University of Trento
University IUAV of Venezia

Tao Liu

EQUIVALENT LINEARIZATION ANALYSIS METHOD FOR BASE-ISOLATED BUILDINGS

Advisor:
Prof. Enzo Siviero
Università IUAV di Venezia, Venice, Italy

Co-Advisors:
Prof. Qilin Zhang, Prof. Tobia Zordan
Tongji University, Shanghai, China
Prof. Bruno Briseghella
Fuzhou University, Fuzhou, China

2014

UNIVERSITY OF TRENTO

Department of Civil, Environmental and Mechanical Engineering

Final Examination 10 / April / 2014

Board of Examiners

Prof. Maurizio Piazza	(Università degli Studi di Trento)
Prof. Andrea Prota	(Università degli Studi di Napoli Federico II)
Prof. Carmelo Gentile	(Politecnico di Milano)
Prof. Helmut Wenzel	(Universität für Bodenkultur Wien)

SUMMARY

Base isolation system, as one of the most popular means to mitigate the seismic risks, often exhibits strong nonlinearity. To simplify the procedure of structural design, bilinear force-deformation behavior is recommended for isolation systems in most modern structural codes. Although base isolation system can be analyzed through nonlinear time history method, solving of a system with a large number of degrees of freedom may require an exorbitant amount of time. As a substitute, the equivalent linearization method is frequently used. Apparently, under given earthquake ground motions, the accuracy of equivalent linearization analysis method is significantly related to the estimation of equivalent linear properties. How to improve the estimation accuracy of this approximate method constitutes a subject of wide and deep interest among researchers around the world.

In this research, the equivalent linearization analysis method for base-isolated buildings was investigated. The literature survey on related aspects of base-isolated buildings was carried out firstly. Then, the estimation accuracy of fifteen equivalent linearization methods selected from the literatures was evaluated when subjected to twelve earthquake ground motions. After that, from simplicity to complexity, the base-isolated buildings were modeled using single-degree-of-freedom (SDOF) systems and multi-degree-of-freedom (MDOF) systems, respectively. For both considered systems, more comprehensive parametric analyses were performed with varying the parameters selected from the isolation system and the superstructure. Accordingly, improved equivalent linearization methods were derived for SDOF and MDOF systems to improve the prediction accuracy of the maximum displacement of isolation systems.

Based on the proposed equivalent linearization methods, different analysis methods for base-isolated buildings were assessed, including equivalent static linear analysis, response spectral analysis, linear and nonlinear time history analyses. It was found that with the proposed equivalent linearization methods equivalent linear analyses could yield more accurate results when compared with the equivalent linearization method recommended by structural codes. As a result, the proposed equivalent linearization method could be potentially useful for the design and analysis of base-isolated buildings, as least in the preliminary stage of structural design.

SOMMARIO

L'isolamento alla base, ormai divenuto una delle tecniche piu' utilizzate per la riduzione del rischio sismico, e' caratterizzato da un comportamento non lineare.
Al fine di semplificare la procedura di calcolo, quasi tutte le piu' attuali normative propongono di utilizzare un modello forza-deformazione bi-lineare.
Nonostante le strutture isolate alla base possano essere analizzate attraverso analisi non lineari al passo, tali calcolazioni sono generalmente molto onerose dal punto di vista computazionale per sistemi a molti gradi di liberta'. In alternativa a cio' viene spesso utilizzato un metodo lineare equivalente. L'accuratezza del metodo lineare equivalente e', definita una certa azione sismica di input, significativamente legata alla stima delle proprieta' lineari equivalenti. La precisione delle analisi basate su questo metodo e come aumentarla rappresenta un interessante tema di ricerca per gli studiosi in tutto il mondo.

In questa ricerca si analizza il metodo lineare equivalente per l'analisi di strutture isolate alla base e si arriva a formulare un proprio modello. Nella prima parte della tesi viene riportato lo stato dell'arte sui metodi di analisi delle strutture isolate alla base e si analizza l'accuratezza di 15 diversi metodi di linearizzazione selezionati fra quelli presenti in letteratura sotto l'azione di 12 segnali sismici diversi.
Successivamente si effettua un analisi parametrica andando a studiare l'influenza nella risposta dei parametri piu' importanti che caratterizzano il sistema di isolamento e la sovrastruttura e modellando la struttura sia come un sistema ad un solo grado di liberta' (SDOF) che a molti gradi di liberta' (MDOF). In base ai risultati ottenuti si propongono dei nuovi modelli lineari equivalenti in grado di cogliere piu' accuratamente per SDOF e MDOF lo spostamento massimo del sistema di isolamento.

Utilizzando i modelli lineari equivalenti proposti, si analizza poi l'influenza dei vari tipi di analisi (analisi statica lineare, analisi spettrale, analisi dinamica lineare e non lineare) sui risultati ottenuti concludendo che anche adottando un'analisi linaere il metodo esposto sembra essere in grado di minimizzare gli errori rispetto a quelli contenuti nelle normative.
In conclusione il modello lineare equivalente sviluppato in questa tesi sembra poter essere utillizzabile in modo affidabile per la progettazione e l'analisi di strutture isolate alla base, almeno in fase di progettazione preliminare.

DEDICATION

to my parents
and
my girlfriend

ACKNOWLEDGEMENTS

Grateful thanks to Prof. Enzo Siviero and Prof. Qilin Zhang
for their deep insights and supports
during my study in Italy.

Grateful thanks to Prof. Tobia Zordan and Prof. Bruno Briseghella
for their great kindest helps and advices
not only in my studies but also in my livings,
to make this research work possible.

Sincere thanks to all my dear friends.

CONTENTS

CHAPTER 1

1. INTRODUCTION

Base isolation systems, as one of most effective methods to mitigate the seismic hazards, have been widely used in practical projects. Due to the existence of the strong nonlinearity, structural design of base-isolated buildings is often performed using nonlinear time history analysis. However, this method requires precise finite element models of the base-isolated buildings and an exorbitant amount of solving time. Furthermore, in the initial stage of structural design, many structural configurations are not well-defined. Therefore, approximate analysis methods of base-isolated buildings are generally performed for the sake of simplicity. One of the best known approximate methods is the equivalent linear analysis method based on equivalent linearization of isolation systems.

1.1. Background

Earthquake, which is considered to be one of the most destructive natural disasters, has caused great loss of life and severe damage to property in recent years.

On 12 May 2008, the great Wenchuan earthquake (Myiamoto, 2008) with a magnitude of 8.0 (Ms) occurred in Sichuan province of China, killing an estimated 68000 people. According to the state media, almost 80% of buildings were destroyed in the quake and the direct economic loss from the disasters is 841.5 billion RMB (US$122.7 billion), as seen in Fig. 1.

In central Italy, the 2009 L'Aquila earthquake (Myiamoto, 2009) occurred on 6 April 2009 and was rated 6.3 on the moment magnitude scale. The earthquake caused significant damage to more than 10000 buildings in the L'Aquila area, as presented in Fig. 2. 308 people were killed in this earthquake and the total cost including financial losses and reconstruction efforts, is expected to exceed US$16 billion.

In New Zealand, The magnitude 6.3 earthquake (Myiamoto, 2011a) occurred on 22 February 2011 severely damaged New Zealand's second-largest city Christchurch. In this earthquake, 185 people were killed and the total losses were estimated over US$12 billion, making it the second-deadliest natural disaster recorded in New Zea-

land. Many buildings had been damaged; it was estimated that more than 30% of the brick and stone buildings in the Central Business District (CBD) had either collapsed or sustained major damage (see Fig. 3).

On 11 March 2011, an Earthquake of Magnitude (Mw) 9.0 (Myiamoto, 2011b) occurred off the Pacific Coast of Tohoku, Japan. This is the fourth largest earthquake in the world and the largest in Japan since instrumental recordings began in 1900. According to National Police Agency of Japan, there were 15870 deaths and 3203 missing, as well as 129426 buildings totally collapsed, with a further 265240 buildings 'half collapsed', and another 727054 buildings partially damaged (see Fig. 4). The earthquake and tsunami caused over US$200 billion damage in Japan and resulted in a nuclear accident with explosions and leaks in three reactors at the Fukushima I (Daiichi) Nuclear Power station.

Nowadays, although earthquake engineering makes great progress, seismic design of structures is still a challenge for structural designers and earthquake engineers, especially when considering structures subjected to great earthquakes or buildings built before with inadequate seismic resistance. People have been very active in finding new ways to protect buildings against earthquakes.

Fig. 1 Structural damage caused by Wenchuan earthquake (Myiamoto, 2008)

Fig. 2 Structural damage caused by L'Aquila earthquake (Myiamoto, 2009)

Fig. 3 Structural damage caused by Christchurch earthquake (Myiamoto, 2011a)

Fig. 4 Structural damage caused by Tohoku earthquake (Myiamoto, 2011b)

Base isolation has been proved to be one of the most successful techniques to mitigate the risk to life and property from strong earthquakes, which shifts the fundamental natural period of a structure to the long period range, e.g., two to four seconds, by placing horizontally flexible isolation devices at the base of the structure to physically decouple it from the ground.

The first record of seismic isolation is an 1870 U.S. Patent filed in San Francisco for a double concave rolling ball bearing, described as an “Earthquake-proof building” (Touaillon, 1870). Although the concept of seismic isolation dates back more than one hundred years, it has only been practiced in the world for the last three decades.

One of the goals of seismic isolation is to shift the fundamental frequency of a structure away from the dominant frequencies of earthquake ground motion and the fundamental frequency of the fixed base superstructure (Naeim & Kelly, 1999). The other purpose is to provide an additional means of energy dissipation, thereby limiting the transfer of seismic energy to the superstructure. Both of them can be illustrated in Fig. 5.

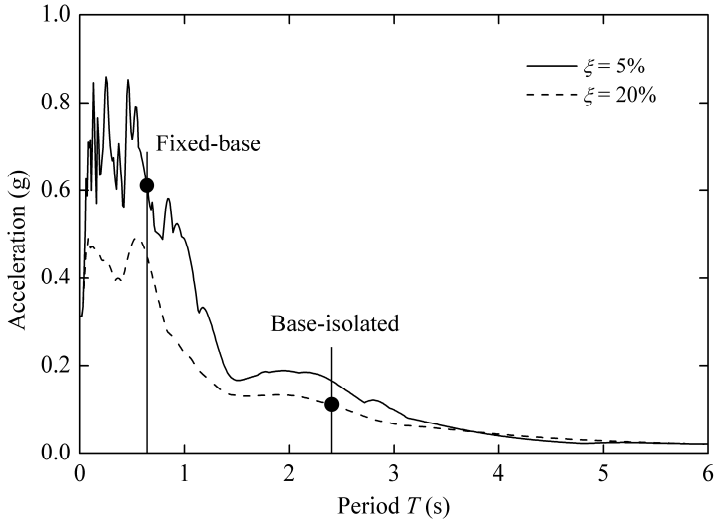

Fig. 5 Goals of base-isolation systems

A base-isolated building can be achieved in both design of new buildings and retro-fit of existing buildings by inserting seismic isolation devices between building and foundation. In general, seismic isolation devices are supposed to provide a single or a combination of the following functions:

- vertical-load carrying capability combined with increased lateral flexibility and high vertical rigidity;
- energy dissipation, hysteretic or viscous;
- re-centering capability;
- lateral restraint (sufficient elastic stiffness) under non-seismic service lateral loads.

Although different hypotheses on the constitutive law for the isolation devices have been developed (Wen, 1976; Hwang et al., 2002; Bhuiyan et al., 2009; Amin et al., 2002; Amin et al., 2006), a bilinear force-deformation behavior is generally recommended in most cases to simplify the design procedure, which can be characterized by the initial elastic stiffness K_i, the strain hardening ratio α, and the yield strength F_y, as presented in Fig. 6.

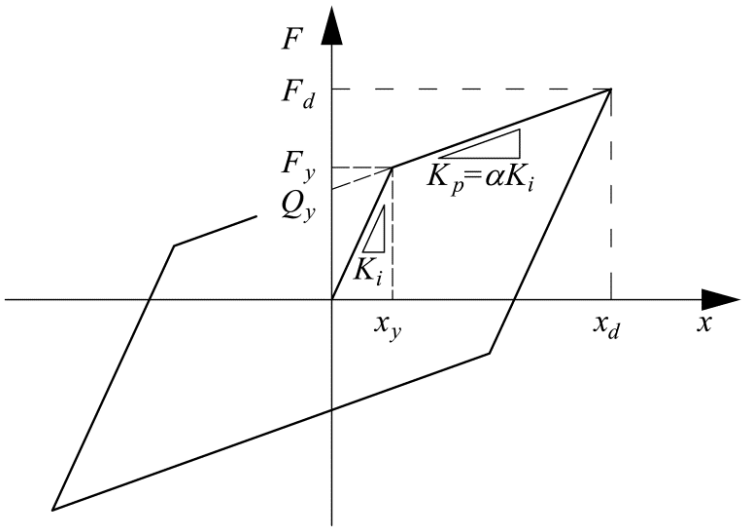

Fig. 6 Bilinear hysteretic model

For a bilinear hysteretic system, the equation of motion under earthquake excitation is given by:

$$M\ddot{x}(t)+C\dot{x}(t)+F\left(x(t),\dot{x}(t)\right)=-M\ddot{x}_g(t) \tag{1}$$

where $\ddot{x}(t)$, $\dot{x}(t)$, and $x(t)$ are the acceleration, velocity, and displacement, respectively, of the system relative to the ground; C is the damping coefficient; $F\left(x(t),\dot{x}(t)\right)$ is the restoring force; M is the mass of the system; and $\ddot{x}_g(t)$ is the ground acceleration.

Of course, the motion equations can be solved exactly through nonlinear time history method. However, solving of a system with a large number of degrees of freedom may require an exorbitant amount of time when time history analysis methods are used. Also, the enormous amount of output results from such a system may be so detailed that it is impractical for engineers to summarize. Furthermore, in the initial stage of structural design, many structural configurations are not well-defined, such as the arrangement and the hysteretic properties of seismic isolation bearings. Thus, there will always be a need for good approximate methods of analysis of nonlinear systems (Guyader & Iwan, 2006).

Of the approximate methods, the equivalent linearization analysis method is best known (Lin & Miranda, 2009). The underlying premise of this method is that the base-isolated structure can be adequately modelled using a viscously damped elas-

tic structure whose stiffness and damping characteristics are selected such that the maximum displacement responses of the two systems are approximately equal, as shown in Fig. 7.

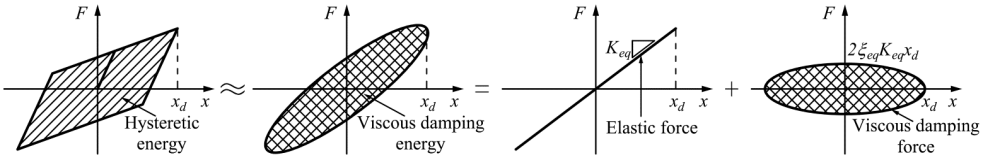

Fig. 7 Equivalent linearization of bilinear hysteretic behavior

Replacing the bilinear system with a viscously damped elastic system, the differential equation of motion may be expressed as:

$$M\ddot{x}_{eq}(t)+C_{eq}\dot{x}_{eq}(t)+K_{eq}x_{eq}(t)=-M\ddot{x}_{g}(t) \tag{2}$$

where $\ddot{x}_{eq}(t)$, $\dot{x}_{eq}(t)$, and $x_{eq}(t)$ are the acceleration, velocity, and displacement, respectively, of the equivalent linear system relative to the ground; C_{eq} is the equivalent damping coefficient; K_{eq} is the equivalent stiffness.

Ideally, if no seismic energy is transmitted, the superstructure remains literally unaffected by a seismic attack. Conversely, the isolators must be capable of undergoing the movements imposed by the ground shaking, while maintaining their ability to carry gravity loads from the superstructure to the ground. So, the maximum deformation of the isolator is considered to be a very important indictor in structural design of base-isolated buildings.

Under a given earthquake ground motion, the response of nonlinear system is related to the hysteretic properties of the isolators and the structural damping specified in the base-isolated buildings, while that of the equivalent linear system is a function of the equivalent period of vibration and the equivalent viscous damping ratio. Denoting Δ_{ex} and Δ_{ap} are the peak displacements respectively solved by Eq. (1) and Eq. (2), the objective of equivalent linearization method is to seek an appropriate linear elastic system (i.e., K_{eq} and C_{eq}) such that the ratio of approximate to exact maximum displacement Δ_{ap}/Δ_{ex} equals to 1.0. Therefore, the estimation of equivalent linear properties is of significant importance to the accuracy of equivalent linear analysis.

According to different treatments in estimating equivalent period and equivalent viscous damping ratio, several analytical or empirical formulas used in equivalent linear elastic analysis were developed in the past decades, which will be further described in the art of state. Most of them are the functions of the strain hardening ratio and the displacement ductility ratio. However, the estimation accuracy of these various equivalent linearization methods is strongly related to different assumptions when they are derived or fitted. Although many researchers have contributed a significant number of works, there are still many aspects need to be investigated in order to gain better equivalent linearization method used for analysis of base-isolated buildings.

To simplify structural design of base-isolated buildings, equivalent linearization analysis method is often proposed by many modern codes. However, in order to model the behavior of isolation system as being equivalent linear, several requirements must be met.

Therefore, in modern codes, equivalent linearization of seismic isolation system cannot always be applied. If equivalent linearization analysis method is conducted, nonlinear properties of seismic isolation system must be adjusted to satisfy the limited conditions, which will be very inconvenient. In addition, the selected isolation bearings may be unavailable on the market. Thus, the code-recommended equivalent linearization method makes simplified analysis of base-isolated buildings only applicable in very limited cases.

1.2. Objectives of the Research

To extend the application scope of equivalent linearization analysis method for base-isolated buildings, a large amount of work has been performed, such as parametric analyses, optimization analyses and regression analyses. Meanwhile, a large number of parameters are considered separately.

Specifically, the main contributions of this study are presented as follows:

1) Fifteen equivalent linearization methods are evaluated to give a general understanding in equivalent linearization technique. Comments on the accuracy of different equivalent linearization methods are given to make their applications more appropriate in practical design.

2) More comprehensive parametric study is performed for base-isolated buildings characterized by SDOF systems. The influence of different parameters, such as strain hardening ratio, initial period and ductility ratio, on the estimation accuracy of maximum displacement response is identified.

3) According to optimization analysis and regression analysis, an improved equivalent linearization method is proposed for SDOF bilinear systems in order to obtain more accurate results.

4) Similarly, the equivalent linearization method recommended in structural specifications and the method proposed for SDOF systems are further examined based on MDOF base-isolated systems. Specifically, the effect of the ratio between the equivalent period and superstructure period on the prediction accuracy of the maximum displacement response is investigated.

5) Accordingly, for MDOF base-isolated systems, the equivalent linearization method used for SDOF systems is improved by taking into account the influence of the ratio between the equivalent period and superstructure period.

6) Based on the code-recommended linearization method and the proposed methods for SDOF and MDOF systems, different methods, including equivalent linear static analysis, response spectral analysis, and linear and nonlinear time history analyses are used for analysis of MDOF base-isolated buildings. Evaluations on the accuracy of different equivalent linear analysis methods are given.

1.3. Layout of the Thesis

This research seeks to examine the equivalent linearization of base-isolated buildings with bilinear hysteretic isolators and to propose more accurate equivalent linearization method used for simplified design of base-isolated buildings. Both SDOF and MDOF systems are considered to simulate the base-isolated buildings. Based upon the improved equivalent linearization models, the detailed procedures to perform linear static analysis and response spectral analysis, which provide a simple way to design base-isolated structures, are described and the results are compared with linear and nonlinear time history analysis.

This dissertation is composed of 7 chapters as described below.

Chapter 1 gives the background and objectives of the research. The background shows several great earthquakes in recent years and explains the need for seismic upgrading of structures using base isolation system. Then, the concept of equivalent linearization technique is briefly introduced.

Chapter 2 provides a literature review of the major previous works conducted in seismic isolation. The review includes many aspects involved in the present study, such as the isolator devices, the effectiveness of base isolation system, equivalent linearization methods, modeling of superstructure damping in base-isolated structures, the lateral force distribution along the height of base-isolated buildings, and so on.

Chapter 3 evaluates fifteen equivalent linearization methods based on bilinear SDOF system when subjected to twelve ground motions. Using a program specifically developed in MATLAB and OpenSees, a large number of parametric analyses are performed. The accuracy of various methods to estimate the maximum displacement response is investigated.

Chapter 4 derives an improved equivalent linearization method for general bilinear SDOF systems. In a wider parameter space, parametric analyses are performed again for equivalent linearization methods selected from Chapter 3. Successively, optimization analyses and regression analyses are carried out to derive an improved formula used to estimate the equivalent damping ratio. In addition, the proposed method (Liu I method) is validated using another twelve recorded ground motions.

Chapter 5 investigates the accuracy of equivalent linearization methods applied to base-isolated structures characterized by MDOF systems. Both the method recommended in codes (R&H method) and Liu I method are considered. Similar to the previous Chapter, an improved method for MDOF systems (Liu II method) is proposed through correcting Liu I method.

Chapter 6 compares various equivalent linear analyses used for base-isolated buildings, such as equivalent linear static analysis, response spectral analysis, and linear time history analysis. The results from these analysis methods are compared with those from nonlinear time history analysis. For the sake of comparison, both code-recommended equivalent linearization method and the proposed equivalent linearization methods are considered in equivalent linearization analysis of base-isolated buildings

In the end, the main findings of this research are summarized and recommendations for future work are presented.

CHAPTER 2

2. STATE-OF-ART

A comprehensive literature survey helps not only to deepen the basic knowledge on the studied subject but also to emphasize advantages and disadvantages of previous experiences, so to give researchers space for further improvements. To provide a unitary framework, a detailed literature survey about the topic of seismic base isolation system is presented.

First of all, different isolation devices are briefly introduced as well as the efficiency of seismic isolation to mitigate the damage of structures. Then, the past efforts to achieve equivalent linearization methods are reviewed. After that, the modelling methods of viscous damping in the superstructure of base-isolated buildings are summarized. Finally, different methods to estimate lateral force distributions along the height of multi-storey base-isolated buildings are presented.

2.1. Seismic Isolation Systems

A number of studies have provided comprehensive reviews of various aspects of the development, theory, and application of seismic isolation systems. For instance, Kelly (Kelly, 1986) provided a historical perspective dating back to the rudimentary beginnings of seismic isolation technology, followed by a complete chronology of research and development efforts. Buckle and Mayes (Buckle & Mayes, 1990) also included a thoughtful historical discussion as well as a comprehensive list of the early applications that paved the way for acceptance and wider adoption. Taylor et al. (Taylor et al., 1992) presented a review of the use of elastomers in seismic isolation bearings, with emphasis on their long-term behavior. A mid-1990s report provided information on several subtopics including theory, experiments, and application of sliding bearings, hybrid testing, and development and practice in several countries (Soong & Constantinou, 1994). Jangid and Datta (Jangid & Datta, 1995) presented an updated state-of-the-art review of the behavior of base-isolated buildings to seismic excitations. The review included the literature on theoretical aspects of seismic isolation, parametric behavior of base-isolated buildings and experimental studies to verify some of the theoretical findings. A brief review of the

earlier and current base-isolation devices (proposed or implemented) was given, and aspects for future research in the area of base islation were also included.

As the volume of information on seismic isolation has grown exponentially over the past 10-15 years, the attempts at a comprehensive review have diminished. Yet, several focused reviews have emerged. Kunde and Jangid (Kunde & Jangid, 2003) prepared a comprehensive review of research and application of seismic isolation to bridges, including analytical, experimental and parametric studies. Symans et al. (Symans et al., 2003) reviewed the development and application of seismic isolation and damping systems for wood frame structures, which are uniquely challenging to isolate due to the inherent flexibility of the framing system and relatively light mass. In different countries, such as USA (Wiles, 2008), Europe (Martelli & Forni, 1998), Japan (Pan et al., 2005), China (Pan et al., 2012) and New Zealand (Robinson, 1995), detailed review of base isolation system could be also found.

Regarding the isolation devices, they can be classified into two basic types: elastomeric bearings and sliding bearings. The elastomeric bearings with low horizontal stiffness shift fundamental time period of the structure to avoid resonance with the excitations. The sliding isolation system is based on the concept of sliding friction.

1) Elastomeric Base Isolation Systems

The first category of elastomeric bearings (i.e., the laminated rubber bearings), as shown in Fig. 8, is most commonly used base isolation system. Laminated rubber bearings can be categorized as: (1) low-damping natural rubber; and (2) high-damping rubber.

Low-damping natural rubber material exhibits nearly linear shear stress-strain behavior up to 150% shear strain, after which the material stiffens. Natural rubber with durometer hardness of 50 is typically used for seismic applications having a shear modulus that ranges from 0.65 MPa to 0.9 MPa. In general, for low-damping natural rubber the equivalent damping ratio ξ ranges between 2% and 3% at 100% shear strain. In order to control the displacements across the isolation interface, external supplemental damping devices such as yielding steel bars, plates, or viscous fluid dampers are typically used in parallel with low-damping natural rubber bearings.

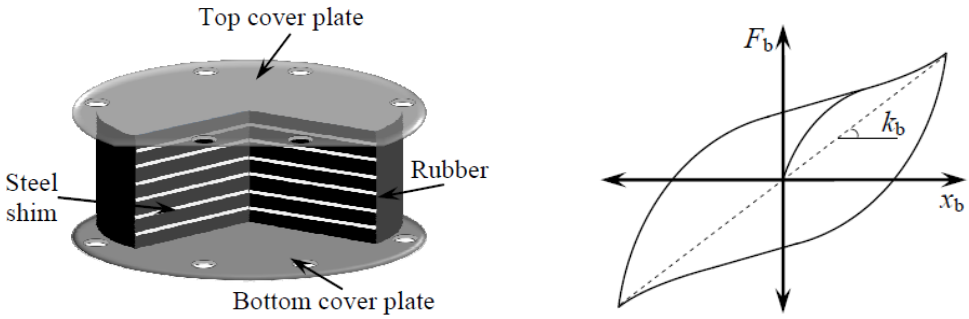

Fig. 8 Laminated rubber bearings and its force-deformation behavior

To achieve a higher level of damping, carbon black and other fillers can be added to the raw rubber during the mixing process to produce high-damping rubber bearings (HDRBs) (Naeim & Kelly, 1999). The equivalent damping ratio of high-damping rubber bearings can range from 10% to 20% at 100% shear strain. Although the range of shear modulus for high-damping rubber is similar to that for low-damping rubber, the fillers increase the hardness and thus the shear modulus of the rubber so that it can be difficult to achieve low shear modulus and high levels of damping simultaneously.

As mentioned by many researchers, the mechanical behavior of HDRBs is generally characterized by strain-rate-dependent hysteresis property. Hwang et al. (2002) have developed an analytical model to describe the damping and restoring forces of HDRBs. Both stiffness and damping coefficients are expressed in terms of a higher order polynomial function of the relative displacement and velocity of the bearing. All parameters of the model are determined from the cyclic loading tests of a particular bearing by utilizing the nonlinear least-square method. However, the physical basis of the mathematical model incorporating the rate-dependence to describe the stiffness and the damping coefficients is not clearly explained. Tsai et al. (Tsai et al., 2003) have developed a rate-dependent analytical model of HDRBs by extending the Wen's hysteretic model (Wen, 1976) in an incremental form. This model has described the restoring force in terms of the strain as well as velocity induced forces. Dall'Asta and Ragni (Dall'Asta & Ragni, 2006) have conducted cyclic shear tests and simple relaxation tests to identify the rate-dependent mechanical properties of HDRBs. On the basis of the experimental results, they have proposed a rate-dependent analytical model of HDRBs. The physical basis of the mathematical model describing the elasticity behavior of HDRBs is ambiguous and the mathematical model cannot adequately describe for a general loading condition. Other analytical models for HDRBs have been proposed by many researchers (Hwang & Ku, 1997; Hwang & Wang, 1998; Koh & Kelly, 1990) based on the results of the

shaking table tests of seismically isolated bridge decks. In these proposed models, the fractional derivative of the relative displacement is used rather than the relative velocity term of the equation of motion. In recent, Bhuiyan et al. (Bhuiyan et al., 2009) developed an elasto-viscoplastic rheology model of HDRBs for seismic analysis on the basis of experimental observations. In their model, the Maxwell model is extended by adding a nonlinear elastic spring and an elasto-plastic model (spring-slider) in parallel. Based on the comparison between the simulations and the experimental results, the proposed model is able to predict the nonlinear viscosity in loading and unloading of the HDR bearings in addition to other inelastic behavior.

The second category of elastomeric bearings is lead-rubber bearings (LRB) (Robinson, 1977; Robinson, 1982), as presented in Fig. 9. This kind of isolator bearing was first introduced and used in New Zealand in the late 1970s. Therefore, they are also referred as N-Z systems. The lead-rubber bearings behave essentially as hysteretic damper device and widely studied in the past (Kelly et al., 1972; Kelly et al., 1977; Skinner et al., 1975).

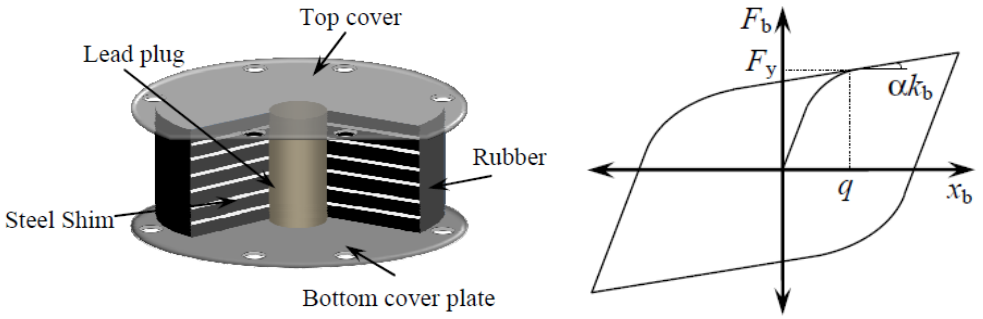

Fig. 9 Lead-rubber bearing and its force-deformation behavior

LRB system provides the combined features of vertical load support, horizontal flexibility, restoring force and damping in a single unit. To provide an additional means of energy dissipation, a central lead core is added. The lead-plug deforms plastically under shear deformation, enhancing the energy dissipation capabilities compared to the low-damping natural rubber bearing.

In general, the lead yields at a relatively low stress of about 10 MPa in shear and behaves approximately as an elasto-plastic solid. The interrelated simultaneous process of recovery, recrystallization and grain growth is continuously restoring the mechanical properties of the lead. The lead has good fatigue properties during cy-

clic loading at plastic strains. More important, lead is readily available at high purity of 99.9 per cent required for its predictable mechanical properties.

Due to plastic deformation of the lead core, the energy dissipation mechanism is primary hysteretic. A Bouc-Wen or rate independent plasticity model (Nagarajaiah et al., 1991) is typically used for analytically modelling the shear force-horizontal deformation response of LRBs. Under bi-directional loading, the bearing model is coupled in the two orthogonal horizontal directions through a circular yield surface.

However, the Bouc-Wen based hysteretic models do not account for the effect of heating in the lead-core with repeated cycling that leads to degradation in the characteristic strength. To account for the effects of heating in LRBs, many theoretical models have been developed and experimentally verified (Kalpakidis & Constantinou, 2009a; Kalpakidis & Constantinou, 2009b). But, thermo-mechanical models (Kalpakidis et al, 2010) that account for heating and strength degradation in LRBs have not been widely implemented for the analysis and design of LRB systems. Ozdemir and Dicleli (Ozdemir & Dicleli, 2012) investigated the effect of lead core heating and associated strength deterioration on the seismic response of bridges isolated with LRBs as a function of the characteristics of the isolator and near fault ground motions with forward rupture directivity effect.

The vertical force-deformation behavior is typically assumed to be linear with stiffness equal to the compressive stiffness of the bearing, though multi-linear models are possible. A model that includes the influence of vertical load on the effective horizontal stiffness and lead-core yield strength was developed by Ryan et al. (Ryan et al., 2005) and has been implemented in OpenSees (Mazzoni et al., 2007). In order to account for the second-order effects due to vertical load at large horizontal displacement, many models have been developed (Iizuka, 2000; Yamamoto et al., 2009; Kikuchi et al., 2010) and are capable of exhibiting zero or negative tangential horizontal stiffness (Sanchez et al., 2012). However, these models have not been widely adopted due to the extensive experimental data required to calibrate the model parameters.

2) Sliding Base Isolation Systems

One of the most popular techniques for seismic isolation is through the use of sliding isolation devices. The sliding systems exhibit excellent performance under a variety of severe earthquake loading and are very effective in reducing the large levels of the superstructure acceleration. These isolators are characterized by their insen-

sitivity to the frequency content of earthquake excitation, because of the tendency of sliding system to reduce and spread the earthquake energy over a wide range of frequencies. In addition, since the frictional force is proportional to the mass of the structure, the center of mass and the center of resistance of the sliding support coincide, thus the torsion effects produced by the asymmetric building can be diminished.

(a) Pure Friction System

The simplest sliding isolation system, used popularly for bridges in particular, is the pure friction (P-F) system based on the mechanism of sliding friction (Westermo & Udwadia, 1983), as shown in Fig. 10. The use of layer of sand or roller in the foundation of the building is the example of P-F base isolator. Under normal conditions of ambient vibrations, and small magnitude earthquakes, P-F system acts like a fixed base system due to the static frictional force. However, for large earthquakes, the static value of frictional force is overcome, and sliding occurs with reduced dynamic resistance thereby reducing the accelerations transferred to the structures. The horizontal frictional force at the bearing interface offers resistance to the motion, and dissipates energy. The coefficient of friction of P-F system varies significantly with the nature of friction surface. Coulomb's frictional model is often used to model the limiting frictional force. It should be noted that in this model the frictional coefficient is independent of the sliding velocity.

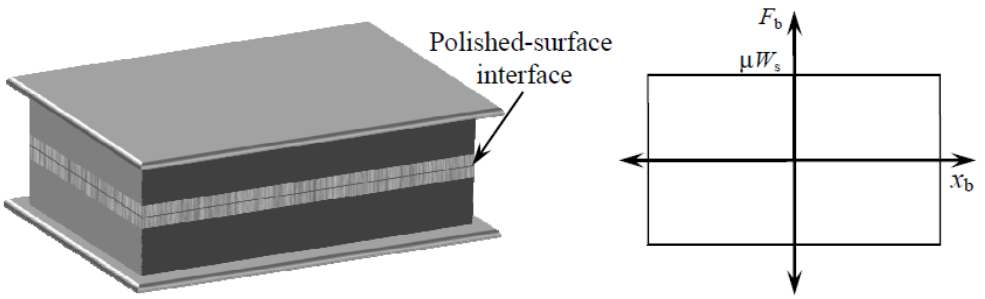

Fig. 10 Lead-rubber bearing and its force-deformation behavior

(b) Friction Pendulum System

When P-F systems are used, supplemental devices are indispensable to provide restoring capacity, and to check on the excessive displacements across isolation layers. Therefore, combined the concept of a pendulum type response with P-F sys-

tem, friction pendulum system (FPS) is developed (Zayas et al., 1987; Zayas et al., 1990), as shown in Fig. 11.

The concept of FPS is marked by sliding of an articulated slider on spherical concave chrome surface. The slider is faced with a bearing material which results in development of friction force while concave surface produces restoring force. FPS is activated only when the inertia forces caused by earthquakes overcome the static value of friction and coefficient of friction depends upon the velocity attained. The FPS develops a lateral force equal to the combination of the mobilized frictional force, and the restoring force that develops because of the rising of the structure along the spherical concave surface (Matsagar & Jangid, 2003). In practice structural design, rigid-plastic model is often used to represent the characteristics of FPS (Liu et al., 2014c).

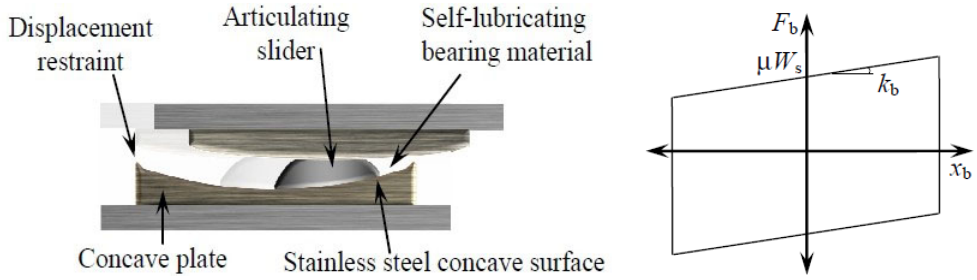

Fig. 11 Friction pendulum bearing and its force-deformation behavior

As discussed by Constantinou et al. (Constantinou et al., 1990), the coefficient of friction is strongly related to the sliding velocity and normal pressure, so it is both velocity and pressure dependent. In addition, the variation of normal force also has significant influence on the response behavior of FPS (Almazán et al., 1998; Briseghella et al., 2013).

In the past years, many research efforts were made to develop refined models for FPS. Eröz and DesRoches (Eröz & DesRoches, 2008) presented a new model for the FPS that can represent the variation of the normal force and friction coefficient, bi-directional coupling and large deformation effects during nonlinear dynamic analyses. The influence of various parameters had been highlighted via nonlinear time-history analyses of a multi-span continuous bridge.

Almazán and De la Llera (Almazán & De la Llera, 2002) developed a theoretically 'exact' model to account for large deformation kinematics and the associated P-Δ effects in FPS isolators. Their study pointed out that small deformation kinemat-

ics may lead, in the case of impulsive motions, to discrepancies in global response quantities, relative to the 'actual' response, as large as 30 per cent. These discrepancies increased up to 50 per cent for local response quantities such as normal isolator forces.

2.2. Efficiency of Base Isolation System

There had been several analytical studies in the past to demonstrate the effectiveness of seismic isolation for earthquake-resistant design of buildings, which could be involved to structural response or cost effectiveness.

Shatnawi et al. (Shatnawi et al., 2008) studied the response of the rubber-steel bearing isolation system. The structural responses were computed using two material models. These are: a hyperviscoelastic material model (Al-Shatnawi, 2001) that is linked with ABAQUS as a user defined material model (UMAT), and another large strain hyperelastic material model that exists within the ABAQUS software (i.e., Ogden type). Structural response of the rubber bearings were found to have good agreement with those obtained when using the hyperelastic Ogden model of ABAQUS. Moreover, the non-linear seismic responses of a fixed-base and base-isolated steel frame structures were analyzed. The results showed a great efficiency of using the rubber bearing isolation in uncoupling both structures from the seismic ground motion helping both of them to sustain the earthquake excitation. This is observed by elongating the period of the structure and reducing the horizontal accelerations, lateral-forces and the relative horizontal roof displacement. However, better results were observed for the high-rise structures, because their period was longer than the period of the low-rise structures which reduced the effect of the earthquake excitation on this type of structures. In addition, it had been proved that the used material model was more effective to capture the behavior of the base-isolated structures expressing a notable reduction in acceleration and an increase in the structural resistance to earthquake excitations.

Matsagar and Jangid (Matsagar & Jangid, 2008) investigated seismic responses of structures retrofitted using base isolation devices. The retrofitting of various important structures using seismic isolation technique by incorporation of the layers of isolators at suitable locations was studied, such as historical buildings, bridges, and liquid storage tanks. Different types of isolation devices, such as elastomeric bearings and sliding systems were evaluated for their performance to investigate the effectiveness of the base isolation in seismic retrofitting. The response of the retrofit-

ted structural system was obtained numerically by solving the governing equations of motion under different earthquakes and compared with the corresponding conventional structure without any retrofit measures. The results showed that the seismic response of the retrofitted structures reduced significantly in comparison with the conventional structures depicting effectiveness of the retrofitting done through the base isolation technique. That study also distinctively elaborated on the methods of construction in retrofitting works involving base isolation.

Lee et al. (Lee et al., 2008) investigated the statistics of peak elastic and inelastic responses of structures with tuned mass dampers (TMD) or base isolation devices (BID) under seismic excitations, and assessed the cost-effectiveness of structures with an option of installing these devices in mitigating seismic risk. For the assessment, a structure was modelled as a two-degree-of-freedom system; one degree-of-freedom represented a main structure and the other represented an auxiliary system (i.e., TMD or BID). The hysteretic behavior of the main structure and auxiliary system was approximated by the Bouc-Wen model. A parametric study of linear and nonlinear responses of the system was carried out by using 381 ground motion records, and the ratios of the maximum displacement and ductility demand of the system with auxiliary devices to those without were considered as a measure of effectiveness of TMD/BID. The linear and nonlinear responses were also incorporated for assessing possible damage states and damage costs in the lifecycle cost analysis. The analysis results indicated that TMD reduced peak structural responses by as much as 10%-15%, depending on the mass ratio, and was effective for structures with longer vibration periods. The effectiveness of TMD decreased as the seismic excitation level increased and its installation could have a negative impact on the structure. The results for BID systems showed that BID significantly reduced peak structural responses by as much as 70%-80% and was particularly beneficial for structures with shorter vibration periods. This effectiveness decreased as the seismic excitation level increased, since the degradation of structures leaded to the elongation of the vibration period. It was also indicated that bilinear base isolators, although slightly less effective than linear ones, can be useful for practical applications, since peak displacement demands in isolators were reduced. Furthermore, the lifecycle cost analysis results illustrated that TMD reduced the expected lifecycle cost by about up to 2.5% in terms of the initial construction cost, whereas BID reduced it by about up to 16%.

Zekioglu et al. (Zekioglu et al., 2009) described the performance-based seismic design of the Sabiha Gökçen International Airport (SGIA) Terminal Building in Istanbul, Turkey utilizing seismic-isolation concept with triple-friction-pendulum devices. The

structural system was analyzed using equivalent static, linear dynamic and time history procedures, including a "beyond the code requirement" investigation of the structural members at MCE hazard with FEMA recommended acceptance criteria per the selected performance objectives. A comparative study was performed showing the effectiveness of the current code based analysis and design procedures. Overall, the seismically isolated structure met and surpassed the performance objectives while achieving an 80% reduction in the base shear (relative to the fixed-base building model), significant decreased in the story drift (83%) and floor accelerations (90%).

Alhana and Altun (Alhana & Altun, 2009) carried out bi-directional non-linear time history analyses of a 4-story base isolated benchmark building under near-fault and far-fault earthquakes. This building was designed according to UBC97 and the isolation system was composed of high damping rubber bearings with the bi-linear force-displacement behavior. Design displacements were estimated using UBC97 parameters. Results showed that UBC97 predicted isolator displacements successfully. A major improvement in the superstructure performance was achieved as the floor accelerations, inter-story drifts and base shear can be significantly reduced altogether.

Sayani and Ryan (Sayani & Ryan, 2009) developed a response index for rapid prototyping of response as a function of system characteristics. Based on response history analysis to a suite of motions, constant ductility spectra were generated for fixed-base and isolated buildings. Both superstructure force (base shear) and deformation demands in base-isolated buildings were lower than in fixed-base buildings responding with identical deformation ductility. When evaluated for a life safety performance objective, the superstructure design base shear of an isolated building was competitive with that of a fixed-base building with identical ductility, and the isolated building generally had improved response. Isolated buildings can meet a moderate ductility immediate-occupancy objective at low design strengths, whereas comparable ductility fixed-base buildings failed to meet the objective.

Mitu et al. (Mitu et al., 2010) presented the analyses of the efficiency for a base isolation system. To portray the hysteretic behavior of the devices used for seismic protection the Bouc-Wen model was used. The nonlinear first order equation which can describe the evolution of force developed by one device for almost any loading pattern were added to the system of equations which modelled the dynamical behavior of the protected building. Using Matlab-Simulink software, the model was employed to investigate the efficiency of the base isolation devices by comparing

the seismic response of protected and unprotected buildings subjected to strong seismic actions. The simulation results advocated the efficiency of using passive seismic protection devices with hysteretic characteristics, which included in the same element both the elastic and the dissipative properties necessary to reduce the structural seismic response. The base isolation systems can provide an important reduction of accelerations transmitted to the structure, such that the structural elements remained in the elastic field.

Tulei et al. (Tulei et al., 2010) analyzed the possibility of implementing modern solutions for the seismic rehabilitation of buildings in Romania. A 5-storey reinforced concrete framed structure located in Bucharest was upgraded in accordance to the present Romanian codes. In order to draw conclusions regarding the influence of the site conditions on the structural response, the building was considered in different seismic zones from Romania, for which the response spectrum had the same PGA values, but different corner periods. The efficiency of two solutions based on passive control devices was analyzed, namely base isolation with lead-rubber elastomeric bearings and in structure linear viscous dampers. The analyses results showed the use of viscous dampers significantly reduced the relative lateral displacements, but leaded to lesser reductions of the base shear forces. However, the base isolation system can reduce the base shear force with 84-86% and it was considered to be the most efficient solution for ensuring the building seismic safety.

Wu (Wu, 2010) examined the dynamic characteristics of an eccentric five-storey benchmark model isolated with laminated rubber bearings and lead core rubber bearings using a shaker table and four different ground motions. Important differences between the two isolator types were identified. The laminated rubber bearings were found to be similar to lead core rubber bearings in protecting torsional deformation of the model but were more effective than lead core rubber bearings in reducing model relative displacement. Lead core rubber bearings rendered a smaller torsional angle and absolute deformation of the base isolation system, a more stable structural system. Therefore, base isolation can greatly reduce torsional as well as translational response of building structures.

Komur et al. (Komur et al., 2011) performed nonlinear dynamic analyses of 4- and 8- storey reinforced concrete structures as isolated and fixed-base types. Lead-rubber bearing (LRB) was used as an isolation system. Nonlinear behavior of both isolation system and super-structure were considered in the modelling. The behaviors of designed models under dynamic loads were analyzed using Ruaumoko computer software. Erzincan, Marmara and Duzce Earthquakes were chosen as the

ground motions. Results showed that in base-isolated structures large reduction was observed in acceleration values, base shear forces and relative storey displacements with respect to conventional structures. As a result of decreasing relative storey displacements, the accelerations acting on superstructure were damped at base level and the internal forces in superstructures were reduced. On the other hand, the displacements and periods of base-isolated structures were increased comparing with fixed-base structures.

Branco and Guerreiro (Branco & Guerreiro, 2011) presented a comparative study of the performance of different seismic retrofitting techniques, implemented in a model of an existing masonry building. The first part of the study considered the testing of different methodologies to strengthen the building floors, to enable them to behave as stiff diaphragms. In the second stage, the seismic protection of the building was studied with these different solutions: insertion of concrete walls, the use of a base isolation solution, and the implementation of viscous dampers. Based upon the observed results, the solution that presented the best response, considering the measured displacements, was the solution with concrete walls, although the results were very close to those from the viscous dampers. The base isolation system presented higher absolute displacements, but was the one that conducted the smallest relative displacements. According to the tensile stresses evaluation, the best results were reached by the base isolation system, followed by the concrete walls.

Thakare and Jaiswal (Thakare & Jaiswal, 2011) studied a 3-storey R.C building with elastomeric lead rubber bearing having bilinear force deformation behavior. The performance of fixed-base and base-isolated building was compared through seismic analysis method. Based upon the obtained results, it was found that base isolation reduced the design parameters (i.e. base shear and bending moment) in the structural members above the isolation interface by around 4-5 times. The shear and bending moments were reduced due to the higher period of the base isolated structure which resulted in lower acceleration acting on the structure and also, due to the increased damping in the structure. It had been found that the base shear reduced 55%-60% in response spectrum analysis, whereas base shear reduced by 70%-80% in time history analysis. In general, the peak displacements obtained by the time history analysis were less than those from the response spectrum analysis. The authors concluded that this was because the damping due to hysteretic effect was more than the equivalent damping considered in the response spectrum method.

Bedrinana (Bedrinana, 2011) evaluated the cost-effectiveness as well as the seismic safety of a base-isolated building located in Peru. A methodology to evaluate quantitatively the seismic risk and the cost-effectiveness of a base-isolated building during its lifetime was presented. The process started with the hazard analysis and the earthquake ground motion generation in the studied area. Lima area was considered in that study. Series of artificial earthquake ground motions were generated by a stochastic method in the studied area. Then a preliminary seismic design of the target building was carried out according to the Peruvian seismic code. To get the response distribution of the target building, several dynamic nonlinear analyses were performed by using the generated artificial motions as input waves. By assuming a structural response distribution, the seismic risk analysis was performed in terms of three structural parameters such as: inter-storey drift ratio (IDR), floor acceleration (FA) and the structural damage index (DI). The damage of the target building was evaluated by using damage index. Results showed that the total damage in conventional building was considerably larger than isolated building. The expected value of the total damage index in 50 years, with 10% of exceedance probability, for the fixed building had a value of about 2.47 times larger than isolated one. Although the initial total structural cost in the isolated building was larger than that in fixed one, the total structural cost in isolated building was much smaller for long time interval. So, base isolated building was cheaper than fixed building during the lifetime of the target building when large damage was expected.

Islam et al. (Islam et al., 2012) provided incorporation of lead-rubber bearing (LRB) and high damping rubber bearing (HDRB) as base isolators in addition to focussing on the changes of structural parameters for isolating effects in the region of medium risk seismicity. Nonlinear models of LRB and HDRB had been built up. The design of base isolators for building construction was covered along with structural feasibility. Linear static, free vibration and nonlinear dynamic time domain analyses were performed for both isolated and non-isolated buildings under site specific bi-directional earthquake. That study revealed that for medium rise buildings, isolation can significantly reduce seismic response in soft to medium stiff soil. The reduction of overturning base moment due to isolation indicated that the building became more stable compared to the fixed base structure. Modelled non-linear bearings had been found to be suitable to cope with the precise nonlinearities. The building experienced more flexibility even when using the same structural element configuration. In addition, the flexibility of the structure envisaged some sort of savings due to reduced structural responses through incorporation of the isolator. In seismic vulnerable areas where the main concern was the mitigation of the seismic instability

with the support of critical components, results showed the effectiveness of base isolation system in terms of lessening structural responses under seismic loading.

In another work of Islam et al. (Islam et al., 2010), the design of base isolators for a building along with its structural and economic feasibility was addressed. Linear static as well as dynamic (time history and response spectrum) analyses had been carried out for both isolated and non-isolated buildings. Similar analyses had also been repeated for buildings with different heights but similar plan areas. That study revealed that for low-to-medium rise buildings, isolation system can reduce seismic force along with some savings in structural cost of the building, though incorporating base isolators increase the overall price and installation cost. A meticulous review indicated that savings may be in the order of 5%-10% of the total structural cost of the respective building.

Briseghella et al. (Briseghella et al., 2012) investigated the application of base isolation system to an old R.C. buildings built in the 70's and 80's, which was damaged by the L'Aquila earthquake occurred in Italy. Different kinds of analysis (response spectral, pushover and nonlinear dynamic analysis) were performed by Midas/Gen according to Eurocode8. Results had been compared among the original building and buildings retrofitted by different interventions. Although both "column cut" and "Lift up" strategies can reduce the seismic vulnerability of existing building, the later exhibited better performance than the former. In addition, the "column cut" technique generally implies a reduction of the free floor height and strength of structural elements in elevation, so stairs and elevators need special design. But the "Lift up" system has not the disadvantages above and preserves the architectural and functional character of the construction. So, "Lift up" technique is more attractive and should be widely applied in the retrofitting of existing building. Furthermore, from the economic point of view, "column cut" technique and "Lift up" system were equivalent in the presented case.

Kilar et al. (Kilar et al., 2013) analyzed the effects and costs of implementing a base isolation system for the mitigation of the seismic risk of an existing externally-braced steel frame rack structure by means of nonlinear static (pushover) analysis. Various plan asymmetric variants, with different realistic distributions of the payload mass and occupancy levels, had been investigated under two seismic intensities (a_g = 0.175 *g* and 0.25 *g*). The results obtained were presented as floor plan projection envelopes of the top displacements and as plastic hinge damage patterns of the superstructure. In the presented cost evaluation, the cost of the implementation of the proposed base isolation system was compared with the estimated costs of

structural repairs to the damaged structural members of the superstructure, as well as with estimated expenses of the downtime period and content damage. The results had shown that base isolation was, in general, not economically feasible for lower ground motion intensities, whereas it could be of great benefit in the case of moderate and high intensities. A simple rough cost estimation study, based on the obtained plastic hinge patterns, showed that the inclusion of the downtime period costs and content damage costs might be important parameters, which could make such an isolation system viable also for lower ground motion intensities. The other benefits brought by seismic isolation, such as savings on the building design costs, reductions in the threat to employees' lives, were not included in that study.

2.3. Equivalent Linearization Methods

Equivalent linearization of the nonlinear system greatly simplifies the problem and provides an approximate estimate of the response of a structure equipped with hysteretic devices. This approach is reflected in current design and analysis guidelines for structures incorporating passive energy dissipation systems (FEMA, 1997; AASHTO, 2002; BSSC, 2003; CEN, 2004; D.M., 2008). It must be clearly understood, however, that this equivalent linearization for structures incorporating hysteretic devices should be used only for preliminary design and for estimating the dynamic response. The addition of this equivalent viscous damping will always cause a reduction of the dynamic response of a single-degree-of-freedom (SDOF) system for any seismic input signal. Because of the nonlinear nature of actual hysteretic devices, the results obtained with the linear system with equivalent viscous damping may be non-conservative.

Equivalent linearization of base-isolated buildings can be made by computing the effective period of vibration and the equivalent viscous damping for an equivalent SDOF system. According to different treatments in estimating equivalent period and equivalent viscous damping ratio, several analytical or empirical formulas used in equivalent linear elastic analysis were developed in the past decades. Generally, they can be classified into two main groups according to the definition of the equivalent period of vibration (or equivalent stiffness). The first group includes methods with the equivalent period defined using the concept of secant stiffness at design displacement of systems. In the second group of the existing equivalent linearization methods, the equivalent stiffness of the equivalent linear systems is determined using other derived or fitted formulas.

2.3.1 Equivalent Linearization Methods Based on Secant Stiffness

The first group of equivalent linearization methods considered in this research comprises those proposed by Rosenblueth and Herrera (Rosenblueth & Herrera, 1964), Gulkan and Sozen (Gulkan & Sozen, 1974), JPWRI (JPWRI, 1992), Kowalsky (Kowalsky, 1995), Blandon and Priestley (Blandon & Priestley 2005), Jara and Casas (Jara & Casas, 2006), Dicleli and Buddaram (Dicleli & Buddaram, 2007), and Jara et al. (Jara et al., 2012). Here, for the purpose of brevity, they are abbreviated as R&H, G&S, JPWRI, Kow, B&P, J&C, D&B, and J&O method.

Based on harmonic loading, Rosenblueth and Herrera firstly proposed the secant stiffness at maximum deformation as the basis for selecting the period ratio. Considering the idealized bilinear hysteresis model, equivalent stiffness can be determined based upon the concept of secant stiffness, as shown in Fig. 12, namely:

$$K_{eq} = \frac{F_d}{x_d} \tag{3}$$

where

$$F_d = K_i x_y + K_p \left(x_d - x_y \right) \tag{4}$$

Therefore,

$$K_{eq} = \frac{K_i x_y + K_p \left(x_d - x_y \right)}{x_d} = K_i \left[\frac{x_y}{x_d} + \frac{K_p}{K_i} \left(1 - \frac{x_y}{x_d} \right) \right] \tag{5}$$

Let denote $\mu = x_d / x_y$ and $\alpha = K_p / K_i$, and substitute them in the above expression, that is:

$$K_{eq} = K_i \left[\frac{1}{\mu} + \alpha \left(1 - \frac{1}{\mu} \right) \right] = K_i \frac{1 + \alpha \left(\mu - 1 \right)}{\mu} \tag{6}$$

Once the equivalent stiffness is determined, the equivalent period and initial period can be computed using the following equations, respectively.

$$\begin{cases} T_{eq} = 2\pi\sqrt{M / K_{eq}} \\ T_0 = 2\pi\sqrt{M / K_i} \end{cases} \tag{7}$$

Finally, period ratio can be given as:

$$T_{eq} / T_0 = \sqrt{K_i / K_{eq}} = \sqrt{\mu / \left[1 + \alpha\left(\mu - 1\right)\right]} \tag{8}$$

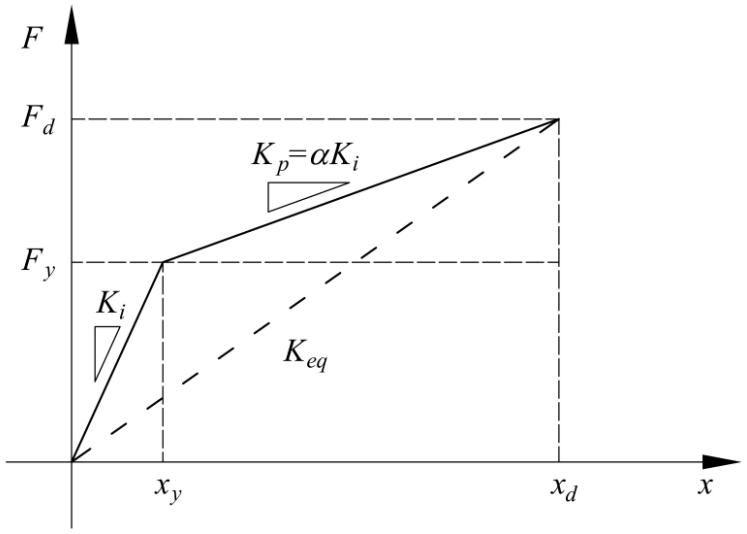

Fig. 12 The concept of secant stiffness

Hysteretic damping ratio of bilinear system can be determined through equating the energy dissipated by one cycle of the bilinear model with the energy dissipated by one cycle of harmonic response of linear elastic system at resonance. Considering symmetric steady-state response of bilinear systems, the hysteresis energy dissipated by one cycle (i.e., the area of enclosed by hysteresis loop, see Fig. 13) can be expressed as:

$$E_H = 4S_{OABC} = 4S_{O'ABC'} = 4Q_y\left(x_d - x_y\right) = 4x_y\left(K_i - K_p\right)\left(x_d - x_y\right) \tag{9}$$

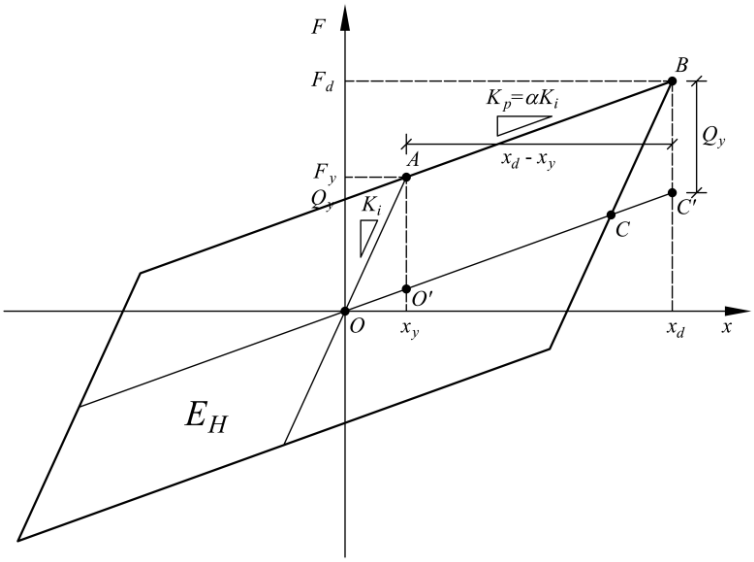

Fig. 13 Hysteresis energy dissipated by one cycle of the bilinear model

For linear elastic systems with a damping ratio ξ and a secant stiffness *K*, the damping energy dissipated by one cycle of harmonic response is defined by the area of the ellipse shown in Fig. 14.

$$E_D = \pi \cdot x_d \cdot \left(2\xi K x_d\right) = 2\pi\xi K x_d^2 \tag{10}$$

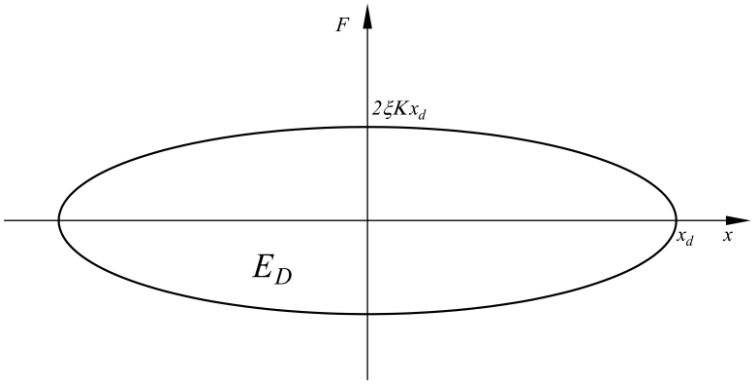

Fig. 14 Damping energy dissipated by one cycle of harmonic response

Substituting K_{eq} for *K* in Eq. (10) and employing the equal energy dissipation principle (i.e., $E_H = E_D$), first proposed by Jacobsen (Jacobsen, 1930), the hysteretic damping ratio of the equivalent linear systems can be derived:

$$\xi_{hyst} = \frac{E_H}{2\pi K_{eq} x_d^2} = \frac{4x_y\left(K_i - K_p\right)\left(x_d - x_y\right)}{2\pi K_{eq} x_d^2} = \frac{4\left(1 - K_p / K_i\right)\left(x_d / x_y - 1\right)}{2\pi\left(x_d / x_y\right)^2}\frac{K_i}{K_{eq}} \tag{11}$$

Considering $\mu = x_d / x_y$, $\alpha = K_p / K_i$ and $K_i / K_{eq} = \mu / [1+\alpha(\mu -1)]$, the hysteretic damping ratio ξ_{hyst} can be rewritten as:

$$\xi_{hyst} = \frac{2\left(1-\alpha\right)\left(\mu -1\right)}{\pi\mu\left[1+\alpha\left(\mu -1\right)\right]} \tag{12}$$

If the inherent viscous damping ratio of bilinear systems ξ_0 is considered, the equivalent viscous damping ratio can be finally expressed as:

$$\xi_{eq} = \xi_0 + \xi_{hyst} = \xi_0 + \frac{2\left(1-\alpha\right)\left(\mu -1\right)}{\pi\mu\left[1+\alpha\left(\mu -1\right)\right]} \tag{13}$$

This method is also referred to as geometric stiffness method, which has been adopt by many structural codes, such as AASHTO (AASHTO, 2002), Eurocode8 (CEN, 2004) and the new Italian code (D.M., 2008).

Gulkan and Sozen (Gulkan & Sozen, 1974) found that a reduction in stiffness and an increase in energy dissipation capacity are two basic characteristics of reinforced concrete structures to mitigate the structural response when subjected to strong ground motions. Both can be related to the maximum displacement. They concluded that the maximum dynamic response of reinforced concrete structures, as represented by SDOF systems, can be approximated by linear response analysis using a reduced stiffness and a substitute viscous damping ratio. Based on Takeda hysteretic model (Takeda et al., 1970) and a series of experimental investigations on reinforced concrete frames, they proposed a simpler and more convenient empirical equation for computing equivalent viscous damping, which is expressed as:

$$\xi_{eq} = \xi_0 + 0.2\left(1 - 1/\sqrt{\mu}\right) \tag{14}$$

In order to get more accurate estimation of peak displacement of inelastic systems, JPWRI (JPWRI, 1992) proposed the concept of effective design displacement,

which is set to be 70 per cent of the maximum design displacement, to compute the period ratio and equivalent viscous damping ratio. Substituting 0.7μ for μ in Eq. (8) and Eq. (12), the equivalent linear properties can be rewritten as:

$$T_{eq} / T_0 = \sqrt{\frac{0.7\mu}{1+\alpha\left(0.7\mu-1\right)}} \tag{15}$$

$$\xi_{eq} = \xi_0 + \frac{2\left(1-\alpha\right)\left(0.7\mu-1\right)}{0.7\pi\mu\left[1+\alpha\left(0.7\mu-1\right)\right]} \tag{16}$$

Assuming the energy absorbed in a single cycle of the inelastic systems and of the equivalent linear systems is the same, Kowalsky (Kowalsky, 1995) derived an equation for the equivalent viscous damping ratio based on the secant stiffness and Takeda hysteretic model (Takeda et al., 1970). The equivalent viscous damping ratio is given by:

$$\xi_{eq} = \xi_0 + \frac{1}{\pi}\left[1-\mu^n\left(\frac{1-\alpha}{\mu}+\alpha\right)\right] \tag{17}$$

where *n* is stiffness degradation factor, with a suggested value of 0 for steel structures and 0.5 for RC structures. In this study, the value of 0.5 is considered.

Blandon and Priestley (Blandon & Priestley, 2005) found that in general Jacobsen's approach in combination with secant stiffness at maximum displacement overestimates the equivalent viscous damping and proposed modified design equations for equivalent viscous damping used in direct displacement-based design method:

For elasto-plastic hysteretic model:

$$\xi_{eq} = \xi_0 + \frac{0.904}{\pi}\cdot\left(1-\frac{1}{\mu^{0.5}}\right)\cdot\left(1+\frac{1}{\left(T_{eq}+0.85\right)^2}\right) \tag{18}$$

For bilinear hysteretic model:

$$\xi_{eq} = \xi_0 + \frac{1.230}{\pi} \cdot \left(1 - \frac{1}{\mu^{0.5}} - 0.1 \cdot \alpha \cdot \mu\right) \cdot \left(1 + \frac{1}{\left(T_{eq} + 0.85\right)^4}\right) \tag{19}$$

Jara and Casas (Jara & Casas, 2006) proposed a simple empirical expression of equivalent viscous damping ratio to improve the displacement prediction of equivalent linearization methods when applied to bridges supported on LRBs. The provided formulas for computing the equivalent viscous damping ratio is expressed as:

$$\xi_{eq} = \xi_0 + 0.05 ln\mu \tag{20}$$

They concluded that, using the proposed model, the displacement prediction of the equivalent linear elastic analysis could be improved and a lower scattering of results could be obtained over the whole range of the ductility. However, they also suggested that more research is needed to determine the equivalent linearization parameters and the influence of the earthquake characteristics.

Dicleli and Buddaram (Dicleli & Buddaram, 2007) evaluated the equivalent linear elastic analysis for seismic-isolated structures represented by SDOF systems and found that the equation of equivalent viscous damping ratio used in the design of seismic-isolated structures must incorporate the equivalent period of the structure and the frequency characteristics of ground motion in order to acquire a more accurate estimation of seismic response quantities. Modifying the existing equation for estimating the equivalent viscous damping ratio, a new equation was proposed to yield more reasonable estimates of the actual nonlinear responses, which can be expressed as:

$$\xi_{eq} = \xi_0 + \frac{2\left(1-\alpha\right)\left(\mu-1\right)}{\pi\mu\left[1+\alpha\left(\mu-1\right)\right]} \sqrt{0.41\left(\frac{T_{eq}}{T_0} - 1\right)} \tag{21}$$

Jara et al. (Jara et al., 2012) recognized that the dynamic characteristics of earthquake ground motions, ductility capacities, type of hysteretic relationships, and stiffness degradation characteristics of the structure were aspects that strongly affected both the equivalent stiffness and the energy dissipation capacity of the systems; nevertheless, these conditions had not been adequately accounted for in the analyses. Then, they proposed a new expression to evaluate the equivalent viscous

damping ratio derived from the particular characteristics of bridges supported on bi-linear hysteretic bearings, as shown below:

$$\xi_{eq} = \xi_0 + \zeta ln\mu \leq 0.30 \tag{22}$$

where the coefficient ζ = 0.065 for earthquakes recorded on firm soils and ζ = 0.085 for earthquakes recorded on soft soils. In the present research, the average value ζ = 0.075 is considered.

2.3.2 Equivalent Linearization Methods not Based on Secant Stiffness

Under earthquake loading, most of the time the displacement of the systems would be much smaller than the maximum response, thus the equivalent viscous damping ratio computed using the equal energy dissipation principle would lead to an under-estimation of the peak response. Iwan and Gates (Iwan & Gates, 1979) proposed the average stiffness and energy (ASE) damping model, as expressed in Eqs. (23) - (24), to improve the accuracy of equivalent linearization method.

$$T_{eq} / T_0 = \sqrt{\frac{\mu}{1+\alpha(\mu-1)+(1-\alpha)ln\mu}} \tag{23}$$

$$\xi_{eq} = \xi_0 + \frac{6(1-\alpha)(\mu-1)^2 + \pi\xi_0\left[(1-\alpha)(3\mu^2-1)+2\alpha\mu\right]}{2\pi\mu^2\left[1+\alpha(\mu-1)+(1-\alpha)ln\mu\right]} \tag{24}$$

In another work of Iwan (Iwan, 1980), various approximate methods were evaluated and the equivalent viscous damping ratio was found to be overestimated for most of the considered ductility range. Then empirical equations to estimate the period ratio and equivalent damping ratio were derived as follows:

$$T_{eq} / T_0 = 1 + 0.121(\mu-1)^{0.939} \tag{25}$$

$$\xi_{eq} = \xi_0 + 0.0587(\mu-1)^{0.371} \tag{26}$$

The relationship between period ratio and equivalent viscous damping ratio was represented by:

$$\xi_{eq} - \xi_0 = 0.1352\left(\frac{T_{eq}}{T_0} - 1\right)^{0.3952} \tag{27}$$

Hwang and Sheng (Hwang & Sheng, 1993) examined equivalent stiffness and equivalent viscous damping ratio of seismically isolated bridges. To improve the prediction of Iwan (Iwan, 1980) model, the data obtained by Iwan and Gates (Iwan & Gates, 1979) were used to fit an assumed function for the relationship between the equivalent period ratio and ductility ratio. The proposed formula was presumed to be an exponential function rather than a power function of ductility ratio, which is expressed in Eq. (28). However, the formula used for computation of the equivalent damping ratio is kept the same as Eq. (25).

$$T_{eq} / T_0 = 1 + ln\left[1 + 0.13\left(\mu - 1\right)^{1.137}\right] \tag{28}$$

Hwang and Chiou (Hwang & Chiou, 1996) proposed an equivalent linearization model for the analysis of base-isolated bridges with LRBs, which was derived in a modified form from AASHTO guide specifications for seismic isolation through an identification method. A total of 15 ductility ratios up to 50 and a stiffness ratio of 0.15 were assigned in that study. The provided formulas for computing period ratio and equivalent viscous damping ratio are respectively expressed as:

$$T_{eq} / T_0 = \sqrt{\frac{\mu}{1 + \alpha\left(\mu - 1\right)}}\left(1 - 0.737\frac{\mu - 1}{\mu^2}\right) \tag{29}$$

$$\xi_{eq} = \xi_0 + \frac{2\left(1 - \alpha\right)\left(\mu - 1\right)}{\pi\mu\left[1 + \alpha\left(\mu - 1\right)\right]}\frac{\mu^{0.58}}{6 - 10\alpha} \tag{30}$$

Based on ASE model, Ou (Ou et al., 1998) proposed the average stiffness and damping (ASD) model, in which the equivalent period is the same as that in ASE model. However, the equivalent viscous damping ratio was expressed as:

$$\xi_{eq} = \xi_0 + \frac{2\left[1+\alpha\left(\mu-1\right)+\mu\left(1-\alpha\right)ln\mu-\mu\right]}{\pi\mu\left[1+\alpha\left(\mu-1\right)+\left(1-\alpha\right)ln\mu\right]} \tag{31}$$

Kwan and Billington (Kwan & Billington, 2003) proposed the relations between equivalent period T_{eq} and equivalent damping ratio ξ_{eq} for the equivalent linearization approach. Results from the simulations indicated that neither the secant stiffness method nor existing empirical methods were adequate in accounting for the influence of hysteretic behavior on the equivalent linear system parameters. Optimal T_{eq} and ξ_{eq} values from extensive time history analyses of SDOF systems with six types of hysteretic behavior and a period range of 0.1 s to 1.5 s were used to derive the new relations, which are presented as follows:

$$T_{eq} / T_0 = 0.8\mu^{C_1} \tag{32}$$

$$\xi_{eq} = \frac{2C_2}{\pi}\left(\frac{T_{eq}}{T_0}\right)^2\frac{\mu-1}{\mu^2} + 0.55\left(\frac{T_{eq}}{T_0}\right)^2\xi_0 \tag{33}$$

For elastoplastic, moderately and slightly degrading hysteretic systems, values of C_1 and C_2 are set to be 0.5 and 0.56 respectively according to their research.

In order to have the measure of goodness of the optimal equivalent linear parameters according to some sense of engineering acceptability, Guyader and Iwan (Guyader & Iwan, 2004) introduced an improved capacity spectrum method solution procedure that had been adopted as one of the three solution procedures to be presented in FEMA-440 (FEMA, 2005). In that study, the optimal pair of T_{eq} and ξ_{eq} was taken as the values that maximize the probability that the percentage error between the actual nonlinear systems and their equivalent linear counterparts was within the range -10% to +20%. Several hysteretic systems including bilinear, stiffness degrading, strength degrading and pinching models were considered. The proposed empirical equations were shown in Eq. (34).

For μ < 4.0:

$$T_{eq} / T_0 = 1 + 0.1262\left(\mu-1\right)^2 - 0.0224\left(\mu-1\right)^3 \tag{34a}$$

$$\xi_{eq} = \xi_0 + 0.05073(\mu - 1)^2 - 0.01083(\mu - 1)^3 \quad (34b)$$

For $4.0 \le \mu \le 6.5$:

$$T_{eq} / T_0 = 1.1713 + 0.1194(\mu - 1) \quad (34c)$$

$$\xi_{eq} = \xi_0 + 0.1169 + 0.01579(\mu - 1) \quad (34d)$$

For $\mu > 6.5$:

$$T_{eq} / T_0 = 1 + 0.87\left(\sqrt{\frac{\mu - 1}{1 + 0.10[(\mu - 1) - 1]}} - 1\right) \quad (34e)$$

$$\xi_{eq} = \xi_0 + 0.24383\frac{0.36(\mu - 1) - 1}{\left[0.36(\mu - 1)\right]^2}\left(\frac{T_{eq}}{T_0}\right)^2 \quad (34f)$$

2.3.3 Comparison Between Different Equivalent Linearization Methods

When equivalent linearization analysis method is performed, it is obviously noted that the proper estimation of equivalent linear properties is crucial for the results. Structural engineers never stop seeking more accurate linear elastic methods to approximate peak response of nonlinear systems. Meanwhile, there are multiple references to evaluate the accuracy of different equivalent linearization methods.

Iwan and Gates (Iwan & Gates, 1979) assessed the potential of various linearization techniques to estimate the peak response of certain SDOF hysteretic oscillators exposed to strong ground motion. Inelastic response spectra were constructed for a range of response ductility. An effective linear period and damping were calculated for each system and ductility by determining those parameters which minimized an RMS response spectrum error. Conclusions were presented concerning the effects of deterioration, stiffness degradation, cracking and ductility on the effective linear system parameters.

Hwang (Hwang, 1996) compared and evaluated various equivalent linear analysis methods for base-isolated regular bridges, including the equivalent linear analysis models specified by the American Association of State Highway and Transportation Officials (AASHTO) and the Japanese Public Works Research Institute (JPWRI). In addition, the model used by the California Department of Transportation (CALTRANS) and the model proposed by Huang and Chiou (Hwang & Chiou, 1996) were also included. It was concluded that the total shear force transmitted by bilinear hysteretic bearings was better determined using the CALTRANS model and the model proposed by Huang and Chiou in which the force was calculated based on the hysteretic characteristics of the bearings when the maximum or design displacement had been obtained. Based on the evaluation of prediction accuracy, it was found that, for the purpose of practical analysis, the equivalent linear time history analysis with the iteration procedure can predict the maximum inelastic response more accurately than the response spectrum analysis.

Franchin et al. (Franchin et al., 2001) discussed three aspects related to the method of analysis for linear or linearized isolated bridge, namely (i) classical modal analysis, using real modes and the diagonal terms of the modal damping matrices, still provide a fully acceptable approximation, (ii) parametric study conducted shown that none of the linearized expressions in current use gives satisfactory results for both the displacement and the force responses, a requirement for a reliable design of an isolated bridge and (iii) a rational, approximate procedure for equivalent damping applicable to all types of structures with non-proportional damping, which in the case of bridges can be shown to reduce to the expression provided in the Japanese bridge design guidelines.

Miranda and Ruiz-García (Miranda & Ruiz-García, 2002) carried out an investigation comparing the capabilities of different performance based methodologies (including methodologies based on equivalent linearization) in estimating the inelastic displacement for Takeda, modified Clough, stiffness degrading and elastoplastic system using 264 ground motion records. The findings suggested that R&H method for estimating the equivalent viscous damping factor was not conservative for structures with high hysteretic energy absorption. However, due to smaller equivalent damping ratios from the Goulkan and Sozen, Iwan's and Kowalsky's methods, better results were produced when compared with R&H method.

Matsagar and Jangid (Matsagar & Jangid, 2004) analyzed the influence of isolator characteristics on the seismic response of base-isolated structures modeled as MDOF systems. It was observed that the code-recommended equivalent linear

elastic-viscous damping model (i.e., R&H method) of a bi-linear hysteretic system overestimated the design bearing displacement and underestimated the superstructure acceleration. In addition, the authors concluded that the response of base-isolated structures was significantly influenced by the shape of hysteresis loop of isolator.

Dicleli and Buddaram (Dicleli & Buddaram, 2007) evaluated the equivalent linear elastic analysis for SDOF systems, concluding that the linearized model underpredicted the design displacement using the existing effective viscous damping ratio. It was found that the accuracy of the equivalent linear analysis results was affected by the peak ground acceleration to peak ground velocity ratio of the ground motion as well as the intensity of the ground motion relative to the characteristic strength of the isolator.

Lin and Miranda (Lin & Miranda, 2009) presented a statistical study that evaluated the accuracy of four equivalent linear methods which allowed the maximum deformation demands of nonlinear structures to be estimated from the maximum deformation demands of the equivalent linear ones. Three of them are defined by displacement ductility ratios, and the other is defined by lateral strength ratios. They concluded that if the linear response-history analyses were adopted to obtain the highly damped displacement responses, all three equivalent linearization methods predicted the mean approximate maximum inelastic displacements well for systems with periods of vibration greater than about 0.75 s. However, they simply overestimated those with an exponential tendency for systems with periods of vibration less than 0.75 s. However, the Lin and Miranda method (defined by lateral strength ratios) leaded to good estimations of the mean approximate maximum inelastic displacements whatever the strength ratio and the period of vibration are.

Mavronicola and Komodromos (Mavronicola & Komodromos, 2011) investigated the appropriateness of various literature-proposed relationships for the linearization of stiffness and the conversion of hysteretic to equivalent viscous damping of LRBs, concluding that usage of the proposed relationships resulted in overestimation of the maximum relative displacements at the isolation level and leaded to large response discrepancies in comparison with those computed by the more accurate bi-linear model. Therefore, considering that the linear elastic analysis was, in general, conservative, regarding the estimation of the maximum relative displacements at the isolation level, linear elastic analysis may be used, under certain limitations, only in the preliminary design of a seismically isolated building. Finally, the authors

strongly recommended that for the final analysis of a seismically isolated building, the more accurate bilinear inelastic analysis should be used.

As is known to all, the estimation accuracy of equivalent linearization analysis method is strongly related to various parameters, such as the hysteretic model, inherent viscous damping ratio and inputted seismic excitations. Even for a given hysteretic model (for example, the bilinear hysteretic model), the determination of equivalent linear properties is heavily dependent on the strain hardening ratio, the initial period and the ductility ratio. Although many research works have been contributed to evaluate the accuracy of different equivalent linearization methods proposed in literatures, their scopes are very limited. For instance, in the study done by Miranda and Ruiz-García, the maximum considered ductility ratio is 6. However, for base-isolated buildings, the ductility ratio of isolation systems could be much larger. Though very difficult to account for all parameters, much more works need to be done to get better insights into the application of equivalent linearization analysis method for seismically-isolated buildings.

2.4. Modeling of Viscous Damping in Base-isolated Buildings

All structures exhibit some degree of energy dissipation during free vibration or seismic loading to reduce the level of response. Generally, there are three sources of energy loss, i.e., hysteretic damping, radiation damping and inherent damping in the structure (Wilson, 2000). For low amplitude response, the determined damping values will contain only contributions from radiation damping and inherent damping in the structure. For higher levels of response, hysteretic damping will be added, which will act together with the previously defined radiation and structural damping mechanisms to absorb the input energy. In general, radiation damping exists at the supports of the structure. The vibration of structure strains the foundation material near the supports and causes stress waves to radiate into the infinite foundation. This can be significant if the foundation material is soft relative to the structural stiffness. In the present study, for simplicity, the radiation damping component is omitted. Thus, for linear systems, the energy dissipation will be done only with the inherent damping in the structure while in nonlinear systems hysteretic damping and inherent damping will work together after the structure yields.

In the numerical model of structures, irrespective of linear or nonlinear, mass and stiffness matrices can be straightforwardly assembled because they are based on easily identified and quantified physical properties. However, because there is no

physical counterpart for the structural damping, it is impractical to determine the damping matrix directly from the properties of materials and structural members.

Hysteretic damping can be automatically considered in response history analysis through explicit modeling of force-deformation relationship of construction materials of structural elements, which is considered to be the most appropriate mathematical model for representing the structural damping (Clough & Penzien, 2003). It is worth noting that hysteretic damping can be only used in nonlinear dynamic analysis. If the whole structure or most of it remains linear elastic, using hysteretic damping to simulate the structural damping will not be a wise option.

The inherent damping in structures accounts for all other energy dissipation mechanisms except hysteretic damping. In most applications, analysts usually linearize the inherent damping by assuming that it is linear viscous, namely the damping force is directly proportional to the velocity. It can be found that linear viscous damping is frequency dependent, but is not displacement dependent, which differs from hysteretic damping. As an approximation of hysteretic damping, viscous damping, which takes the form of a damping matrix of constant coefficients multiplying a vector of velocities of the degrees of freedom, is mathematically convenient.

To diagonalize the damping matrix and apply the modal superposition approach, classical damping matrix is normally required so that the multiple-degree-of-freedom (MDOF) system can be transformed into a set of single-degree-of-freedom (SDOF) systems. The general form of a classical damping matrix for a MDOF system was proposed by Caughey (Caughey, 1960), which can be expressed as:

$$C = M\sum_{i=0}^{N\text{-}1} a_i \left[M^{-1}K \right]^i \tag{35}$$

where N is the number of DOFs in the system and a_i are constants, which can be arbitrarily chosen, depending on the modal damping characteristics desired.

Considering the general form of a classical damping matrix for a MDOF system, as shown in Eq. (35), the first two terms are found to be a_0M and a_1K. Hence, three classical damping matrices can be formulated:

$$\begin{aligned} C_{M-p} &= a_0 M && \textit{Mass-proportional damping} \\ C_{S-p} &= a_1 K && \textit{Stiffness-proportional damping} \\ C_{Rayleigh} &= a_0 M + a_1 K && \textit{Rayleigh damping} \end{aligned} \tag{36}$$

After spectral decomposition of the equations of motion for a linear MDOF system, it is straightforward to derive:

$$M^{(l)} = \left[\phi^{(l)}\right]^{\mathrm{T}} M \phi^{(l)} \tag{37}$$

$$K^{(l)} = \left[\phi^{(l)}\right]^{\mathrm{T}} K \phi^{(l)} \tag{38}$$

$$\omega^{(l)} = \sqrt{K^{(l)} / M^{(l)}} \tag{39}$$

where $M^{(l)}$ and $K^{(l)}$ are the l^{th} normal-coordinate generated mass and stiffness, respectively. $\omega^{(l)}$ and $\phi^{(l)}$ are used to denote the l^{th} modal frequency and its corresponding modal shape. Similarly, the normal-coordinate generated critical damping can be derived as:

$$C_{cr}^{(l)} = 2M^{(l)}\omega^{(l)} \tag{40}$$

Thus, the l^{th} modal damping ratio $\xi^{(l)}$ can be determined using the following equation:

$$\xi^{(l)} = \frac{C^{(l)}}{C_{cr}^{(l)}} = \frac{M^{(l)} \sum_{k=0}^{N\text{-}1} a_k \left[K^{(l)} / M^{(l)}\right]^k}{2M^{(l)}\omega^{(l)}} = \frac{1}{2\omega^{(l)}} \sum_{k=0}^{N\text{-}1} a_k \left[\omega^{(l)}\right]^{2k} = \frac{1}{2} \sum_{k=0}^{N\text{-}1} a_k \left[\omega^{(l)}\right]^{2k-1} \tag{41}$$

This equation reveals that $\xi^{(l)}$ is a function of the modal frequency $\omega^{(l)}$. Based on Eq. (41), the l^{th} modal damping ratios corresponding to Mass-proportional, Stiffness-proportional and Rayleigh damping models are computed to be:

$$\xi_{M-p}^{(l)} = \frac{a_0}{2}\frac{1}{\omega^{(l)}}$$
$$\xi_{S-p}^{(l)} = \frac{a_1}{2}\omega^{(l)} \tag{42}$$
$$\xi_{Rayleigh}^{(l)} = \frac{a_0}{2}\frac{1}{\omega^{(l)}} + \frac{a_1}{2}\omega^{(l)}$$

It is evident that the desired damping ratios can be specified for any number of natural modes by assigning an equal number of terms to the series in Eq. (42). This will result in a system of simultaneous equations and the solutions of which yield the appropriate damping coefficients.

For instance, let denote ξ_0 to be the desired damping ratio specified for different natural modes. For Mass- and Stiffness-proportional damping models, the coefficients a_0 and a_1 can be computed respectively by assuming the damping ratio ξ_0 for any one mode:

$$\begin{aligned} a_0 &= 2\xi_0\omega_i \\ a_1 &= 2\xi_0 / \omega_i \end{aligned} \tag{43}$$

where ω_i is the frequency of the selected mode *i*.

Considering Rayleigh damping, the coefficients a_0 and a_1 can be simultaneously determined by assuming the same damping ratio ξ for two selected modes,

$$\begin{cases} \xi_0 = \dfrac{a_0}{2}\dfrac{1}{\omega_i} + \dfrac{a_1}{2}\omega_i \\ \xi_0 = \dfrac{a_0}{2}\dfrac{1}{\omega_j} + \dfrac{a_1}{2}\omega_j \end{cases} \Rightarrow \begin{cases} a_0 = 2\xi_0\dfrac{\omega_i\omega_j}{\omega_i + \omega_j} \\ a_1 = 2\xi_0\dfrac{1}{\omega_i + \omega_j} \end{cases} \tag{44}$$

where ω_i and ω_j are the frequencies of modes *i* and *j*, respectively. The two modes *i* and *j* are chosen to ensure nearly the same amount of damping for all the modes significantly contributing to the response of the structure. Typically, ω_i is selected to be the frequency of the first mode, and ω_j corresponds to a higher mode.

After determining these coefficients, the damping matrix is known from Eq. (36) and the damping ratio in any other mode is given by Eq. (42), as shown in Fig. 15. To

simplify the subsequent assessments for different damping models, the frequency ω_i included in Eqs. (43-44) is assumed to be the frequency of the first (or fundamental) mode of the considered structure while ω_j in Eq. (44) is selected as the frequency of the second mode.

Although there is no requirement that the damping matrix used in response history analysis of structures must be classical, classical damping is generally used in many commercial finite element programs. Apparently, the choice of a damping model (i.e., Mass-proportional damping, Stiffness-proportional damping, Rayleigh damping or Caughey damping) as well as the selection of frequencies to compute damping coefficients could lead to many different approaches of modeling viscous damping. Furthermore, in nonlinear dynamic analysis of structures, the selection of stiffness matrix (i.e., initial stiffness or tangent stiffness) to compute the frequencies of structure and to develop the damping matrix also produces substantially different results. Modeling of viscous damping constitutes a major source of uncertainty in dynamic analysis and an open issue to experimental and analytical research.

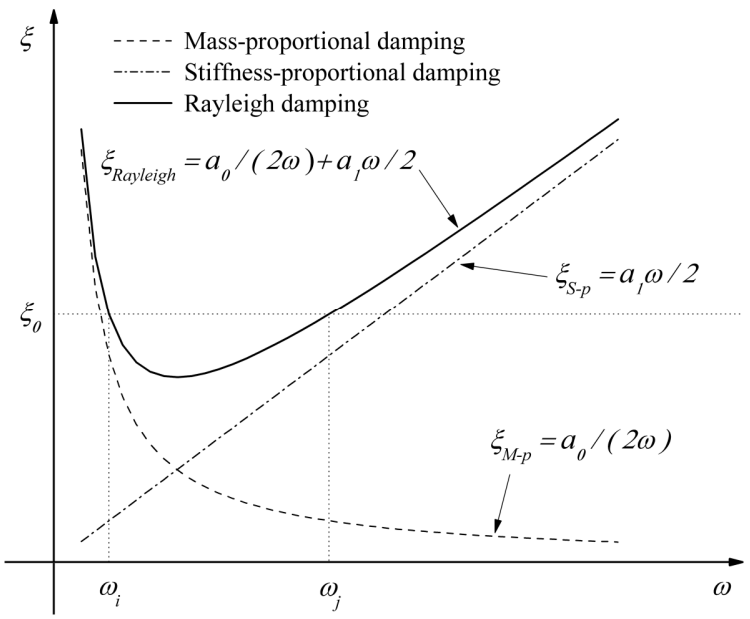

Fig. 15 Relationship between damping ratio and frequency for different damping models

The issue of modeling viscous damping had been explored extensively for nonlinear dynamic analysis of fixed-base structures. Léger and Dussault (Léger & Dussault, 1992) investigated the effects of various mathematical models to represent viscous damping in nonlinear seismic analysis of MDOF structures. Various structural performance indices were selected to characterize the nonlinear seismic response.

Results shown that a tangent Rayleigh damping model using proportionality coefficients that are updated at each time step provided a rational control of the damping in nonlinear seismic analyses. Charney (Charney, 2008) underlined the appearance of artificial damping due to the mass participation and evaluated the effect of initial and inelastic stiffness on the viscous damping forces through inelastic analysis of a simple five-story structure. The author also provided some recommendations for performing analysis where the artificial damping was eliminated, or at least controlled. Erduran (Erduran, 2012) evaluated the effects of Rayleigh damping model on the engineering demand parameters of two steel moment-resisting frame buildings. Again, it was demonstrated that mass-proportional damping leaded to high damping forces compared with restoring forces and might lead to overestimation of floor acceleration demands. As a remedy, Rayleigh damping models anchored at reduced modal frequencies was recommended by the author to produce reasonable damping forces and floor acceleration demands.

Not only in nonlinear dynamic analysis but also in linear dynamic analysis, the implement of linear viscous damping has significant influence on the structural response. Chopra (Chopra, 2007) agreed that Rayleigh damping cannot be applied unless similar damping mechanisms are distributed throughout the structure. However, when the system consists of two or more subsystems with disparate energy dissipation properties, the resultant damping of the combined system is non-classical and the classical Rayleigh damping will not be applicable any more. Base-isolated structure is just the case needs to be treated with caution, which is composed of two subsystems: the superstructure and the isolation system. The superstructure has typical modal damping ratios of 5% or less, whereas the equivalent damping ratio of the isolation system considering the complete structural mass generally exceeds 10%. If the classical damping is still used to model the actual damping, problems may occur. Hall (Hall, 2006) demonstrated problems encountered from the use (or misuse) of Rayleigh damping through a series of examples, one of which was base-isolated structure. The author found that, if the Mass-proportional damping term is applied, unrealistic high viscous damping will be obtained, which significantly suppresses the structural response. Thus, only Stiffness-proportional damping model was recommended with the secant stiffness of seismic isolator. Ryan and Polanco (Ryan & Polanco, 2008) also concluded that Rayleigh damping model resulted in undesirable suppression of the first mode response of base-isolated structure and they recommended the application of Stiffness-proportional damping instead of Rayleigh damping to the superstructure of base-isolated structures. Pant et al. (Pant et al., 2013) investigated the effects of modeling viscous damping on the response of base-isolated reinforced concrete struc-

tures subjected to earthquake ground motions. Many different approaches of modeling viscous damping, developed within the framework of Rayleigh damping, were evaluated through the comparison of results between shaking table test and finite element simulation of a reduced-scale three-storey building. Results shown that Stiffness-proportional damping, where the coefficient multiplying the stiffness matrix is calculated from the frequency of the base-isolated structure with the post-elastic stiffness of the isolation system could provide reasonable estimates of the peak response indicators. Furthermore, nonlinear modal time-history analysis was also considered in their study. It was found that for nonlinear modal time-history analysis, frequency-dependent damping is more appropriate than constant damping.

Although these studies provided insight to the effects of different damping model on the simulated seismic behavior of base-isolated structures, the majority of structural analysis programs still use the conventional way of modeling viscous damping and may not be aware of these potential problems because damping forces are seldom included in the output results. Hence, the effect of various approaches of modeling viscous damping is important to the practical analysis and design of base-isolated structures.

2.5. Lateral Force Distributions in Base-isolated Buildings

To simplify the design procedure, equivalent static analysis or equivalent linear analysis, is generally recommended in structural codes (ICBO, 1997; NEHRP, 1997; CEN, 2004; ASCE, 2005; D.M., 2008). Based on the practical observation, the response of a base-isolated building is dominated by its first mode of vibration, in which the horizontal displacements are concentrated at the isolation level, while the superstructure moves almost like a rigid body. Thus, an equivalent elastic SDOF system can be utilized to simulate the base-isolated building. It can be found that the equivalent linearization method, which is used to estimate the maximum displacement of isolator bearings, does not provided the lateral force distributions over the height of the superstructure. Consequently, several equations to predict the distribution of lateral force in base-isolated buildings are proposed by many researchers.

Adopted by the European Seismic Code (CEN, 2004) and the new Italian Seismic code (D.M., 2008), the uniform acceleration profile over the height of the building is assumed and the equivalent static seismic forces (F_i) are computed by distributing

the design base shear (V_b) over the height of the structure, proportionally to the storey masses (m_i), namely:

$$F_i = V_b \frac{m_i}{\sum m_i} \tag{45}$$

This lateral load pattern is provided for regular low-rise buildings equipped with isolation systems that can be modelled with equivalent linear viscous-elastic behavior (CEN, 2004). In addition, there are several limited conditions on the applicability of equivalent linear analysis. For instance, base-isolated buildings are limited to five storeys.

To account for the higher mode contributions generated by possibly nonlinear behavior of the isolation systems, an inverted triangular distribution of storey accelerations over the height of the structure is assumed. This method has been adopted by many seismic codes (ICBO, 1997; NEHRP, 1997; ASCE, 2005; ICC, 2000; GB50011, 2001), in which the equivalent static seismic force are computed by distributing the design base shear (V_b) over the height of the structure, proportionally to the product of storey masses (m_i) and storey height (h_i):

$$F_i = V_b \frac{m_i \cdot h_i}{\sum m_j \cdot h_j} \tag{46}$$

In the US seismic code, the applicability of equivalent linear analysis is limited to base-isolated buildings that not exceed four storeys.

The current Protective Systems Committee (PSC) (SEAONC, 1986) has also considered options to revise the static force distribution. One option was to add a concentrated force F_b at the base level proportional to the base mass, while retaining the inverted triangle lateral force distribution to the superstructure. This distribution is given by the following equations:

$$F_b = \frac{V_b}{W} W_1 \tag{47}$$

$$F_i = \frac{(V_b - F_b)}{R_I} \cdot \frac{W_i \cdot h_i}{\sum_n W_n \cdot h_n} \tag{48}$$

In Japan, the shear force coefficient on the superstructure in the recommendation for design of base-isolated buildings (AIJ, 2001) is as follows:

$$\alpha_i = \alpha_f + a_i \cdot \overline{\alpha}_i \cdot \alpha_s \tag{49}$$

where α_i, α_f, α_s are the shear force coefficient of *i*-th story of base-isolated buildings, elastomeric isolator and elasto-plastic dampers, respectively. $\overline{\alpha}_i$ is the optimum yield shear force coefficient distribution considered the natural periods and weight distribution. a_i is given by Eq. (50). Where *N* is the number of structure story, $\overline{a}$ is given by Eq. (51).

$$a_i = \left\{ \left(\overline{a} - 1 \right) / \left(N - 1 \right) \right\} i + \left(N - \overline{a} \right) / \left(N - 1 \right) \tag{50}$$

$$\begin{cases} \overline{a} = 3.1238 - 0.1238 \cdot b_s & 1 \le b_s < 10 \\ \overline{a} = 2.0127 - 0.0127 \cdot b_s & 10 \le b_s < 80 \\ \overline{a} = 1.0 & 80 \le b_s \end{cases} \tag{51}$$

where b_s is the ratio of horizontal stiffness of the first story of superstructure in base fixed condition to that of dampers in isolated condition ($b_s = k/k_s$).

However, it has been pointed out that the above-mentioned method likely underestimates the seismic response (Takayama et al., 2002). The following cases are more possible: 1) superstructure doesn't behave as rigid-body and 2) seismic isolator has high-stiffness, i.e., the higher-mode responses will be generated. In other words, seismic forces and floor accelerations of the superstructure are amplified more than ideal isolation system. This phenomenon counteracts the purpose of isolation system. Thus, Kobayashi and Matsuda (Kobayashi & Matsuda, 2012) proposed a response amplification factor β_i considering higher-mode responses to evaluate the seismic response properly.

$$\alpha_i = \alpha_f + \beta_i \cdot A_i \cdot \alpha_s \tag{52}$$

$$\beta_i = \frac{\alpha_i - \alpha_f}{A_i \cdot \alpha_s} \tag{53}$$

$$\beta_i = \left\{\left(\overline{\beta} - 1\right)/\left(N - 1\right)\right\} i + \left(N - \overline{\beta}\right)/\left(N - 1\right) \tag{54}$$

$$\begin{aligned} &\overline{\beta} = \frac{s}{I^2} + t \quad \left(\overline{\beta} \le u\right) \\ &I = T_{b1} / T_0 \\ &s = 0.26 h_{eq} + 0.29 \left(\text{upper limit} = 5.0\right) \\ &t = 0.60 \\ &u = 0.09 h_{eq} + 1.28 \left(\text{upper limit} = 3.0\right) \end{aligned} \tag{55}$$

Lee et al. (Lee et al., 2001) investigated the UBC-91 (ICBO, 1991) and UBC-97 (ICBO, 1997) static lateral load procedures for isolated structures and found the inverted triangular force distribution overestimated the maximum seismic responses of most base-isolated buildings, even when the isolation system exhibits a strong nonlinear behavior or large effective damping values. Therefore, they proposed a new formula for the vertical distribution of seismic load. Similarly, Tsai et al. (Tsai et al., 2003) also proposed modified equations for the vertical distribution of equivalent static seismic loads, considering the influence of the first mode of vibration on the base-isolated structures. The proposed equations can be expressed as follows:

$$F_i = V_b \frac{m_i \cdot \left(1 + \dfrac{\varepsilon}{H_e} \cdot h_i\right)}{\sum m_j \cdot \left(1 + \dfrac{\varepsilon}{H_e} \cdot h_j\right)} \tag{56}$$

where $\varepsilon = \omega_b^2 / \omega_s^2$, ω_s being the circular frequency of the fix-base structure and ω_b that of the base-isolated structure with the superstructure assumed to behave like a rigid body. H_e represents the effective height of the equivalent SDOF system of the base-isolated structure, considering the flexibility of the superstructure. In the equation proposed by Lee et al., $H_e = 0.6H$ for framed and $H_e = 0.7H$ for shear wall structures, respectively whilst Tsai et al. assume $H_e = H$, where H is the total height of the superstructure.

In essence, the force distribution given by Eq. (56) corresponds to a trapezoidal distribution of storey acceleration over the height of the structure, which tends to a uniform distribution when ε << 1 (i.e. when the superstructure becomes much stiffer than the isolation system).

Many research works (Kelly, 2001; Skinner et al., 1993; Constantinou et al., 1993; Winters & Constantinou, 1993) had concluded that the envelope profiles of the storey shear-forces can significantly differ from those derived from Eqs. (45-46), even when the base-isolated structure complies with the requirements for the applicability of equivalent linear analysis. Moreover, they found that the envelope profiles of the storey shear-forces can vary considerably from one case to another, mainly due to the following three factors: (i) the degree of non-linearity of the isolation system and more precisely the "fatness" of its force-displacement cyclic behavior, (ii) the number of storeys of the building and (iii) the fundamental period of vibration of the superstructure in the fixed-base configuration.

To quantify the degree of non-linearity of the isolation system, Skinner et al. (Skinner et al., 1993) introduced the non-linearity factor *NL*, defined as the ratio of the area of the hysteresis loops (W_d) at the design displacement (D_d) of isolation system to that of the corresponding rectangle:

$$NL = \frac{W_d}{4 \cdot D_d \cdot F_d} \tag{57}$$

where F_d being the restoring force at the design displacement D_d. The studies by Skinner et al. confirmed the importance of the *NL* factor with respect to the shear-force distribution in base-isolated buildings. Furthermore, it can be found that the non-linearity factor *NL* is proportional to the equivalent viscous damping ratio ξ (see Eq. (11)).

$$\xi_{is} = \frac{1}{4\pi} \cdot \frac{W_d}{W_s} = \frac{W_d}{2\pi \cdot F_d \cdot D_d} \tag{58}$$

Efforts have been made to derive enhanced equivalent static force distributions, able to predict accurately the maximum seismic response of a base-isolated building, even for medium-rise buildings with strongly nonlinear isolation systems. Based on the results of extensive nonlinear time history analysis on multi-storey framed buildings equipped with isolation systems with an idealized bilinear hysteretic force-

displacement behavior, Andriono and Carr (Andriono & Carr, 1991a; Andriono & Carr, 1991b) proposed the following equivalent static force distribution:

$$F_i = V_b \frac{m_i \cdot h_i^p}{\sum m_j \cdot h_j^p} \tag{59}$$

It is similar to Eq. (46), except for the exponent "*p*". The authors found that *p* is strongly correlated to the non-linearity factor *NL* and the fundamental period of vibration of the fixed-base structure (T_{fb}) (Andriono & Carr, 1991b), but they did not provide any analytical or graphical relationship to derive *p* as a function of these two parameters.

Similar results have been found by York and Ryan (Ryan & York, 2007; York & Ryan, 2008), who proposed the following formulas:

$$F_i = \frac{V_s}{R} \frac{m_i \cdot h_i^k}{\sum_n m_n \cdot h_n^k} \tag{60}$$

$$\frac{V_s}{V_b} = \left(\frac{M_s}{M} \right)^{(1-2.2\xi)} \tag{61}$$

$$k = 13 \cdot \xi \cdot T_{fb} \tag{62}$$

where V_s is the superstructure base shear (derived from the global base shear V_b based on the ratio of the superstructure mass to the total mass of the building). The exponent "*k*" is expressed, through regression analyses, as a function of the equivalent viscous damping ratio ξ and of the fundamental period of vibration of the superstructure in the fixed-base configuration (T_{fb}).

In the research study of Khoshnoudian and Mehrparvar (Khoshnoudian & Mehrparvar, 2008), a new formulation for vertical distribution of base shear was proposed, as shown below:

$$F_x = a \frac{w_x}{\sum_n w_i} V_s + (1\text{-}a) \frac{w_x \cdot h_x}{\sum_n w_i \cdot h_i} V_s \tag{63}$$

This method was based on the combination of the two previously presented formulas (i.e., uniform and triangular) by means of a scaling factor *a*. The simplicity of the proposed method makes it a possible substitution for vertical distribution formula in the future codes. However, this formula is limited by the number of superstructure storeys, i.e., not exceeding six storeys.

In a recent work done by Cardone et al. (Cardone et al., 2009), the authors presented a new approach for the evaluation of accurate lateral force distributions for the linear static analysis of base-Isolated buildings, as shown in the following:

$$F_i = V_b \frac{m_i \cdot \Delta_i}{\sum m_j \cdot \Delta_j} \tag{64}$$

The design base shear is distributed along the height of structures in proportion to storey masses m_i and corresponding displacements Δ_i:

$$\phi_{1i} = \cos\left[\left(\frac{T_{is}}{T_{fb}}\right)^{-1} \cdot \left(1 - \frac{i}{N}\right) \cdot \frac{\pi}{2}\right] \tag{65}$$

$$\phi_{ji} = \cos\left[\left(2N - 2\right) \cdot \frac{\pi}{2} \cdot \frac{i}{N}\right] \qquad \text{for} \quad j \geq 2 \tag{66}$$

The new “displacement” profiles are obtained as linear combinations of the approximate first three modal shapes.

$$\Delta_i^* = \phi_{1i} + a_2 \cdot \phi_{2i} + a_3 \cdot \phi_{3i} \tag{67}$$

where ϕ_{1i}, ϕ_{2i} and ϕ_{3i} are the approximate shapes of the first, second and third mode of vibration, respectively. Based on the parameters from Table 1, a_2 and a_3 for bilinear hysteretic model can be defined as:

$$\begin{cases} a_2 = m \cdot NL^p \cdot \left(\dfrac{T_{is}}{T_{fb}}\right)^{(r-q)} \\ a_3 = 0.7 \cdot a_2 \end{cases} \tag{68}$$

Storeys	m	p	q	r
3	$0.3\text{-}0.1T_1/T_{fb}$ (valid for T_1/T_{fb} <3)	2.5	0.5	2.0
5	$0.7\text{-}0.3T_1/T_{fb}$ (valid for T_1/T_{fb} <2.3)	2.5	0.5	2.0
8	$1.0\text{-}0.5T_1/T_{fb}$ (valid for T_1/T_{fb} <2)	2.5	0.5	2.0

Table 1

Parameters governing the analytical expression of a_2 for buildings with LRB/HDRB isolation systems

In essence, the proposed lateral force distributions depend on a factor measuring the degree of nonlinearity of the isolation system and on the ratio between the effective period of the base-isolated structure (T_{is}) and the fundamental period of the fixed-based structure (T_{fb}), which is fully compatible with the Direct Displacement-Based Design (DDBD) method.

CHAPTER 3

3. EVALUATION OF EQUIVALENT LINEARIZATION METHODS

In this Chapter, fifteen equivalent linearization methods selected from the literatures are assessed based on single-degree-of-freedom (SDOF) systems with bilinear hysteretic behavior. A large number of numerical simulations are performed using a program developed by MATLAB in combination with OpenSees. The influence of ductility ratio and initial period on the accuracy of various methods to estimate the maximum inelastic displacement of bilinear SDOF systems is investigated when subjected to twelve earthquake ground motions. Eventually, comments on the accuracy of different equivalent linearization methods are given to make their applications more appropriate in practical design of base isolation systems.

3.1. Equivalent Linearization Methods Considered

As described in Chapter 2.3, a total of fifteen equivalent linearization methods are considered in this Chapter. The important characteristics of them are summarized in Table 2. It can be noted that several of the considered models have not been calibrated against a bilinear oscillator, such as equivalent linearization methods G&S and Kow. But, for the methods K&B and G&I, more than one hysteresis type is considered. Consequently, it is to be expected that the equivalent linearization methods that best simulate the bilinear one, i.e., the reference type, may well not the best ones to emulate the response of other hysteresis types. However, only the bilinear hysteresis type is focused and discussion of other hysteresis types is out of the scope of this study.

Equivalent linearization methods	Hysteretic type	Strain hardening ratio α	Ductility ratio μ
R&H (Rosenblueth & Herrera, 1964)	Bilinear	$0.0 \le \alpha \le 1.0$	$1 < \mu$
G&S (Gulkan & Sozen, 1974)	Takeda without hardening	$\alpha = 0.0$	$1 < \mu$
JPWRI (JPWRI, 1992)	Bilinear	$0.0 \le \alpha \le 1.0$	$1 < \mu$
Kow (Kowalsky, 1995)	Takeda with post-yield hardening	$\alpha = 0.05$	$1 < \mu$
B&P (Blandon & Priestley, 2005)	Elastic-perfectly plastic, Bilinear	$0.0 \le \alpha \le 0.2$	$2 \le \mu \le 6$
J&C (Jara & Casas, 2006)	Bilinear	$0.05 \le \alpha \le 0.15$	$1 \le \mu \le 40$
D&B (Dicleli & Buddaram, 2007)	Bilinear	$0.01 \le \alpha \le 0.2$	$2 \le A_p W/Q_y \le 10$*
J&O (Jara et al., 2012)	Bilinear	$0.05 \le \alpha \le 0.15$	$1 < \mu \le 30$
ASE (Iwan & Gates, 1979)	Bilinear	$0.0 \le \alpha \le 1.0$	$1 < \mu$
Iwan (Iwan, 1980)	Elastic-perfectly plastic	$\alpha = 0.0$	$1 < \mu \le 8$
H&S (Hwang & Sheng, 1993)	Bilinear	$\alpha = 0.05$	$1 < \mu \le 8$
H&C (Hwang & Chiou, 1996)	Bilinear	$\alpha = 0.15$	$2 \le \mu \le 50$
ASD (Ou et al., 1998)	Bilinear	$0.0 \le \alpha \le 1.0$	$1 < \mu$
K&B (Kwan & Billington, 2003)	Elastic-perfectly plastic, Slightly degrading, Moderately degrading, Slip, Origin-oriented, Bilinear elastic	-	$2 \le \mu \le 8$
G&I (Guyader & Iwan, 2004)	Bilinear, Stiffness degrading, Strength and stiffness degrading, Pinching	-	$1.25 \le \mu \le 10$

Note: A_p is the peak ground acceleration, W is the weight acting on isolator and Q_y is the characteristic strength.

Table 2

Summary of the equivalent linearization methods considered in this study.

Regarding the considered bilinear hysteresis model, the strain hardening ratio is set equal to 0.1 and the yield strength is assigned to be 5% of the total weight of the systems. To differentiate the concept of viscous damping and hysteretic damping, the inherent damping ratio of the bilinear SDOF systems is assigned to be zero, namely $\xi_0 = 0$. Herein lies the assumption that the seismic input energy in nonlinear systems is dissipated only through hysteretic behavior. According to the above assumptions, a comparison of equivalent viscous damping ratio of various equivalent linearization methods, as functions of the ductility ratio, is shown in Fig. 16. The first eight legends with thick solid lines denote the first group of equivalent linearization models while the last seven dashed curves present the second group.

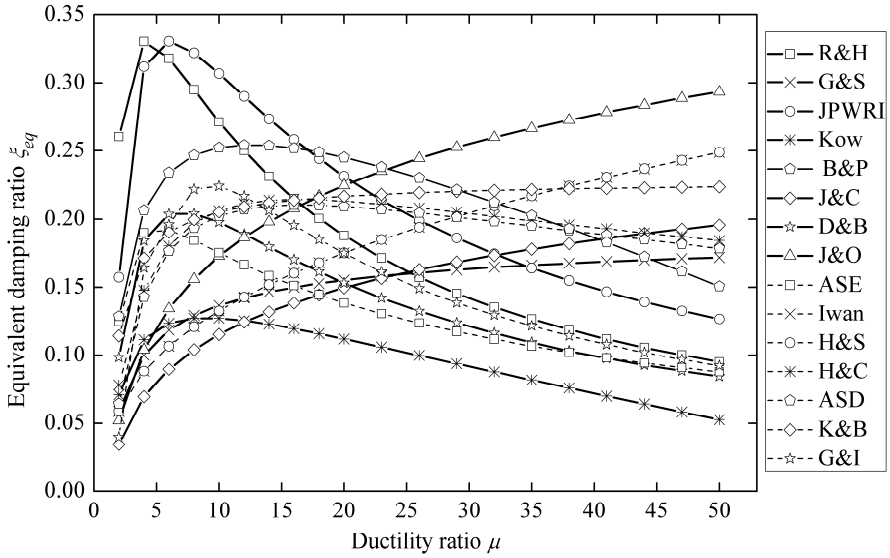

Fig. 16 Comparison of ξ_{eq} computed by different equivalent linearization methods as a function of ductility ratio

As observed from this figure, R&H and JPWRI methods, which are based on equating the energy dissipated per cycle of steady response to harmonic excitation in the nonlinear SDOF systems, yield much higher values of the equivalent damping ratio than other methods when ductility ratio is less than 10. However, method proposed by Kow gives lowest values for ductility ratios greater than 10. Furthermore, two trends of variation of equivalent damping ratio can be observed in this figure, the first one is always increasing, represented by G&S, J&C, J&O, Iwan, H&S and K&B methods, and the other is first increasing and then decreasing, characterized by R&H, JPWRI, Kow, B&P, D&B, ASE, H&C, ASD and G&I methods.

Fig. 17 shows the comparison of period ratio between different equivalent linearization methods. For the equivalent linearization methods using the concept of secant stiffness, the identical period ratio can be obtained except JPWRI method. This is because in this method the equivalent stiffness is determined using the effective design displacement (70%x_d) rather than the maximum design displacement (x_d), as shown in Eq. (15). As can be observed, the period ratios computed using formulas derived by Iwan and K&B lead to relatively high values. However, period ratio calculated using ASE and ASD formulas are the same and yield the lowest values. The formulas of period ratio proposed by H&C, H&S and G&I have a similar trend with those obtained using secant stiffness method.

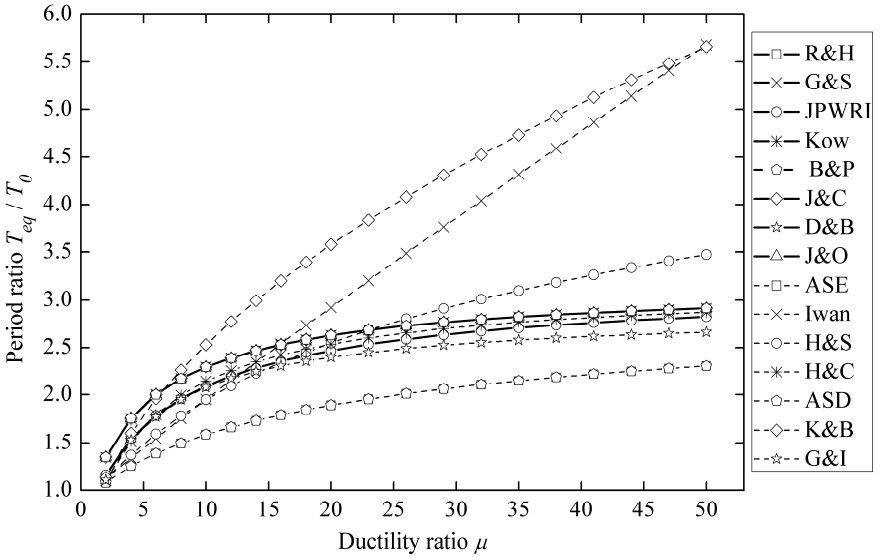

Fig. 17 Comparison of period ratio computed by different equivalent linearization methods as a function of ductility ratio

Due to direct relationship between linear response and equivalent linear properties of the SDOF systems, equivalent linearization methods providing analogous curves in Fig. 16 and Fig. 17 will obtain similar results when subjected to the same seismic loading. In other words, if linear response of the systems has been computed using one of these equivalent linearization methods, then, the variation trend of results obtained through another equivalent linearization method can be roughly expected according to the above curves.

3.2. Earthquake Ground Motions

A set of twelve earthquake time histories is selected from the Pacific Earthquake Engineering Research Center (PEER, 2010) and used as seismic input in this study. All the ground motions are selected based on the following criterions: (1) recorded on stations where enough information exists on the geological conditions; (2) recorded on free field stations or in the first floor of low-rise buildings with negligible soil-structure interaction effects; (3) recorded in earthquakes with surface-wave magnitudes between 6.1 and 7.5; and (4) the records have the peak ground acceleration greater than 0.10 *g*. A complete list of all used ground motions is given in Table 3, including date, earthquake name, magnitude, recorded station, rupture distance to the horizontal projection of the fault, shear-wave velocity in the upper 30 m of the site profile, selected horizontal component, peak ground properties and duration.

Date	Earthquake	M_s*	Station name	R_{rup}* (km)	$V_{s,30}$* (m/s)	Com.* (deg)	PGA (m/s^2)	PGV (m/s)	PGD (m)	Duration (s)
1966	Parkfield	6.2	Temblor pre-1969	16.0	527.9	205	3.504	0.215	0.038	30.3
1971	San Fernando	6.6	Castaic-Old Ridge Route	22.6	450.3	021	3.177	0.156	0.024	30.0
1972	Managua-Nicaragua-01	6.2	Managua- ESSO	4.1	288.8	090	4.131	0.214	0.060	26.0
1979	Imperial Valley-06	6.5	Compuertas	15.3	274.5	015	1.826	0.138	0.029	36.0
1980	Mammoth Lakes-01	6.1	Convict Creek	6.6	338.5	090	4.084	0.232	0.047	30.0
1980	Victoria- Mexico	6.3	Cerro Prieto	14.4	659.6	045	6.091	0.316	0.131	24.5
1983	Coalinga-01	6.4	Parkfield-Cholame 2WA	44.7	184.8	000	1.069	0.113	0.026	40.0
1989	Loma Prieta	6.9	Foster City-Menhaden Court	45.6	126.4	270	1.048	0.206	0.080	30.0
1992	Cape Mendocino	7.0	Petrolia	8.2	712.8	000	5.782	0.481	0.219	36.0
1994	Northridge-01	6.7	LA-Wonderland Ave	20.3	1222.5	095	1.101	0.087	0.018	30.0
1995	Kobe-Japan	6.9	Kakogawa	22.5	312.0	000	2.466	0.187	0.058	41.0
1999	Kocaeli- Turkey	7.5	Izmit	7.2	811.0	090	2.153	0.298	0.171	30.0

* M_s is the surface-wave magnitude of recorded earthquake; R_{rup} is the rupture distance to the horizontal projection of the fault; $V_{s,30}$ is shear-wave velocities in the upper 30 m of the site profile; Com. is the horizontal component of the considered ground motions.

Table 3

Recorded earthquake ground motions.

3.3. Assessment Procedure

The accuracy of different approximate methods is examined through comparison of results between nonlinear time history analysis (NTHA) and equivalent linear time history analysis (LTHA). Detailed procedures to perform both NTHA and LTHA analysis of seismically-isolated buildings are described as well as a specifically developed program within MATLAB and OpenSees (Liu et al., 2014a).

Fundamental period of base-isolated buildings is generally considered to range between 1.5 s and 3.0 s (Tena-Colunga & Zambrana-Rojas, 2006). However, in order to restrain the base displacement when subjected to strong winds or small earthquakes, base isolation systems are expected to have a relatively high initial stiffness, i.e., a relatively low initial period. Thus, a total of 15 initial periods of vibration between 0.1 s and 1.5 s are assigned for isolation systems with period increments equal to 0.1 s. Furthermore, as mentioned by Hwang and Chiou (Hwang & Chiou, 1996), ductility ratio demanded by an earthquake ground motion on seismic isolation systems may be up to 20 and higher. Therefore, a set of 20 ductility ratios between 2 and 50 are considered with increments equal to 2 for ductility ratios between 2 and 20 and 3 for ductility ratios greater than 20.

Exact maximum inelastic displacement is computed based on the bilinear properties and the predefined displacement ductility ratio. Thus, an iterative scaling process of the selected ground motion will be performed until the computed displacement ductility demand is, within a tolerance, equal to the desired displacement ductility ratio. The scaling factor will be considered satisfactory if the relative error between computed and specified ductility ratio is within 1 per cent.

NTHA of bilinear SDOF systems is conducted using the Open System for Earthquake Engineering Simulation (OpenSees) (Mazzoni et al., 2007) due to its modularity and high execution speed. Bilinear force-deformation behavior is modeled by elastomericBearing element in Opensees, and Newmark step-by-step integration method (Newmark, 1959) (parameters β = 0.25 and γ = 0.5) is used with a constant time step of 0.005 s to compute nonlinear response of SDOF systems.

For LTHA, the equivalent linear properties can be determined based on predefined displacement ductility ratios and hysteretic characteristics of the systems. Here are the steps to estimate the maximum inelastic displacement using LTHA method:

Step 1: Calculate the period of vibration of equivalent linear systems using the equations for period ratio corresponding to different equivalent linearization methods;

Step 2: Compute the equivalent viscous damping ratio of equivalent linear systems using the equations for equivalent damping ratio corresponding to different equivalent linearization methods;

Step 3: Compute the response time history of equivalent linear systems with linear response history analysis based on the equivalent linear properties computed in steps 1 and 2. Note that the seismic input should be the scaled earthquake record used in NTHA analysis to produce the specified displacement ductility ratio.

Step 4: Calculate the approximate maximum inelastic displacement as the maximum absolute value of displacement response computed in step 3.

To perform numerical analyses expediently and systematically, a program is developed using MATLAB in conjunction with OpenSees, as presented in Fig. 18. In this program, the function of OpenSees is to compute the time history response of linear or nonlinear systems, while MATLAB is used to control the global operations, such as parameter input, OpenSees calling and result processing.

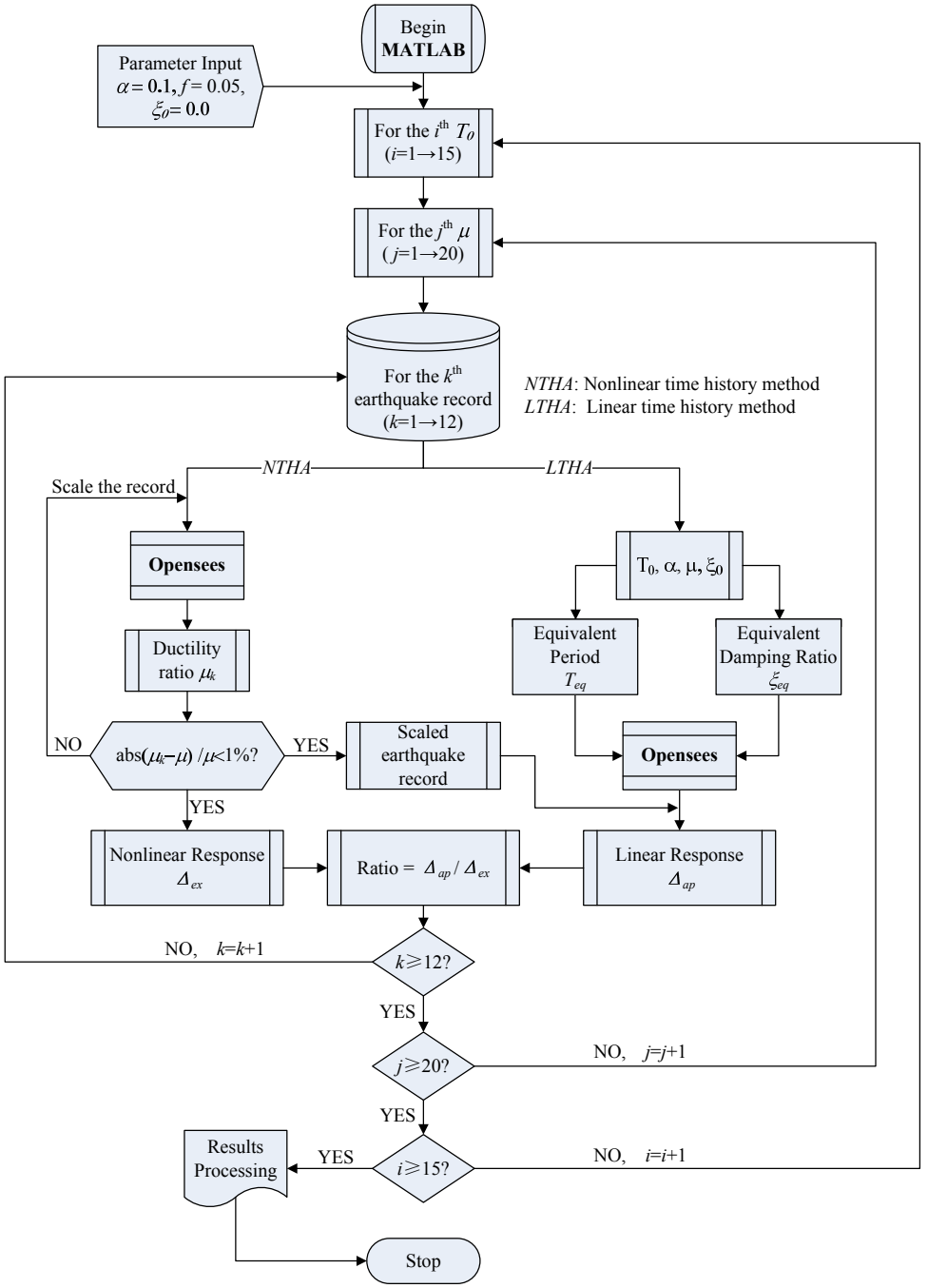

Fig. 18 Flowchart of the specifically developed program

3.4. Results of Parametric Study

For each earthquake record and each initial period, exact maximum inelastic response are computed for each value of ductility ratio previously specified between 2 and 50. Therefore, a total of 15×20×12 = 3600 inelastic displacement demands are computed by iteration as part of this investigation. Accordingly, 15×(15×20×12) = 54000 linear time history analyses are conducted based on equivalent linear properties determined by 15 different approximate methods. For each initial period and each level of inelastic deformation, ratios of approximate to exact maximum inelastic displacement corresponding to each equivalent linearization method, as shown in Eq. (70), are averaged over the 12 ground motions.

$$R = \frac{1}{N}\sum_{l=1}^{N}\frac{\Delta_{ap,l}\left(T_{eq},\xi_{eq}\right)}{\Delta_{ex,l}\left(T_0,\alpha,\mu,\xi_0\right)} \tag{69}$$

where N is the number of earthquake records.

In the following illustrations, ratios smaller than one indicate that the approximate method underestimates on average the exact maximum displacement in inelastic systems and ratios larger than one mean that the approximate method overestimates on average the exact maximum inelastic displacement. Furthermore, in order to assess the dispersion of ratios computed using different earthquake ground motions, the standard deviation of the ratios is also investigated, as given by:

$$\sigma\left(R\right) = \sqrt{\frac{1}{N-1}\sum_{l=1}^{N}\left(\frac{\Delta_{ap,l}\left(T_{eq},\xi_{eq}\right)}{\Delta_{ex,l}\left(T_0,\alpha,\mu,\xi_0\right)} - R\right)^2} \tag{70}$$

3.4.1 Estimation Accuracy of the First Grouped Methods

In this subsection, the accuracy of the first group of investigated equivalent linearization methods to estimate the maximum inelastic displacement of bilinear SDOF systems is plotted in the same order that they were introduced in Chapter 2.3.1 as well as the standard deviation of the measured ratios.

Fig. 19 presents mean approximate to exact ratios and their standard deviations corresponding to R&H method. As observed from this figure, the maximum inelastic

displacement is underestimated by R&H method for ductility ratios less than 10 due to the high damping ratios, particularly when initial period of vibration is longer than about 0.3 s. However, for ductility ratio greater than 10, good estimations are obtained and relative errors are on average smaller than 10 per cent. In general, regarding standard deviation of the measured ratios, larger dispersions will be obtained for relatively low ductility ratios, and the initial period has no significant effect on the standard deviation.

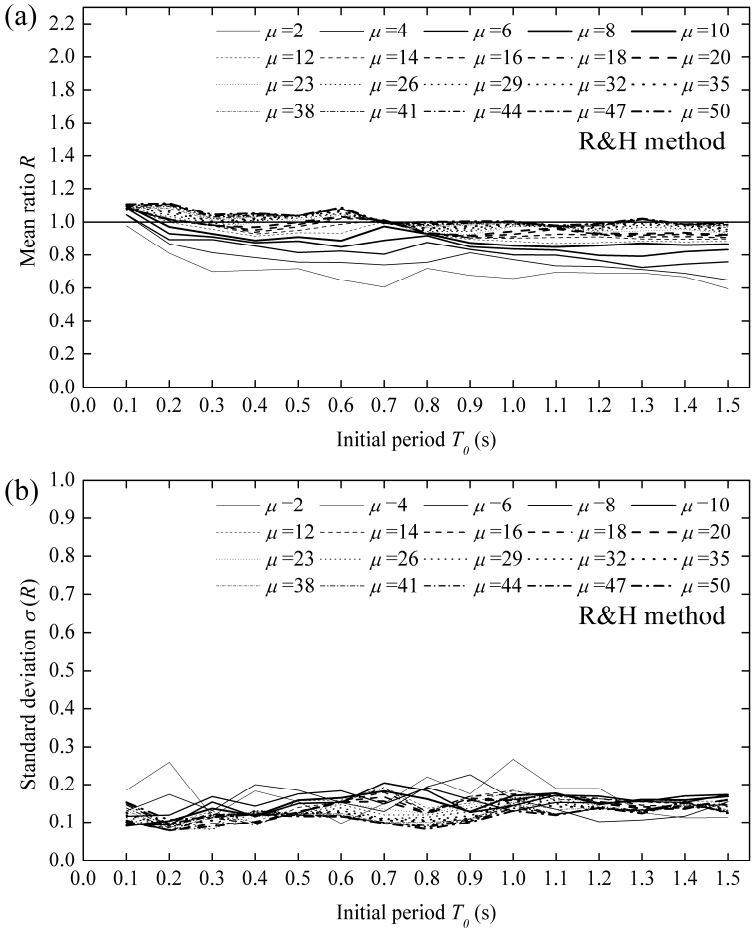

Fig. 19 Estimation accuracy of R&H method: (a) mean ratios R and (b) standard deviation of measured ratios σ (R)

Results corresponding to G&S method are shown in Fig. 20. In this figure, it is noted that the maximum displacement of bilinear SDOF systems is overestimated for low ductility ratios and underestimated for high ones. Furthermore, the estimation accuracy increases as the initial period of vibration increases. The maximum error

is up to 50 per cent for systems with initial period of 0.1 s, and then decreases to 40 per cent for systems with initial period of 0.9 s, finally less than 20 per cent for that with 1.5 s. However, the initial period does not produce significant effects for systems with high ductility ratios ranging from 23 to 50. Similar to the mean values of peak displacement ratios, standard deviation of the measured ratios is remarkably influenced by the level of inelastic deformations.

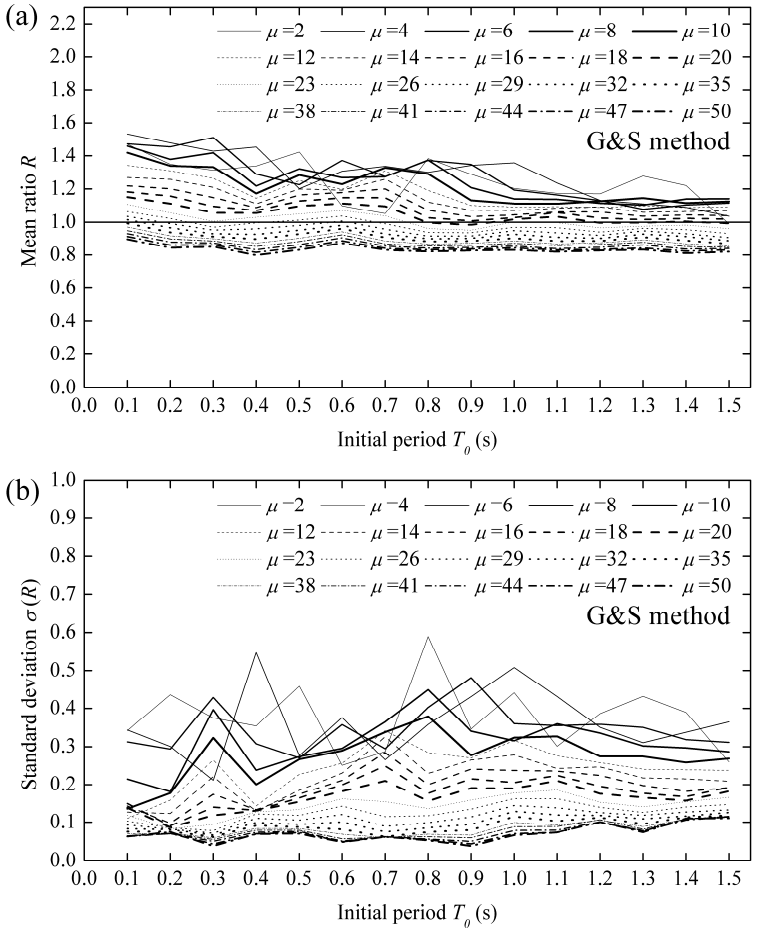

Fig. 20 Estimation accuracy of G&S method: (a) mean ratios R and (b) standard deviation of measured ratios σ (R)

When equivalent linearization method proposed by JPWRI is used, the maximum inelastic displacements are underestimated for all level of ductility ratio, as shown in Fig. 21. For bilinear SDOF systems with low ductility ratio less than 20, this method produces underestimations that on average are 20 per cent, while the errors decrease to 10 per cent on average for systems with ductility ratio greater than 20. In

addition, the influence of initial period of bilinear systems on the accuracy of JPWRI method is not remarkable, especially when ductility ratios are greater than 20. Although the peak inelastic displacements are underestimated, standard deviation of the measured ratios is generally in the order of 0.1.

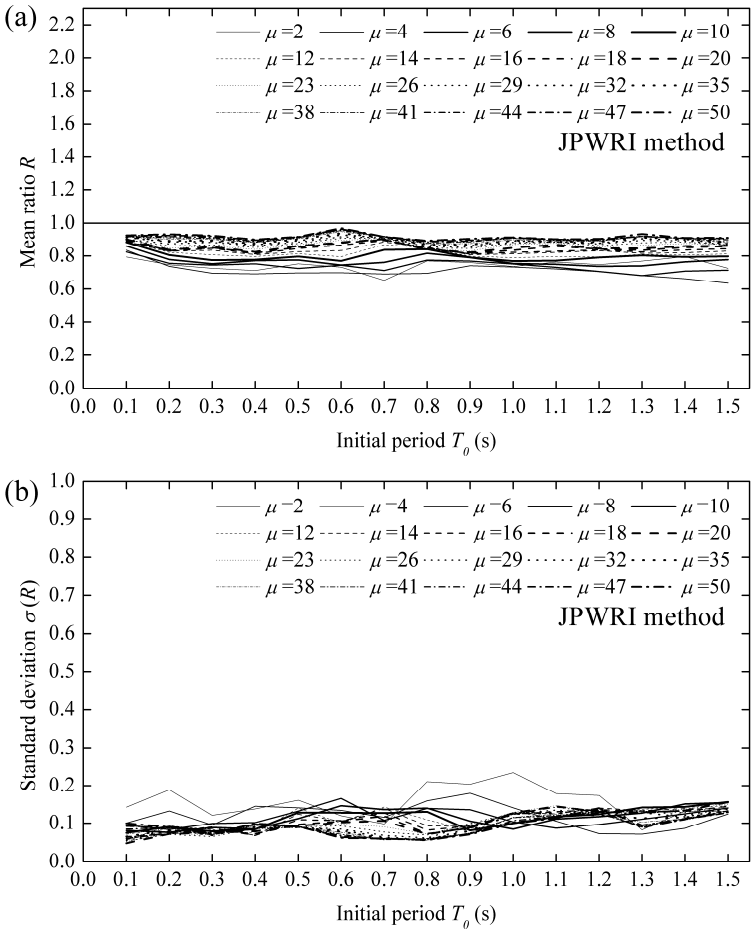

Fig. 21 Estimation accuracy of JPWRI method: (a) mean ratios R and (b) standard deviation of measured ratios σ (R)

Kow method tends to yield conservative estimates of the maximum inelastic displacement, as presented in Fig. 22. The estimation accuracy increases as the initial period of vibration increases, which is on average 30 per cent for initial periods from 0.1 s to 0.4 s, 25 per cent between 0.4 s and 0.7 s, 20 per cent between 0.7 s and 1.0 s and 15 per cent for that from 1.0 s to 1.5 s. Accordingly, effect of ductility ratio on the accuracy of estimation has the same variation trend as that of initial period. Compared with the mean ratios, their standard deviations are more sensitive to ductility ratio and initial period.

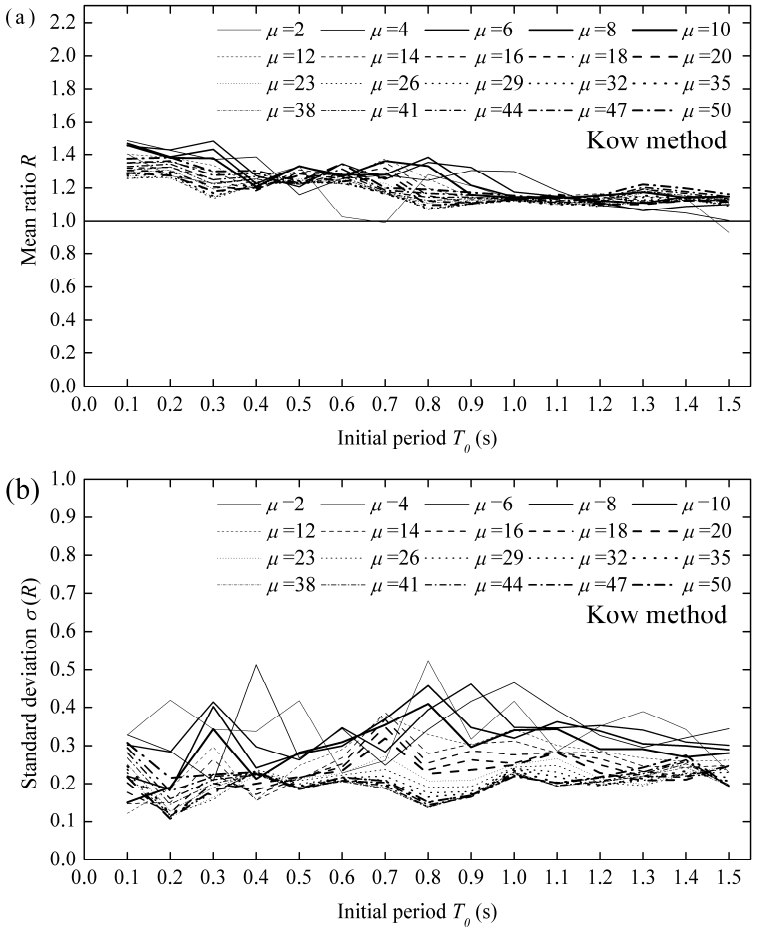

Fig. 22 Estimation accuracy of Kow method: (a) mean ratios R and (b) standard deviation of measured ratios σ (R)

Fig. 23 illustrates the results obtained from B&P method. It can be observed that the estimation accuracy decreases with increasing the ductility ratio. The peak displacement is accurately predicted for ductility ratio less than 6. This is because the ductility ratio used in B&P method is limited to 6. For high ductility ratios, the peak displacement is in general underestimated. In addition, B&P method is nearly independent to the initial period. The standard deviation of the mean ratio is found to increase with increasing the initial period and to decrease with increasing the ductility ratio.

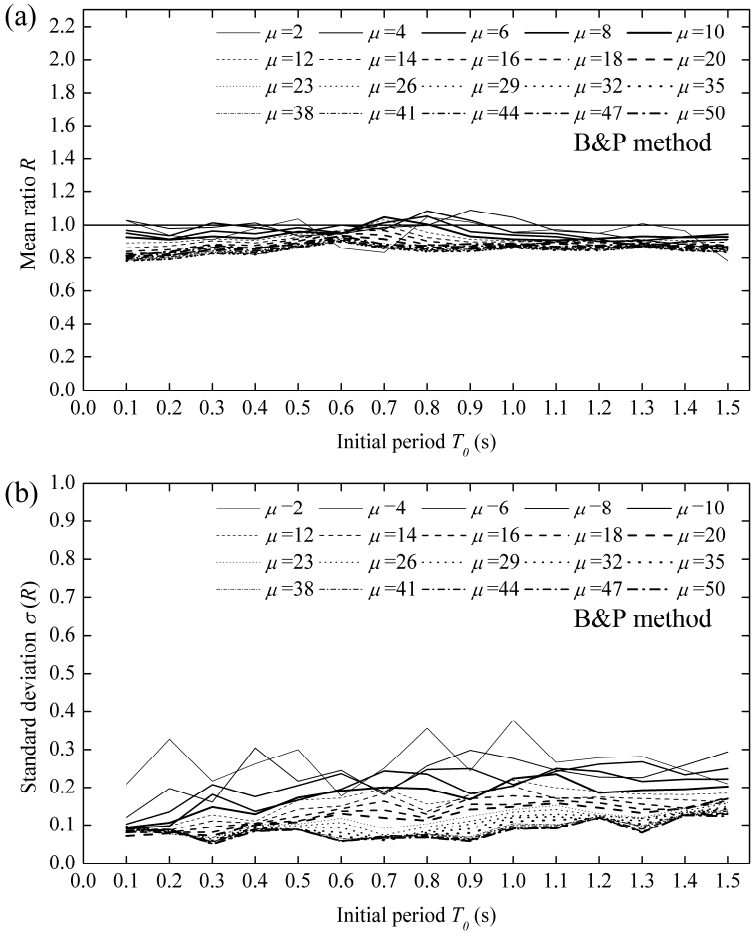

Fig. 23 Estimation accuracy of B&P method: (a) mean ratios R and (b) standard deviation of measured ratios σ (R)

Fig. 24 illustrates the results obtained from J&C method. As seen from the figure, the peak displacement is overestimated in regions with low ductility ratios while underestimated in regions with high ductility ratios. For ductility ratios between 23 and 35, this method produces satisfied accuracy with average error of 10 per cent. The variation of estimation accuracy of peak displacement is more sensitive in low-ductility region than that in high-ductility region. For any bilinear SDOF system having an initial period longer than 0.9 s, the maximum inelastic displacement estimated by J&C method will keep constant for a specific ductility ratio between 12 and 50. It is interesting to find that the variation trends of both mean value and standard deviation of the measured ratios are in general the same when comparing Fig. 19 with Fig. 24. However, as are presented, the estimates of G&S method are considered

to be more accurate than that from J&C method. Thus, equivalent linear properties determined by G&S method are more appropriate than those computed by J&C method.

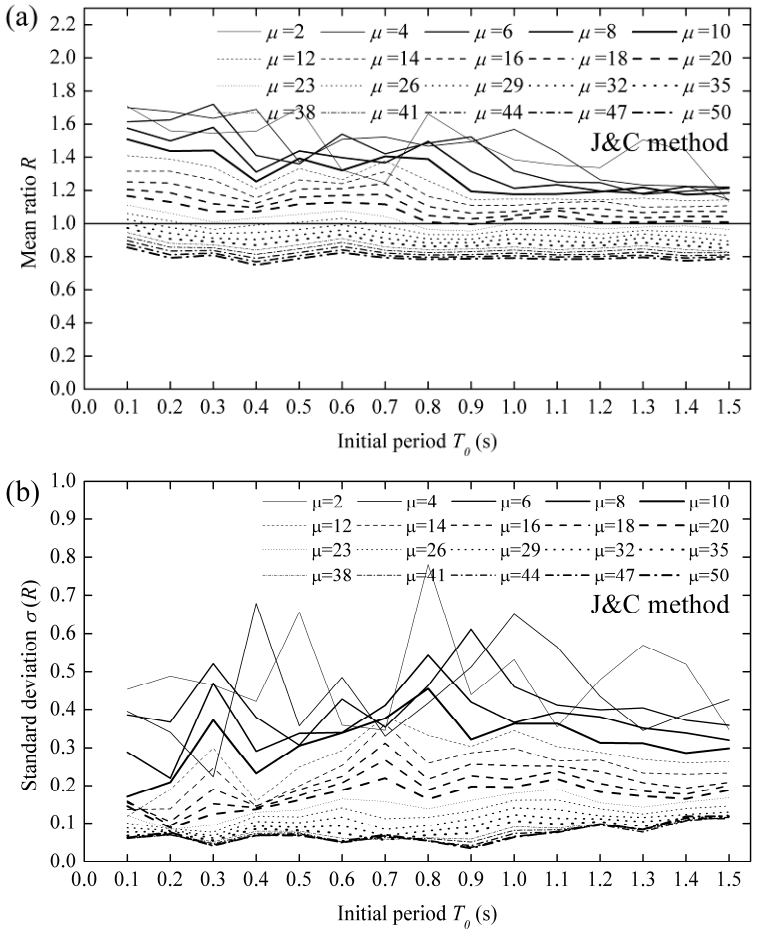

Fig. 24 Estimation accuracy of J&C method: (a) mean ratios R and (b) standard deviation of measured ratios σ (R)

Fig. 25 presents the mean approximate to exact displacement ratios and their standard deviations calculated by D&B method. For ductility ratios less than 10, the ratios are significantly influenced by the initial periods. But, the estimation accuracy of D&B method is nearly independent of ductility ratio when it is greater than 10. In general, it can be seen that estimation accuracy increases as the initial period increases. Best estimation is yielded for bilinear systems with initial periods longer than 0.8 s and with ductility ratios greater than 10, which is on average less than 5 per cent. The dispersion of ratios is found to be lower for systems with high ductility ratio than that with low ductility ratio.

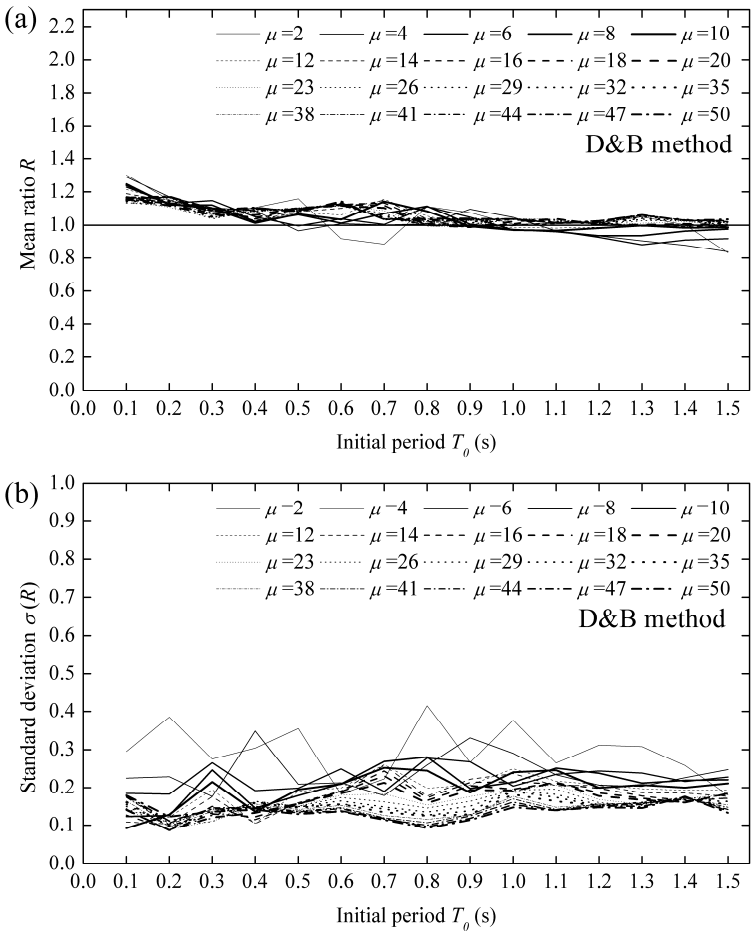

Fig. 25 Estimation accuracy of D&B method: (a) mean ratios R and (b) standard deviation of measured ratios σ (R)

The equivalent viscous damping ratio computed by J&O method is 1.5 times that from J&C method. It can be expected that the mean ratios of approximate to exact maximum displacement will decrease at all levels of initial period and ductility ratio, as shown in Fig. 26. Having the same variation trend of equivalent viscous damping ratio, results obtained by J&O method are just the downward migration of that from J&C method. Thus, J&O method does not improve the estimation accuracy. However, compared with the results from J&C method, relatively low dispersion of measured ratios is obtained using J&O method.

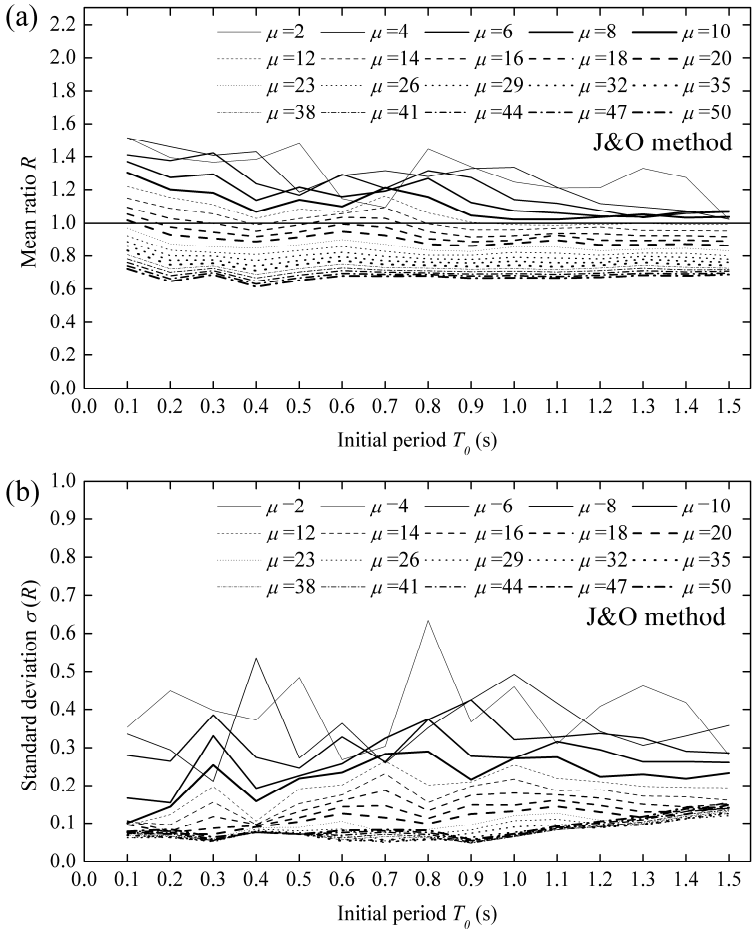

Fig. 26 Estimation accuracy of J&O method: (a) mean ratios R and (b) standard deviation of measured ratios σ (R)

3.4.2 Estimation Accuracy of the Second Grouped Methods

Results of last seven equivalent linearization methods are given here and they are plotted using an identical format of illustrations compared with the former subsection and in the order that they were introduced in Chapter 2.3.2.

Accuracy of ASE method to estimate the maximum displacement of bilinear SDOF systems is presented in Fig. 27. Mean ratios of approximate to exact maximum displacement are generally underestimated for all levels of ductility ratio. As noted from this figure, errors between LTHA with ASE method and NTHA decrease with increasing initial period and displacement ductility ratio. Better estimations are produced by this method for systems with initial periods longer than 0.5 s and with duc-

tility ratio greater than 12, which has an error on average less than 10 per cent. It is very interesting to note, unlike the first group of equivalent linearization methods, standard deviation of the measured ratios computed by ASE method increases with increasing the level of inelastic deformation.

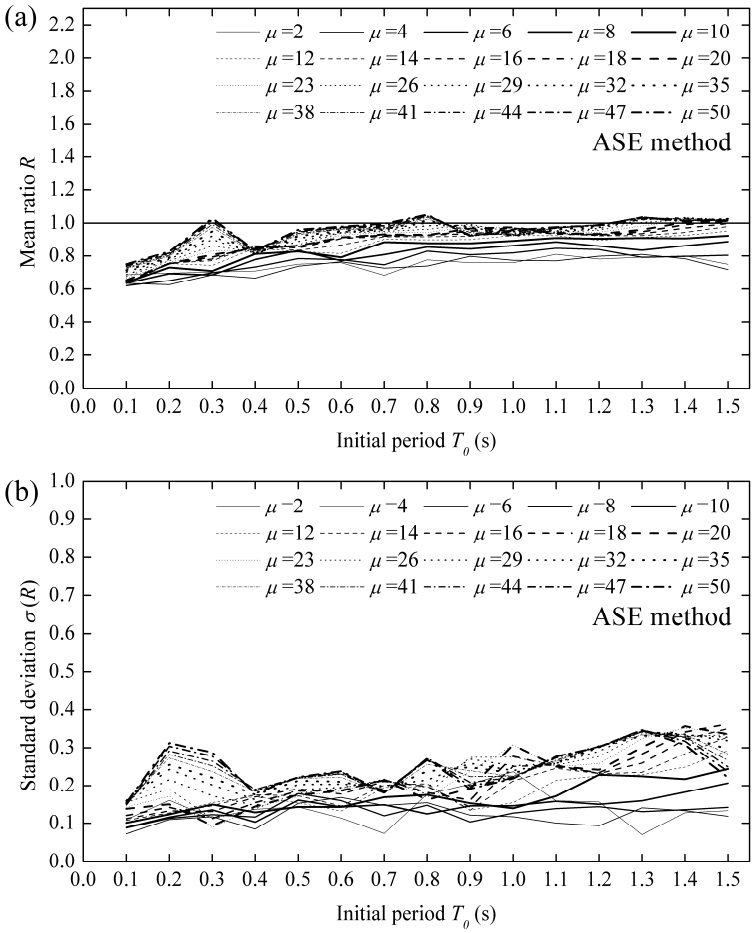

Fig. 27 Estimation accuracy of ASE method: (a) mean ratios R and (b) standard deviation of measured ratios σ (R)

Fig. 28 plots mean approximate to exact displacement ratios calculated by Iwan method. According to Iwan's work, the formulas are applicable for structures within the mid-period range of 0.4 s - 4.0 s, hence no evaluation for short period structures was provided. In addition, the ductility ratio considered is up to 8, which is much less than that of seismic isolation systems. From Fig. 28, it is found that significant deviations will be obtained when the ductility ratio is greater than 20, especially for initial period less than 0.4 s. No regularity between the estimation accuracy and initial period is identified for systems with ductility ratio less than 12, which shows fluc-

tuations in the whole range of initial period. However, in high-ductility regions, maximum displacement estimated by Iwan method decreases with increasing the initial period. It can be also seen that both mean and standard deviation of displacement ratios are very sensitive to initial period.

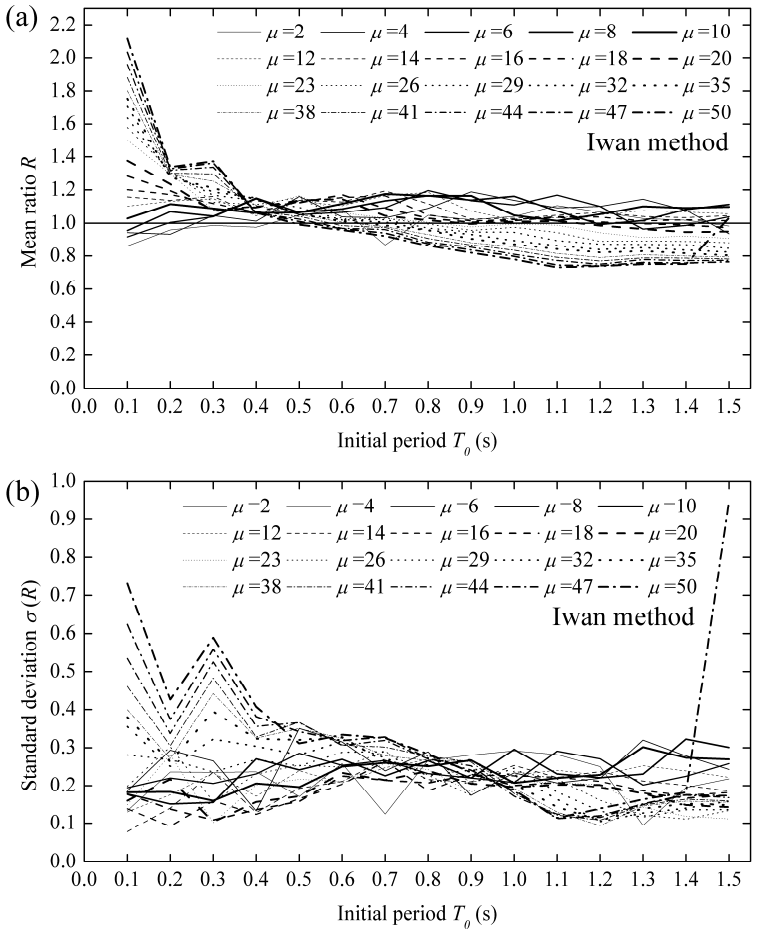

Fig. 28 Estimation accuracy of Iwan method: (a) mean ratios R and (b) standard deviation of measured ratios σ (R)

Mean and standard deviation of displacement ratios computed by H&S method are shown in Fig. 29, which has the same equivalent damping equation to Iwan method but gives much lower period ratio for ductility ratios greater than 15. Thus, the equivalent linear elastic systems determined by H&S method are stiffer and the maximum inelastic displacement is expected to decrease compared with that computed using Iwan method. As observed from this figure, mean ratios of approximate to exact displacement demand are nearly identical with that from Iwan method for bilinear SDOF systems with ductility ratio less than 15. However, for ductility ratios

greater than 15, estimation accuracy is significantly improved as well as the standard deviation of measured ratios.

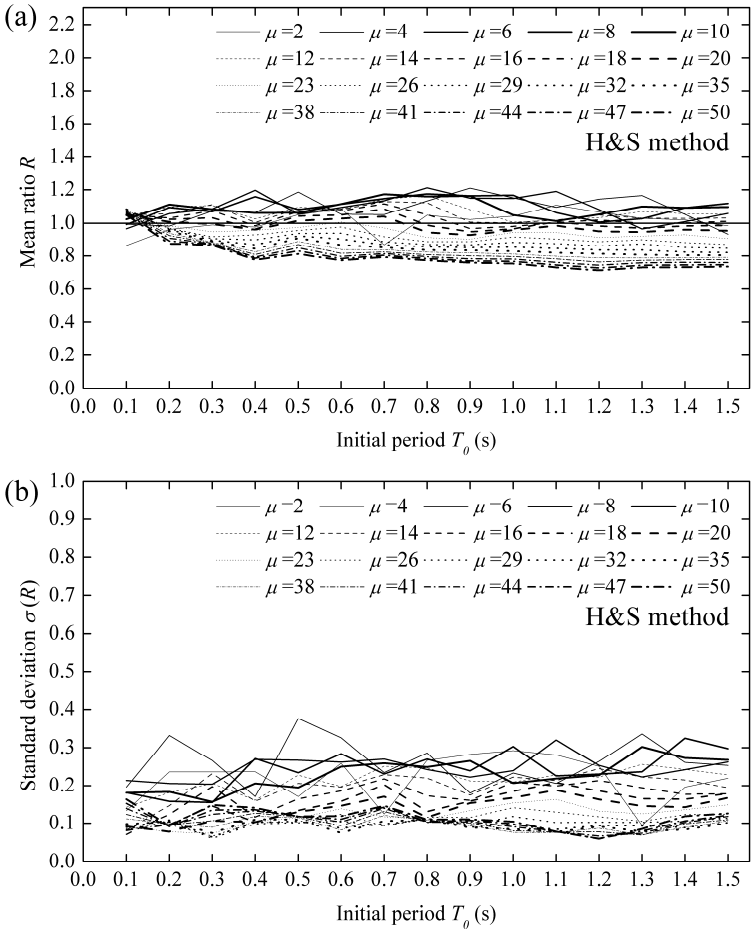

Fig. 29 Estimation accuracy of H&S method: (a) mean ratios R and (b) standard deviation of measured ratios σ (R)

Fig. 30 presents the mean approximate to exact displacement ratios calculated using H&C method. In general, the maximum displacement is underestimated on average by 10 per cent. The estimation accuracy is found to decrease with increasing the ductility ratio. Furthermore, compared with H&S method, the mean ratios from H&C method are less sensitive to the variation of initial period, especially when the ductility ratio is greater than 20. When H&C method is utilized, to a certain extent, standard deviation of measured ratios decreases compared with H&S method.

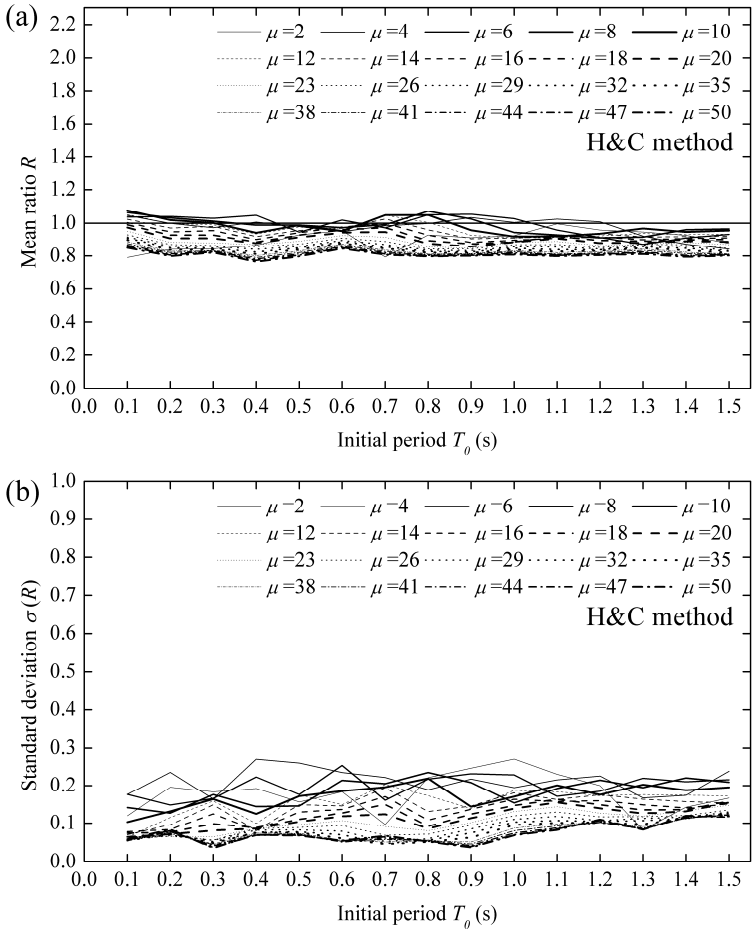

Fig. 30 Estimation accuracy of H&C method: (a) mean ratios R and (b) standard deviation of measured ratios σ (R)

Compared with ASE method, the same period ratio formula is utilized in ASD method, but the computed equivalent viscous damping ratio is much greater when the ductility ratio is larger than 10, which can be reviewed in Fig. 16. Thus, variation trends of estimation accuracy can be expected according to differences of damping ratio between ASD and ASE methods, as shown in Fig. 31. Estimation accuracy of ASD method increases compared with the results shown in Fig. 27 when ductility ratio is less than 10. However, significant underestimations are produced when ductility ratio is greater than 10. Generally, both mean and standard deviation of measured ratios increase as the initial period increases, which is more obvious for high ductility ratios.

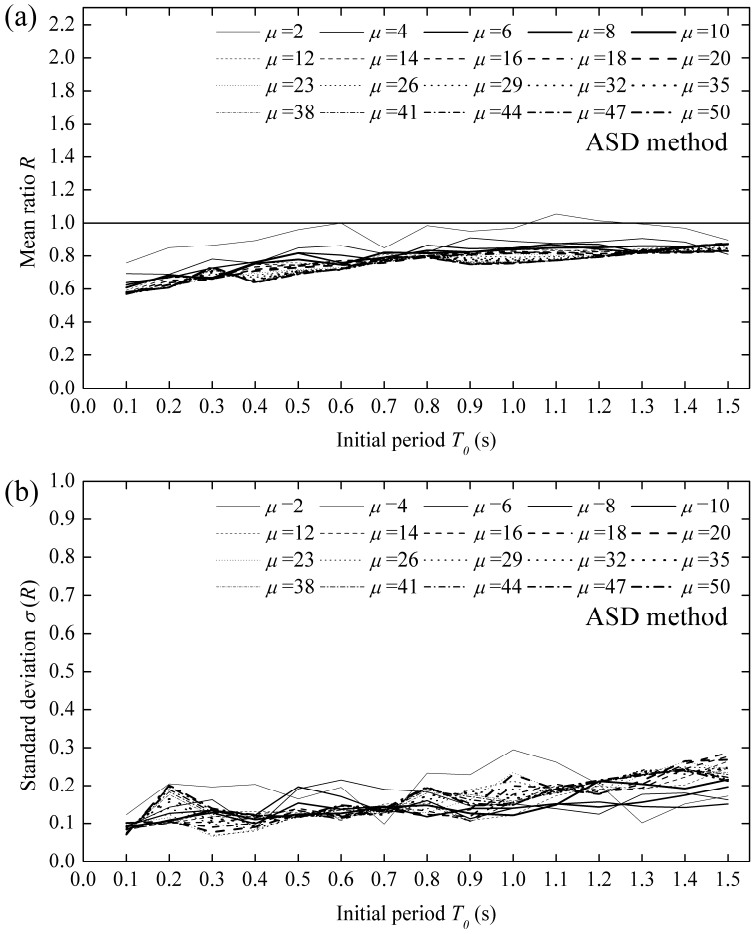

Fig. 31 Estimation accuracy of ASD method: (a) mean ratios R and (b) standard deviation of measured ratios σ (R)

Fig. 32 presents mean values of approximate to exact displacement ratios obtained by K&B method. It can be found that it gives satisfactory estimates only in very limited range of ductility ratio and initial period. As the initial period increases, the peak displacement decreases, especially when the high ductility ratios are considered. Due to the assumptions when the formulas are derived, K&B method is not suitable for design of seismically isolated building with high ductility ratios. The standard deviation of measured ratios does not vary too much as the initial period increases for systems with ductility less than 20, while it is significantly affected by initial period when ductility ratio is greater than 20, which is quite similar to the variation trend of results computed using Iwan method.

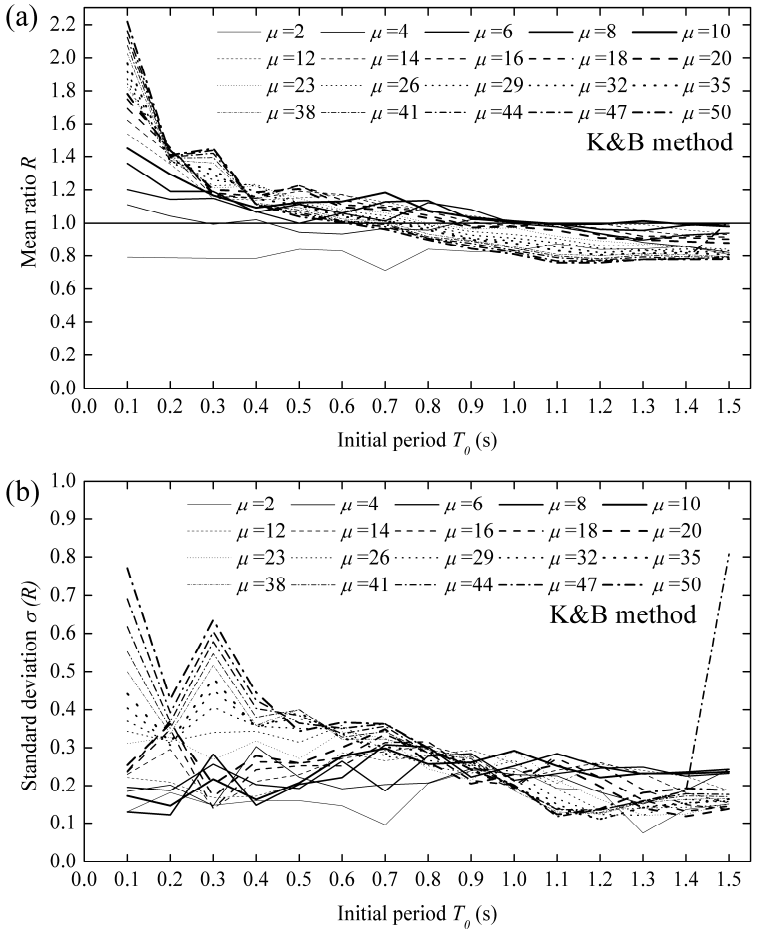

Fig. 32 Estimation accuracy of K&B method: (a) mean ratios R and (b) standard deviation of measured ratios σ (R)

Mean and standard deviation of approximate to exact displacement ratios produced by G&I method are illustrated in Fig. 33. It can be noted that an average error of 10 per cent is obtained for systems with ductility ratio less than 6 and an average error less than 5 per cent for ductility ratio greater than 6. The standard deviation of the results also shows low dispersions expect systems with ductility ratio less than 6. So, G&I method gives high accuracy to estimate the maximum inelastic displacement of SDOF systems with bilinear hysteretic behavior. In addition, the results are nearly independent of initial period and inelastic deformation.

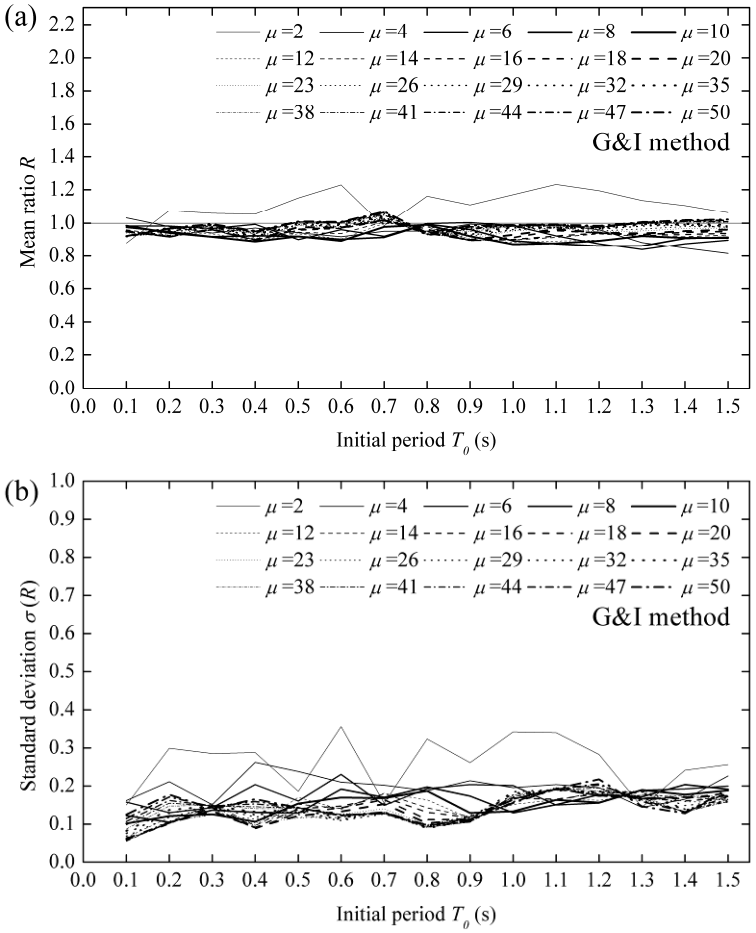

Fig. 33 Estimation accuracy of G&I method: (a) mean ratios R and (b) standard deviation of measured ratios σ (R)

3.4.3 Discussions

From the above results, it is seen that estimation accuracy of peak inelastic displacement is strongly related to different assumptions when various equivalent linearization methods are derived or fitted, namely ranges of ductility ratios, initial periods, and the strain hardening ratio. But one should have in mind that in this study a strain hardening ratio of 0.1 and a yielding strength ratio of 5% normalized by total weight are assumed for the investigated SDOF systems. Although it is very difficult to directly compare the difference of the prediction accuracy between this study and the previous ones due to different range of the considered parameters, the overall

behavior and the general trends of the prediction accuracy can be provided regardless of the discrepancies.

Recommended in recent structural codes and derived based upon the concept of secant stiffness and equal energy dissipation rule, R&H method underestimates the maximum inelastic displacement on average 20 per cent for systems with displacement ductility ratios less than 10. Herein lies the fact that for the relatively low ductility ratio, equivalent viscous damping ratio computed using R&H method is significantly overestimated, especially for bilinear systems with high initial period. However, for high ductility ratios, this method provides satisfied accuracy to estimate the actual maximum nonlinear deformation. Compared with the mean approximate to exact maximum inelastic displacement ratios shown in Fig. 11 in the study of Miranda and Ruiz-García (Miranda & Ruiz-García, 2002), the prediction accuracy of R&H method is improved due to the increase of strain hardening ratio from 0.0 to 0.1. It can be concluded that the accuracy of R&H method overall increases with increasing the strain hardening ratio, which is also consistent with the results observed in the study of Huang (Huang, 1996). Moreover, the mean ratios also increase with increasing the ductility ratio. These are the reasons several requirements must be met in modern codes for the use of equivalent linearization technique. However, this may lead to slightly overestimated results, as seen in Fig. 19 when the initial period is less than 0.6 s and the ductility ratio is larger than 20.

Comparing Fig. 28 in this research with Fig. 11 in Miranda and Ruiz-Garcia's study, Iwan method slightly overestimates the maximum inelastic displacements when the strain hardening ratio 0.1 is used other than zero. Furthermore, large deviation is produced when the ductility ratio is relatively high, especially for systems with short initial period, which is not presented in study of Miranda and Ruiz-García. So, Iwan method is not suitable for analysis and design of seismically-isolated structures. Similar observations can be also found for K&B method in Fig. 31 in this study.

Derived based on Takeda hysteretic model, G&S method and Kow method produce better results for SDOF systems with long initial period than those with short initial period, which agrees with the results from the study of Miranda and Ruiz-García. As described by Miranda and Ruiz-García, the mean approximate to exact maximum inelastic displacement ratios are found to increase as the ductility ratio increases, which is limited to 6. However, the mean ratios computed using G&S method decrease with increasing the ductility ratio in this study, in particular for ductility ratio larger than 12. For Kow method, the variation trend of the measured ratios against the ductility ratio is less clear.

Although G&I method is found to produce high accuracy of estimating the maximum inelastic displacement of bilinear SDOF systems with strain hardening ratio of 0.1 and with yielding strength ratio of 5% normalized by total weight, it should been noted that this model is independent to strain hardening ratio, thereby it may lead to large errors as the strain hardening ratio varies.

In a word, for relatively small ductility ratios, B&P method produces better results compared with other methods. Remembering that R&H method could present good estimates of peak displacement for bilinear systems with relatively high ductility ratios, it can be expected that a more appropriate method should incorporate the equivalent damping ratios computed by B&P method when ductility ratio is small and those obtained using R&H method when ductility ratio is large, which could be referenced when proposing new equivalent linearization methods.

3.5. Summary

Fifteen approximate methods used to estimate the maximum inelastic displacement of bilinear SDOF systems were evaluated when subjected to 12 earthquake ground motions. The strain hardening ratio is set to be 0.1 and the yielding strength is assumed to be 5% of total weight. A large number of parameters were assigned for parametric study, including 15 initial periods ranging from 0.1 s to 1.5 s and 20 ductility ratios from 2 to 50. Therefore, 15×20×12 = 3600 nonlinear displacement demands were calculated by iteration and 15×(15×20×12) = 54000 linear time history analyses were conducted accordingly based on different equivalent linearization methods.

Theoretically, each equivalent linearization method is only suitable for the systems which meet the assumptions when it is derived. However, there is still not a good equivalent linearization method that can predict satisfied results in a wide parameter space. Thus, much work needs to be done to develop a universal method for all the considered cases. According to comparison of results obtained by different equivalent linearization methods, basic trends of variations in equivalent viscous damping ratio and period shift are identified as a function of displacement ductility ratio. To improve the prediction accuracy, period shift based upon secant stiffness or other formulas with similar variation trend can be used. Furthermore, equivalent viscous damping ratio should first increase and then decrease as the ductility ratio increases. However, not only the variation trend but also the quantitative values of equivalent linear properties should be taken into account.

Regarding the standard deviation of measured ratios, it is significantly influenced by displacement ductility ratio. Furthermore, if an equivalent linearization method shows a high accuracy of estimation, a relatively low standard deviation will be obtained accordingly. But the opposite is not always true, which can be verified by JPWRI and ASD methods. Thus, when deriving an equivalent linearization method that used to approximate the maximum inelastic displacement of nonlinear SDOF systems, the key issue is to produce a high accuracy of estimation.

CHAPTER 4

4. IMPROVED EQUIVALENT DAMPING FOR SDOF SYSTEMS

As discussed in the last Chapter, none of the investigated equivalent linearization methods is able to present satisfied estimates of the maximum inelastic displacement in bilinear SDOF systems. In the study of Liu et al. (Liu et al., 2014b), they had proposed an modified equivalent linearization method, but only four initial periods (0.25 s, 0.5 s, 0.75 s, and 1.00 s) were considered in that study. In addition, strain hardening ratio varied from 0.02 to 0.20 with an increment of 0.02, which cannot represent the elastic-perfectly plastic model. Due to the limited parameters, the proposed method may not be suitable for general bilinear SDOF systems.

To obtain better estimation accuracy comprehensively, an improved formula to determine the equivalent viscous damping ratio of SDOF base-isolated buildings is proposed in this Chapter, which simultaneously considers the influence of initial period, ductility ratio and strain hardening ratio. As a research methodology, parametric analyses, optimization analyses and regression analyses are performed successively.

Results show that the proposed formula leads to better estimates of maximum inelastic displacement response in the considered parameter space when compared with R&H and B&P methods. In addition, the proposed equivalent linearization method is validated by the other components of the selected twelve earthquake ground motions

4.1. Parametric Analysis of SDOF Systems

Based on the assumption of secant stiffness, R&H method and B&P method are evaluated through parametric analyses in a wider parameter space, which are considered to produce satisfied results for SDOF bilinear systems with high and low ductility ratios, respectively.

4.1.1 Parameters variation

In order to investigate the estimation accuracy of R&H method and D&B method in a wider parameter space, comprehensive parametric analyses are performed based on the following assumptions or parameters:

a) the yielding displacement of SDOF bilinear isolation system is assigned to be 0.01 m;

b) the elastic damping ratio of SDOF bilinear isolation system is omitted (ξ_0=0);

c) 15 initial periods of vibration T0 between 0.1 s and 1.5 s with period increments equal to 0.1 s;

d) 20 ductility ratios μ between 2 and 50 with increments equal to 2 for ductility ratios between 2 and 20 and 3 for ductility ratios greater than 20;

e) 10 strain hardening ratios α (0.00, 0.01, 0.03, 0.05, 0.075, 0.10, 0.125, 0.15, 0.175 and 0.2).

First, based on the above assumptions or parameters, the equivalent linear properties of substitute systems are examined. Since both R&H method and B&P method apply the concept of secant stiffness, the determined equivalent stiffness or equivalent period is the same. However, the computed equivalent damping ratios are different and compared in Fig. 34.

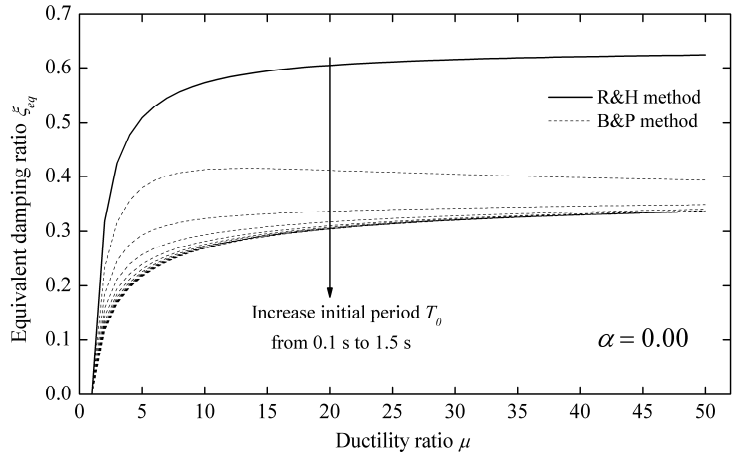

Fig. 34 Comparison of equivalent damping ratios between R&H method and B&P method

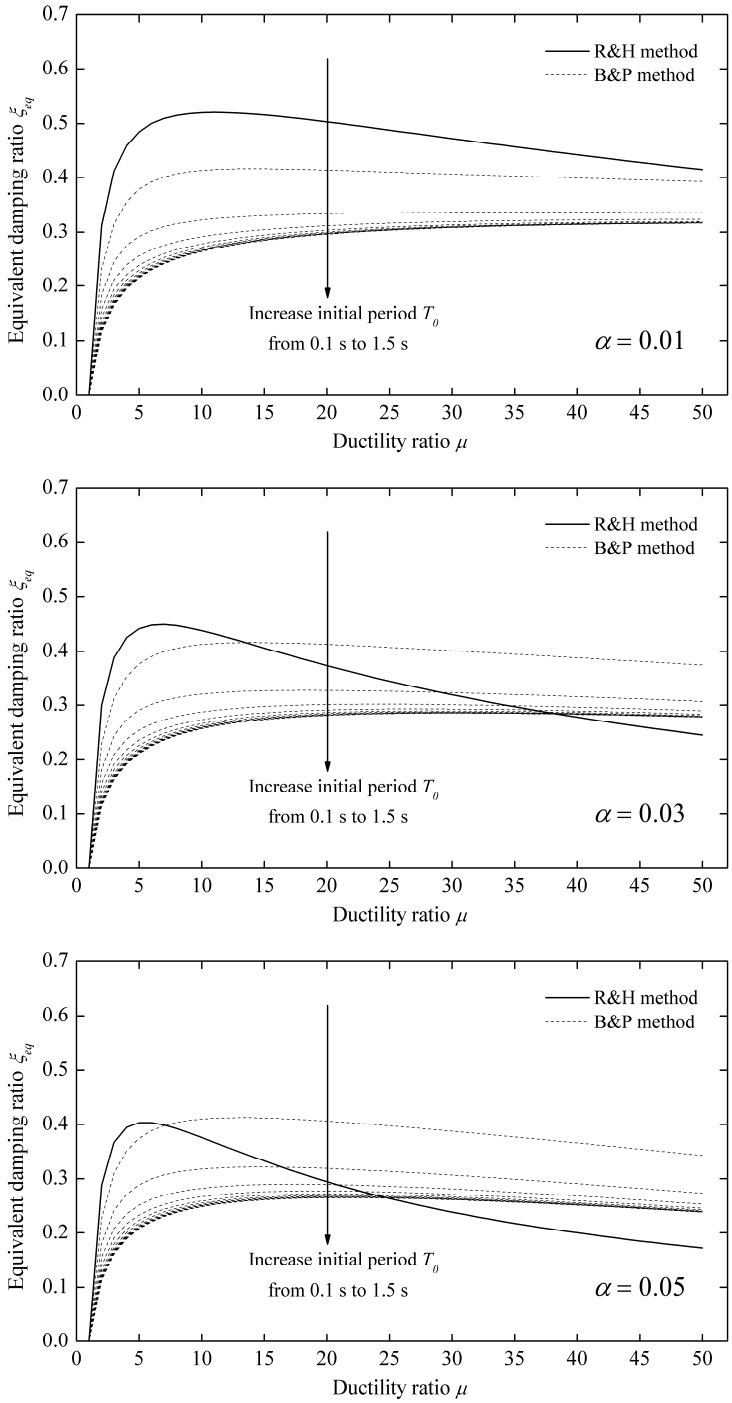

Fig. 34 Comparison of equivalent damping ratios between R&H method and B&P method (continued)

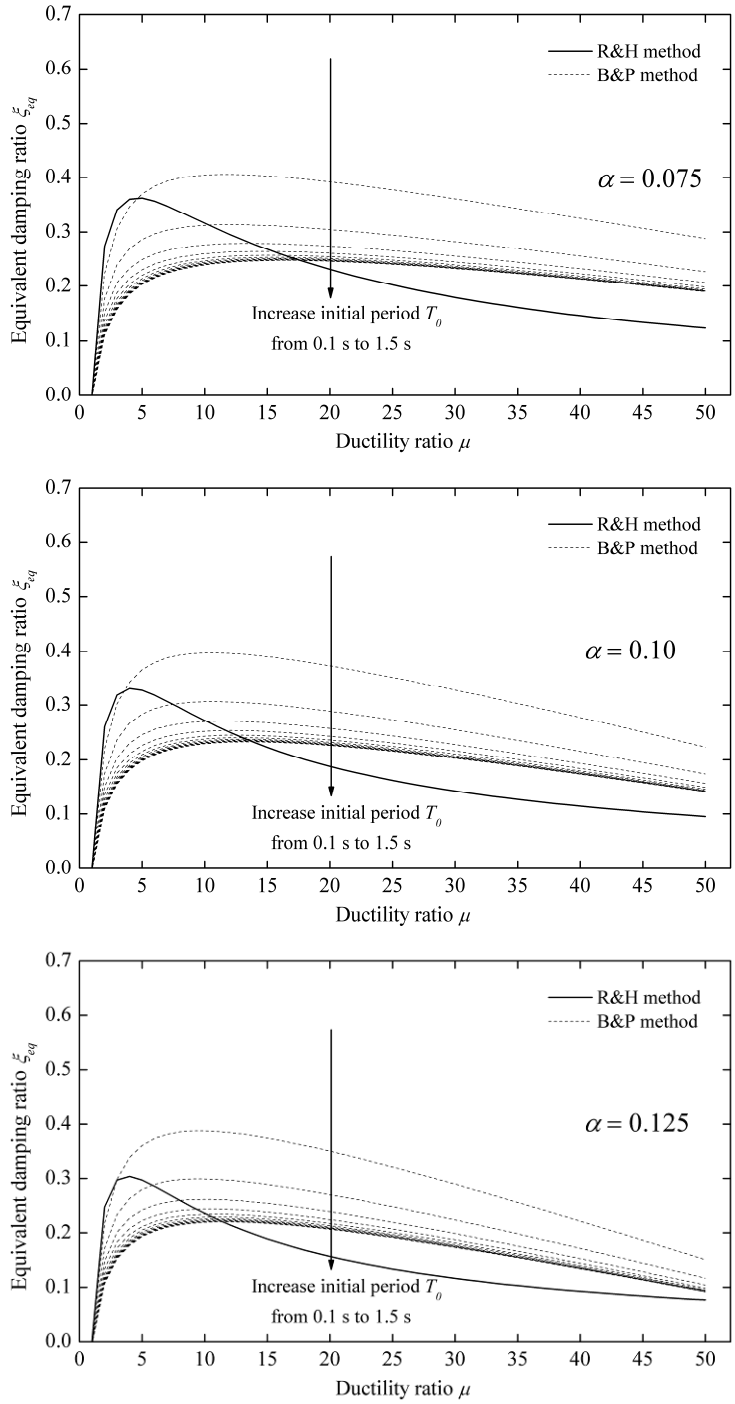

Fig. 34 Comparison of equivalent damping ratios between R&H method and B&P method (continued)

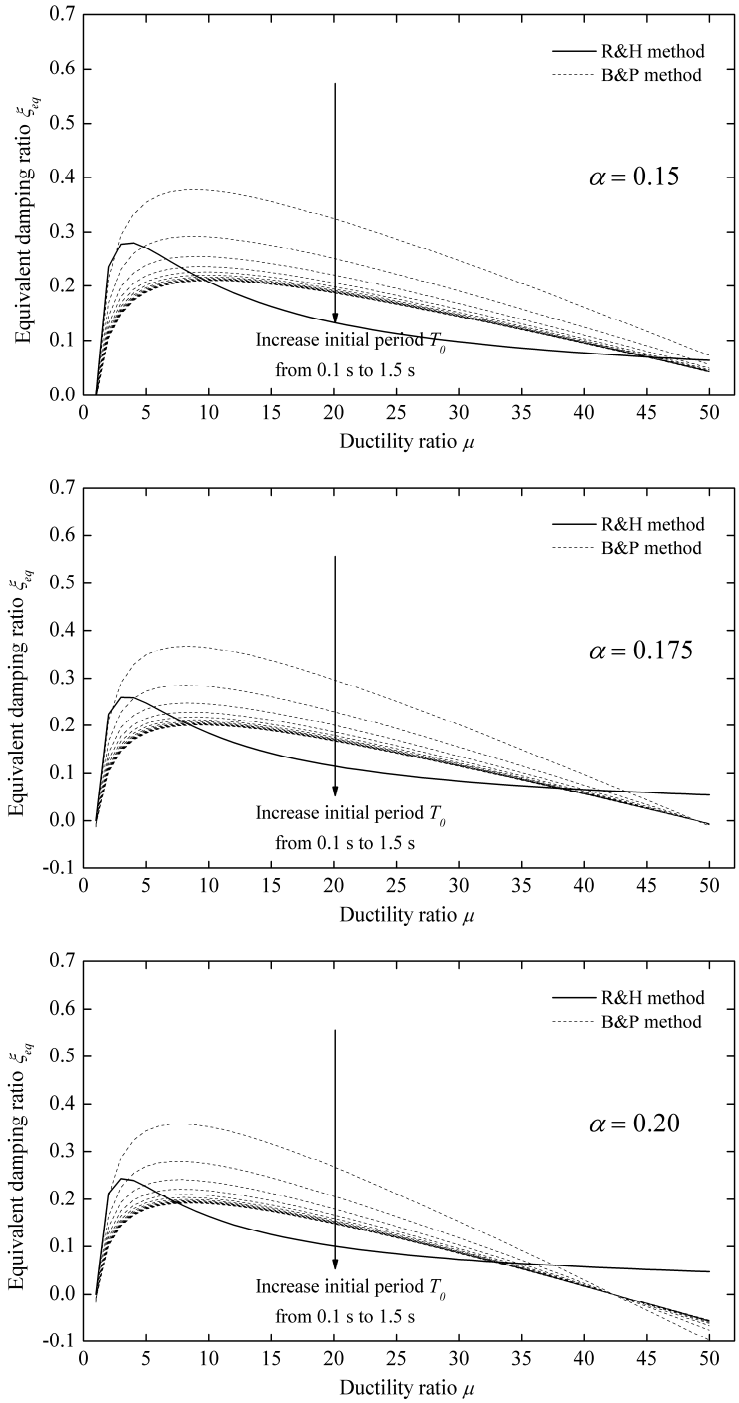

Fig. 34 Comparison of equivalent damping ratios between R&H method and B&P method (continued)

It can be observed that equivalent damping ratios determined by both methods in general first increase and then decrease with increasing the ductility ratio. In addition, in both methods equivalent damping ratio decreases as the strain hardening ratio increases. Since R&H method is independent from period to period, the initial period has no influence on the equivalent damping ratio. However, B&P method is period-dependent and the computed equivalent damping ratio decreases with increasing the initial period of bilinear oscillators for a given ductility level.

Although general variation trend of equivalent damping ratio based on the investigated parameters (i.e., ductility ratio, initial period and strain hardening ratio) is similar, the values of equivalent damping ratio determined using R&H method and B&P method are much different. For strain hardening ratio equal to zero (α = 0.00), equivalent damping ratio from R&H method is much larger than that computed by B&P method for all the ductility levels. However, as the strain hardening ratio increases to 0.05, equivalent damping ratios predicted by B&P method are larger than those estimated by R&H method for SDOF systems with relatively short initial periods and high ductility ratios. It can be expected that the change of equivalent damping ratio is significant with increasing the strain hardening ratio from zero to 0.05, which is also the reason that interval of strain hardening ratio between 0.00 and 0.05 is 0.02 while that from 0.05 to 0.20 is equal to 0.025. With increasing strain hardening ratio to 0.20, equivalent damping ratio estimated by B&P method is again less than that computed by R&H method for large ductility ratio, even a negative value could be obtained for strain hardening ratio equal to 0.20 when ductility ratio is greater than 44. Due to the same method (secant stiffness) to predict the equivalent stiffness (or equivalent period), differences of computed maximum inelastic displacement between both methods could be expected based on comparison of the determined equivalent damping ratios.

Twelve different real earthquake records (Table 3) selected from the Pacific Earthquake Engineering Research Center are still employed here to evaluate the estimation accuracy of both R&H method and B&P method. The assessment methodology is identical to that described in Chapter 3.2 except the incorporation of strain hardening ratio. Similarly, mean ratio *R* is used to evaluate the prediction accuracy of both methods. However, to examine the diversion of the measured ratios, the coefficient of variation C_v is used instead of the standard deviation, which can be defined as the ratio of the standard deviation to the mean:

$$C_v = \sigma(R) / R \tag{71}$$

4.1.2 Estimation accuracy of R&H method for SDOF systems

To clearly present the influence of different parameters on the estimation accuracy of R&H method, mean ratio *R* is plotted against initial period for different ductility ratios and against ductility ratio for different initial periods in Figs. 35-44.

For strain hardening ratio equal to zero, the estimation accuracy significantly depends on initial period. As the initial period increases, the measured ratios *R* first decrease and then keep constant. However, the variation with ductility ratio is less sensitive. On average, the maximum displacement is predicted as only 60% of the exact maximum inelastic displacement except for SDOF oscillators with short initial period. This may be explained by the extremely high damping ratio produced by R&H method (see Fig. 34 with α = 0), which is even greater than 0.6.

It is seen that the estimation accuracy in general decreases with increasing initial period and increases with increasing the ductility ratio for all the considered strain hardening ratios. In addition, the maximum inelastic displacement is underestimated by R&H method for ductility ratios less than 10. However, for relatively high ductility ratio, good estimates of maximum displacement could be produced. Strain hardening ratio has a significant influence on the estimation when it is less than 0.05, but the mean ratio *R* increases slightly with increasing strain hardening ratio from 0.05 to 0.20.

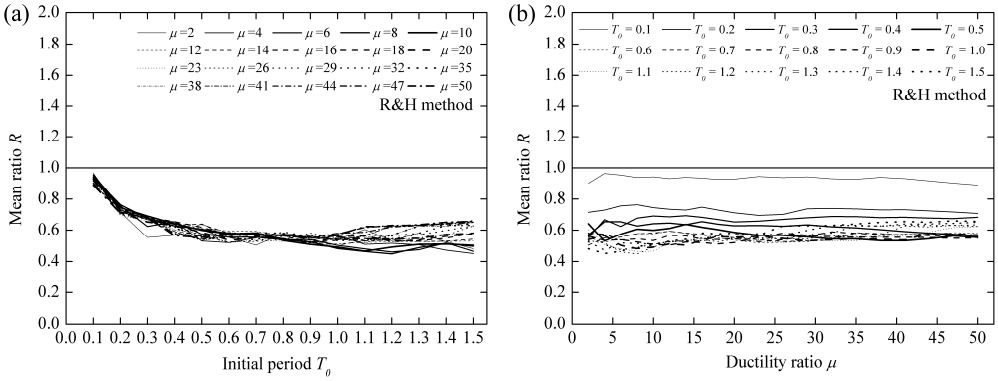

Fig. 35 Estimation accuracy of R&H method based on α = 0.00: (a) against initial period for different ductility ratios and (b) against ductility ratio for different initial periods

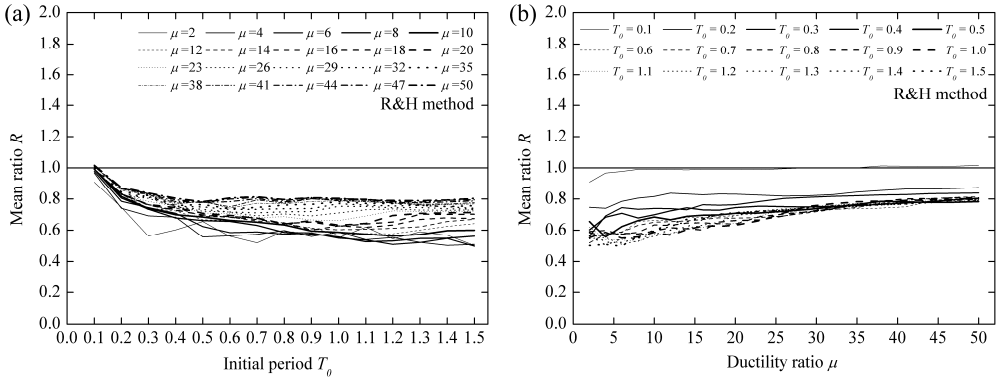

Fig. 36 Estimation accuracy of R&H method based on α = 0.01: (a) against initial period for different ductility ratios and (b) against ductility ratio for different initial periods

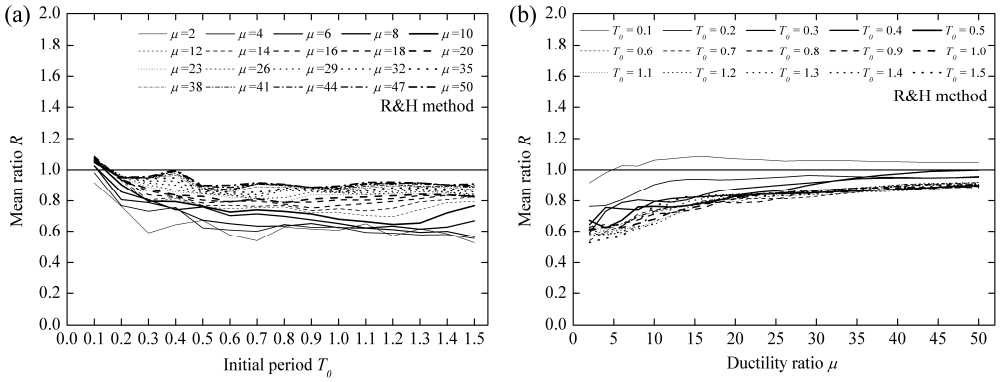

Fig. 37 Estimation accuracy of R&H method based on α = 0.03: (a) against initial period for different ductility ratios and (b) against ductility ratio for different initial periods

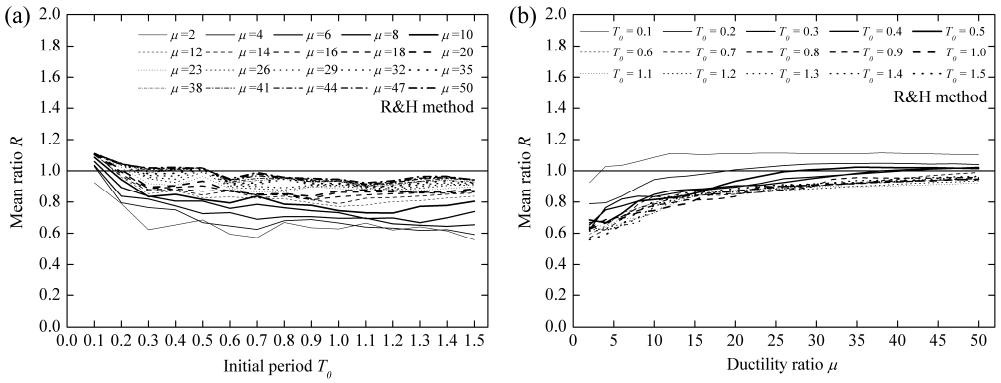

Fig. 38 Estimation accuracy of R&H method based on α = 0.05: (a) against initial period for different ductility ratios and (b) against ductility ratio for different initial periods

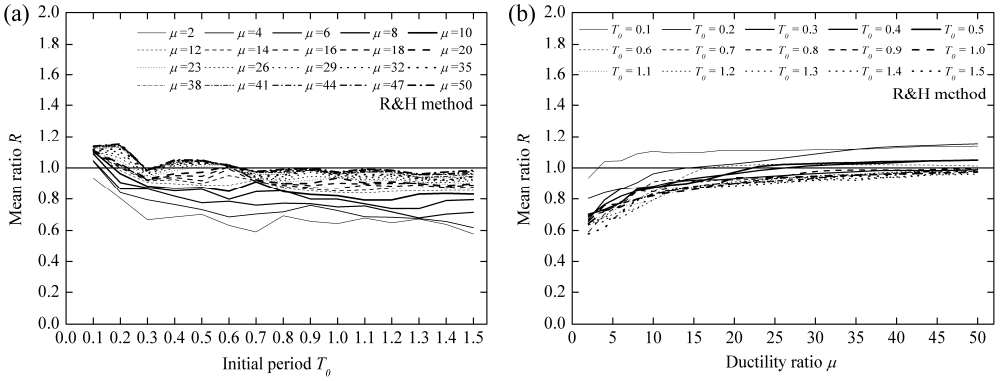

Fig. 39 Estimation accuracy of R&H method based on α = 0.075: (a) against initial period for different ductility ratios and (b) against ductility ratio for different initial periods

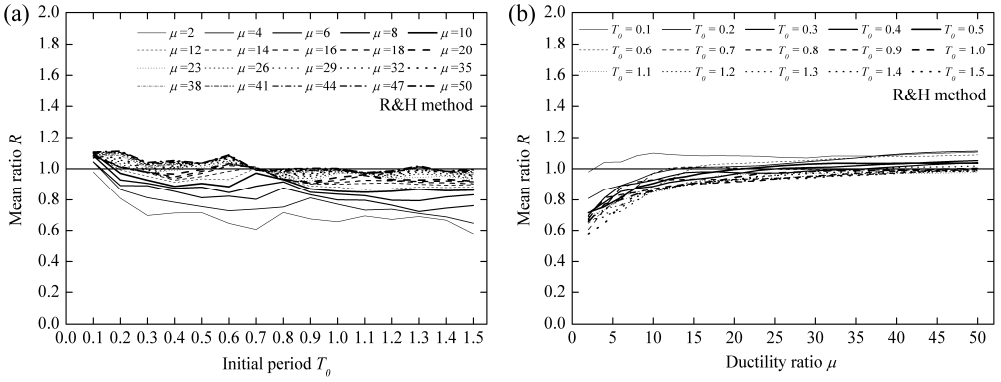

Fig. 40 Estimation accuracy of R&H method based on α = 0.10: (a) against initial period for different ductility ratios and (b) against ductility ratio for different initial periods

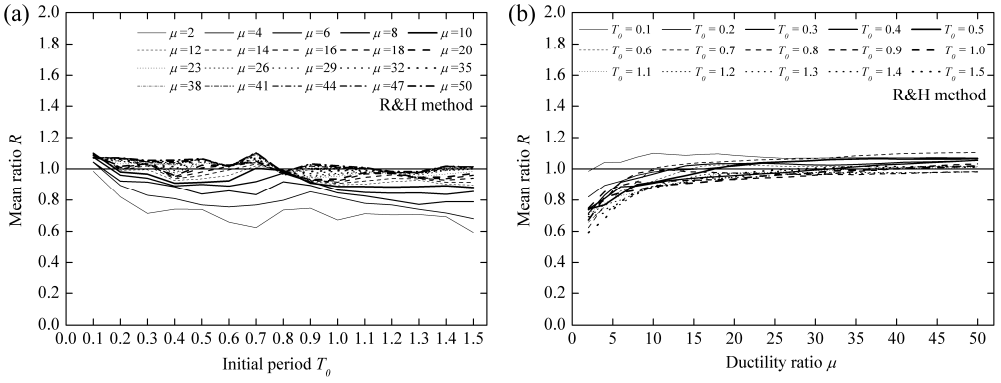

Fig. 41 Estimation accuracy of R&H method based on α = 0.125: (a) against initial period for different ductility ratios and (b) against ductility ratio for different initial periods

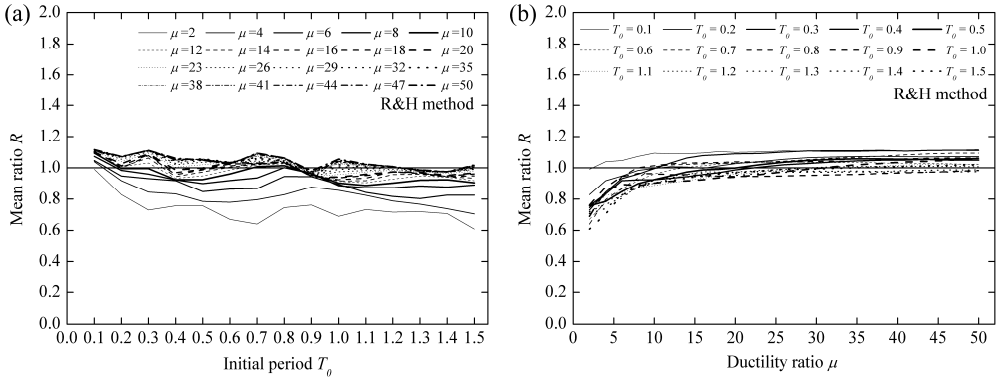

Fig. 42 Estimation accuracy of R&H method based on α = 0.15: (a) against initial period for different ductility ratios and (b) against ductility ratio for different initial periods

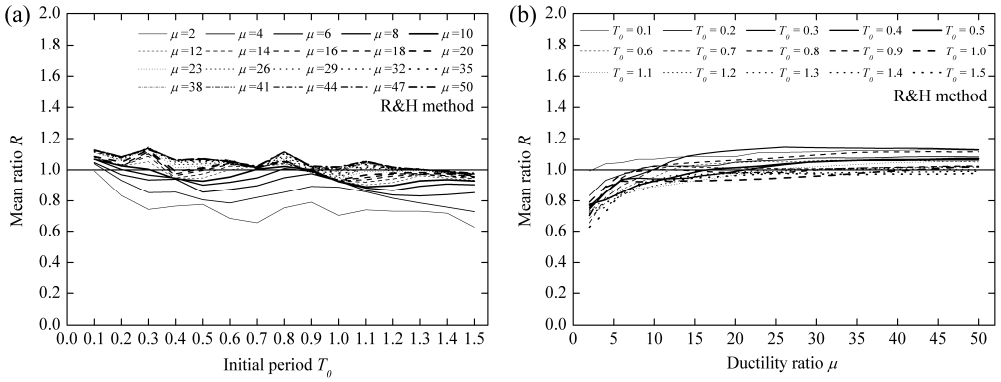

Fig. 43 Estimation accuracy of R&H method based on α = 0.175: (a) against initial period for different ductility ratios and (b) against ductility ratio for different initial periods

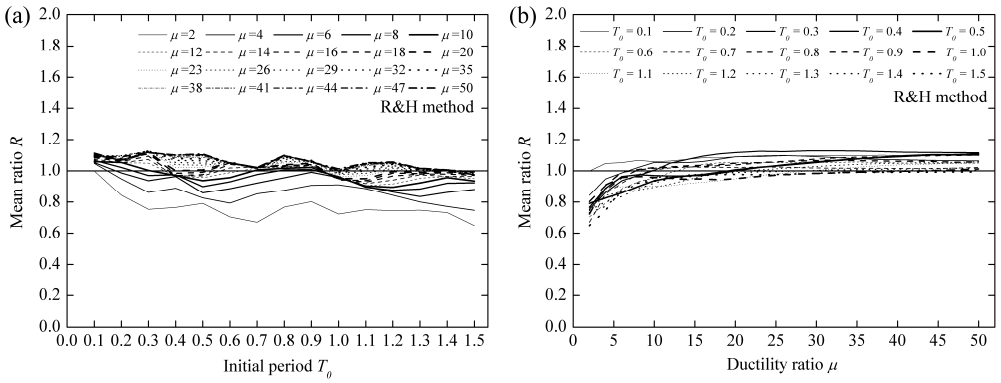

Fig. 44 Estimation accuracy of R&H method based on α = 0.20: (a) against initial period for different ductility ratios and (b) against ductility ratio for different initial periods

The coefficients of variation computed by R&H method are presented in Figs. 45-54. As can be observed from these figures, the initial period has no significant effect on C_v and C_v generally decreases with increasing the ductility ratio. It is found that the C_v also decreases as the strain hardening ratio increases from 0.00 to 0.20. For strain hardening ratio equal to 0.00, C_v varies between 20% and 40%. In addition, C_v is almost independent on the initial period and ductility level of SDOF systems. For strain hardening ratio equal to 0.20, C_v is in general less than 20% except for SDOF systems with low ductility ratios.

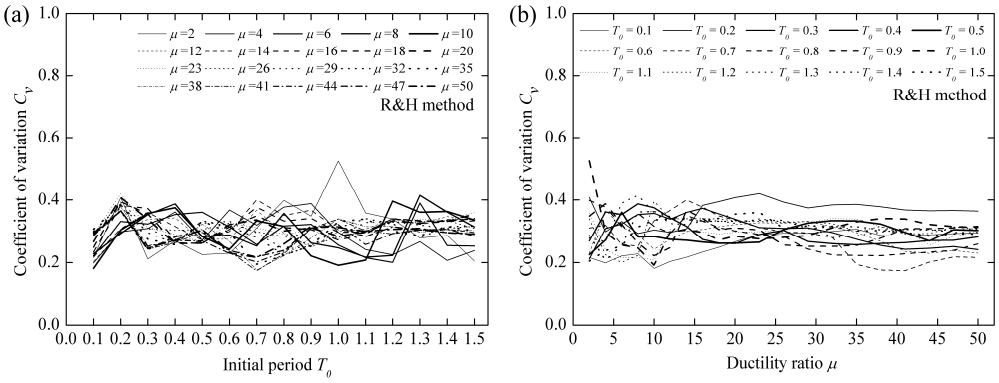

Fig. 45 Coefficient of variation computed based on R&H method and α = 0.00: (a) against initial period for different ductility ratios and (b) against ductility ratio for different initial periods

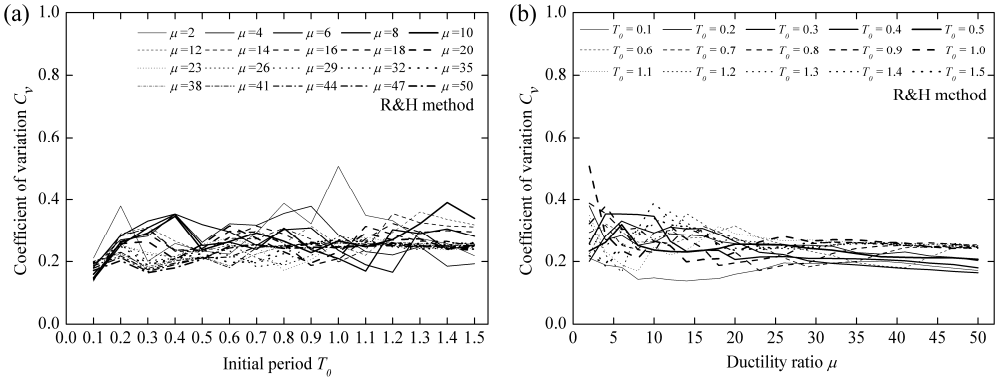

Fig. 46 Coefficient of variation computed based on R&H method and α = 0.01: (a) against initial period for different ductility ratios and (b) against ductility ratio for different initial periods

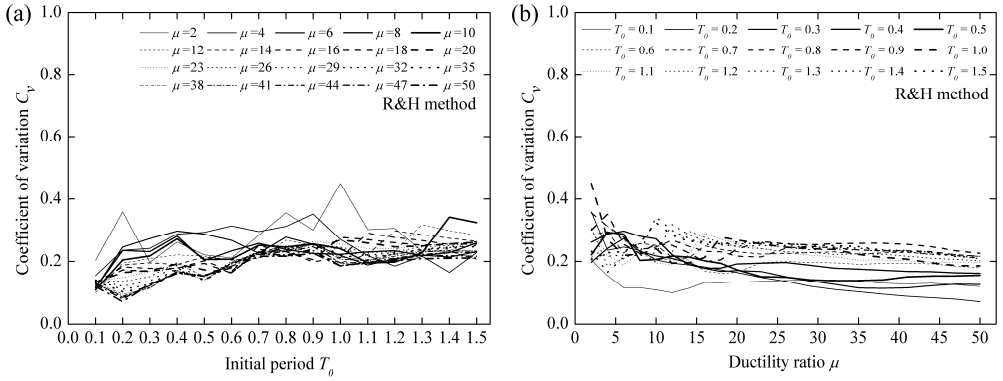

Fig. 47 Coefficient of variation computed based on R&H method and α = 0.03: (a) against initial period for different ductility ratios and (b) against ductility ratio for different initial periods

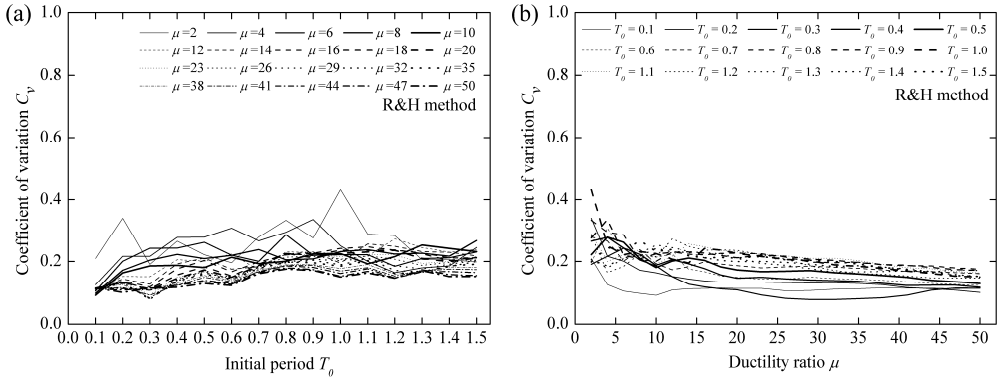

Fig. 48 Coefficient of variation computed based on R&H method and α = 0.05: (a) against initial period for different ductility ratios and (b) against ductility ratio for different initial periods

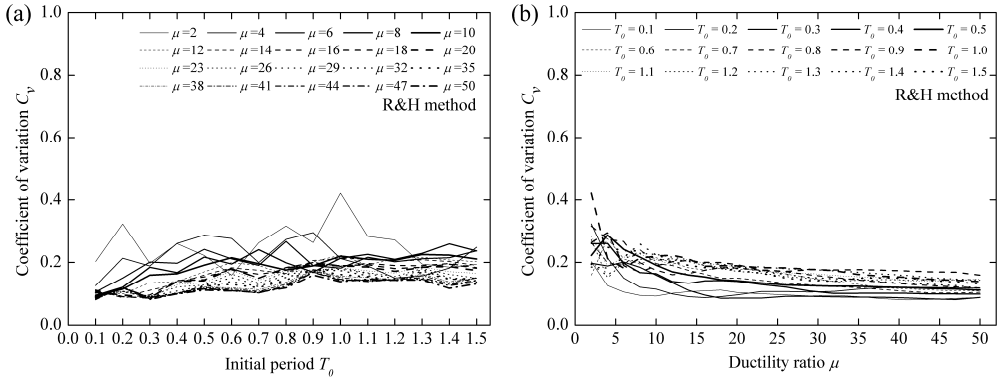

Fig. 49 Coefficient of variation computed based on R&H method and α = 0.075: (a) against initial period for different ductility ratios and (b) against ductility ratio for different initial periods

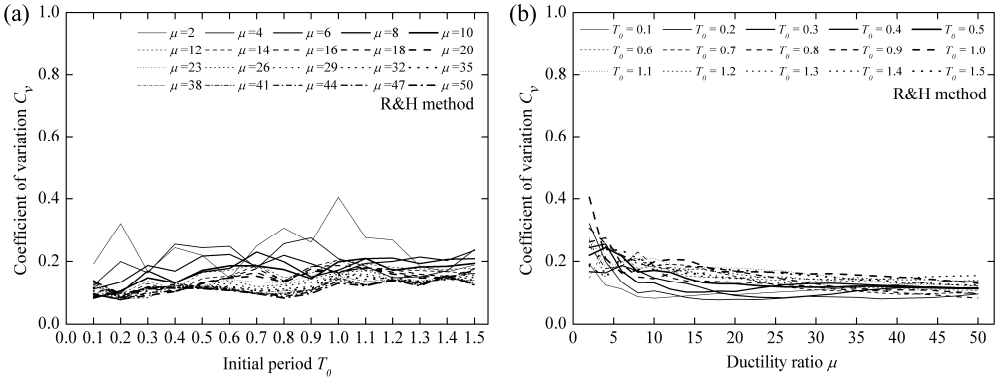

Fig. 50 Coefficient of variation computed based on R&H method and α = 0.10: (a) against initial period for different ductility ratios and (b) against ductility ratio for different initial periods

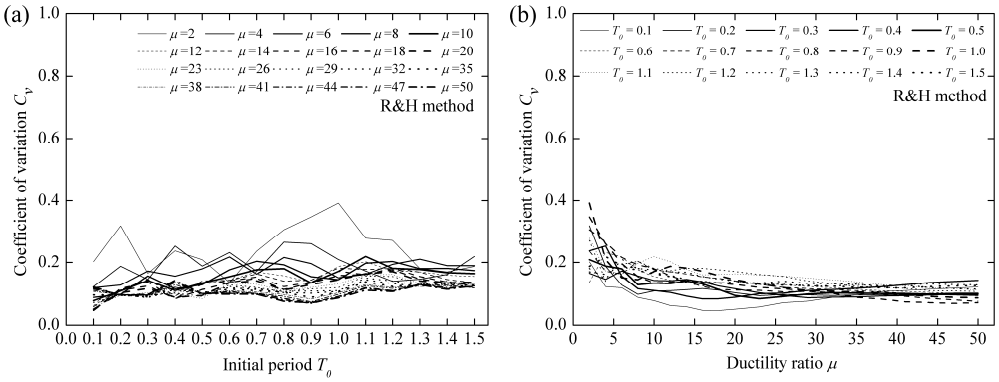

Fig. 51 Coefficient of variation computed based on R&H method and α = 0.125: (a) against initial period for different ductility ratios and (b) against ductility ratio for different initial periods

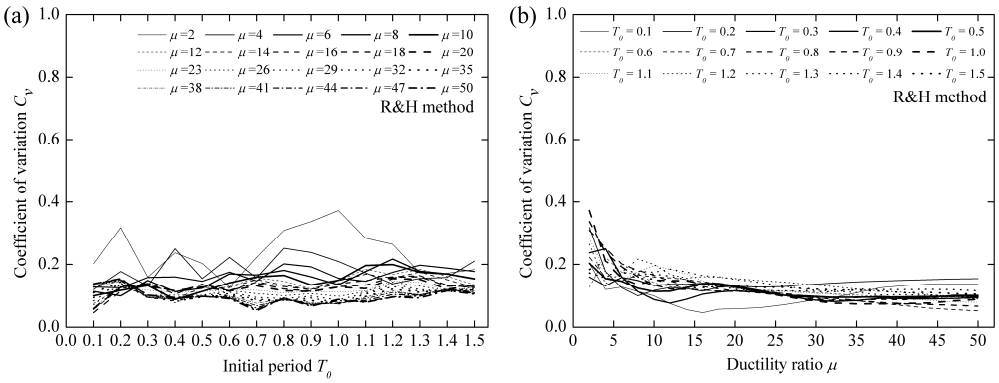

Fig. 52 Coefficient of variation computed based on R&H method and α = 0.15: (a) against initial period for different ductility ratios and (b) against ductility ratio for different initial periods

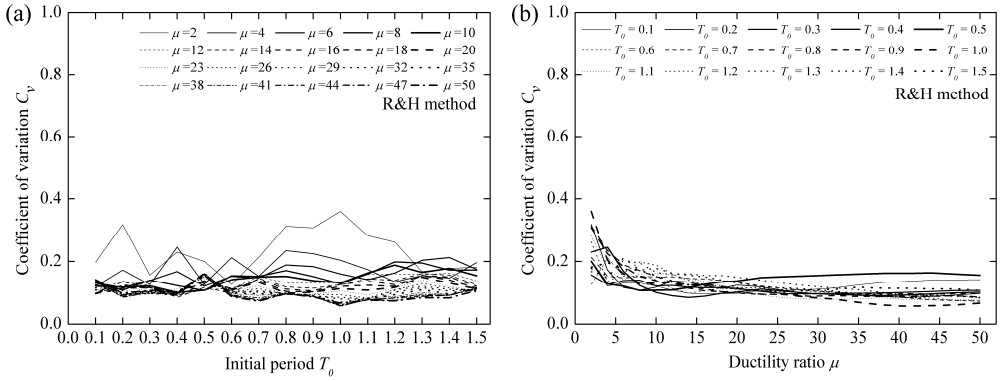

Fig. 53 Coefficient of variation computed based on R&H method and α = 0.175: (a) against initial period for different ductility ratios and (b) against ductility ratio for different initial periods

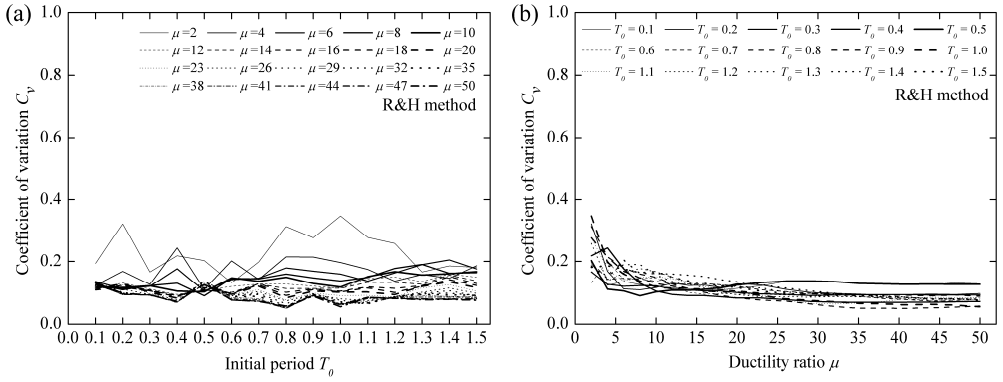

Fig. 54 Coefficient of variation computed based on R&H method and α = 0.20: (a) against initial period for different ductility ratios and (b) against ductility ratio for different initial periods

4.1.3 Estimation accuracy of B&P method for SDOF systems

The mean ratio *R* obtained using B&P method is plotted in Figs. 55-64 for different strain hardening ratios. Considering the zero strain hardening ratio, it is found that the estimation accuracy of the maximum displacement response is largely improved when compared to the results from R&H method. Furthermore, the results are still strongly related to the initial period. As initial period increases, the mean ratio in general deceases. The maximum displacement is overestimated for SDOF systems with short initial period and underestimated for SDOF systems with long initial period. Since the ductility ratio used in B&P method is limited to 6, better accuracy could be found for low ductility ratios than that for high ones. However, errors of the

maximum displacement between nonlinear and linear time history analyses are still quite large in most cases.

Considering the strain hardening ratio equal to 0.05, the mean ratios could be considered independent of the initial period and they in general decease with increasing the ductility ratio. As the strain hardening ratio increases from 0.05 to 0.20, good estimation accuracy could be always obtained when the ductility ratio is less than 10. But, for ductility ratios greater than 10, the mean ratios are significantly related to the ductility ratio. When the strain hardening ratio is equal to 0.2, extremely high mean ratio could be observed for high ductility ratio, which can be explained by the negative equivalent damping ratios determined by B&P method (see Fig. 34 for α = 0.20).

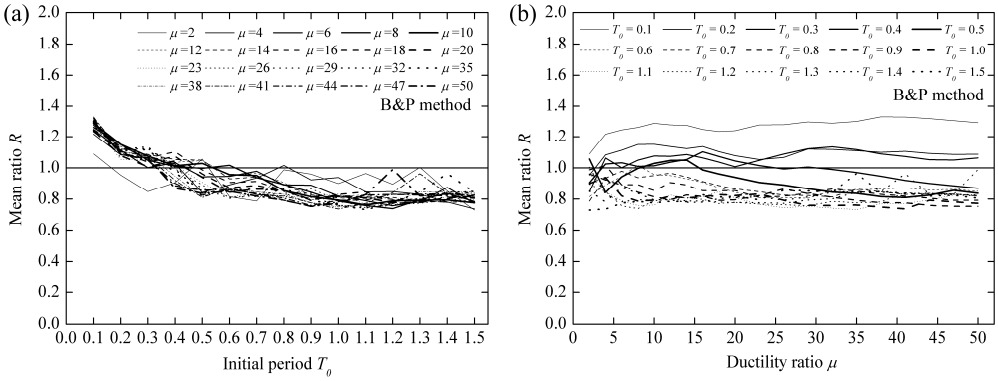

Fig. 55 Estimation accuracy of B&P method based on α = 0.00: (a) against initial period for different ductility ratios and (b) against ductility ratio for different initial periods

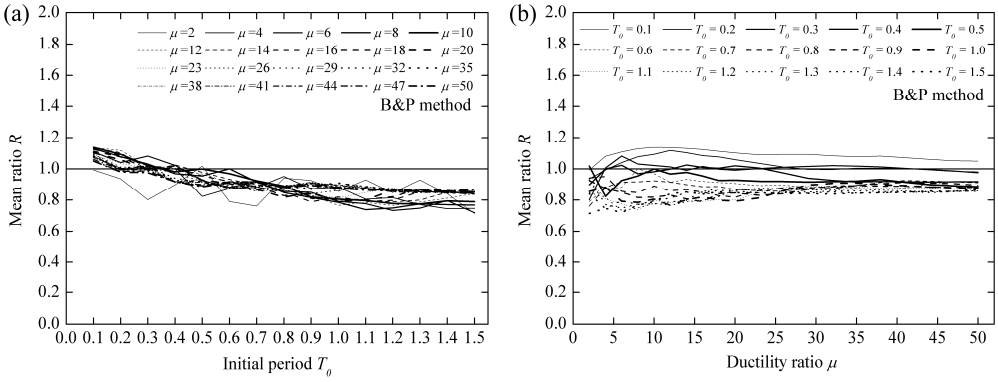

Fig. 56 Estimation accuracy of B&P method based on α = 0.01: (a) against initial period for different ductility ratios and (b) against ductility ratio for different initial periods

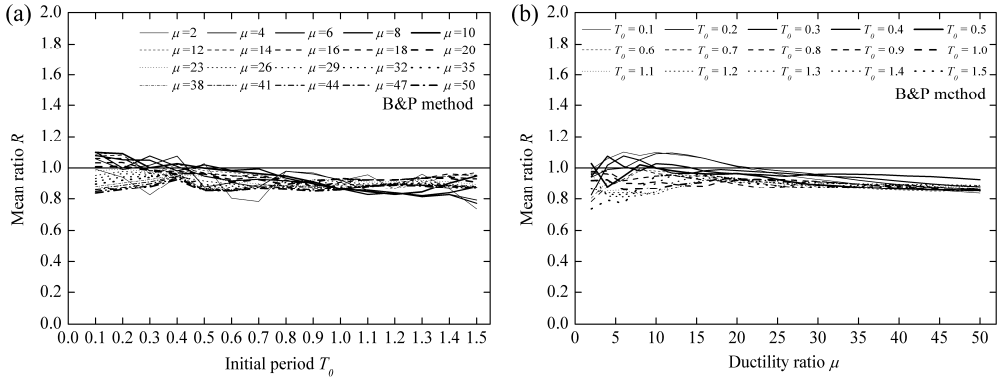

Fig. 57 Estimation accuracy of B&P method based on α = 0.03: (a) against initial period for different ductility ratios and (b) against ductility ratio for different initial periods

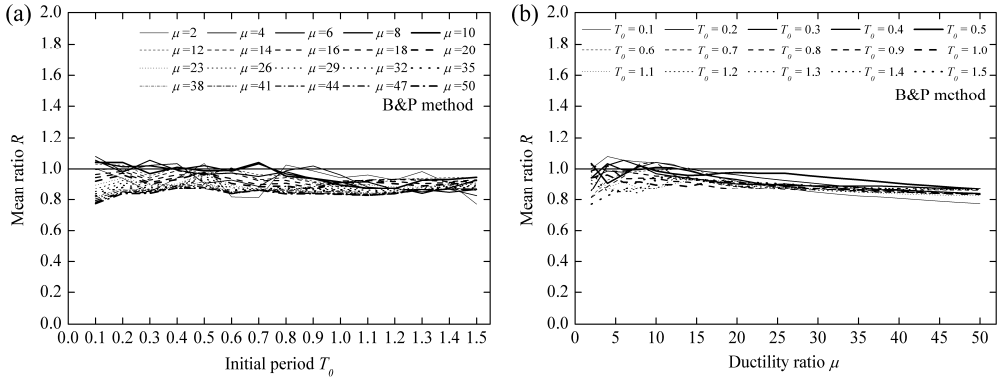

Fig. 58 Estimation accuracy of B&P method based on α = 0.05: (a) against initial period for different ductility ratios and (b) against ductility ratio for different initial periods

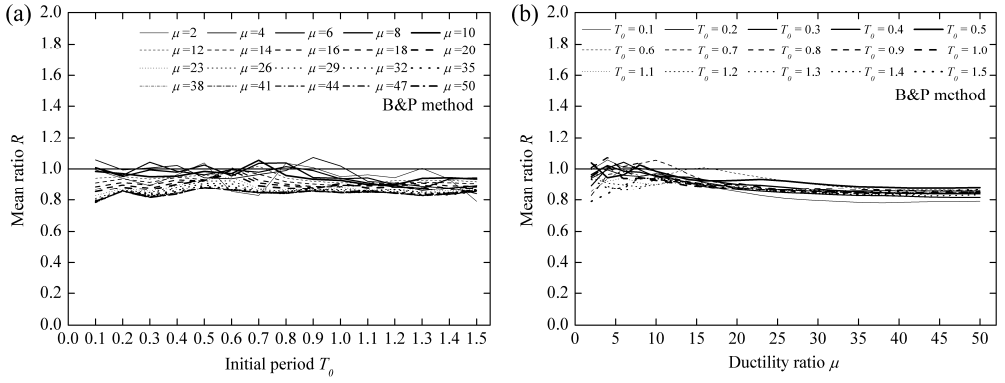

Fig. 59 Estimation accuracy of B&P method based on α = 0.075: (a) against initial period for different ductility ratios and (b) against ductility ratio for different initial periods

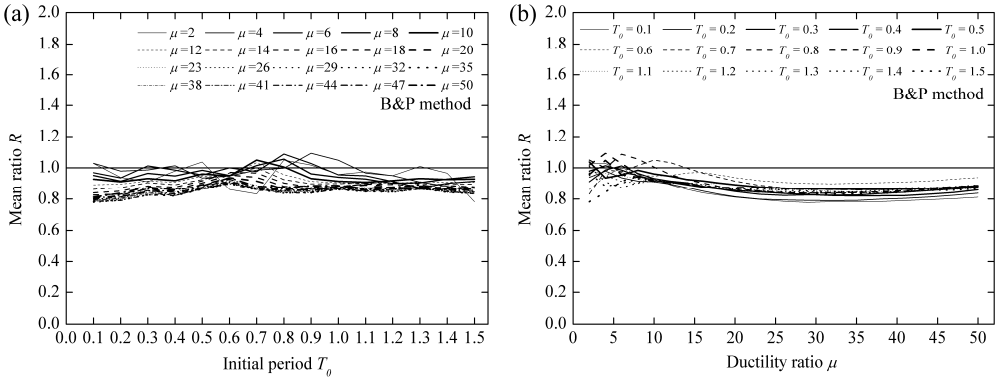

Fig. 60 Estimation accuracy of B&P method based on α = 0.10: (a) against initial period for different ductility ratios and (b) against ductility ratio for different initial periods

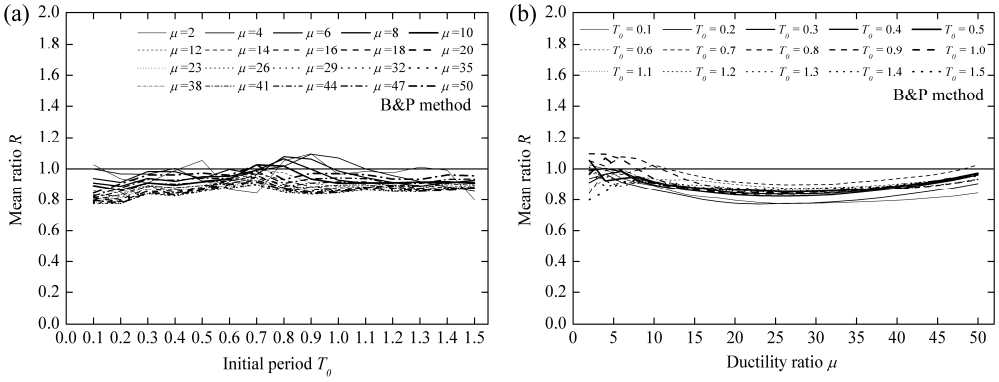

Fig. 61 Estimation accuracy of B&P method based on α = 0.125: (a) against initial period for different ductility ratios and (b) against ductility ratio for different initial periods

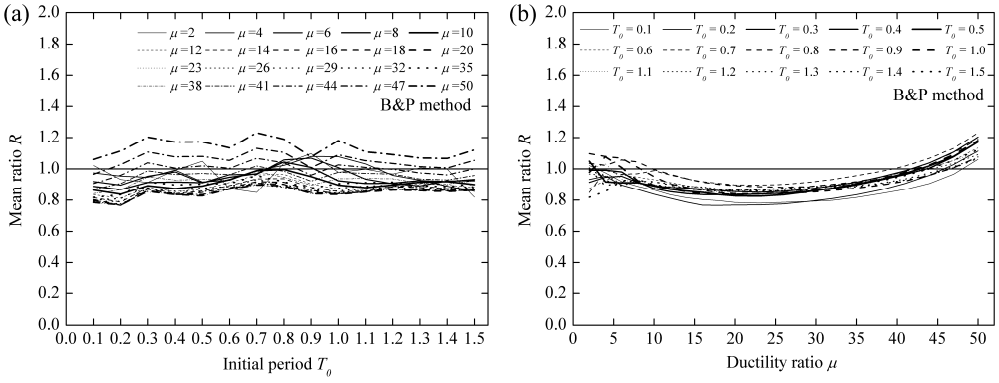

Fig. 62 Estimation accuracy of B&P method based on α = 0.15: (a) against initial period for different ductility ratios and (b) against ductility ratio for different initial periods

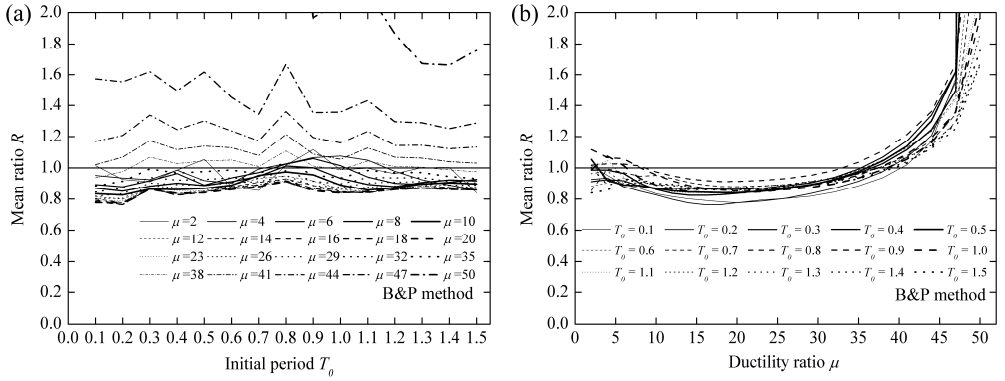

Fig. 63 Estimation accuracy of B&P method based on α = 0.175: (a) against initial period for different ductility ratios and (b) against ductility ratio for different initial periods

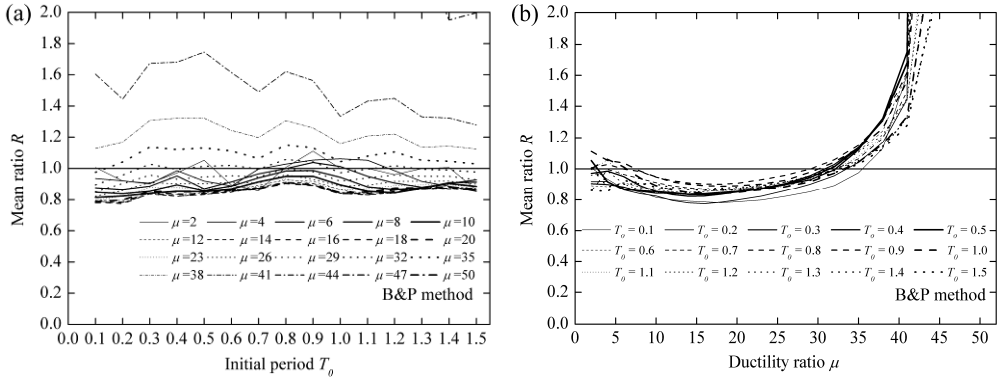

Fig. 64 Estimation accuracy of B&P method based on α = 0.20: (a) against initial period for different ductility ratios and (b) against ductility ratio for different initial periods

Regarding the coefficient of variation C_v obtained from B&P method (see Figs. 65-74), it is on average between 20% and 40% when strain hardening ratio is equal to 0.00, which is similar to R&H method. With increasing strain hardening ratio, smaller C_v could be found. In general, C_v computed by R&H method and B&P method is comparable. However, due to the existence of negative equivalent damping ratio, extremely large C_V can be observed when the strain hardening ratio is greater than 0.175 and the ductility ratio is greater than 40.

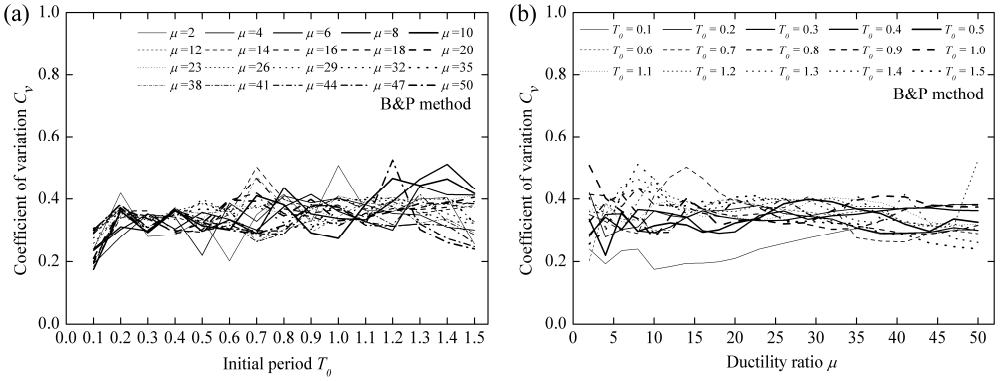

Fig. 65 Coefficient of variation computed based on B&P method and α = 0.00: (a) against initial period for different ductility ratios and (b) against ductility ratio for different initial periods

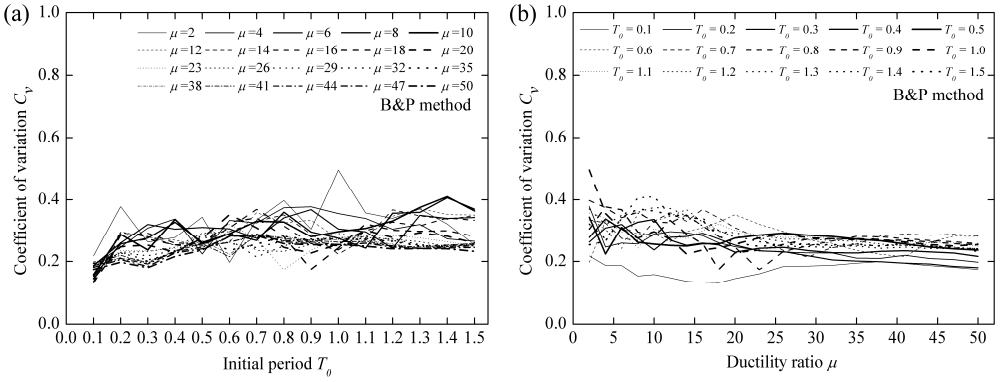

Fig. 66 Coefficient of variation computed based on B&P method and α = 0.01: (a) against initial period for different ductility ratios and (b) against ductility ratio for different initial periods

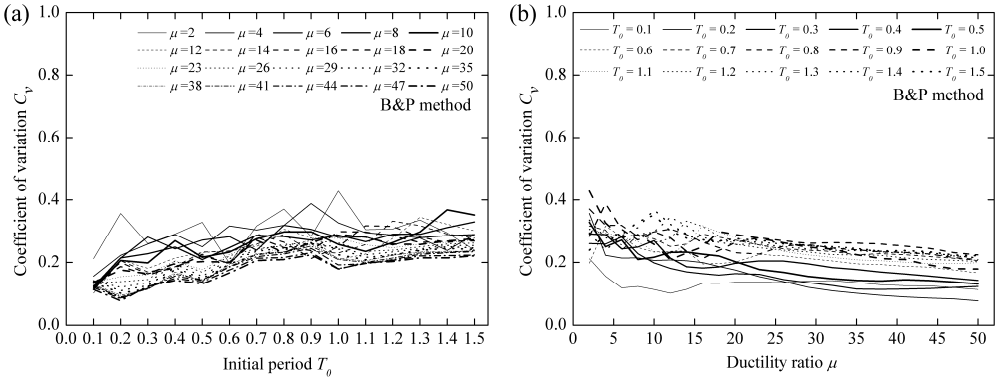

Fig. 67 Coefficient of variation computed based on B&P method and α = 0.03: (a) against initial period for different ductility ratios and (b) against ductility ratio for different initial periods

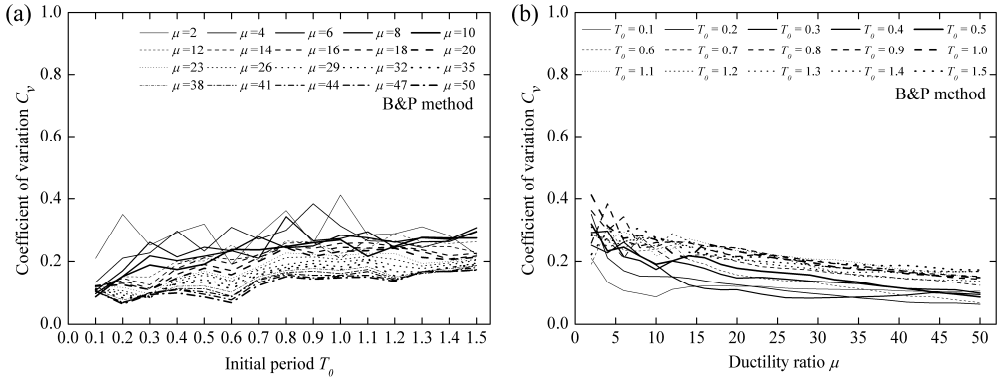

Fig. 68 Coefficient of variation computed based on B&P method and α = 0.05: (a) against initial period for different ductility ratios and (b) against ductility ratio for different initial periods

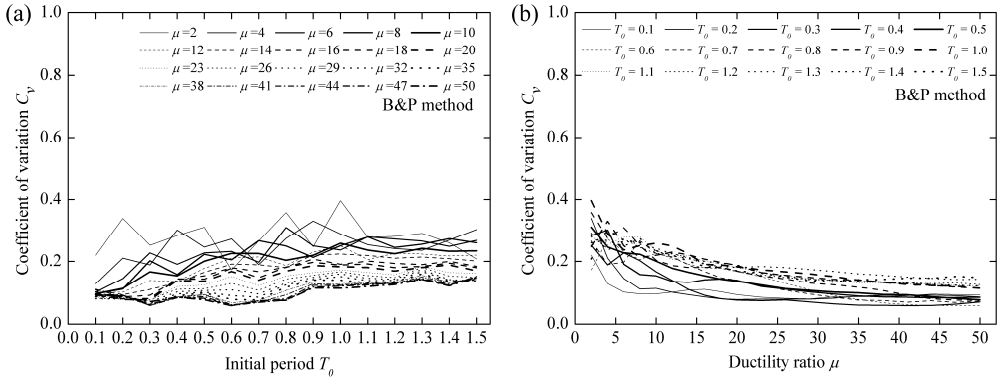

Fig. 69 Coefficient of variation computed based on B&P method and α = 0.075: (a) against initial period for different ductility ratios and (b) against ductility ratio for different initial periods

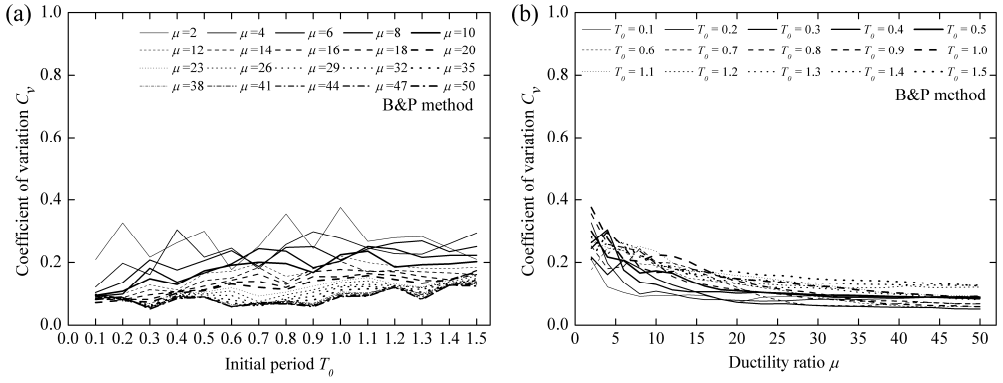

Fig. 70 Coefficient of variation computed based on B&P method and α = 0.10: (a) against initial period for different ductility ratios and (b) against ductility ratio for different initial periods

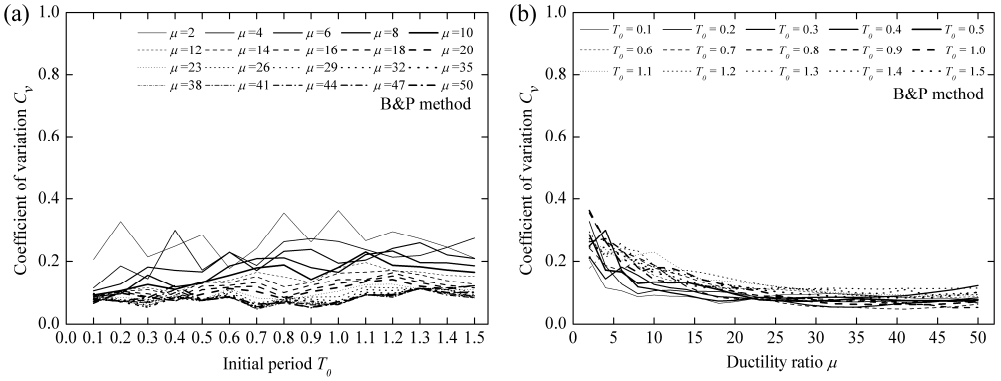

Fig. 71 Coefficient of variation computed based on B&P method and α = 0.125: (a) against initial period for different ductility ratios and (b) against ductility ratio for different initial periods

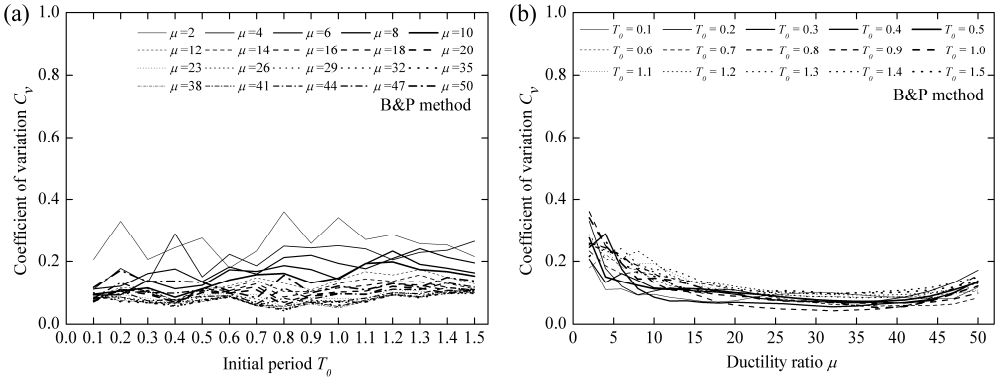

Fig. 72 Coefficient of variation computed based on B&P method and α = 0.15: (a) against initial period for different ductility ratios and (b) against ductility ratio for different initial periods

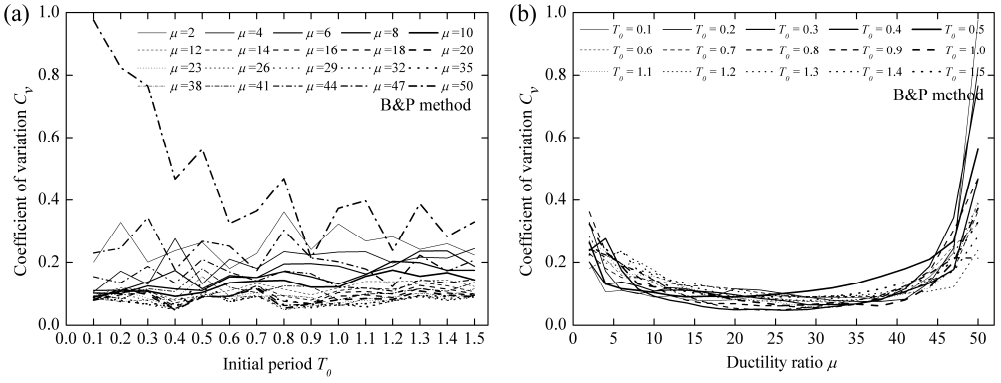

Fig. 73 Coefficient of variation computed based on B&P method and α = 0.175: (a) against initial period for different ductility ratios and (b) against ductility ratio for different initial periods

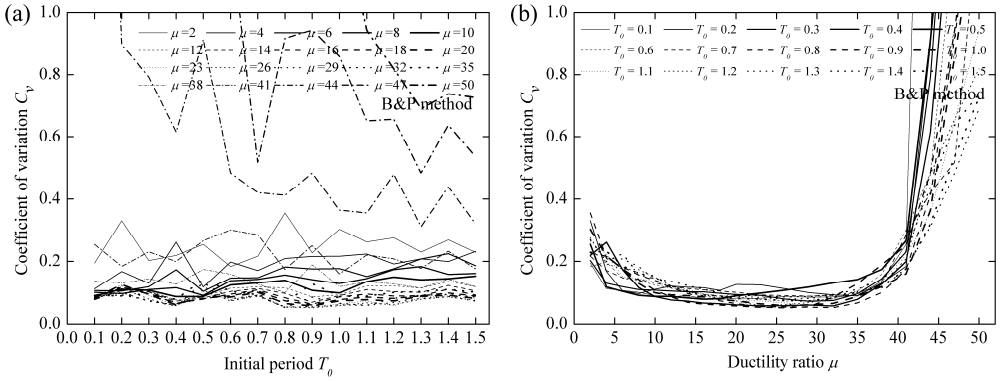

Fig. 74 Coefficient of variation computed based on B&P method and α = 0.20: (a) against initial period for different ductility ratios and (b) against ductility ratio for different initial periods

4.1.4 Discussion

In a word, according to the above observations, R&H method leads to better estimates of the maximum inelastic displacement for bilinear oscillators with relatively high ductility ratio. In fact, several requirements have been specified to make R&H method valid in many modern structural codes. The requirements usually involve the limitation of equivalent stiffness, equivalent damping ratio, and restoring force. In general, for a given strain hardening ratio, these requirements will lead to a lower limit of ductility ratio so that good estimates of maximum displacement could be obtained.

Since B&P method is derived based on the ductility ratio up to 6, better accuracy could be always obtained for low ductility ratios than that for high ones. Although the strain hardening ratio in B&P model is assumed to be 0.2, it can be observed that better results can be produced for lower strain hardening ratio. For instance, when the strain hardening ratio is equal to 0.2 (see Fig. 64), the range of ductility ratio, where satisfied accuracy could be obtained, is from 2 to 6. However, the upper limit of this range is extended to 15 for the strain hardening ratio equal to 0.05 (see Fig. 58). However, one should note that when the strain hardening ratio decreases to zero large error still exists.

As mentioned in Chapter 3, it is seen that R&H method could give satisfied accuracy when the bilinear SDOF systems have high ductility ratio while B&P method leads to good estimates for bilinear SDOF systems with low ductility ratio. To accurately predict the maximum displacement response in the whole range of ductility ratio considered in this study, the equation of equivalent damping ratio should rep-

resent the same results as those obtained by R&H method when ductility ratio is relatively high and as those obtained by B&P method when ductility ratio is relatively low.

4.2. Optimization Analysis of SDOF Systems

Based on the results from parametric analyses, it is observed that R&H method significantly underestimates the maximum inelastic displacement response, and that the prediction accuracy is not well improved using the method proposed by Blandon and Priestley in the whole parametric space. Therefore, to obtain more accurate results, a new equation used for estimating the equivalent damping ratio is required. In order to investigate the exact damping ratio demand that minimizes the difference of maximum displacement response between nonlinear and linear time history analyses, optimization analyses are performed using genetic algorithm.

4.2.1 Optimization Procedure

The second version of “Non-dominated Sorting Genetic Algorithm” (NSGA-II) (Deb, 2002) is used for solving the optimization problems established in this section, which has the following features:

1) A sorting non-dominated procedure where all the individuals are sorted according to the level of non-domination;

2) It implements elitism which stores all non-dominated solutions, and hence enhancing convergence properties;

3) It adapts a suitable automatic mechanics based on the crowding distance in order to guarantee diversity and spread of solutions;

4) Constraints are implemented using a modified definition of dominance without the use of penalty functions.

Detailed process to perform NSGA-II optimization is presented in Fig. 75.

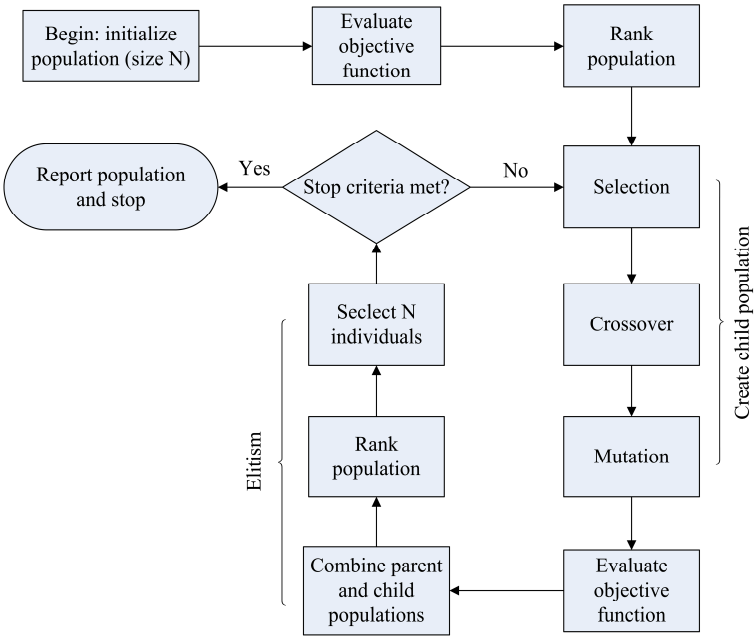

Fig. 75 Flowchart of NSGA-II optimization process

To perform optimization analyses, the variable is assumed to be equivalent damping ratio and the objective function is the relative error of maximum displacement response between nonlinear and linear time history analyses. Here, equivalent stiffness of the SDOF systems is determined by the secant stiffness at the maximum deformation. Initially, 15 damping ratios are randomly generated to form an initial population. In this research, a ranking selection based on the normalized geometric distribution is used and probability of selecting the best individual is set to be 8%. The arithmetic crossover (Kaelo & Ali, 2007), which creates children that are the weighted arithmetic mean of two parents, is used and the crossover probability is set to be 70%. To maintain genetic diversity, non-uniform mutation (Michalewicz et al., 1996) is applied and the mutation probability is assigned to be 2%.

For instance, assuming α = 0.1, T_0 = 0.5 s and μ = 10, the optimization analysis is conducted when subjected to the first ground motion in Table 3. Here, the equivalent stiffness of the bilinear system is still determined by the secant stiffness at the maximum deformation. To obtain the optimal damping ratio ξ_{opt}, the search space is assumed to range from zero to three times the damping ratio computed by R&H model. The tracks of the solution after 10 generations are plotted in Fig. 76.

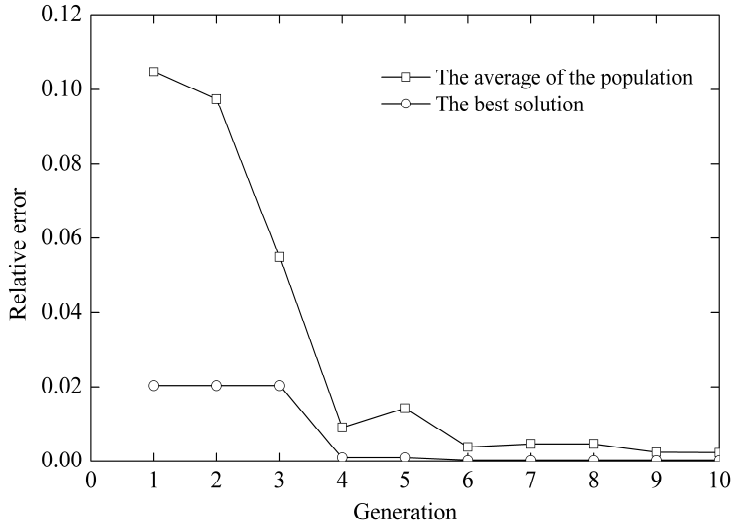

Fig. 76 The track of the NSGA-II optimization for the bilinear system with α = 0.1, T_0 = 0.5 s and μ = 10 when subjected to the first ground motion.

As can be observed, NSGA-II algorithm could find the best solution with good efficiency. In general, the optimal damping ratio can be obtained by several generations. With the optimal damping ratio, response histories of the system computed from both LTHA and NLTH are presented in Fig. 77. To get a clear understanding, only the first 10 seconds of the responses are shown here. It can be seen from this figure, the results from LTHA are in good agreement with those from NLTH. Therefore, the optimal damping ratio calculated by the NSGA-II genetic algorithm could be used to derive an improved expression of the equivalent damping ratio.

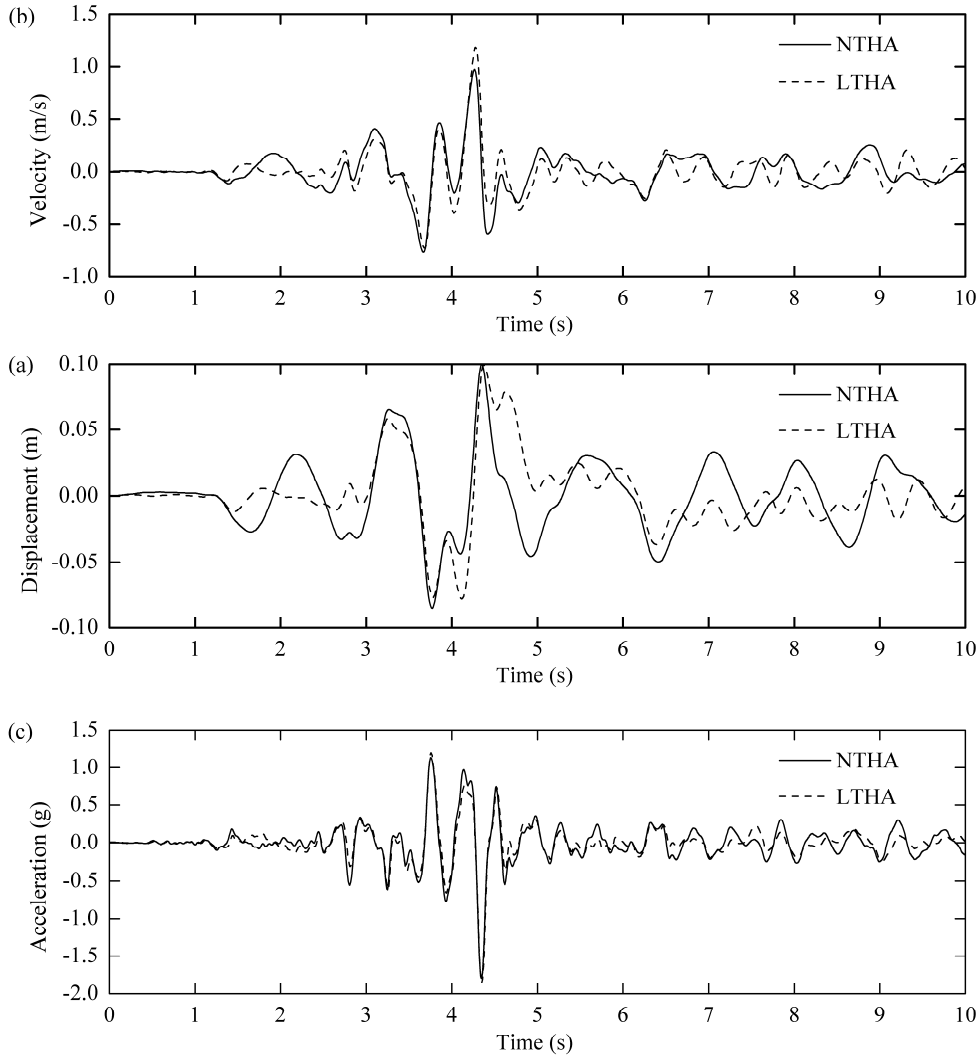

Fig. 77 Comparison of response histories between LTHA and NTHA: (a) displacement, (b) velocity and (c) acceleration

A total of 10×(15×20×12) = 36000 optimal damping ratios will be determined based on the parameter variations, i.e., 10 strain hardening ratios, 15 initial periods, 20 ductility ratios and 12 ground motions. To avoid a locally optimal damping ratio, the NSGA-II algorithm is repeated, where necessary, to make sure all the appropriate to exact maximum displacement ratios are between 0.98 and 1.02. In other words, if appropriate to exact maximum displacement ratio after 15 generations is not in between 0.98 and 1.02, the obtained damping ratio is considered not to be optimal. Then, this iteration is neglected and should be carried out again. As a result, more than 15×36000 = 540000 linear time history analyses will be performed to get 36000 optimal damping ratios for all the cases considered in this research.

To perform these optimization analyses expediently and systematically, a program is developed using MATLAB (MTALAB, 2009) in conjunction with OpenSees (Mazzoni et al. 2007), as presented in Fig. 78. In this program, the rule of OpenSees is to compute the time history response of linear or nonlinear systems, while MATLAB is used to control the global operations and the optimization analyses.

4.2.2 Optimization Results

If a specific strain hardening ratio is considered, the optimal damping ratio is averaged over the selected ground motions for each initial period and each level of displacement ductility, namely:

$$\xi_{opt}\left(i,j\right)=\frac{1}{N}\sum_{k=1}^{N}\xi\left(i,j,k\right) \tag{72}$$

where *i*, *j*, *k* is the index of initial period, ductility ratio and earthquake ground motion, respectively. *N* is the total number of earthquake ground motions.

The averaged optimal damping ratios are shown in Figs. 79-88 for different strain hardening ratios. For strain hardening ratio equal to zero, ξ_{opt} decreases with increasing the initial period of SDOF systems. However, ξ_{opt} first increases and then almost keeps constant as the ductility ratio increases. With increasing the strain hardening ratio, the optimal damping ratio ξ_{opt} decreases overall. Assuming the variation of optimal damping ratio is continuous, sharper changes are expected for small strain hardening ratios. In addition, the influence of initial period on the optimal damping ratio becomes less significant while the effect of ductility ratio is more remarkable. For strain hardening ratio greater than 0.03, the optimal damping ratio first increases and then decreases with increasing the ductility ratio. In theory, according to the equal energy dissipation principle, the equivalent damping ratio changes due to the variation of hysteretic loop of the systems when subjected to earthquake excitations. At the beginning, i.e., small ductility ratio, the hysteretic loops are so thin in horizontal direction that a small equivalent viscous damping ratio will be obtained. Then, as the ductility ratio increases, larger damping ratio can be obtained. However, when a large ductility ratio is considered, hysteretic loops become relatively thin in vertical direction due to the constant yielding strength, and equivalent viscous damping ratio decreases.

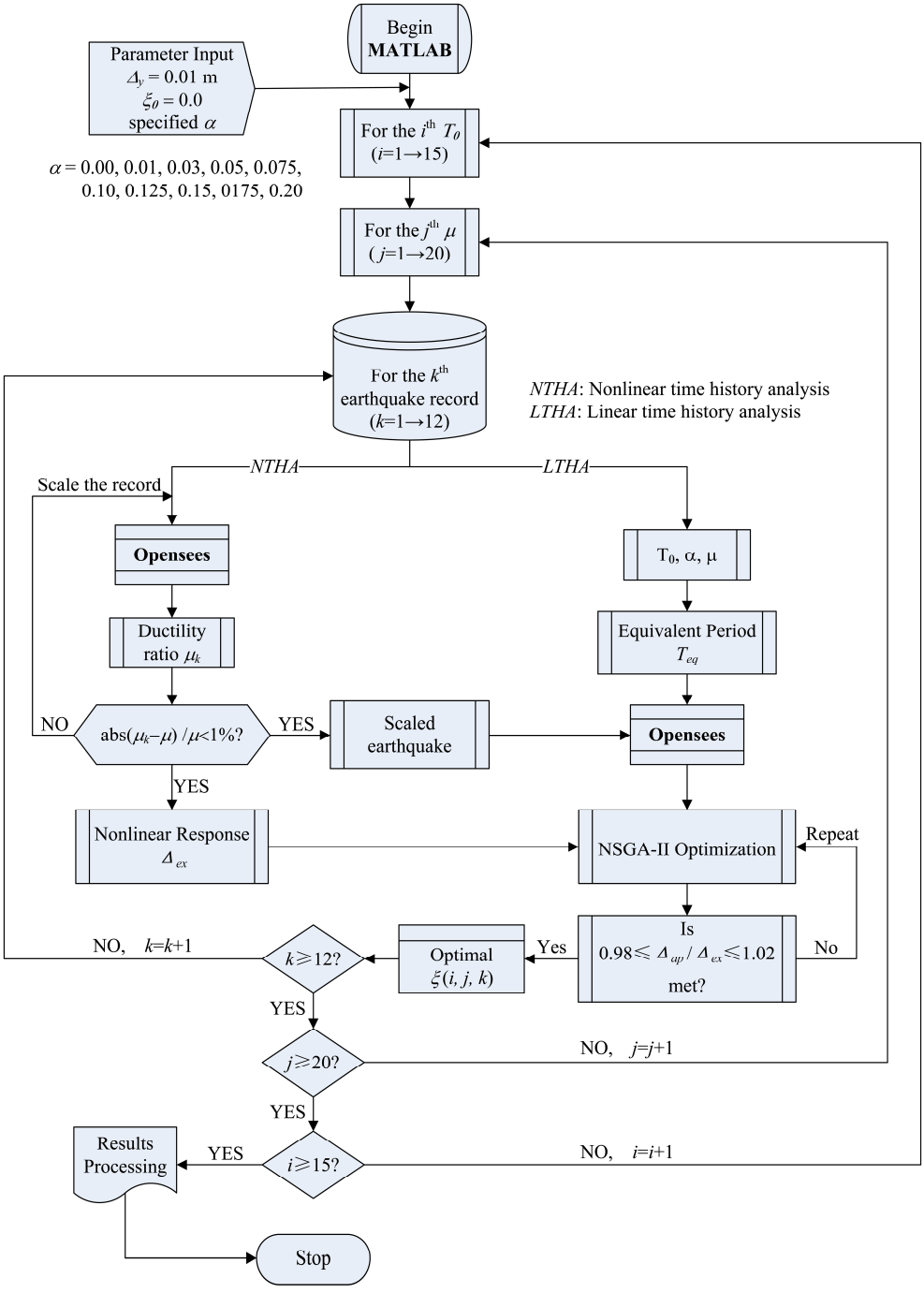

Fig. 78 Flow diagram of the proposed optimization methodology

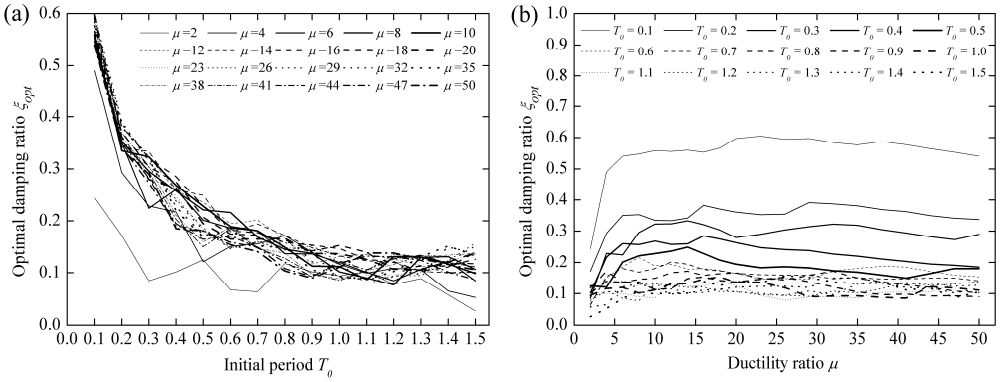

Fig. 79 The optimal damping ratios ξ_{opt} based on α = 0.00: (a) against initial period for different ductility ratios and (b) against ductility ratio for different initial periods

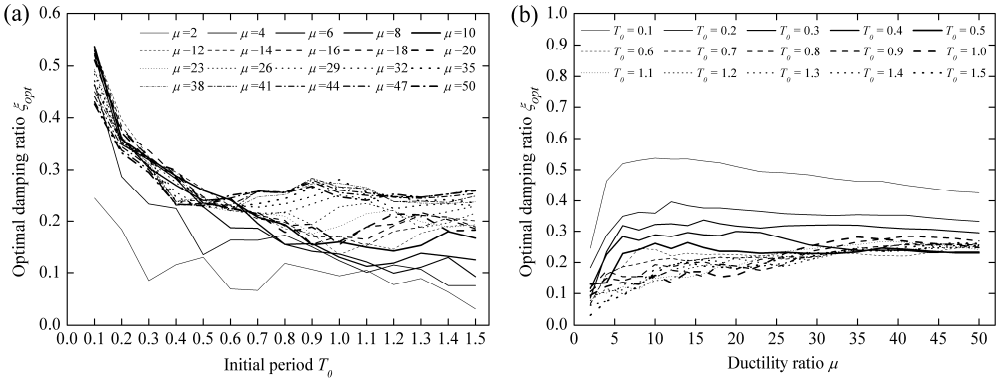

Fig. 80 The optimal damping ratios ξ_{opt} based on α = 0.01: (a) against initial period for different ductility ratios and (b) against ductility ratio for different initial periods

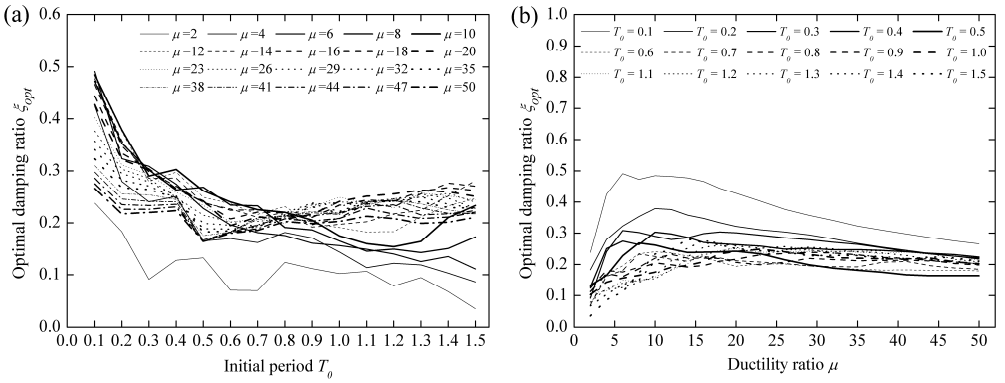

Fig. 81 The optimal damping ratios ξ_{opt} based on α = 0.03: (a) against initial period for different ductility ratios and (b) against ductility ratio for different initial periods

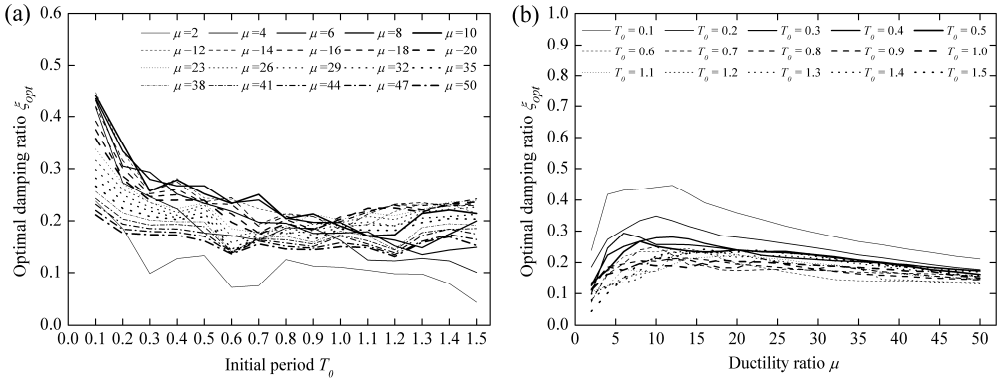

Fig. 82 The optimal damping ratios ξ_{opt} based on α = 0.05: (a) against initial period for different ductility ratios and (b) against ductility ratio for different initial periods

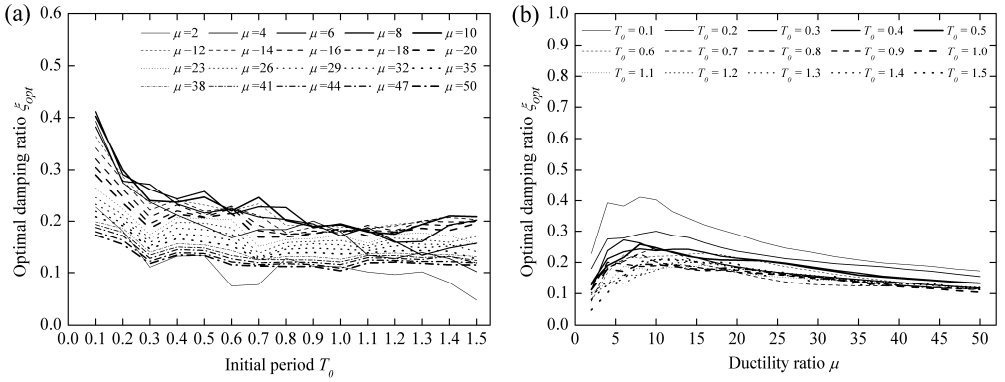

Fig. 83 The optimal damping ratios ξ_{opt} based on α = 0.075: (a) against initial period for different ductility ratios and (b) against ductility ratio for different initial periods

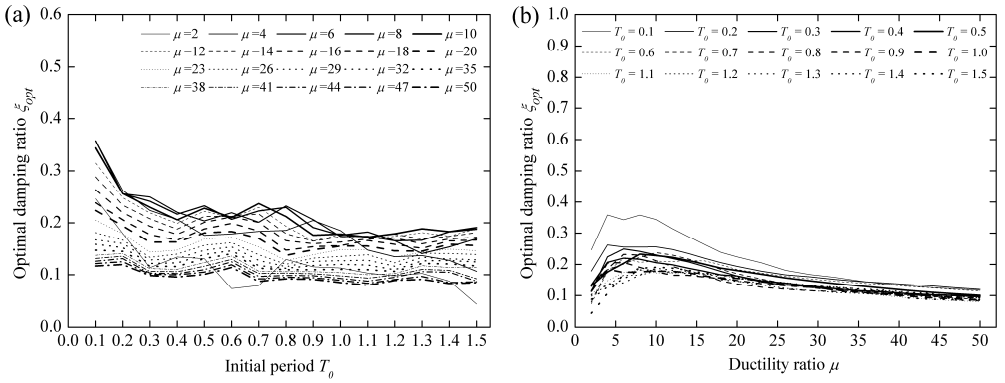

Fig. 84 The optimal damping ratios ξ_{opt} based on α = 0.10: (a) against initial period for different ductility ratios and (b) against ductility ratio for different initial periods

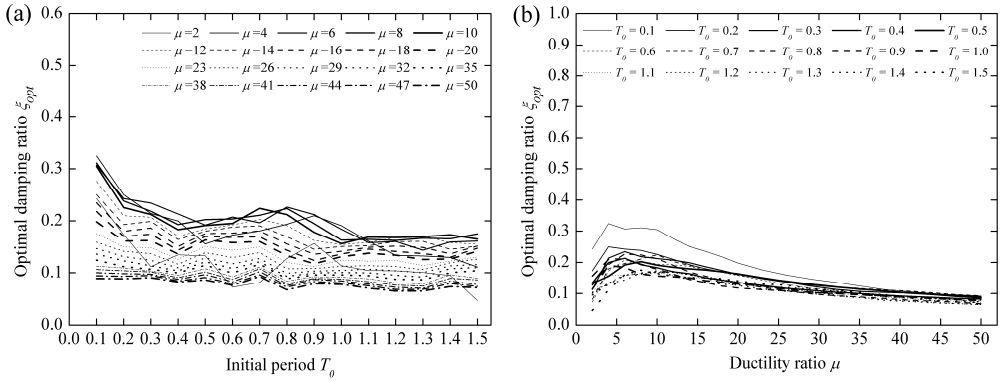

Fig. 85 The optimal damping ratios ξ_{opt} based on α = 0.125: (a) against initial period for different ductility ratios and (b) against ductility ratio for different initial periods

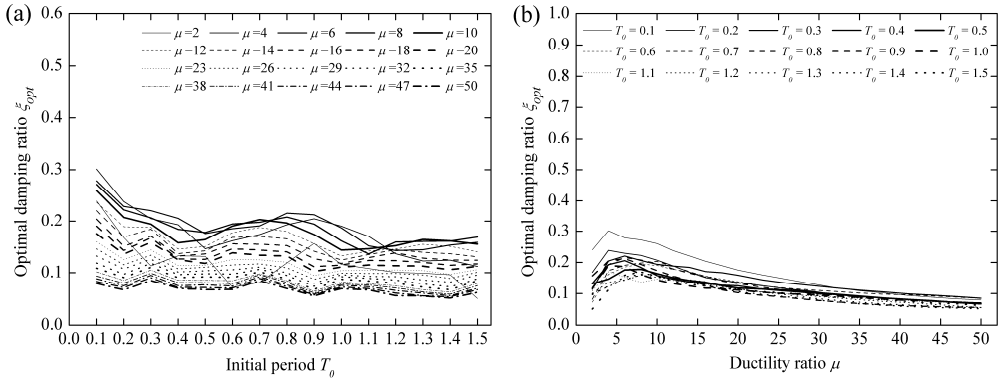

Fig. 86 The optimal damping ratios ξ_{opt} based on α = 0.15: (a) against initial period for different ductility ratios and (b) against ductility ratio for different initial periods

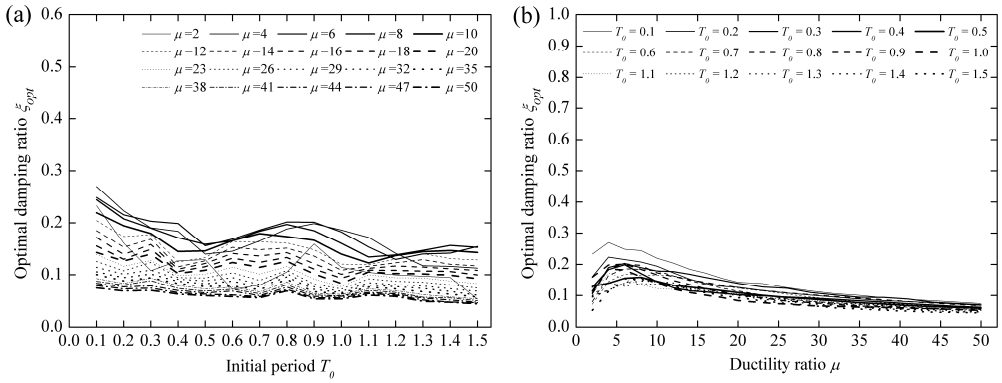

Fig. 87 The optimal damping ratios ξ_{opt} based on α = 0.175: (a) against initial period for different ductility ratios and (b) against ductility ratio for different initial periods

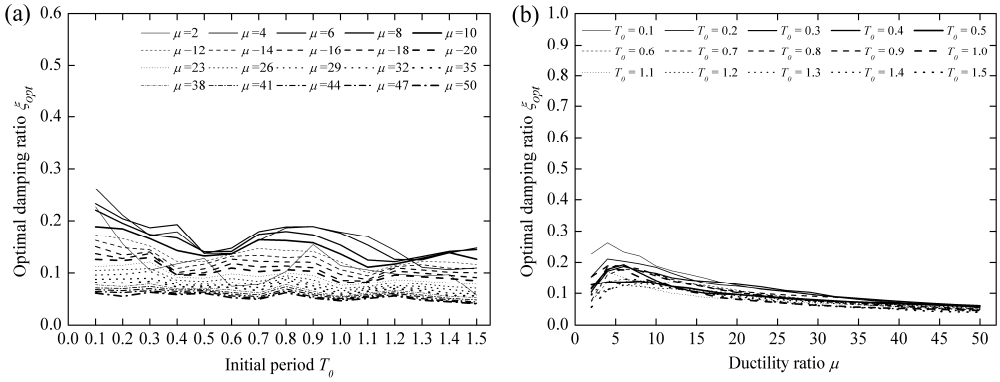

Fig. 88 The optimal damping ratios ξ_{opt} based on α = 0.20: (a) against initial period for different ductility ratios and (b) against ductility ratio for different initial periods

4.3. Regression Analysis of SDOF Systems

Regression analysis is the analysis of the relationship between one variable and another set of variables (SAS, 1999). The relationship is expressed as an equation that predicts a response variable (also called a dependent variable or criterion) from a function of regressor variables (also called independent variables, predictors, explanatory variables, factors, or carriers) and parameters, which can be either 'linear' or 'nonlinear'. Essentially, all models are wrong, but some are useful (Box & Draper, 1987). In this section, regression analysis is performed based on the computed optimal damping ratios to derive the model of equivalent damping ratio as the function of the selected parameters, i.e., strain hardening ratio, initial period and ductility ratio.

How to find the simplest model that adequately fits the observed data is a very difficult task. The best regression equation is not necessarily the equation that explains most of the variance in response variable (the highest R^2). However, it should include all the variables. In addition, the selected equation should be simple (interpretable) and reliable, and the best equation is a compromise between these two.

If an equation of equivalent damping ratio is not able to represent the exact damping ratio demand of hysteretic system, the maximum inelastic displacement response will not be accurately predicted. It can be observed in Chapter 4.2 the optimal damping ratio ξ_{opt} is strongly related to both the initial period and the ductility ratio. Apparently, a linear model is not sufficient to simulate this relationship, and a nonlinear regression analysis is required in this study. To this end, an improved

formula for equivalent damping ratio will be derived through regression analysis in this section.

Although R&H method overestimates the equivalent damping ratio when the ductility ratio is relatively low, there is no additional requirements for the computation of equivalent damping ratio, such as the valid range of strain hardening ratio, initial period and ductility ratio. To propose an improved equation of equivalent damping ratio, modification of R&H method by introducing a factor *F* may be an appropriate option. As a result, the proposed equation of equivalent damping ratio for bilinear model is assumed to have the following form:

$$\xi_{eq} = \xi_0 + \frac{2(1-\alpha)(\mu-1)}{\pi\mu\left[1+\alpha(\mu-1)\right]} \cdot F \tag{73}$$

Now, the problem is to determine the factor *F*. But, the question of selecting an appropriate nonlinear model for this factor is still not solved. The factor *F* could be defined as the ratio of the optimal damping ratios to those calculated using R&H method. In order to investigate the variation trend of factor *F*, it is plotted against initial period for different ductility ratios and against ductility for different initial periods in Figs. 89-98, respectively. As observed in these figures, a power function could be used to simulate the relationship between factor *F* and both variables. Thus, in the present research the factor *F* could be expressed as:

$$F = A \cdot T_0^{\,B} (\mu-1)^C \tag{74}$$

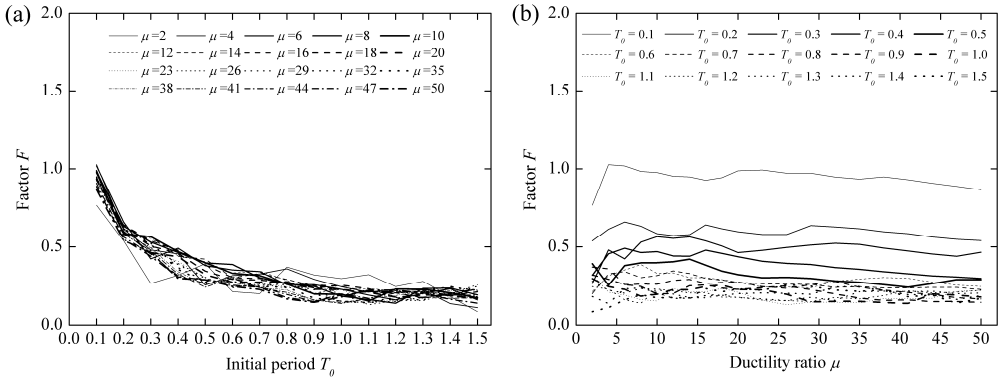

Fig. 89 The factor F based on α = 0.00: (a) against initial period for different ductility ratios and (b) against ductility ratio for different initial periods

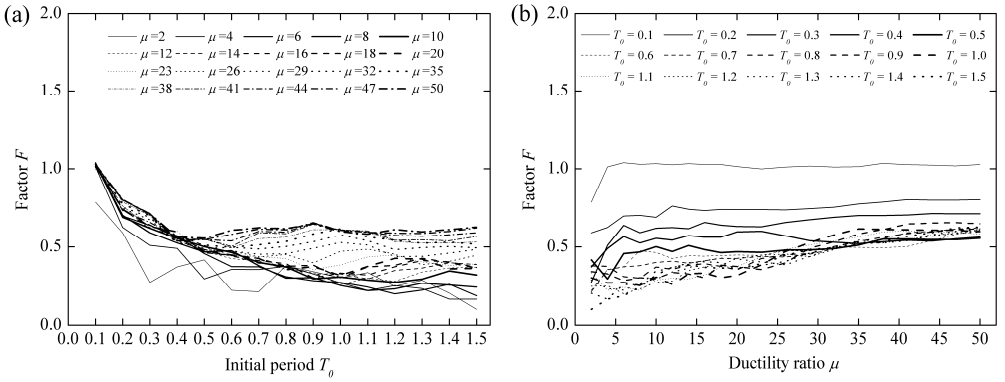

Fig. 90 The factor F based on α = 0.01: (a) against initial period for different ductility ratios and (b) against ductility ratio for different initial periods

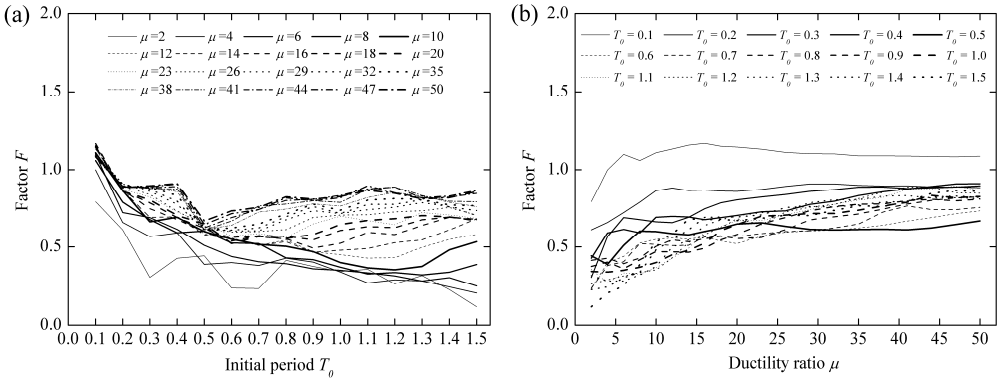

Fig. 91 The factor F based on α = 0.03: (a) against initial period for different ductility ratios and (b) against ductility ratio for different initial periods

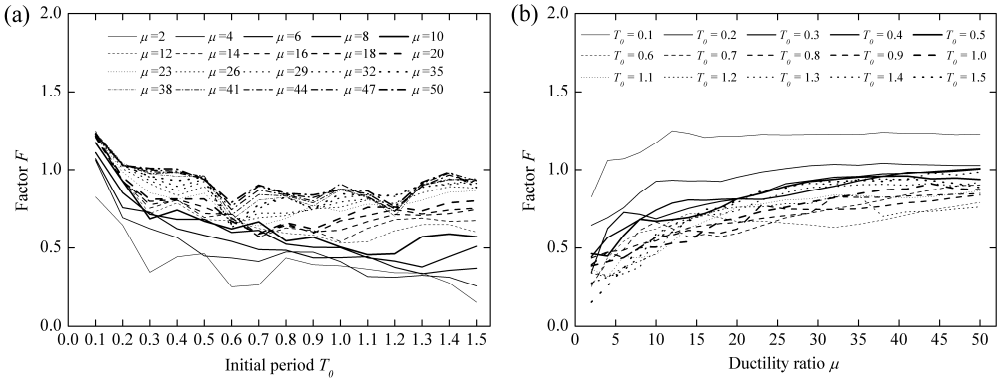

Fig. 92 The factor F based on α = 0.05: (a) against initial period for different ductility ratios and (b) against ductility ratio for different initial periods

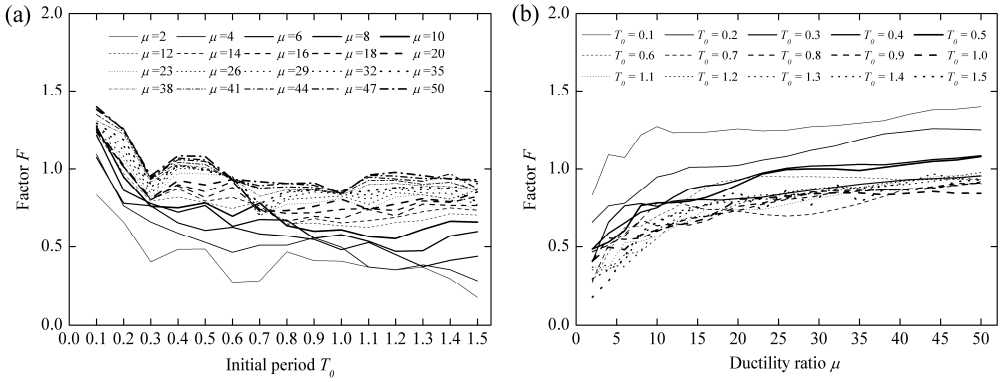

Fig. 93 The factor F based on α = 0.075: (a) against initial period for different ductility ratios and (b) against ductility ratio for different initial periods

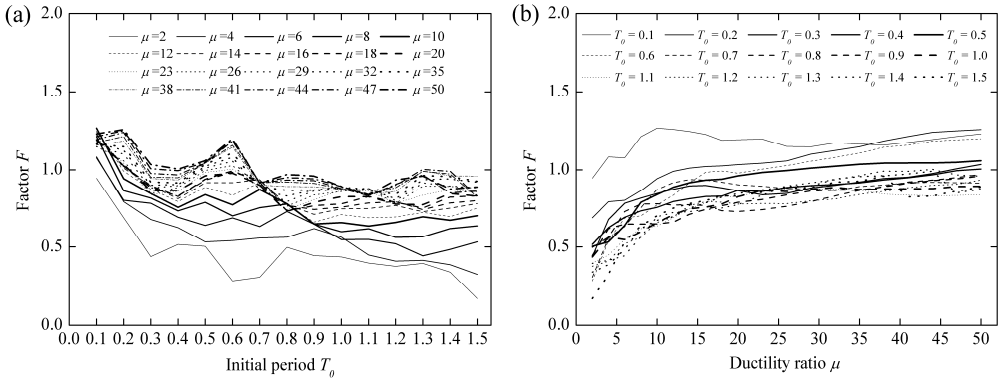

Fig. 94 The factor F based on α = 0.10: (a) against initial period for different ductility ratios and (b) against ductility ratio for different initial periods

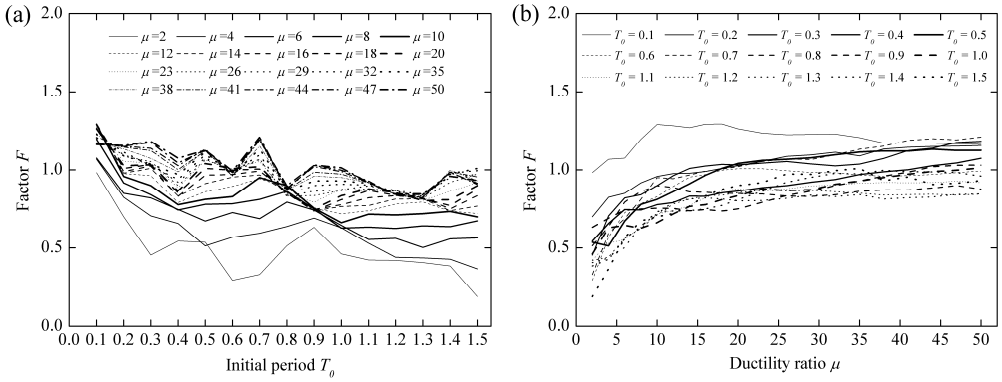

Fig. 95 The factor F based on α = 0.125: (a) against initial period for different ductility ratios and (b) against ductility ratio for different initial periods

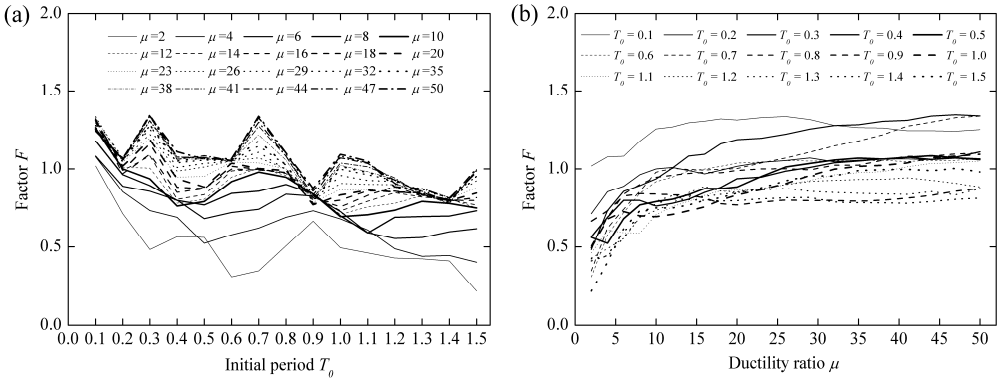

Fig. 96 The factor F based on α = 0.15: (a) against initial period for different ductility ratios and (b) against ductility ratio for different initial periods

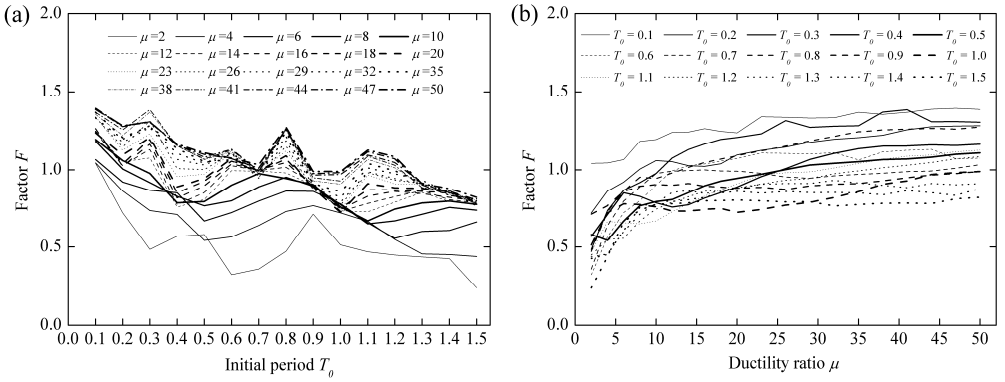

Fig. 97 The factor F based on α = 0.175: (a) against initial period for different ductility ratios and (b) against ductility ratio for different initial periods

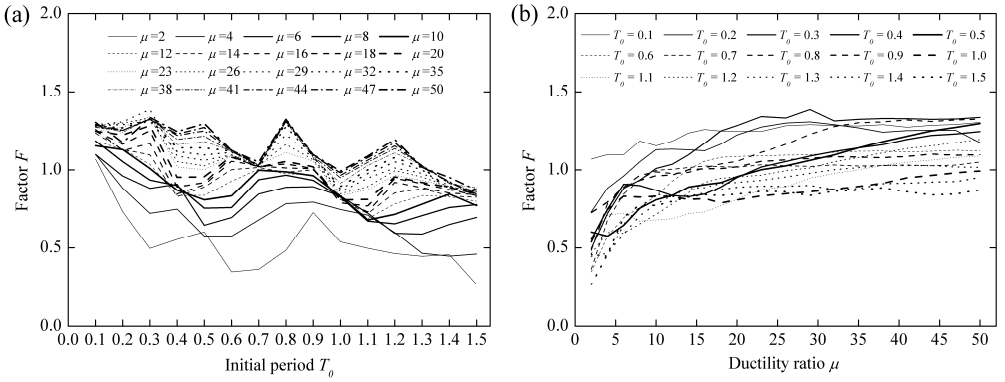

Fig. 98 The factor F based on α = 0.20: (a) against initial period for different ductility ratios and (b) against ductility ratio for different initial periods

Determination of the regression equation is usually done using computer software, particularly when multiple variables are involved. In this study, for a given strain hardening ratio, the parameters *A*, *B* and *C* are determined using the Surface Fitting Toolbox provided by MATLAB. Minimizing the sum of squares of the differences between the actual values of *F* and the values predicted by Eq. (74), parameters *A*, *B* and *C* are obtained and presented in Table 4.

To check the accuracy of surface fitting, the coefficient of determination R^2 and the adjusted R^2 are also calculated. For a perfect fit, $R^2 = 1$. Values less than that indicate that the function fits the data in a less than ideal manner. Excellent fits generally have R^2 values of 0.95 or above and fair to good fits have $R^2 = 0.7$-0.9. To visualize the situation of fits, the collected scatter points and simulated factor *F* are plotted in Figs. 99-108 for various strain hardening ratios. It can be seen that relatively good fits can be obtained. In addition, as stated by Blandon (Blandon & Priestley, 2005), a perfect match is not possible for all the cases because it is necessary to keep a simple form of the equation.

Strain hardening ratio α	Parameters			R^2	*Adj.* R^2
	A	*B*	*C*		
0.00	0.2293	-0.6367	-0.01945	0.9470	0.9467
0.01	0.2698	-0.3463	0.1592	0.8160	0.8148
0.03	0.3256	-0.1982	0.2191	0.7258	0.7240
0.05	0.3711	-0.1892	0.2165	0.7873	0.7859
0.075	0.4110	-0.1930	0.2069	0.8646	0.8637
0.10	0.4750	-0.1512	0.1783	0.8050	0.8036
0.125	0.5153	-0.1450	0.1657	0.7938	0.7924
0.15	0.5338	-0.1513	0.1639	0.7624	0.7608
0.175	0.5376	-0.1644	0.1678	0.8024	0.8010
0.20	0.5573	-0.1408	0.1721	0.7878	0.7864

Table 4
Parameters to determine the factor F

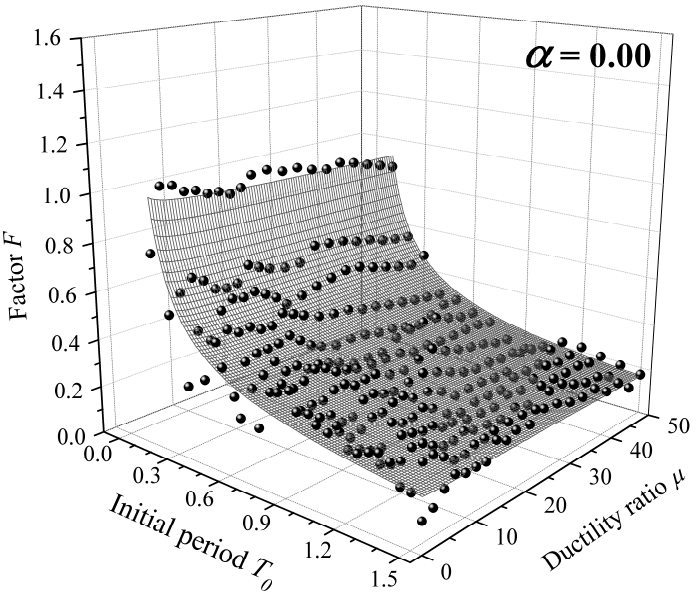

Fig. 99 Surface Fitting of the factor F based on α = 0.00

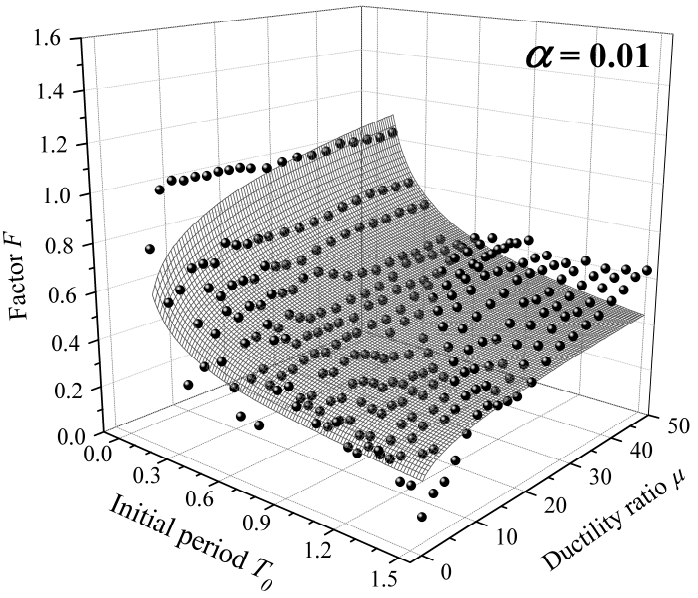

Fig. 100 Surface Fitting of the factor F based on α = 0.01

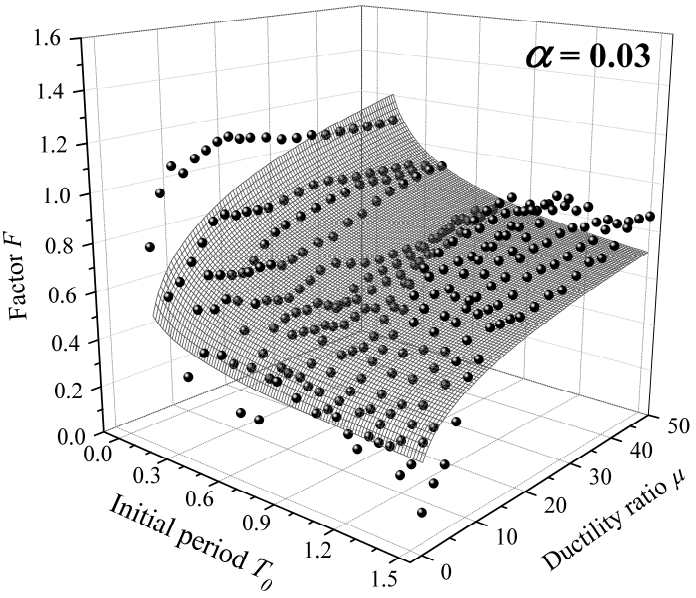

Fig. 101 Surface Fitting of the factor F based on α = 0.03

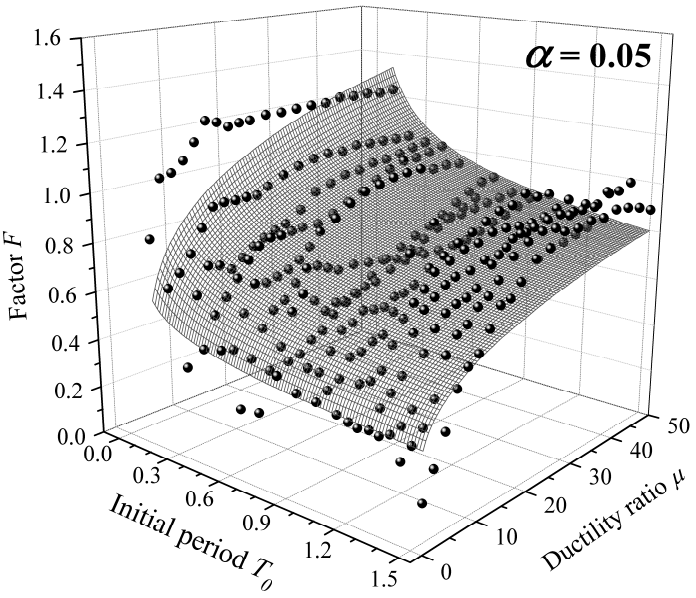

Fig. 102 Surface Fitting of the factor F based on α = 0.05

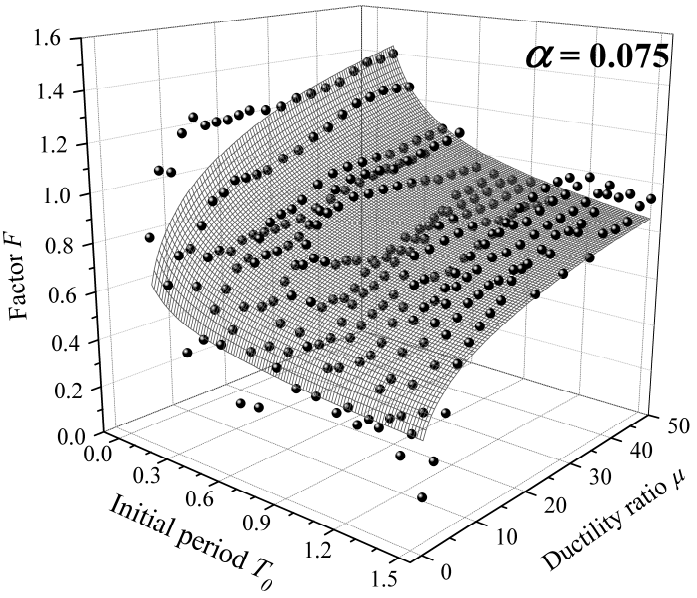

Fig. 103 Surface Fitting of the factor F based on α = 0.075

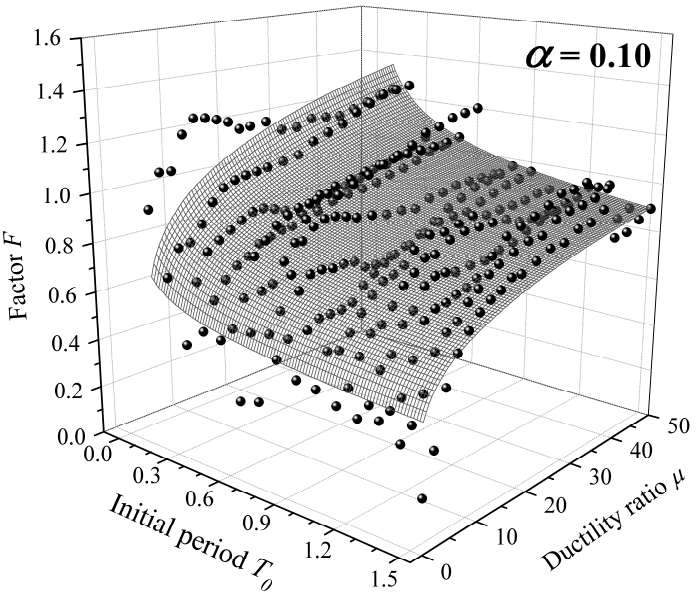

Fig. 104 Surface Fitting of the factor F based on α = 0.10

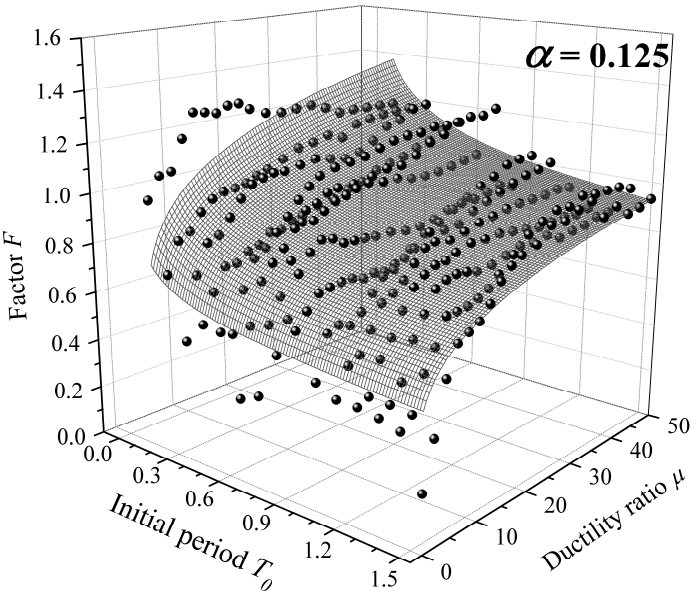

Fig. 105 Surface Fitting of the factor F based on α = 0.125

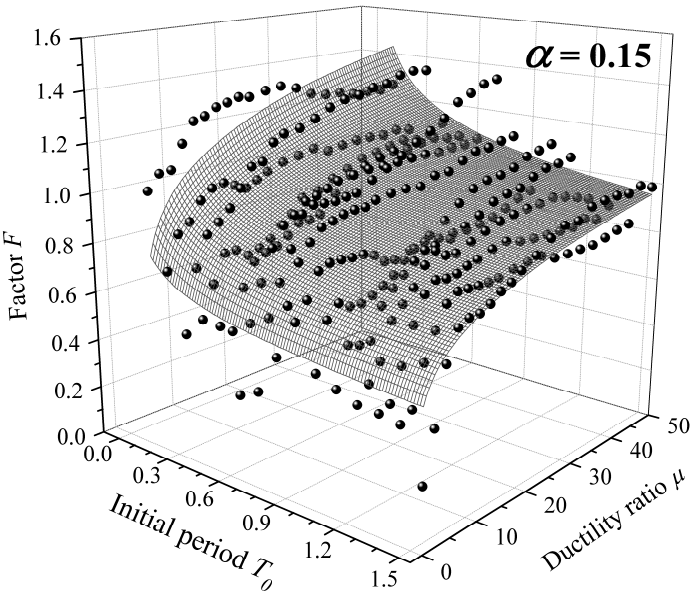

Fig. 106 Surface Fitting of the factor F based on α = 0.15

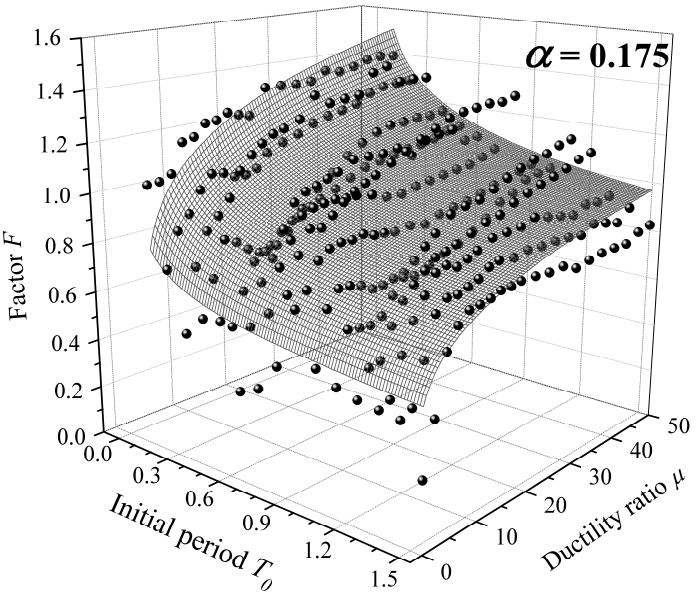

Fig. 107 Surface Fitting of the factor F based on α = 0.175

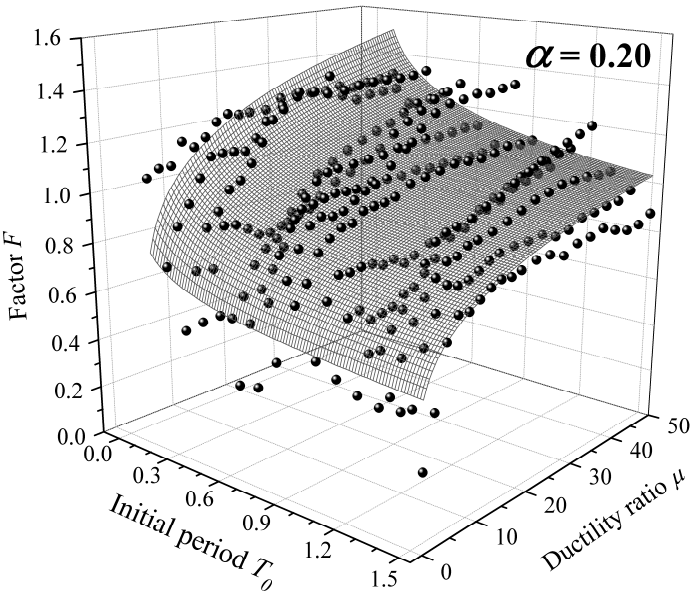

Fig. 108 Surface Fitting of the factor F based on α = 0.2

To consider the effect of strain hardening ratio on the determination of the factor *F*, a simple nonlinear regression procedure is performed using the Curve Fitting Toolbox of MATLAB, as shown in Fig. 109. As can be observed, the relationship between the strain hardening ratio and the parameters to compute the factor *F* can be accurately represented by rational function. One should have in mind that these fitted functions are only valid within the range of strain hardening ratio considered in this study, i.e., 0.00-0.20. For nonlinear hysteretic model with negative stiffness behavior, these assumptions could lead to misunderstanding results, which can be indicated by the variation trend of the parameters *B* and *C* when the strain hardening ratio is less than 0.00.

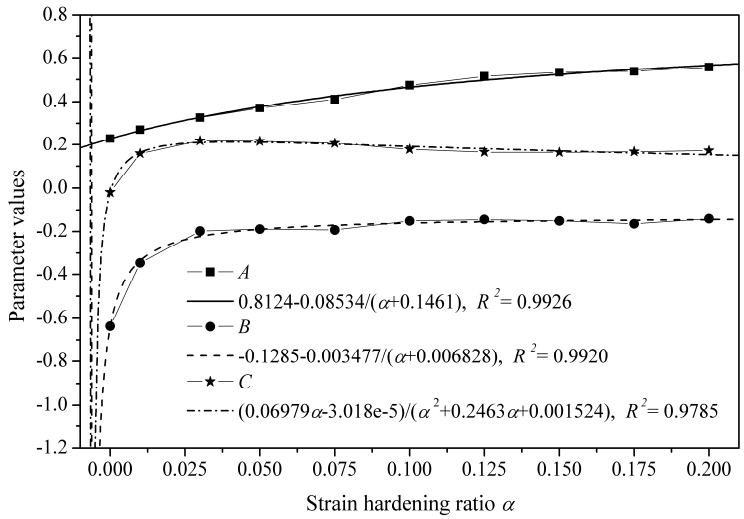

Fig. 109 Nonlinear curve fitting of A, B and C as a function of strain hardening ratio

Finally, the proposed equivalent linearization method used for a general bilinear hysteretic model could be expressed by the following formulas:

Equivalent stiffness:

$$K_{eq} = \frac{1+\alpha\left(\mu-1\right)}{\mu} K_0 \tag{75}$$

or period ratio:

$$\frac{T_{eq}}{T_0} = \sqrt{\frac{\mu}{1+\alpha\left(\mu-1\right)}} \tag{76}$$

Equivalent damping ratio:

$$\xi_{eq} = \xi_0 + \frac{2(1-\alpha)(\mu-1)}{\pi\mu\left[1+\alpha(\mu-1)\right]} \cdot A \cdot T_0^{\,B} (\mu-1)^C \tag{77}$$

where the parameters *A*, *B* and *C* could be defined using the following equation:

$$\begin{cases} A = 0.8124 - \dfrac{0.08534}{\alpha + 0.1461} \\ B = -0.1285 - \dfrac{0.003477}{\alpha + 0.006828} \\ C = \dfrac{0.06979\alpha - 0.00003018}{\alpha^2 + 0.2463\alpha + 0.001524} \end{cases} \tag{78}$$

Equivalent damping ratios computed using the above formulas are compared with the results obtained from R&H method and B&P method, as presented in Fig. 110-119. As described in Chapter 4.2.3, good equation of equivalent damping ratio should represent the same results as those obtained by R&H method when ductility ratio is relatively high and as those obtained by B&P method when ductility ratio is relatively low. It can be seen that the proposed equation of equivalent damping ratio just satisfies this expectation. In addition, all the selected parameters, such as the strain hardening ratio, initial period and ductility ratio, have been considered in the new formula. Therefore, it is expected that the proposed formula could produce much better estimates of the maximum inelastic displacement when compared with R&H method and B&P method.

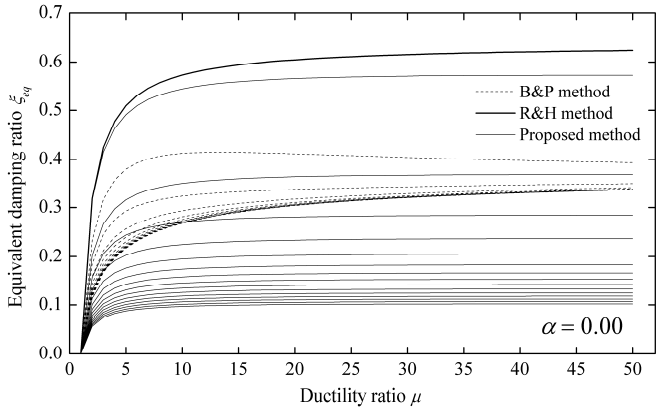

Fig. 110 Comparison of equivalent damping ratios between different methods (α = 0.00)

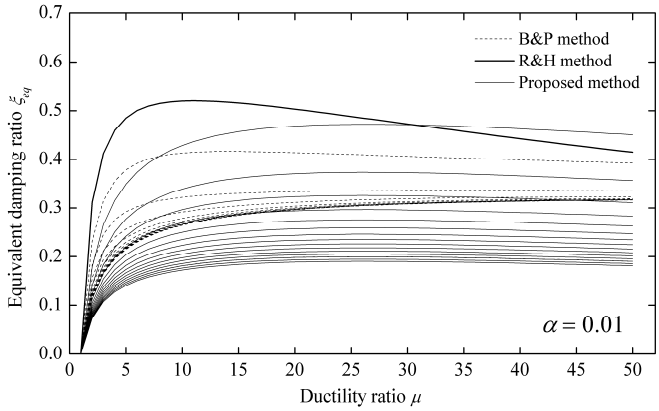

Fig. 111 Comparison of equivalent damping ratios between different methods (α = 0.01)

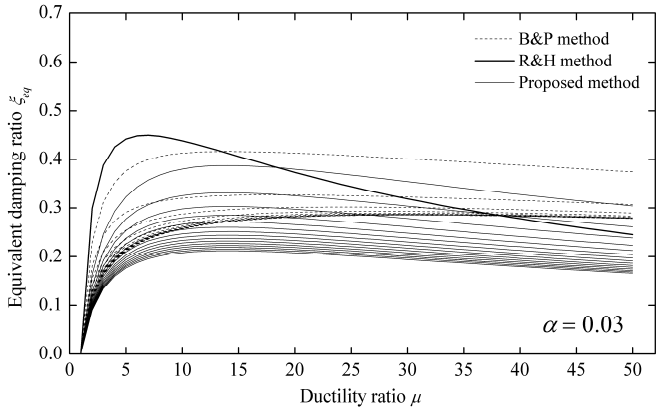

Fig. 112 Comparison of equivalent damping ratios between different methods (α = 0.03)

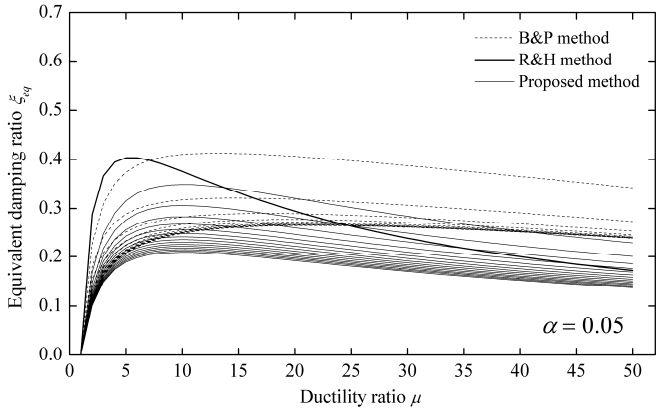

Fig. 113 Comparison of equivalent damping ratios between different methods (α = 0.05)

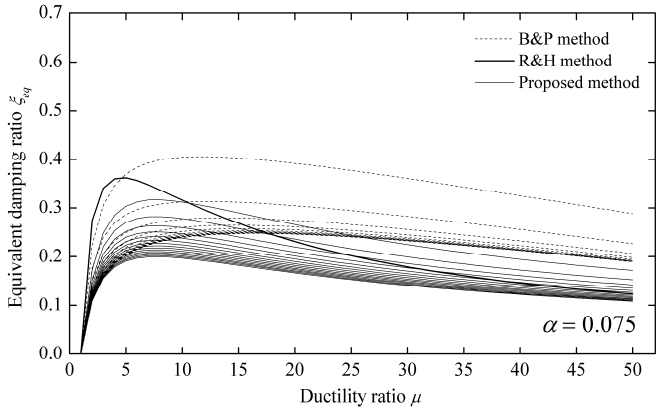

Fig. 114 Comparison of equivalent damping ratios between different methods (α = 0.075)

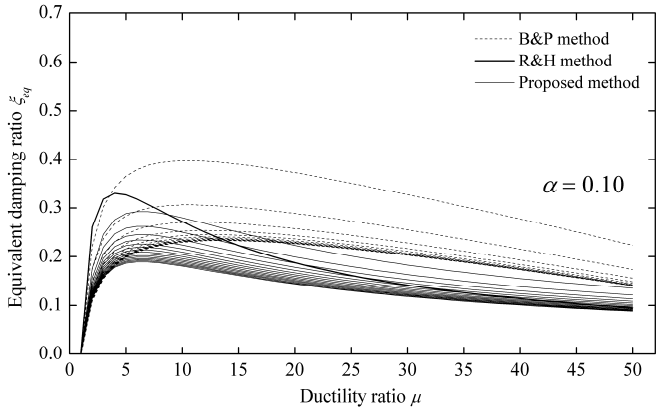

Fig. 115 Comparison of equivalent damping ratios between different methods (α = 0.10)

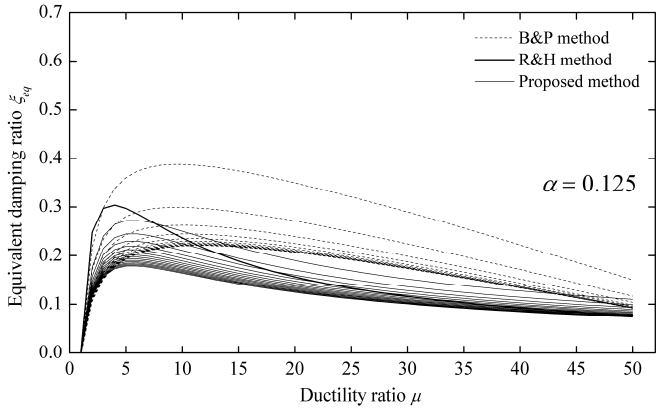

Fig. 116 Comparison of equivalent damping ratios between different methods (α = 0.125)

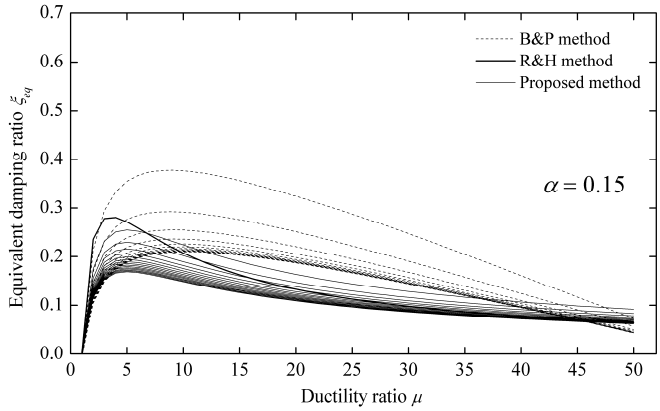

Fig. 117 Comparison of equivalent damping ratios between different methods (α = 0.15)

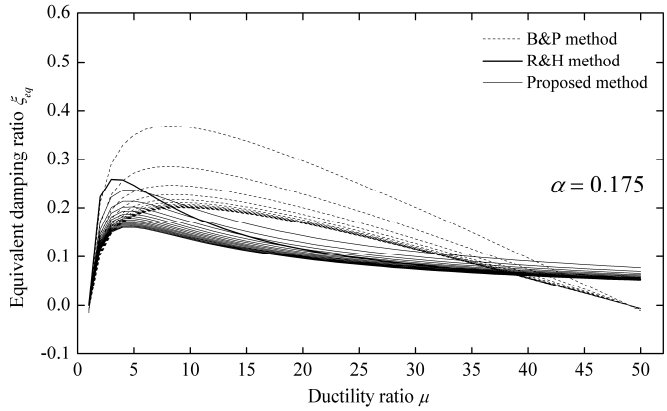

Fig. 118 Comparison of equivalent damping ratios between different methods (α = 0.175)

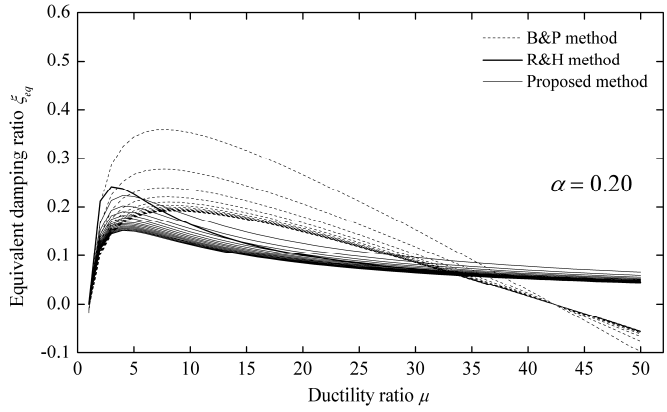

Fig. 119 Comparison of equivalent damping ratios between different methods (α = 0.20)

According to Eq. (76) and Eq. (77), mean approximate to exact displacement ratios are presented in Figs. 120-129, respectively. As can be observed, the estimation accuracy is significantly improved when compared with the results obtained by R&H and B&P methods (Figs. 35-44 and Figs. 55-64), and most of mean approximate to exact displacement ratios range from 0.90 to 1.10, i.e., the relative error between approximate and exact maximum inelastic displacement is less than 10%.

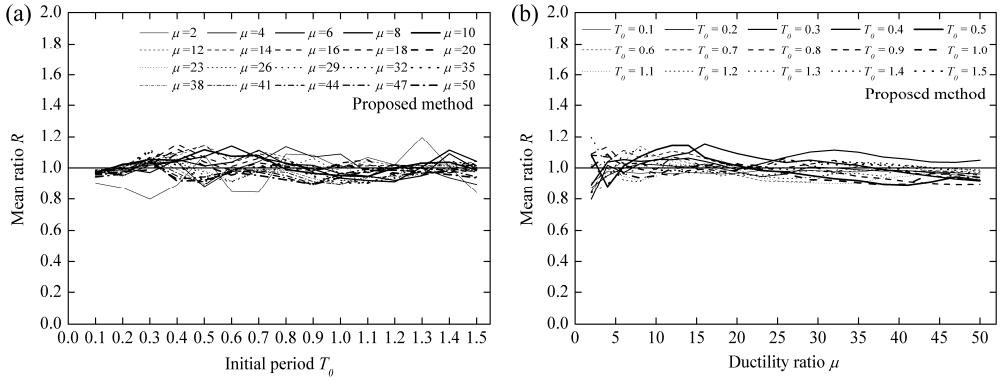

Fig. 120 Estimation accuracy of proposed method based on α = 0.00: (a) against initial period for different ductility ratios and (b) against ductility ratio for different initial periods

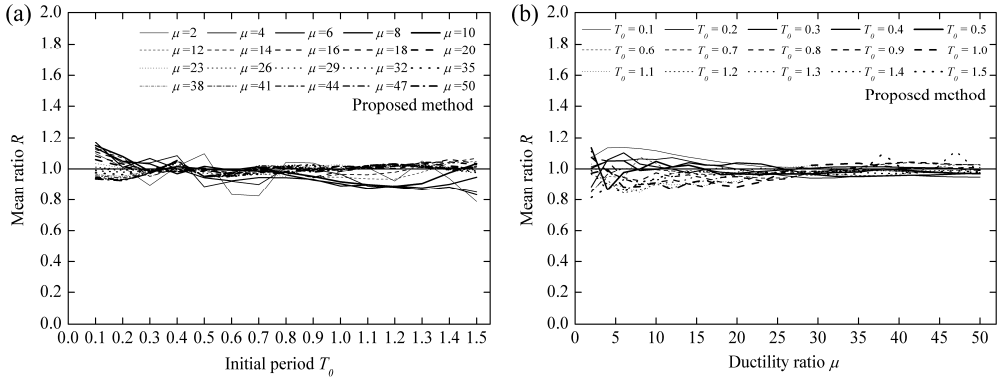

Fig. 121 Estimation accuracy of proposed method based on α = 0.01: (a) against initial period for different ductility ratios and (b) against ductility ratio for different initial periods

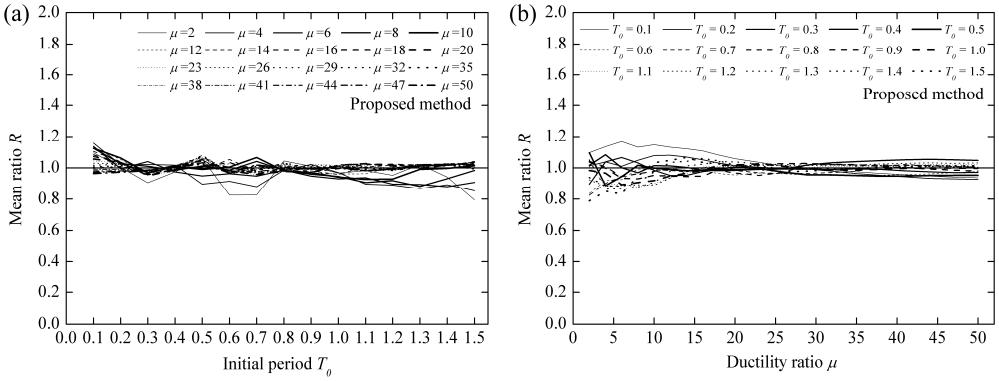

Fig. 122 Estimation accuracy of proposed method based on α = 0.03: (a) against initial period for different ductility ratios and (b) against ductility ratio for different initial periods

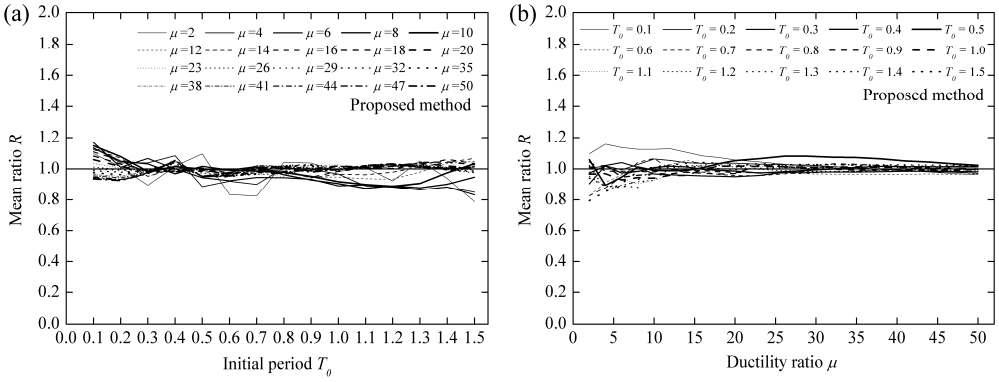

Fig. 123 Estimation accuracy of proposed method based on α = 0.05: (a) against initial period for different ductility ratios and (b) against ductility ratio for different initial periods

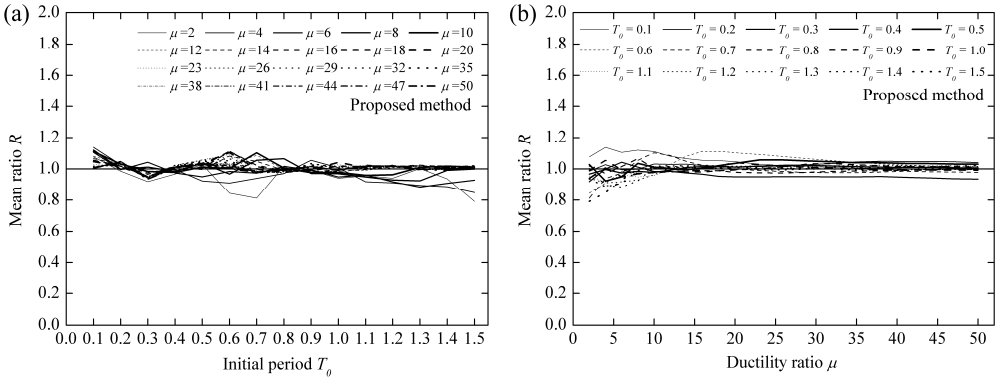

Fig. 124 Estimation accuracy of proposed method based on α = 0.075: (a) against initial period for different ductility ratios and (b) against ductility ratio for different initial periods

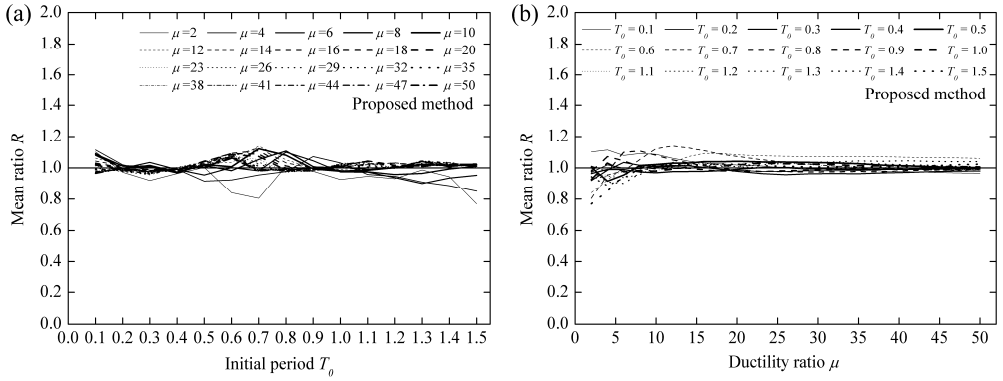

Fig. 125 Estimation accuracy of proposed method based on α = 0.10: (a) against initial period for different ductility ratios and (b) against ductility ratio for different initial periods

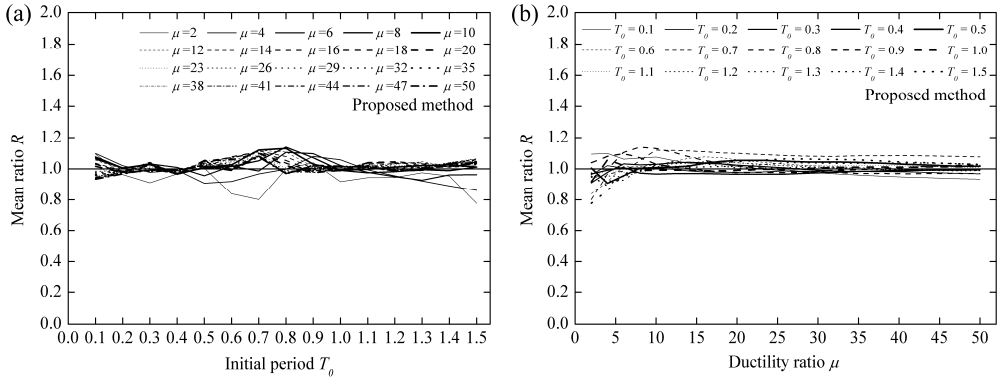

Fig. 126 Estimation accuracy of proposed method based on α = 0.125: (a) against initial period for different ductility ratios and (b) against ductility ratio for different initial periods

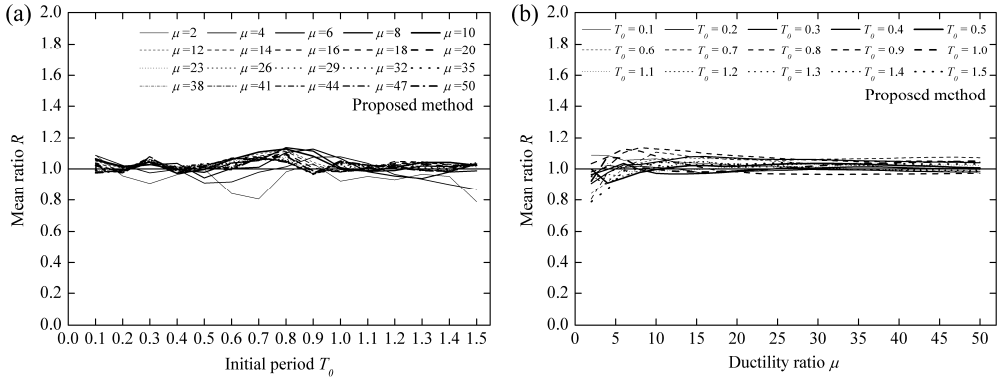

Fig. 127 Estimation accuracy of proposed method based on α = 0.15: (a) against initial period for different ductility ratios and (b) against ductility ratio for different initial periods

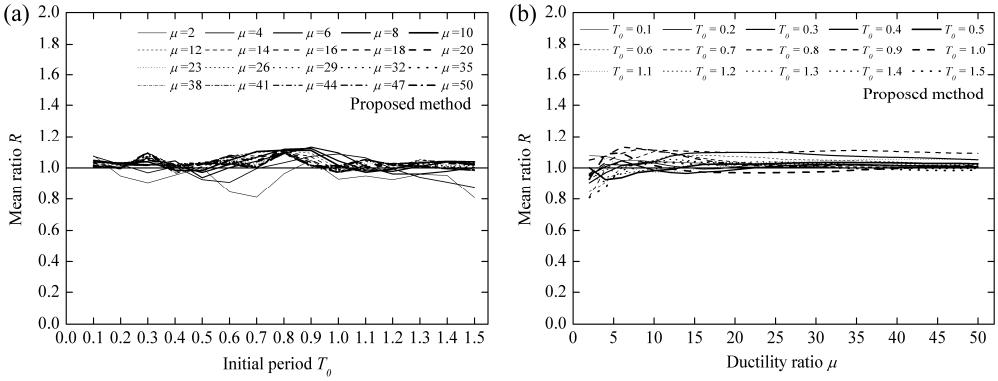

Fig. 128 Estimation accuracy of proposed method based on α = 0.175: (a) against initial period for different ductility ratios and (b) against ductility ratio for different initial periods

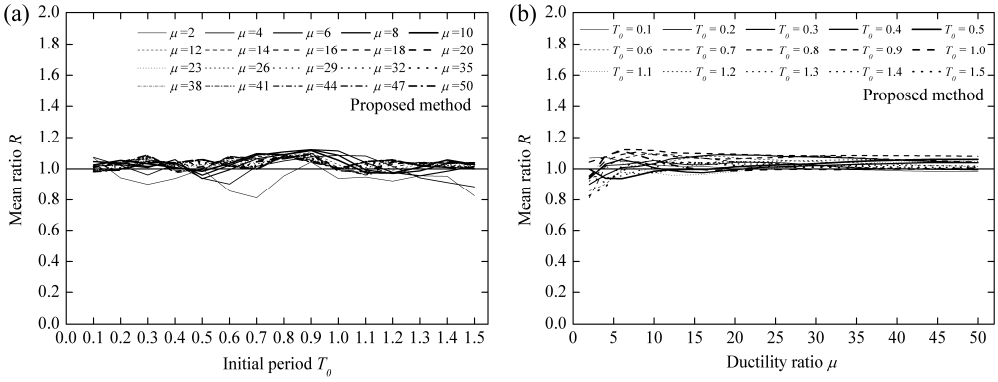

Fig. 129 Estimation accuracy of proposed method based on α = 0.20: (a) against initial period for different ductility ratios and (b) against ductility ratio for different initial periods

For the coefficient of variation C_v, the dispersion obtained by the proposed method is comparable to those from R&H and B&P methods, as shown in Fig. 130-139. In general, C_v slightly increases as the initial period increases and decreases with increasing the ductility ratio. In addition, for larger strain hardening ratio, the coefficient of variation C_v is smaller. Although satisfied accuracy could be obtained by the proposed method, large errors can be still observed for specific earthquake ground motions.

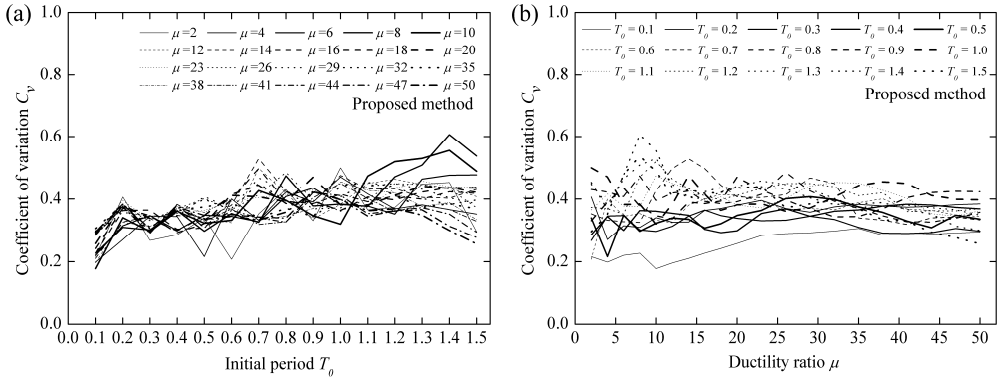

Fig. 130 Coefficient of variation computed by proposed method based on α = 0.00: (a) against initial period for different ductility ratios and (b) against ductility ratio for different initial periods

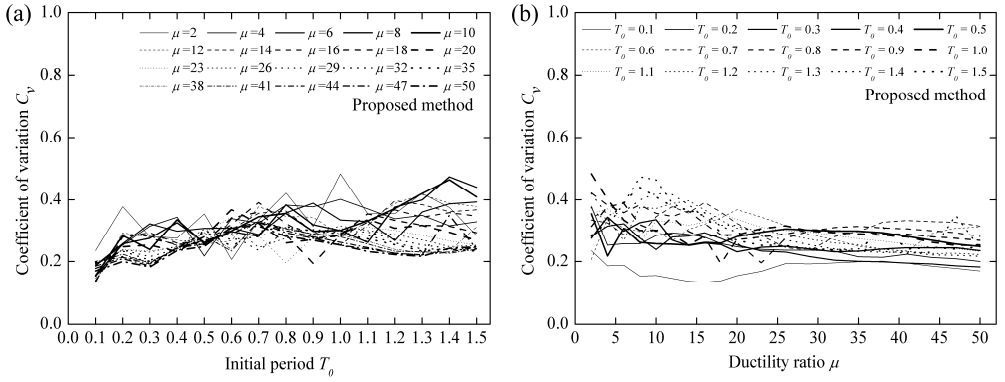

Fig. 131 Coefficient of variation computed by proposed method based on α = 0.01: (a) against initial period for different ductility ratios and (b) against ductility ratio for different initial periods

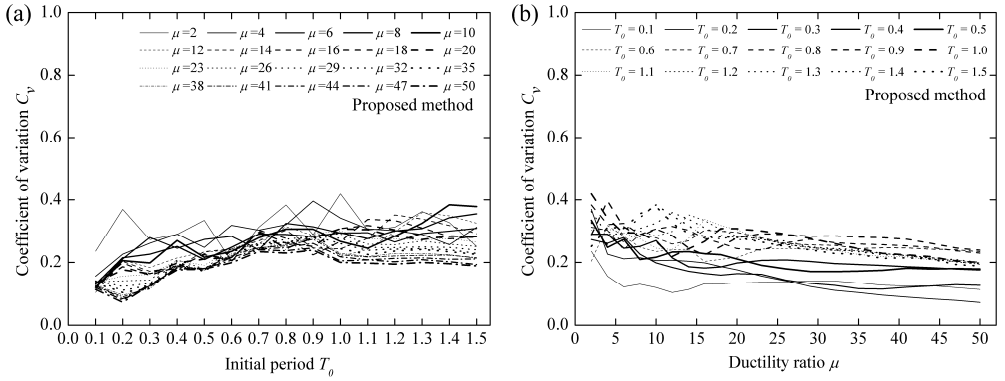

Fig. 132 Coefficient of variation computed by proposed method based on α = 0.03: (a) against initial period for different ductility ratios and (b) against ductility ratio for different initial periods

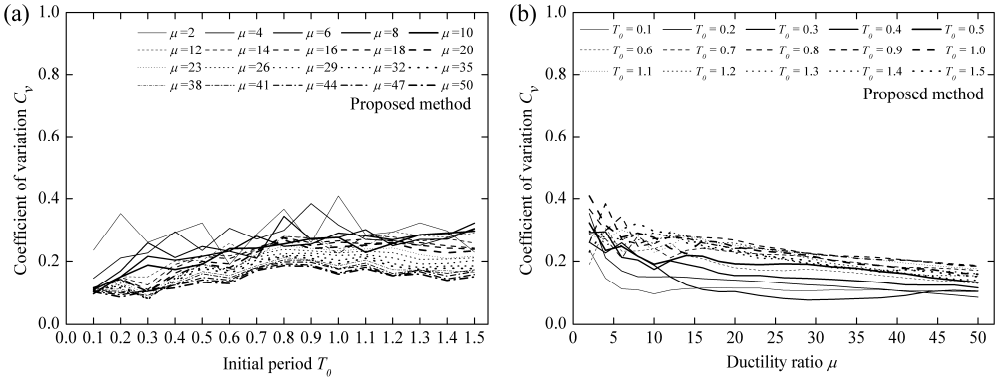

Fig. 133 Coefficient of variation computed by proposed method based on α = 0.05: (a) against initial period for different ductility ratios and (b) against ductility ratio for different initial periods

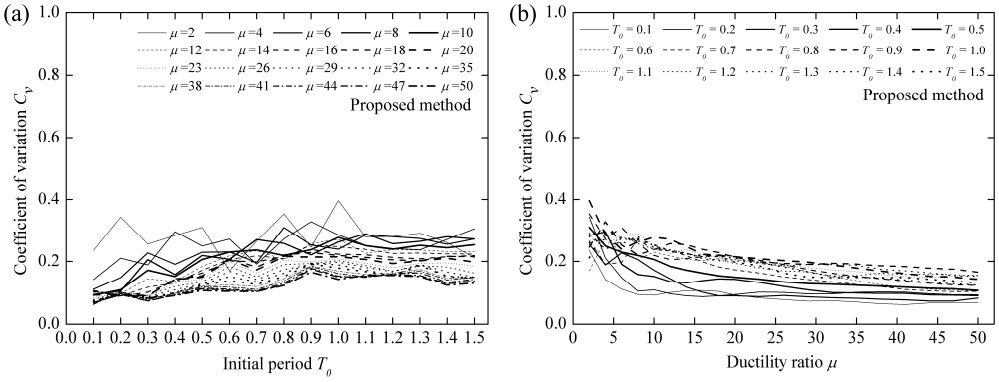

Fig. 134 Coefficient of variation computed by proposed method based on α = 0.075: (a) against initial period for different ductility ratios and (b) against ductility ratio for different initial periods

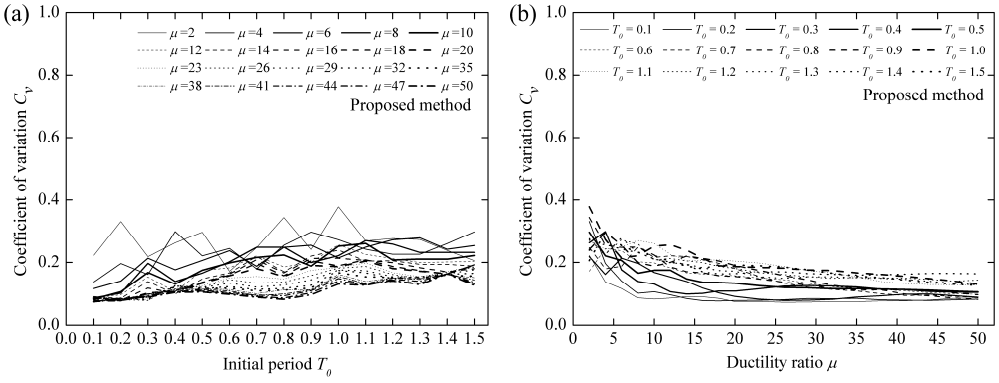

Fig. 135 Coefficient of variation computed by proposed method based on α = 0.10: (a) against initial period for different ductility ratios and (b) against ductility ratio for different initial periods

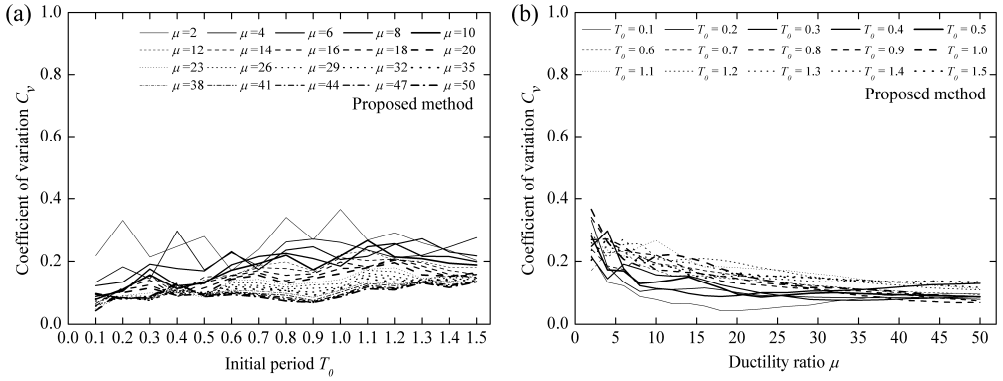

Fig. 136 Coefficient of variation computed by proposed method based on α = 0.125: (a) against initial period for different ductility ratios and (b) against ductility ratio for different initial periods

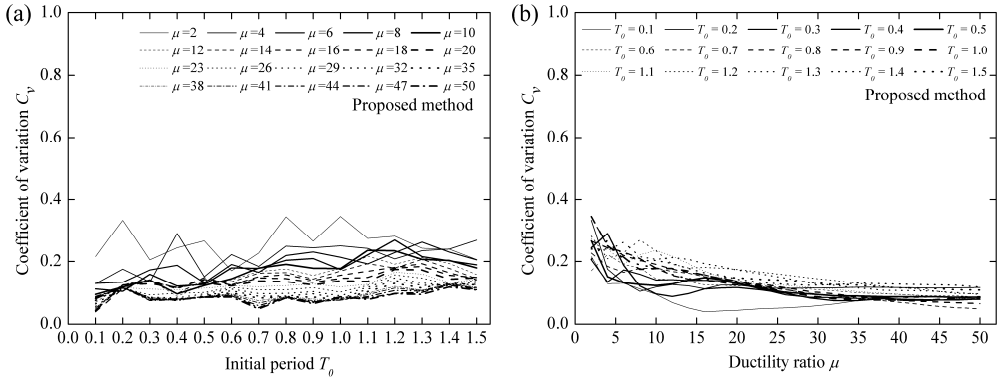

Fig. 137 Coefficient of variation computed by proposed method based on α = 0.15: (a) against initial period for different ductility ratios and (b) against ductility ratio for different initial periods

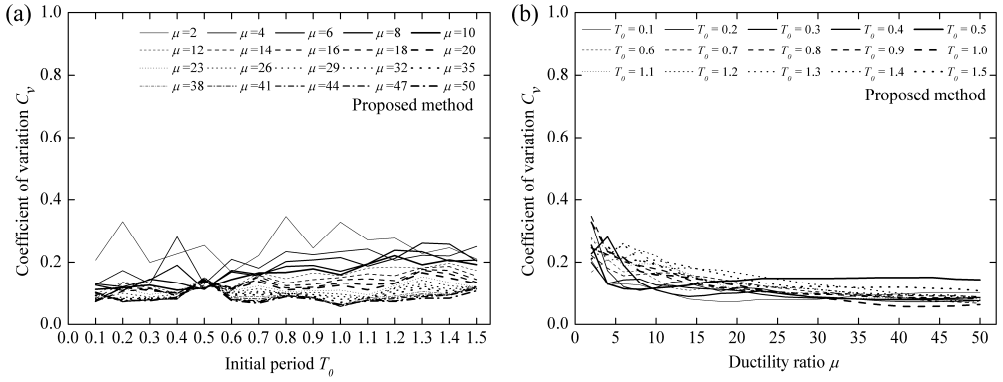

Fig. 138 Coefficient of variation computed by proposed method based on α = 0.175: (a) against initial period for different ductility ratios and (b) against ductility ratio for different initial periods

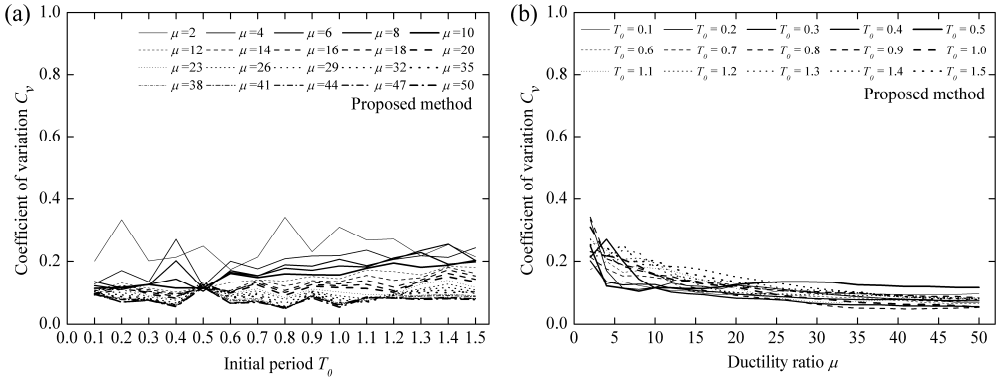

Fig. 139 Coefficient of variation computed by proposed method based on α = 0.20: (a) against initial period for different ductility ratios and (b) against ductility ratio for different initial periods

4.4. Validation of the Proposed Method

The accuracy of equivalent linearization methods is highly affected by the dynamic characteristics of the selected ground motions (Dicleli & Buddaram, 2007). High accuracy could be surely obtained when the ground motions listed in Table 3 are used for validation. But, the proposed formula will be further validated using the other components of the selected ground motions, as presented in Table 5. Validation of the proposed formula is carried out with the same assessment procedure described in Chapter 4.2. The mean ratios of approximate to exact maximum displacement response (Eq. (69)) and the coefficient of variation (Eq. (71)) are still used to examine the estimation accuracy. Due to the space limitation, results from R&H, B&P and proposed methods are examined only based on strain hardening ratios equal to 0.025, 0.075, 0.125 and 0.175. In addition, results are only presented against ductility ratio for different initial periods.

Comparison of mean ratios computed using R&H, B&P and proposed methods are plotted in Figs. 140-143, respectively. As can be seen, the proposed approach is able to produce satisfied estimates of the maximum inelastic displacements in a wide parameter space, although different strain hardening ratios and earthquake ground motions are used. When compared with other two methods, the estimation accuracy of equivalent linearization analysis is significantly improved by the proposed method.

Date	Earthquake	M_s*	Station name	R_{rup}* (km)	$V_{s,30}$* (m/s)	Com.* (deg)	PGA (m/s^2)	PGV (m/s)	PGD (m)	Duration (s)
1966	Parkfield	6.2	Temblor pre-1969	16.0	527.9	295	2.665	0.150	0.034	30.3
1971	San Fernando	6.6	Castaic-Old Ridge Route	22.6	450.3	291	2.629	0.258	0.049	30.0
1972	Managua-Nicaragua-01	6.2	Managua- ESSO	4.1	288.8	180	3.307	0.261	0.082	26.0
1979	Imperial Valley-06	6.5	Compuertas	15.3	274.5	285	1.445	0.095	0.025	36.0
1980	Mammoth Lakes-01	6.1	Convict Creek	6.6	338.5	180	4.330	0.231	0.054	30.0
1980	Victoria- Mexico	6.3	Cerro Prieto	14.4	659.6	315	5.759	0.198	0.095	24.5
1983	Coalinga-01	6.4	Parkfield-Cholame 2WA	44.7	184.8	090	1.115	0.096	0.018	40.0
1989	Loma Prieta	6.9	Foster City-Menhaden Court	45.6	126.4	360	1.138	0.204	0.039	30.0
1992	Cape Mendocino	7.0	Petrolia	8.2	712.8	090	6.496	0.897	0.290	36.0
1994	Northridge-01	6.7	LA-Wonderland Ave	20.3	1222.5	185	1.688	0.118	0.028	30.0
1995	Kobe-Japan	6.9	Kakogawa	22.5	312.0	090	3.380	0.277	0.096	41.0
1999	Kocaeli- Turkey	7.5	Izmit	7.2	811.0	180	1.491	0.226	0.098	30.0

* M_s is the surface-wave magnitude of recorded earthquake; R_{rup} is the rupture distance to the horizontal projection of the fault; $V_{s,30}$ is shear-wave velocities in the upper 30 m of the site profile; Com. is the horizontal component of the considered ground motions.

Table 5

Recorded earthquake ground motions used for numerical validation.

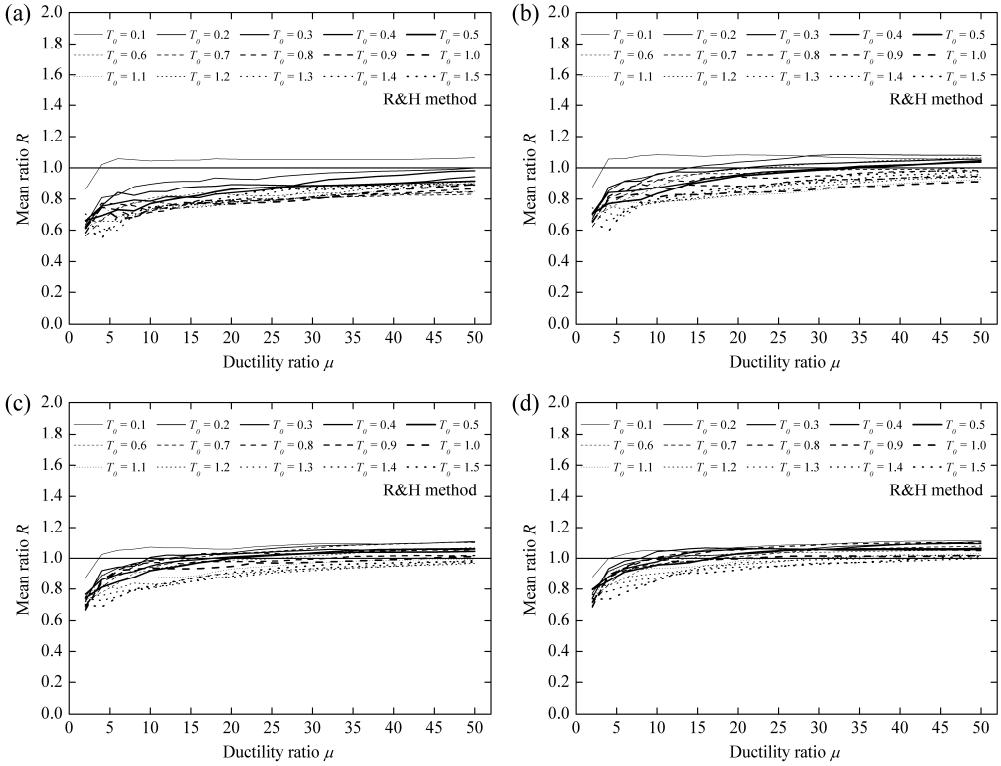

Fig. 140 Validation of mean ratios based on R&H method and (a) α = 0.025, (b) α = 0.075, (c) α = 0.125 and (d) α = 0.175

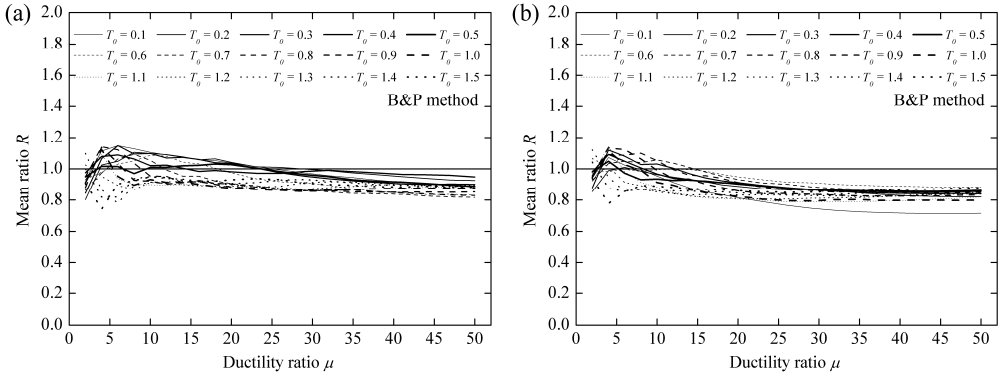

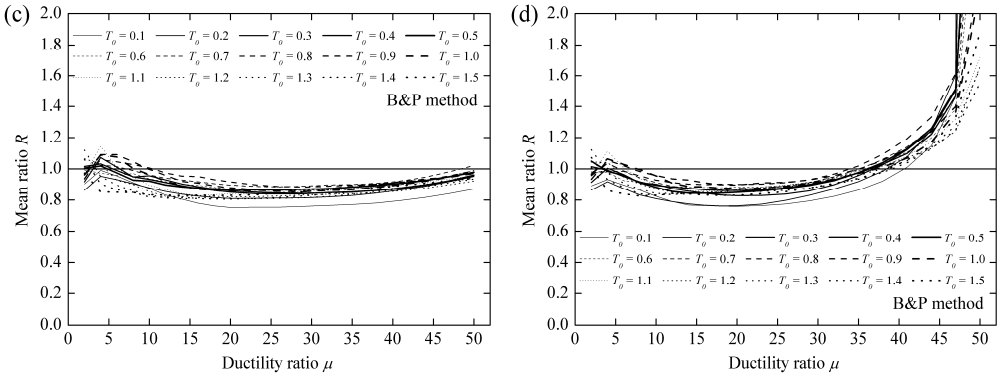

Fig. 141 Validation of mean ratios based on B&P method and (a) α = 0.025, (b) α = 0.075, (c) α = 0.125 and (d) α = 0.175

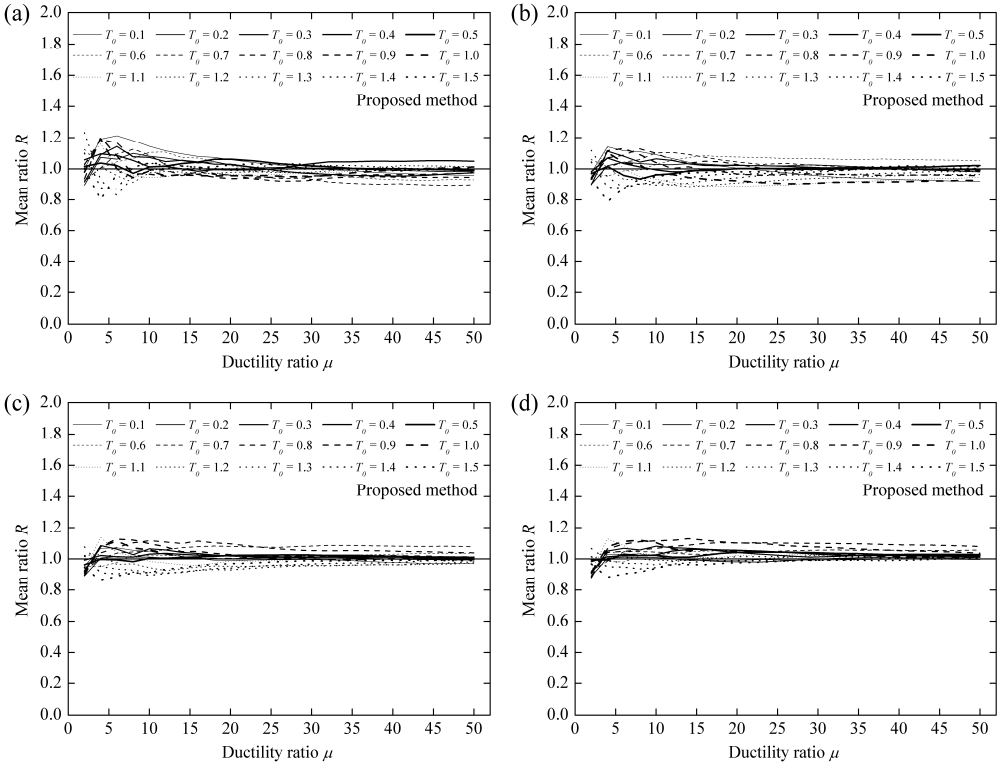

Fig. 142 Validation of mean ratios based on proposed method and (a) α = 0.025, (b) α = 0.075, (c) α = 0.125 and (d) α = 0.175

The coefficients of variation C_v computed using different methods are shown in Figs. 143-145, respectively. It is observed that C_v is even less than the corresponding results computed by the proposed method in the previous sections. Therefore, although different earthquake ground motions are used, the proposed method is robust to yield accurate equivalent damping ratios.

Note that this research focuses on the averaged results over the selected earthquake ground motions, and the influence of dynamic characteristics of input excitations on the prediction accuracy of equivalent linearization method is beyond the scope of this research and it will be addressed in the future study.

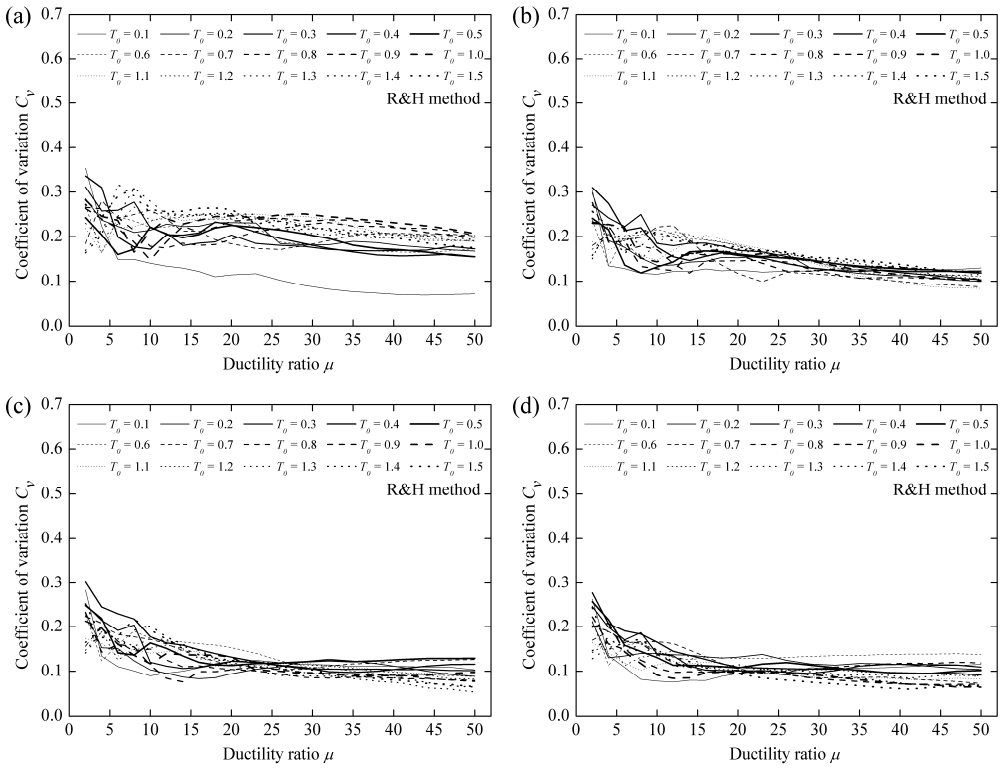

Fig. 143 Validation of coefficient of variation based on R&H method and (a) α = 0.025, (b) α = 0.075, (c) α = 0.125 and (d) α = 0.175

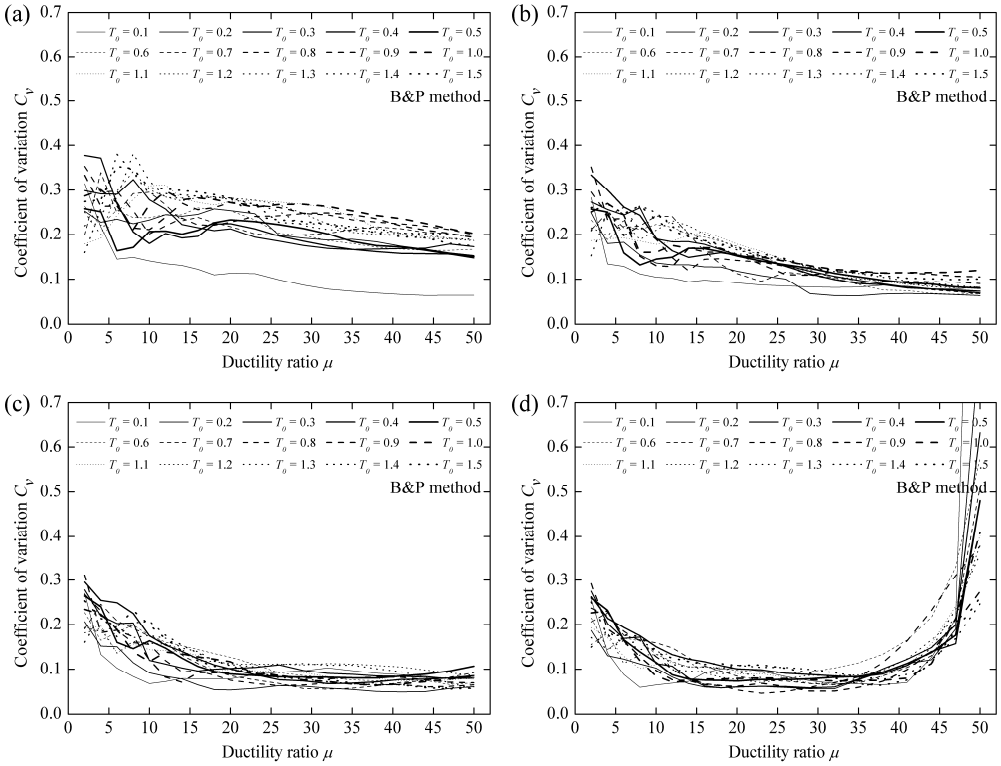

Fig. 144 Validation of coefficient of variation based on B&P method and (a) α = 0.025, (b) α = 0.075, (c) α = 0.125 and (d) α = 0.175

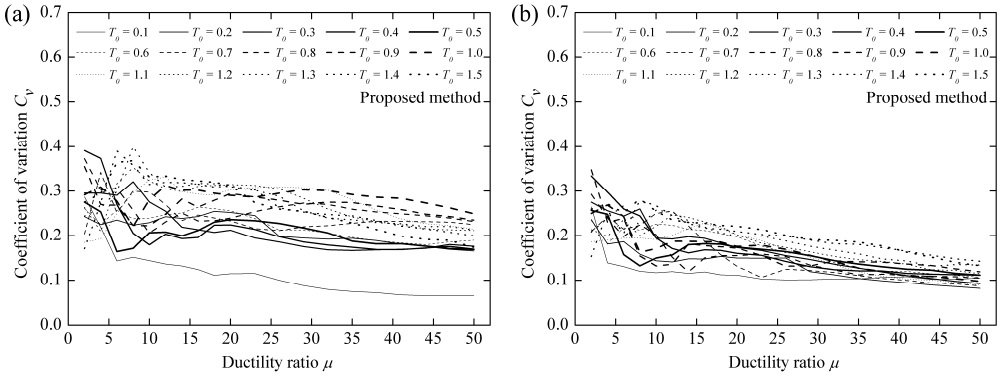

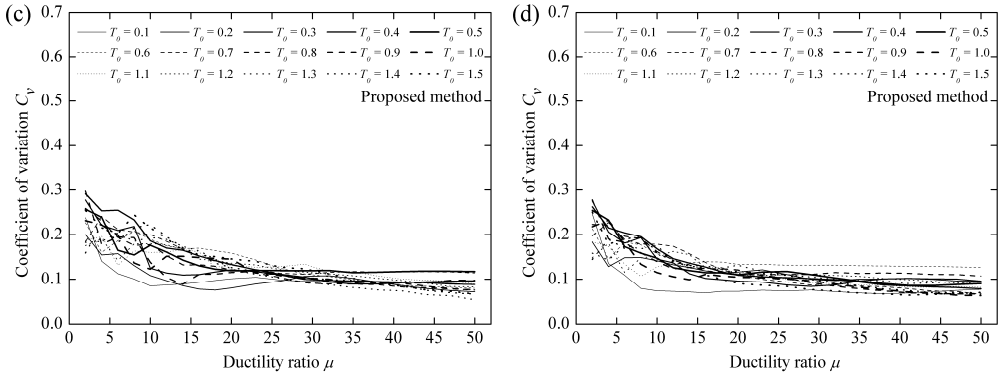

Fig. 145 Validation of coefficient of variation based on proposed method and (a) α = 0.025, (b) α = 0.075, (c) α = 0.125 and (d) α = 0.175

4.5. Summary

This Chapter presents the derivation of an improved formula to determine the equivalent damping ratio of general SDOF bilinear systems. In the research methodology, parametric analyses, optimization analyses and regression analyses are performed successively through MATLAB interfaced with OpenSees. Two different equivalent linearization methods, i.e., R&H method and B&P method, are investigated for the sake of comparison. To present more comprehensive results, a large number of parameters are considered, including 10 strain hardening ratios, 15 initial periods, 20 ductility ratios and 12 earthquake records. A more general formula of equivalent damping ratio is derived through regression analyses of the computed optimal damping ratios.

The accuracy of R&H method and B&P method to predict the maximum inelastic displacement response is investigated and the influences of different parameters on the estimation accuracy are identified. Based on the concept of secant stiffness, the proposed formula of equivalent damping ratio is proved to be able to present the demanded damping ratio used in equivalent linear analysis. In general, using the proposed formula, most of mean approximate to exact displacement ratios range from 0.90 to 1.10, which indicates the relative error between approximate and exact maximum inelastic displacement is less than 10%.

CHAPTER 5

5. IMPROVED EQUIVALENT DAMPING FOR MDOF SYSTEMS

Although equivalent linearization of base isolation systems has been addressed by many research works (Liu et al., 2014d; Zordan et al., 2014), most of them assume the combined system to be SDOF systems, as described in Chapter 4. In other words, the superstructure is assumed to be a rigid body. However, with increasing the height (or natural period) of the superstructure, higher mode effect should be also taken into account; otherwise large errors could be obtained due to the SDOF assumption. This Chapter evaluates the accuracy of equivalent linearization methods to predict the maximum displacement of isolation interface in multi-storey base-isolated buildings. The superstructure is considered to be a shear-type frame building. Three-, six-, nine- and twelve-storey versions of the superstructure frame are considered and modeled as multi-degree-of-freedom (MDOF) systems with lumped masses. Based on the specified parameters, a comprehensive parametric study is performed to examine the influence of the ratio between equivalent period and superstructure period on the estimation accuracy of the maximum displacement of isolation interface under seismic excitations. Results show the prediction accuracy is significantly affected by this ratio and the equivalent linearization method proposed in Chapter 4 is further improved in order to get more accurate results.

5.1. Parametric Analyses of MDOF Systems

In order to evaluate the suitability of different equivalent linearization methods (i.e., R&H method and the proposed method in Chapter 4) in MDOF systems, comprehensive parametric analyses are performed. For the sake of simplicity, equivalent linearization method proposed in Chapter 4 is abbreviated to Liu method.

5.1.1 Parameter Variation and Assessment Procedure

The considered superstructure is a multi-storey shear-type frame building supported on base isolation system, as depicted in Fig. 146. Three-, six-, nine- and twelve-storey versions of the superstructure frame, which are modeled as MDOF systems with lumped masses, are used in this research. They have been assumed to have

the same storey mass at all the levels. For all four superstructure models, the storey height h = 3 m. Storey mass (m_s) has been computed referring to residential buildings with gross floor area of 180 m^2 (specifically, 60000 kg), and the total superstructure mass (M_s) equals the sum of these storey masses. The base mass (m_b) is set to two times the storey mass. At each level of superstructure, inter-storey stiffness (k_s) is assigned to be identical and calibrated so that the fundamental period of the superstructure T_{fb} = 0.3, 0.6, 0.9 and 1.2 s for the three-, six-, nine- and twelve-storey structures with a fixed base, respectively. Presented in Table 6 is the corresponding inter-storey stiffness used for different superstructures. The reduction in stiffness due to P-Δ effects has not been included in the model and the superstructure is assumed to behave rigidly in the axial direction.

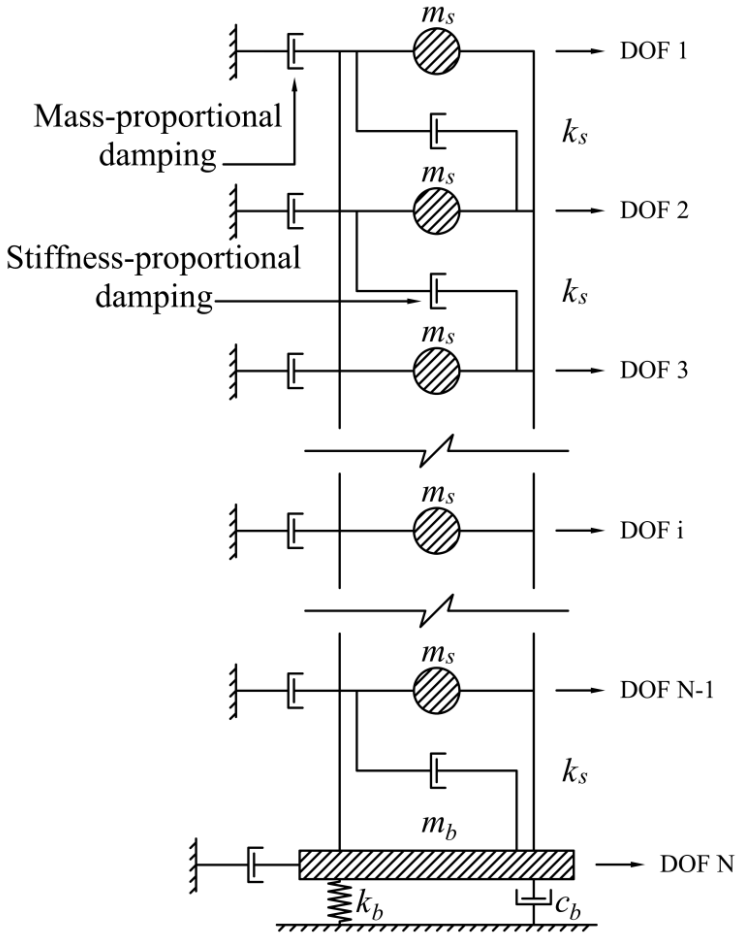

Fig. 146 Layout of the prototype base-isolated structures

Superstructure	Inter-storey stiffness k_s (N/m)
3 storeys (T_{fb} = 0.3 s)	1.328×10^8
6 storeys (T_{fb} = 0.6 s)	1.131×10^8
9 storeys (T_{fb} = 0.9 s)	1.071×10^8
12 storeys (T_{fb} = 1.2 s)	1.042×10^8

Table 6
Inter-storey stiffness of the superstructure models.

Here, four superstructures are used in this chapter, which have 3, 6, 9 and 12 storeys, respectively. Regarding the bilinear base isolation systems, the following assumptions or parameters are specified:

a) the yielding displacement of bilinear isolation system is assigned to be 0.01 m.

b) elastic damping ratio of bilinear oscillators is omitted (ξ_0 = 0).

c) 15 initial periods of vibration T_0 between 0.1 s and 1.5 s with period increments equal to 0.1 s.

d) 20 ductility ratios μ between 2 and 50 with increments equal to 2 for ductility ratios between 2 and 20 and 3 for ductility ratios greater than 20.

e) strain hardening ratios α equal to 0.10.

f) elastic damping ratio of superstructure is set to be 0.05 (ξ_s = 0.05).

The assessment procedure can be seen in Chapter 4, where the difference is that in OpenSees the MDOF systems are used instead of the SDOF systems. According to the results obtained in last chapter, the elastic viscous damping of the superstructure is applied only using the stiffness-proportional damping model.

For a base-isolated structure represented by a linear MDOF system, as shown in Fig. 146, the equations of motion can be expressed as:

$$M\ddot{v}(t)+C\dot{v}(t)+Kv(t)=p(t) \tag{79}$$

where *M*, *C*, *K* are mass, damping and stiffness matrix of the system, respectively; p(t) is the dynamic load vector; $v(t)$, $\dot{v}(t)$, and $\ddot{v}(t)$ are vectors containing the displacements, velocities and accelerations, respectively, at the various degrees of freedom.

Due to the explicit determination of mass and stiffness matrix, the selection of damping matrix produces a great uncertainty in response history analysis. The damping matrix *C* of the combined system can be assembled by combining the superstructure damping matrix C_s with the isolation system damping c_b. The damping matrix for the superstructure C_s can be formed using different damping

models, such as Mass-proportional, Stiffness-proportional and Rayleigh damping model. However, the damping for isolation system c_b can be obtained through the rigid assumption of the superstructure, namely:

$$c_b = 2\left(M_s + m_b\right)\omega_b \xi_b \tag{80}$$

After assembling the mass, stiffness and damping matrix, time history analysis of the base-isolated structure is performed using the Newmark-β time integration method (Newmark, 1959). Although this method is discussed in many textbooks in structural dynamics, a brief description is provided here. The Newmark-β method is based on the solution of an incremental form of the equations of motion. For the equations of motion Eq. (79), the incremental equilibrium equation is:

$$M\Delta\ddot{v}_i + C\Delta\dot{v}_i + K\Delta v_i = \Delta p_i \tag{81}$$

Assuming a certain specific variation for the acceleration within the time interval $\Delta t = t_{i+1} - t_i$, the incremental velocity and acceleration can be written as:

$$\begin{aligned} \Delta\dot{v}_i &= c_1\Delta v_i - c_2\dot{v}_i - c_3\ddot{v}_i \\ \Delta\ddot{v}_i &= c_4\Delta v_i - c_5\dot{v}_i - c_6\ddot{v}_i \end{aligned} \tag{82}$$

where c_i, i = 1, ... , 6, are constants expressed in terms of the algorithm parameters γ, β and Δ_t:

$$\begin{aligned} &c_1 = \frac{\gamma}{\beta\Delta t};\ c_2 = \frac{\gamma}{\beta};\ c_3 = \Delta t\left(\frac{\gamma}{2\beta} - 1\right) \\ &c_4 = \frac{1}{\beta\Delta t^2};\ c_5 = \frac{1}{\beta\Delta t};\ c_6 = \frac{1}{2\beta} \end{aligned} \tag{83}$$

where typically γ = 0,5 and β = 0,25, which yields the constant average acceleration method.

Substituting Eq. (82) and Eq. (83) into Eq. (81), we obtain:

$$\left(c_4 M + c_1 C + K\right)\Delta v_i - \left(c_5 M + c_2 C\right)\dot{v}_i - \left(c_6 M + c_3 C\right)\ddot{v}_i = \Delta p_i \tag{84}$$

which can be solved for Δv_i:

$$\Delta v_i = \Delta \hat{p}_i / \hat{K} \tag{85}$$

where

$$\begin{aligned} \Delta \hat{p}_i &= \Delta p_i + \left(c_5 M + c_2 C\right)\dot{v}_i + \left(c_6 M + c_3 C\right)\ddot{v}_i \\ \hat{K} &= c_4 M + c_1 C + K \end{aligned} \tag{86}$$

Once Δv_i is known, the incremental velocity and acceleration can be obtained from Eq. (82). They, in turn, can be used to obtain the values at the end of the interval:

$$\begin{aligned} v_{i+1} &= v_i + \Delta v_i \\ \dot{v}_{i+1} &= \dot{v}_i + \Delta \dot{v}_i \\ \ddot{v}_{i+1} &= \ddot{v}_i + \Delta \ddot{v}_i \end{aligned} \tag{87}$$

Usually the acceleration is calculated directly from the equations of motion at time t_{i+1} instead of using Eq. (87).

In the following, the steps of the displacement-based Newmark method for the numerical integration of equations of motion (Eq. (81)) are described.

1) Choose time step Δt and parameter γ and β (γ = 0.5 and β = 0.25)
2) Calculate the constants c_1 to c_6 from Eq. (83);
3) Calculate the stiffness matrix *K*, damping matrix *C* and mass stiffness *M*;
4) Initialize the displacement, velocity, and acceleration vectors;
5) Calculate the incremental displacement from Eq. (85) and Eq. (86);
6) Use Eq. (82), then Eq. (87) to obtain incremental velocity and acceleration, and total displacement and velocity at the next time step, respectively;
7) Calculate the acceleration for the next time step using the equations of motion;
8) Repeat from step 5 with the next time step.

According to the above steps, the Newmark-β method is implemented within MATLAB to perform response history analysis systematically.

The selected ground motions are same as Chapter 3 and can be found in Table 3. For each selected version of the superstructure, detailed assessment procedure are presented in Fig. 18 in Chapter 3. Similarly, mean of approximate to exact dis-

placement ratio R and the coefficient of variation C_v are used to investigate the prediction accuracy of different methods:

5.1.2 Accuracy of R&H method

Figs. 147-150 show the computed mean ratios based on R&H method. It is seen that for MDOF systems with 3-storey superstructure the estimation accuracy is almost unchanged when compared with SDOF system (see Fig. 40 (α = 0.10) in Chapter 4), where the superstructure is assumed to be a rigid body. However, for MDOF base-isolated systems with higher superstructure, large difference could be obtained when initial period is less than 0.7 s. Therefore, SDOF assumption is appropriate for relatively low buildings. However, with increasing the height (or the period) of superstructure, better estimation accuracy could be obtained. In general, for relatively small ductility ratios, the maximum inelastic displacement is underestimated to some extent while for large ductility ratio it is overestimated.

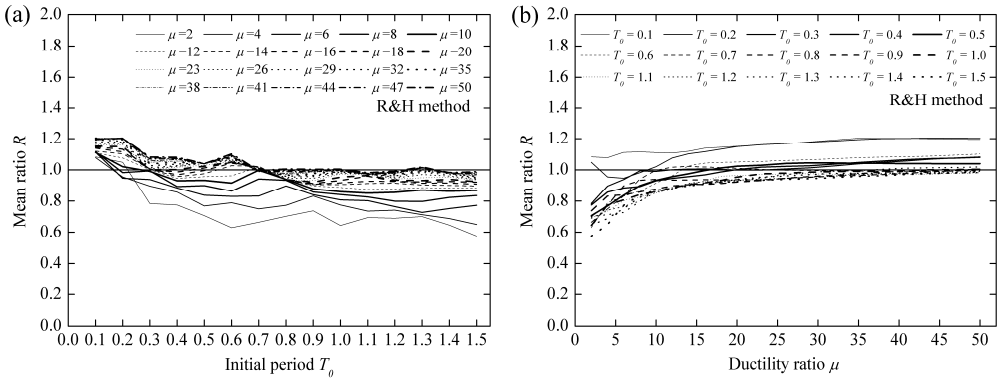

Fig. 147 Estimation accuracy of R&H method based on 3-storey superstructure: (a) against initial period for different ductility ratios and (b) against ductility ratio for different initial periods

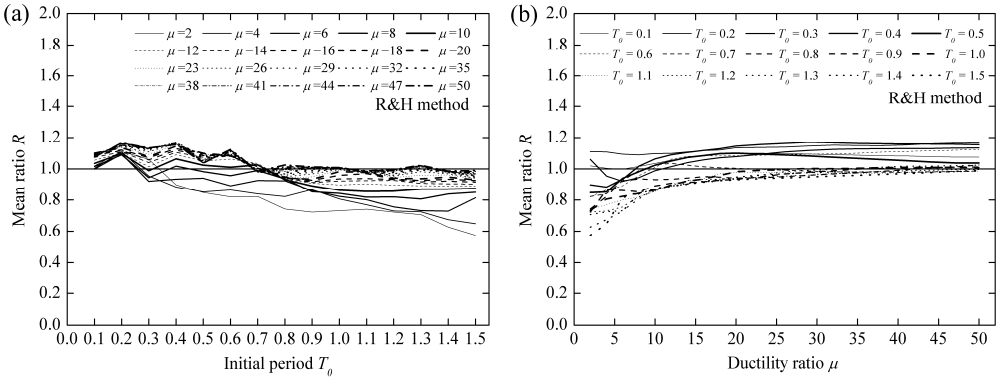

Fig. 148 Estimation accuracy of R&H method based on 6-storey superstructure: (a) against initial period for different ductility ratios and (b) against ductility ratio for different initial periods

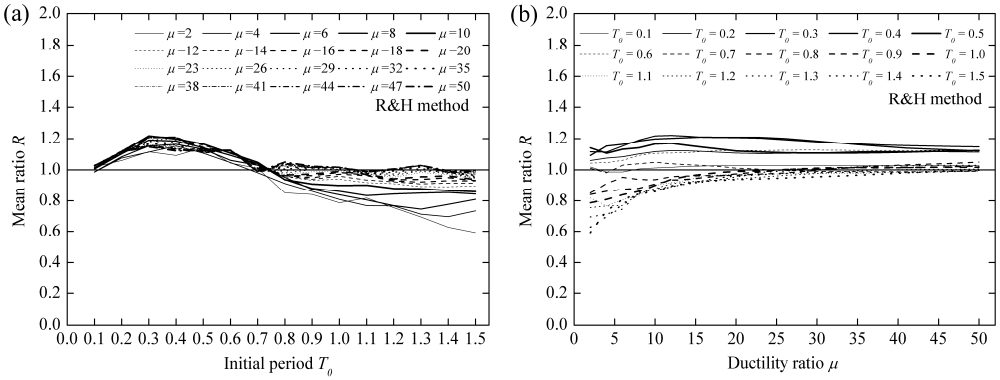

Fig. 149 Estimation accuracy of R&H method based on 9-storey superstructure: (a) against initial period for different ductility ratios and (b) against ductility ratio for different initial periods

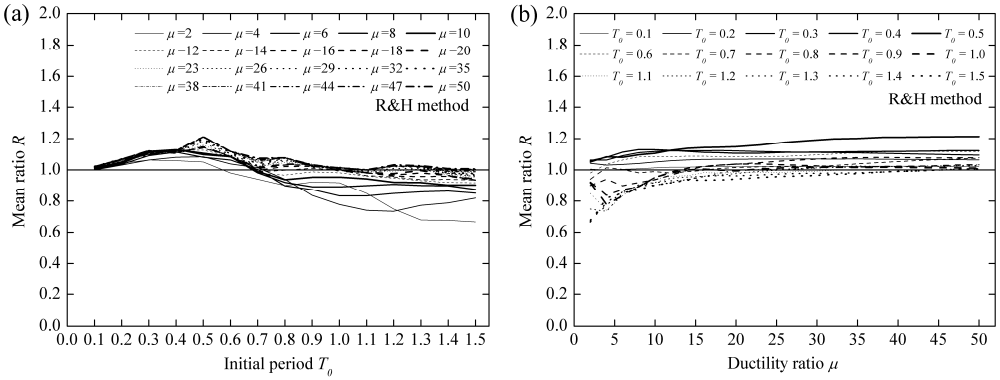

Fig. 150 Estimation accuracy of R&H method based on 12-storey superstructure: (a) against initial period for different ductility ratios and (b) against ductility ratio for different initial periods

The coefficients of variation computed using R&H method are presented in Figs. 151-154 for different superstructures. With increasing the storey number of superstructures, the coefficient of variation in general decreases, in particular for relatively low ductility ratio. In addition, it is found that for a given superstructure the coefficient of variation increases with increasing the initial period and decreases with increasing the ductility ratio.

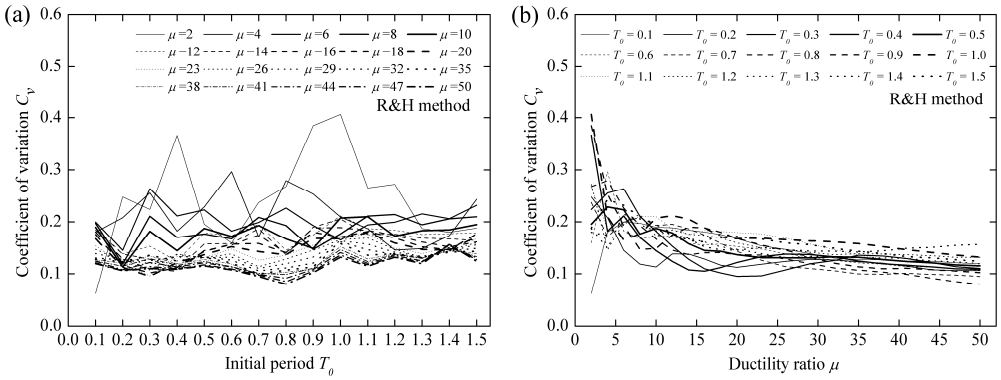

Fig. 151 Coefficient of variation computed based on R&H method and 3-storey superstructure: (a) against initial period for different ductility ratios and (b) against ductility ratio for different initial periods

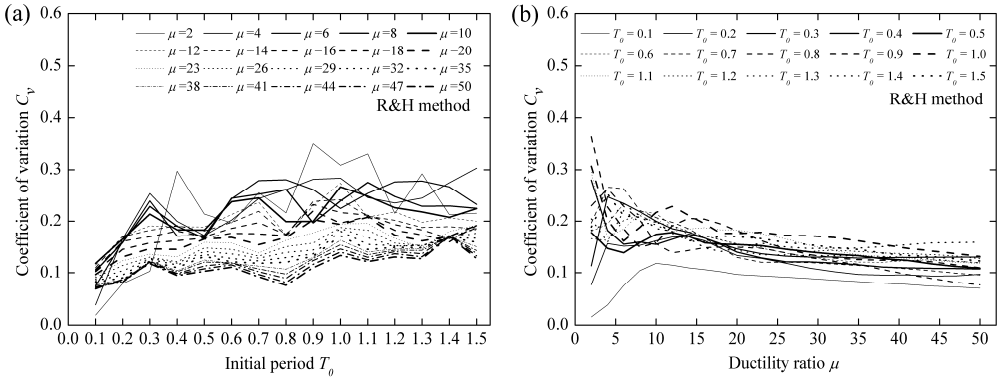

Fig. 152 Coefficient of variation computed based on R&H method and 6-storey superstructure: (a) against initial period for different ductility ratios and (b) against ductility ratio for different initial periods

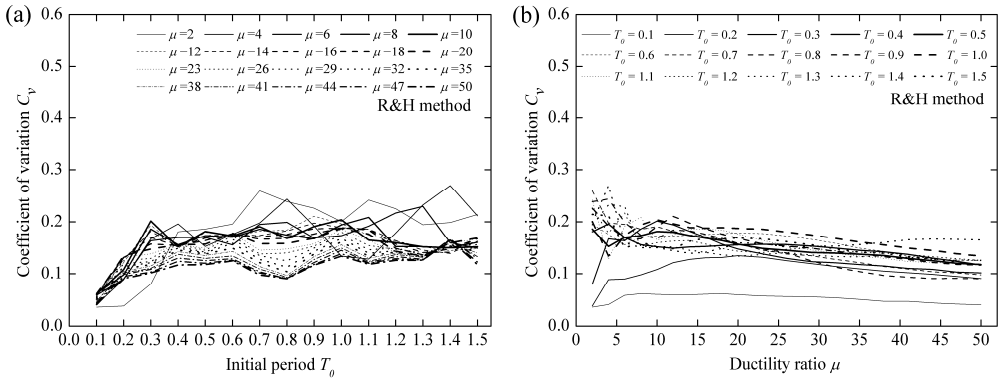

Fig. 153 Coefficient of variation computed based on R&H method and 9-storey superstructure: (a) against initial period for different ductility ratios and (b) against ductility ratio for different initial periods

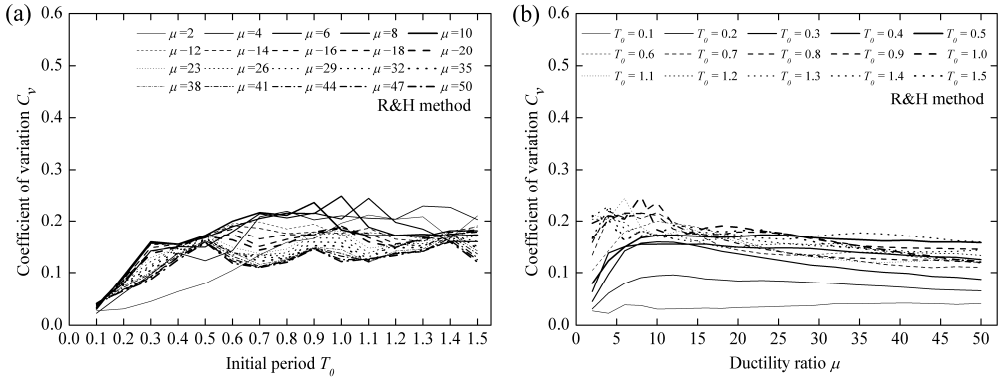

Fig. 154 Coefficient of variation computed based on R&H method and 12-storey superstructure: (a) against initial period for different ductility ratios and (b) against ductility ratio for different initial periods

5.1.3 Accuracy of Liu method

Figs. 155-158 present the mean ratio *R* computed using Liu method. It is found that the estimation accuracy is slightly improved by Liu method when compared with R&H method. In addition, the maximum displacement of isolation interface is in general overestimated by Liu method. With increasing the storey number of the superstructures, the mean ratio *R* increases. Furthermore, the estimation accuracy is only affected by various superstructures in relatively low initial periods. In other words, for relatively high initial periods, there is no significant change in the computed mean ratio *R*.

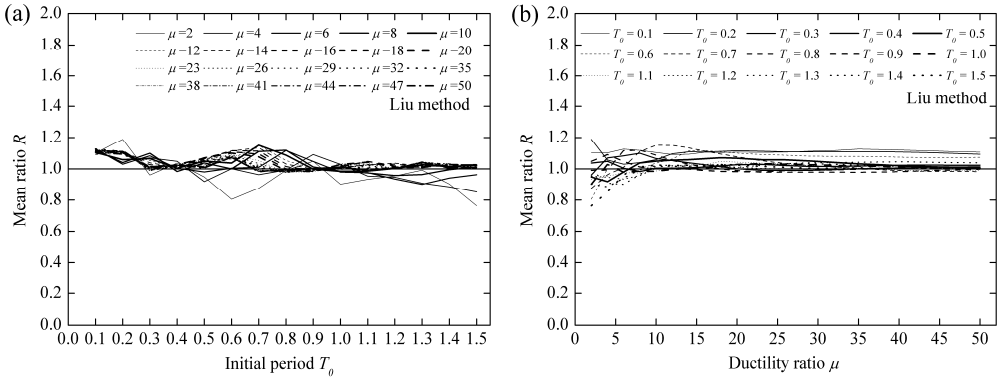

Fig. 155 Estimation accuracy of Liu method based on 3-storey superstructure: (a) against initial period for different ductility ratios and (b) against ductility ratio for different initial periods

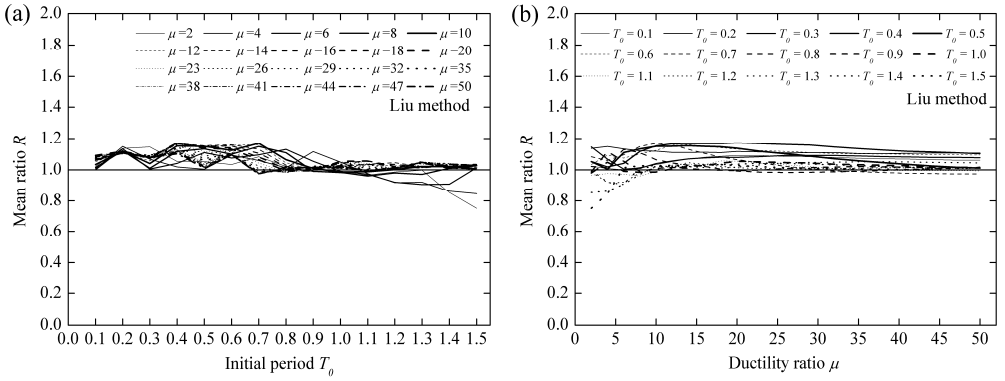

Fig. 156 Estimation accuracy of Liu method based on 6-storey superstructure: (a) against initial period for different ductility ratios and (b) against ductility ratio for different initial periods

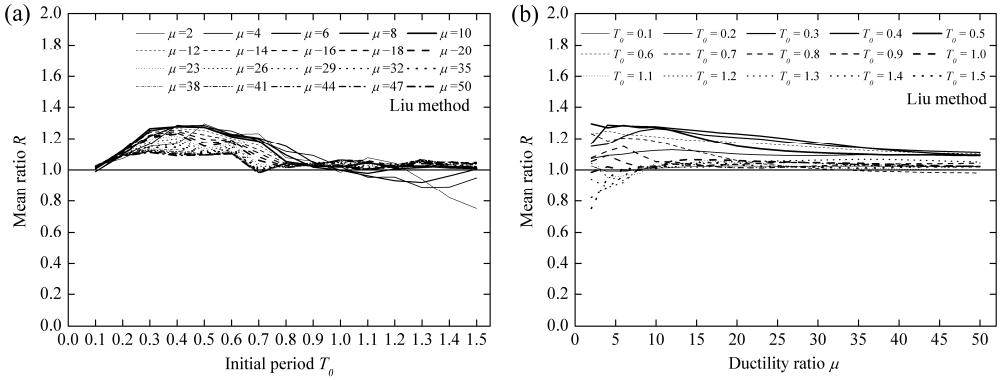

Fig. 157 Estimation accuracy of Liu method based on 9-storey superstructure: (a) against initial period for different ductility ratios and (b) against ductility ratio for different initial periods

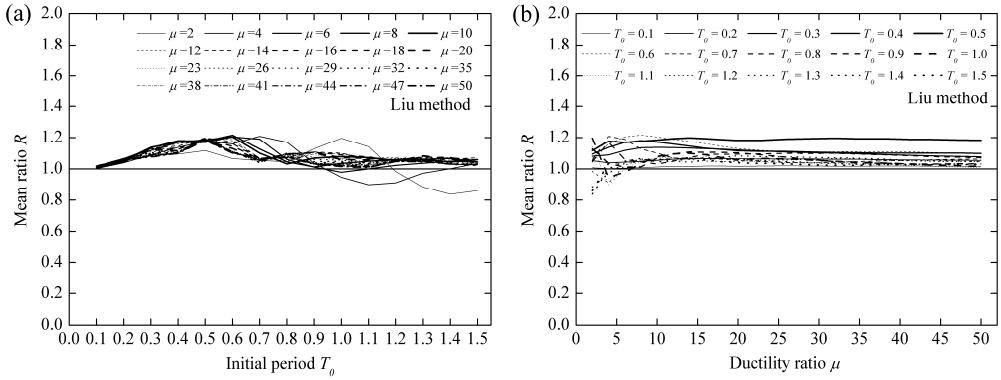

Fig. 158 Estimation accuracy of Liu method based on 12-storey superstructure: (a) against initial period for different ductility ratios and (b) against ductility ratio for different initial periods

Regarding the coefficient of variation C_v, as shown in Figs. 159-162, little larger results could be obtained when compared with R&H method. With varying different parameters, variation trend of C_v is found to be similar to R&H method.

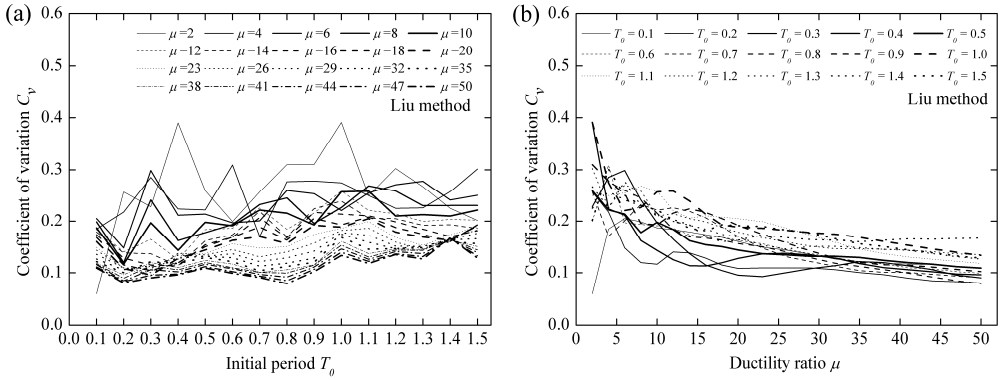

Fig. 159 Coefficient of variation computed based on Liu method and 3-storey superstructure: (a) against initial period for different ductility ratios and (b) against ductility ratio for different initial periods

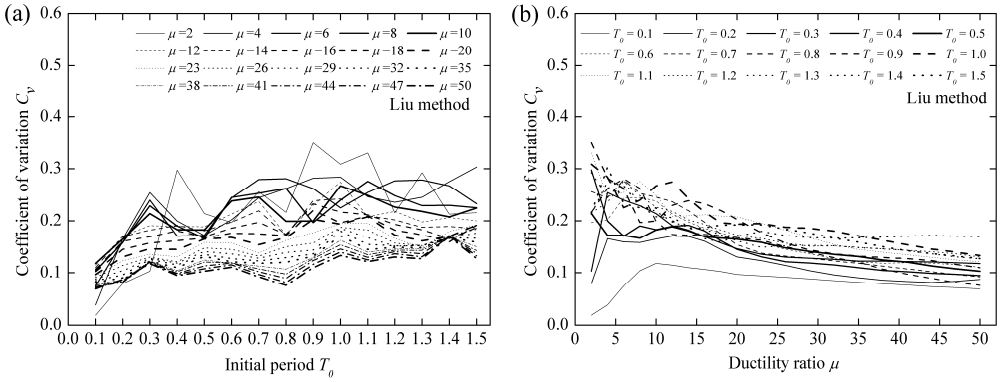

Fig. 160 Coefficient of variation computed based on Liu method and 6-storey superstructure: (a) against initial period for different ductility ratios and (b) against ductility ratio for different initial periods

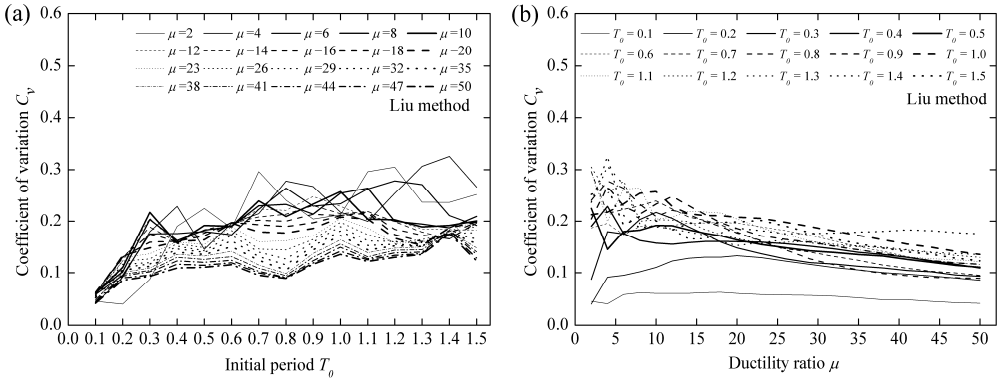

Fig. 161 Coefficient of variation computed based on Liu method and 9-storey superstructure: (a) against initial period for different ductility ratios and (b) against ductility ratio for different initial periods

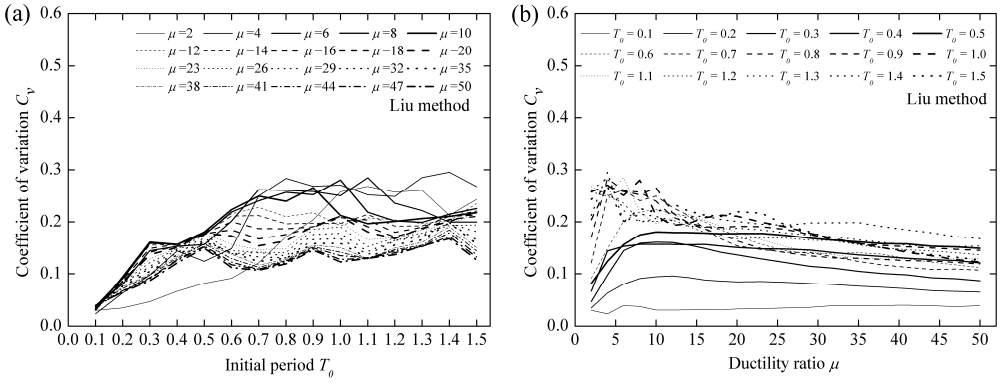

Fig. 162 Coefficient of variation computed based on Liu method and 12-storey superstructure: (a) against initial period for different ductility ratios and (b) against ductility ratio for different initial periods

5.2. Optimization Analyses of MDOF Systems

As observed in last sections, both R&H method and Liu method cannot predict satisfied estimates of the maximum displacement of isolation interface for base-isolated MDOF systems. It is expected that the optimal damping ratio which minimizes the difference of the maximum displacement response between nonlinear and linear time history analysis is significantly affected by the dynamic properties of both superstructure and isolation systems. In this section, optimization analyses are performed to investigate the optimal damping ratios based on the procedures described in previous Chapters. Similarly, the optimal damping ratios are averaged over the selected earthquake records for each initial period and each level of displacement ductility (see Eq. (72)).

The averaged optimal damping ratios are shown in Figs. 163-166 for MDOF systems with different superstructures. It can be observed from this figure, ξ_{opt} in general decreases with increasing the initial period of isolation systems. However, ξ_{opt} first increases and then decreases as the ductility ratio increases except for isolation systems with relatively short initial periods. Significant change in the optimal damping ratio happens when short initial period is considered. But, for the cases with long initial periods and high ductility ratios, the influence of different superstructures is not so remarkable.

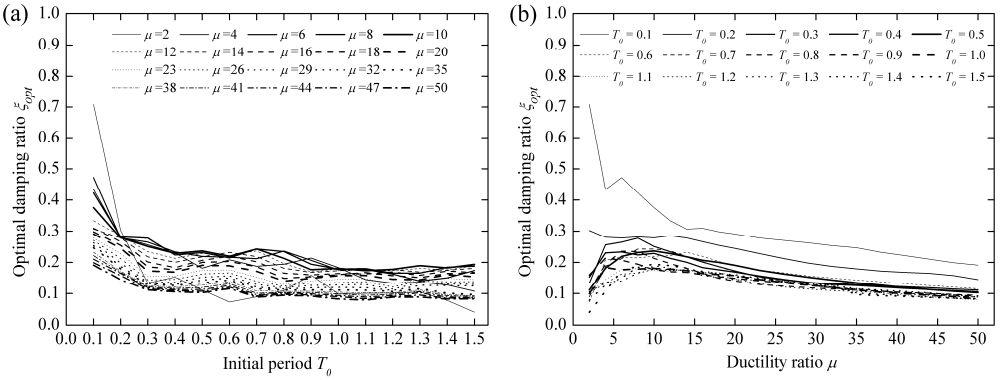

Fig. 163 The averaged optimal damping ratios based on 3-storey superstructure: (a) against initial period for different ductility ratios and (b) against ductility ratio for different initial periods

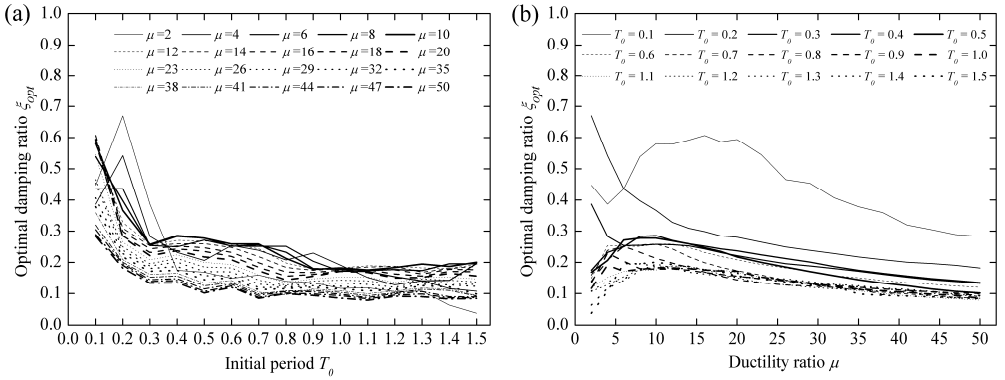

Fig. 164 The averaged optimal damping ratios based on 6-storey superstructure: (a) against initial period for different ductility ratios and (b) against ductility ratio for different initial periods

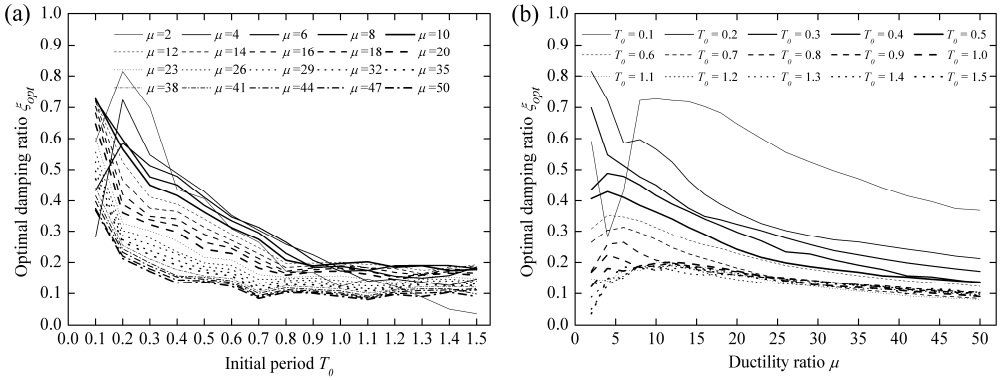

Fig. 165 The averaged optimal damping ratios based on 9-storey superstructure: (a) against initial period for different ductility ratios and (b) against ductility ratio for different initial periods

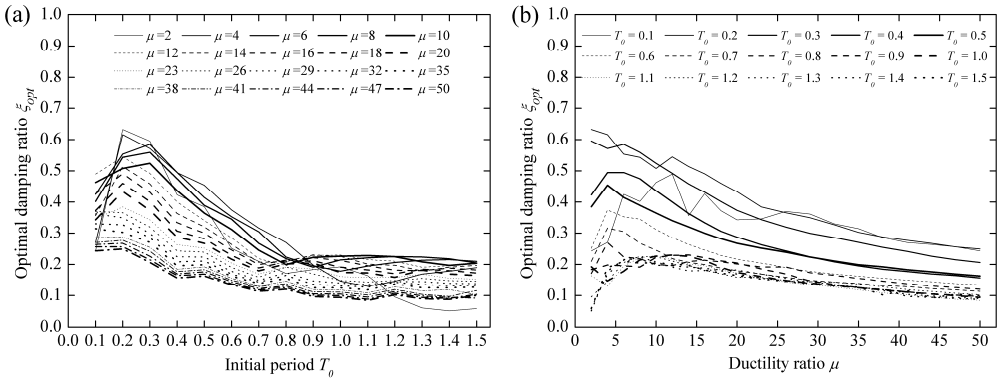

Fig. 166 The averaged optimal damping ratios based on 12-storey superstructure: (a) against initial period for different ductility ratios and (b) against ductility ratio for different initial periods

5.3. Regression Analyses of MDOF Systems

Again, Liu method is modified to take into account the influence of superstructure by regression analysis of the optimal damping ratio computed in Chapter 5.2. A factor *S*, which is a function of the ratio of the superstructure period to the equivalent period, is introduced to Liu method. Thus, the proposed formula of equivalent viscous damping ratio for MDOF systems has the following form:

$$\xi_{eq} = \xi_0 + \frac{2(1-\alpha)(\mu-1)}{\pi\mu\left[1+\alpha(\mu-1)\right]} \cdot A \cdot T_0^{\,B} (\mu-1)^C \cdot S \tag{88}$$

The factor *S* could be computed as the ratio of the optimal damping ratios to those calculated using Liu method. For different superstructures the factors are plotted in Figs. 167-170 against the ratio of equivalent period to superstructure period with fixed base, i.e., T_{eq}/T_{fb}.

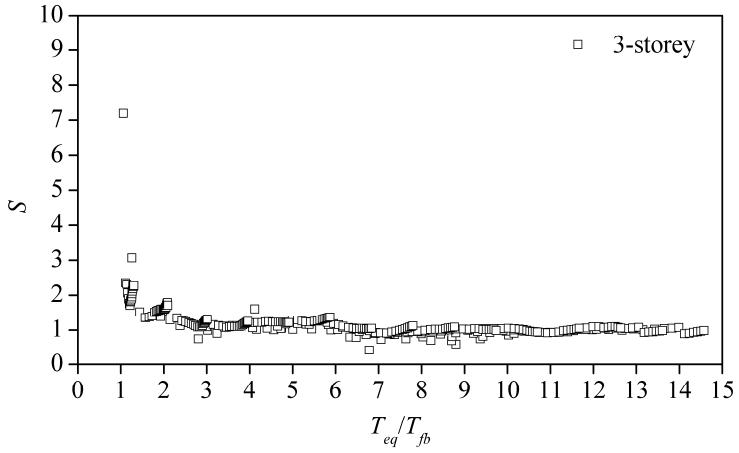

Fig. 167 Values of the factor S for 3-storey base-isolated structures

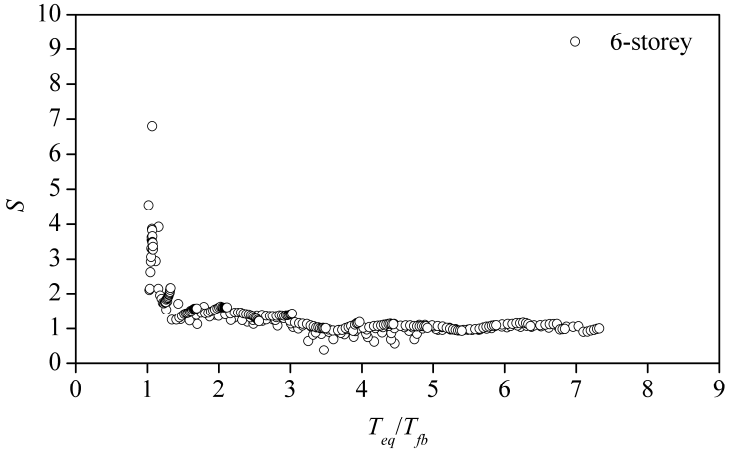

Fig. 168 Values of the factor S for 6-storey base-isolated structures

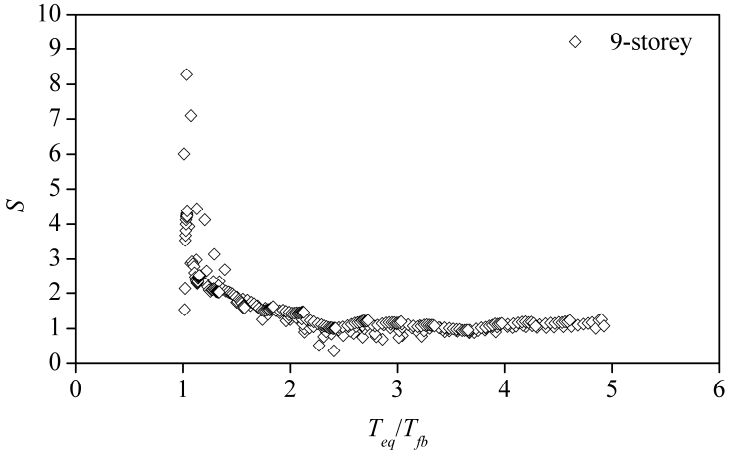

Fig. 169 Values of the factor S for 9-storey base-isolated structures

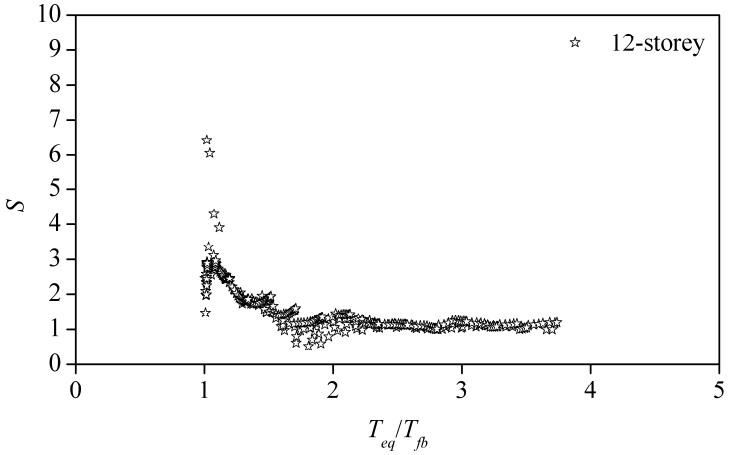

Fig. 170 Values of the factor S for 12-storey base-isolated structures

In the present research, the relationship between S and T_{eq}/T_{fb} is modeled using the following rational function:

$$S = \frac{s_1 \cdot T_{eq}/T_{fb} + s_2}{T_{eq}/T_{fb} + s_3} \tag{89}$$

Minimizing the sum of squares of the differences between the optimal damping ratios and those predicted by Eq. (88) and Eq. (89), parameters s_1, s_2 and s_3 are converged to 0.87, -0.1308 and -0.8094, respectively, with a coefficient of determination R^2 equal to 0.74, as shown in Fig. 171.

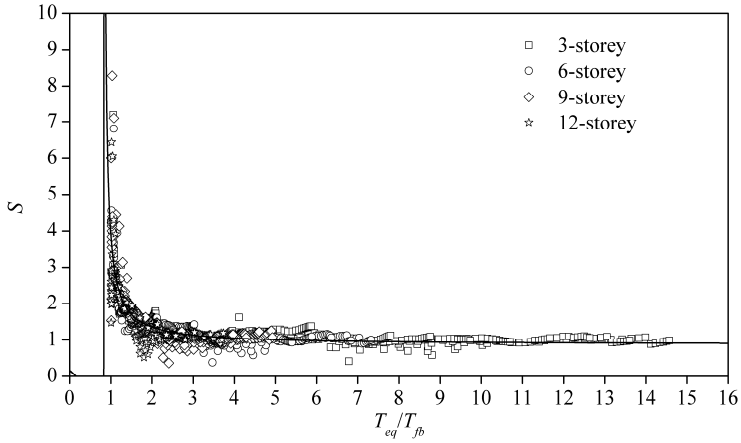

Fig. 171 Regression analysis of the factor S for all considered superstructures

Finally, the proposed formula of equivalent viscous damping ratio used for MDOF base-isolated systems can be expressed as:

$$\xi_{eq} = \xi_0 + \frac{2\cdot(1-\alpha)\cdot(\mu-1)}{\pi\cdot\mu\cdot\left[1+\alpha\cdot(\mu-1)\right]}\cdot A\cdot T_0{}^{B}(\mu-1)^{C}\cdot\left(\frac{0.87\cdot T_{eq}/T_{fb}-0.1308}{T_{eq}/T_{fb}-0.8094}\right) \tag{90}$$

where the parameters A, B and C could be computed based on Eq. (78).

In accordance with Eq. (78) and Eq. (90), mean approximate to exact displacement ratios are computed again and presented in Figs. 172-175. As can be observed, estimation accuracy is significantly improved when compared with the results from Figs. 147-150 and Figs. 155-158, in particular for base-isolated MDOF systems with 9- and 12-storey superstructures.

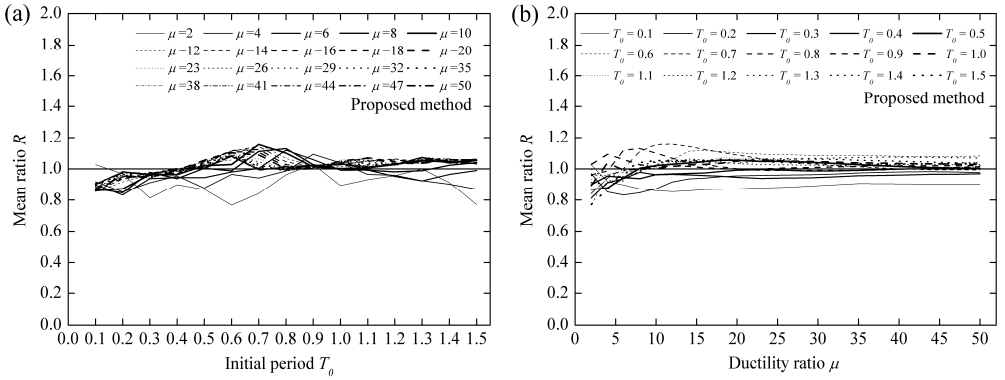

Fig. 172 Estimation accuracy of proposed method based on 3-storey superstructure: (a) against initial period for different ductility ratios and (b) against ductility ratio for different initial periods

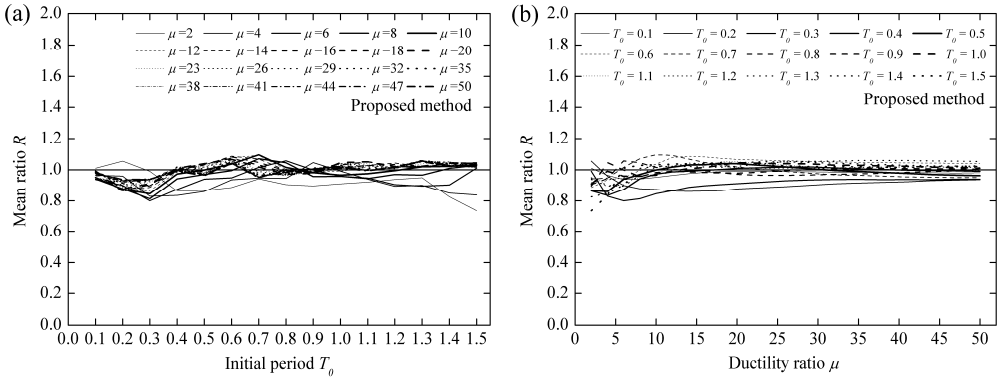

Fig. 173 Estimation accuracy of proposed method based on 6-storey superstructure: (a) against initial period for different ductility ratios and (b) against ductility ratio for different initial periods

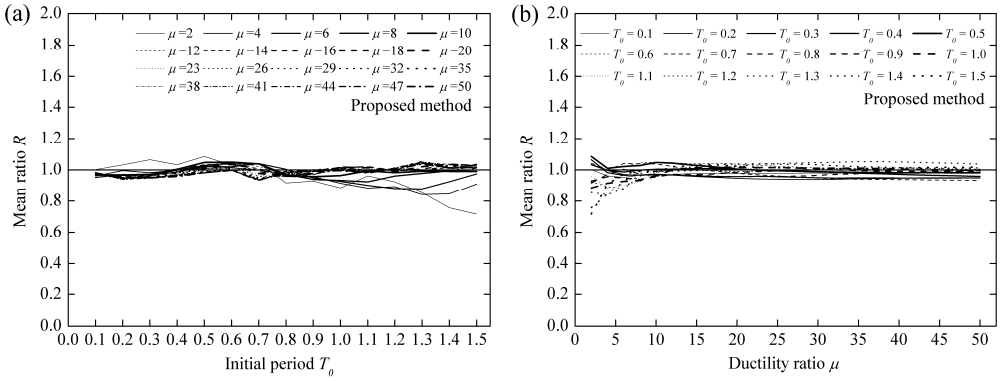

Fig. 174 Estimation accuracy of proposed method based on 9-storey superstructure: (a) against initial period for different ductility ratios and (b) against ductility ratio for different initial periods

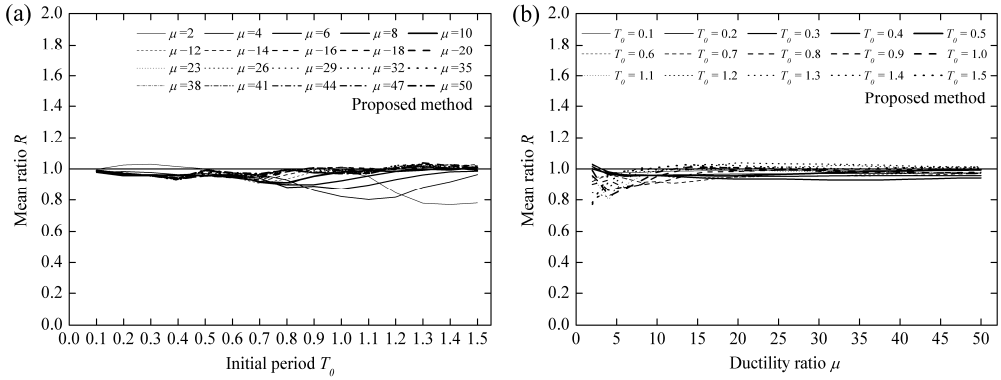

Fig. 175 Estimation accuracy of proposed method based on 12-storey superstructure: (a) against initial period for different ductility ratios and (b) against ductility ratio for different initial periods

The coefficient of variation C_V obtained by the proposed formula is presented in Figs. 176-179. It is seen that C_V in general decreases with increasing the ductility ratio and the initial period. In addition, as the height (or period) of the superstructure increases, C_V decreases overall.

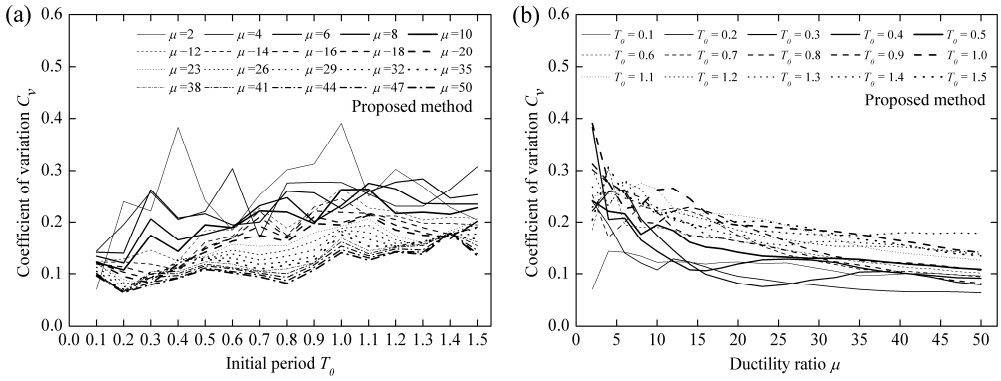

Fig. 176 Coefficient of variation computed based on proposed method and 3-storey superstructure: (a) against initial period for different ductility ratios and (b) against ductility ratio for different initial periods

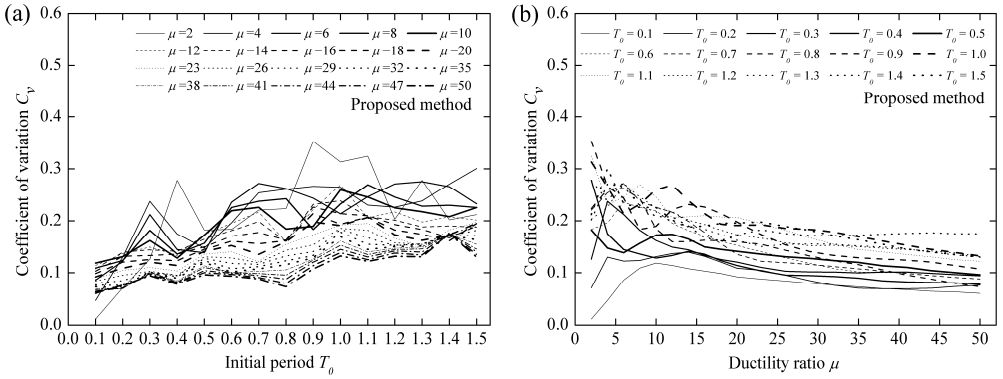

Fig. 177 Coefficient of variation computed based on proposed method and 6-storey superstructure: (a) against initial period for different ductility ratios and (b) against ductility ratio for different initial periods

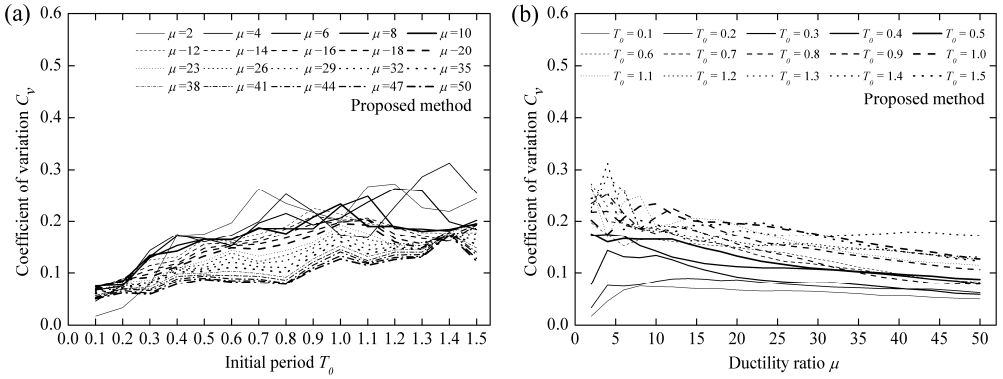

Fig. 178 Coefficient of variation computed based on proposed method and 9-storey superstructure: (a) against initial period for different ductility ratios and (b) against ductility ratio for different initial periods

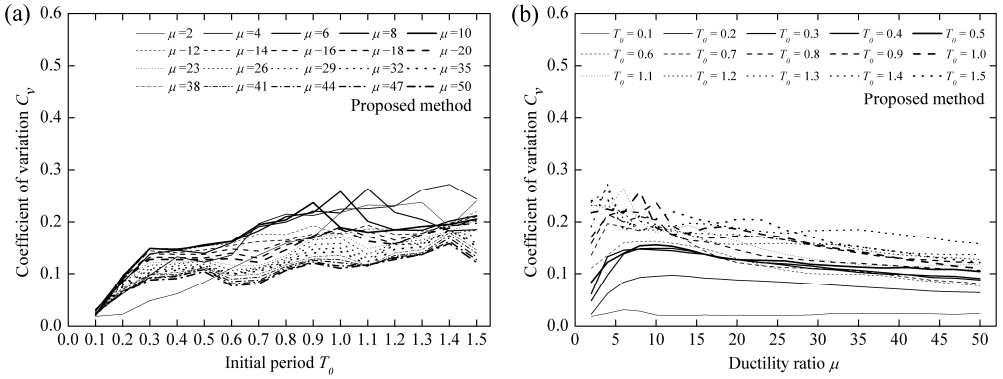

Fig. 179 Coefficient of variation computed based on proposed method and 12-storey superstructure: (a) against initial period for different ductility ratios and (b) against ductility ratio for different initial periods

5.4. Summary

In this Chapter, equivalent linearization methods are investigated based on MDOF base-isolated buildings. Both R&H method and Liu method are not able to accurately predict the maximum displacement of isolation systems when the bilinear isolation systems having short initial periods and small ductility ratios. It is found that the ratio between equivalent period and superstructure period has important influence on the estimation accuracy of equivalent linearization analysis. In other words, if this ratio is relatively large ($T_{eq}/T_{fb}>3$), the superstructure can be assumed to be a rigid body, otherwise large errors could be obtained due to the SDOF assumption.

In order to incorporate the effect of superstructure, Liu method is further modified. An improved equivalent linearization method is derived using similar procedure described in Chapter 4. Results show that the prediction accuracy is significantly improved by the newly proposed method and the relative error between approximate and exact maximum inelastic displacement is less than 10%.

CHAPTER 6

6. STRUCTURAL ANALYSES OF BASE-ISOLATED BUILDINGS

Modern seismic codes (CEN, 2004; D.M., 2008) provide rules to analysis and design base isolated structures in which the isolation system is located below the main mass of the structure. The seismic performance assessment of such base-isolated buildings can be carried out by linear and/or nonlinear structural analysis methods (Di Sarno et al., 2011).

Here, the recent Italian seismic code (D.M., 2008) is focused, in which the structural analysis of structures with base isolation can be conducted as follows:

- *Equivalent static linear analysis;*
- *Linear dynamic analysis (either modal or linear response history);*
- *Nonlinear dynamic analysis (nonlinear response history).*

In this Chapter, the suitability of different analysis methods is investigated with the equivalent linearization technique recommended in code (R&H method) and those proposed in Chapter 4 and 5. Here, for the sake of clarity, the equivalent linearization methods proposed in Chapter 4 (SDOF systems) and 5 (MDOF systems) are abbreviated to Liu I method and Liu II method.

6.1. Introduction

Nonlinear dynamic analysis is deemed compulsory whenever the isolation system cannot be represented by an equivalent linear model; an adequate constitutive relationship should thus be formulated and implemented in the structural analysis scheme.

However, as mentioned in Italian seismic code (D.M., 2008), linear analyses, either static or dynamic, may be employed if the isolation system can be modeled with equivalent linear visco-elastic behavior, if it consists of devices such as laminated elastomeric bearings, or with bilinear hysteretic behavior if the system consists of elasto-plastic types of devices.

When equivalent linear analysis is considered, effective stiffness (K_{eff}) and effective viscous damping (ξ_{eff}) are utilized to model each isolator unit. The effective response quantities (K_{eff} and ξ_{eff}) are computed at lateral displacements relative to the limit state under consideration, where the effective stiffness K_{eff} corresponds to the secant stiffness at the total design displacement and the effective damping ξ_{eff} of the bearing devices quantifies the energy dissipated under cyclic loads. For higher modes outside this range, the modal damping ratio of the complete structure should be that of a fixed base superstructure.

Since the design displacement of isolator unit is unknown at the beginning, the linearization of the isolator constitutive law is an iterative procedure. However, the number of iterations for convergence tends to be rather low to match the 5% error recommended in the seismic standards; generally less than 5 iterations are sufficient.

In order to model the behavior of isolation system as being equivalent linear, all the following conditions specified in Italian seismic code (D.M., 2008) must be met:

(1) The equivalent stiffness, K_{eq}, should be greater or equal to 50% of the secant stiffness for cycles with displacement equal to 20% of the design displacement, as shown in Fig. 180, namely:

$$\frac{K_{eq}}{K_{0.2eq}} = \begin{cases} \dfrac{1+\alpha(\mu-1)}{\mu}\dfrac{0.2\mu}{1+\alpha(0.2\mu-1)} & if\ \mu \geq 5 \\ \dfrac{1+\alpha(\mu-1)}{\mu} & if\ \mu < 5 \end{cases} \geq \frac{1}{2} \tag{91}$$

Simplifying the above inequality, the relationship between μ and α can be derived in order to satisfy this requirement, which can be expressed as:

$$\begin{cases} \mu \geq \max\left(\dfrac{3(1-\alpha)}{\alpha}, 5\right) \\ \mu < \min\left(\dfrac{2(1-\alpha)}{1-2\alpha}, 5\right) \end{cases} \tag{92}$$

Considering the maximum strain hardening ratio α = 0.2 and the second item of Eq. (92), the ductility ratio has to be less than 2.67, which is not suitable for seismic iso-

lation system subjected to design earthquakes. So, in this study, only the first item of Eq. (92) is considered.

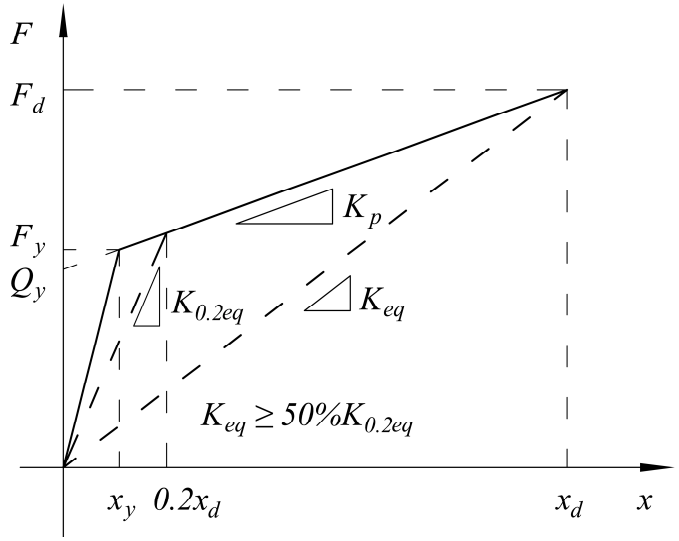

Fig. 180 Requirement of equivalent stiffness in linearization of bilinear behavior

(2) The equivalent damping ratio, ξ_{eq}, of seismic isolation system should be less than 30%, that is:

$$\xi_{eq} = \xi_0 + \frac{2(1-\alpha)(\mu-1)}{\pi\mu\left[1+\alpha(\mu-1)\right]} \leq 0.30 \tag{93}$$

(3) The force-displacement characteristics of seismic isolation system do not vary more than 10% due to the rate of loading and the variation of vertical load. In order to simplify the assessment procedure, the force-displacement characteristics of isolation system are assumed to be independent of the above aspects in this study.

(4) To provide sufficient re-centering capability, increase of the force in isolation system for displacements between $0.5x_d$ and x_d is not less than 2.5% of the total gravity load above the system, as presented in Fig. 181. Similar to requirement (1), considering the performance of seismic isolation system subjected to design earthquakes, conditions when ductility ratio is less than 2.0 are neglected in this study.

Substituting F_y/f for the total weight of isolation system and considering the definition of strain hardening ratio and ductility ratio, this requirement can be expressed as:

$$\Delta F = F_d - F_{0.5d} = 0.5x_d K_2 \geq 2.5\% x_y K_1 / f \tag{94}$$

Separating the ductility ratio from the inequality, the effective range of μ is obtained as below:

$$\mu \geq \frac{1.0}{20\alpha f} \tag{95}$$

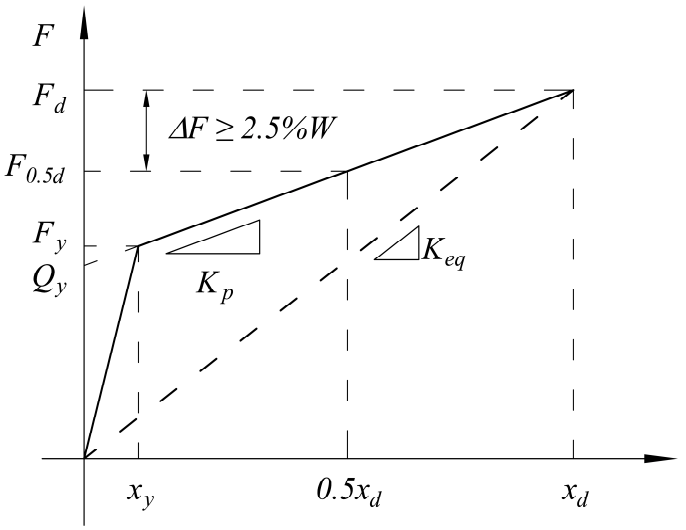

Fig. 181 Requirement of restoring force in linearization of bilinear behavior

It can be noted that equivalent linear properties of seismic isolation system are only related to the ductility ratio μ and strain hardening ratio α in R&H method. The yield strength of seismic isolation system is assigned to be 5% of the structural weight, which is also applicable to the following parametric study. Assuming α ranges from 0.02 to 0.20 and μ varies between 2 and 50, final feasible region determined by requirements (1), (2) and (4) is presented in Fig. 182. As can be observed in this figure, the feasible region is dominated by requirements (1) and seismic isolation systems with high values of α and μ are suitable for the procedure of equivalent linearization. However, in most cases, equivalent linearization of seismic isolation system is not permitted. Thus, under a given earthquake ground motion, adjusting

the bilinear properties of seismic isolation system so as to satisfy the limited condition may become very inconvenient. In addition, the selected isolation bearings may be unavailable on the market.

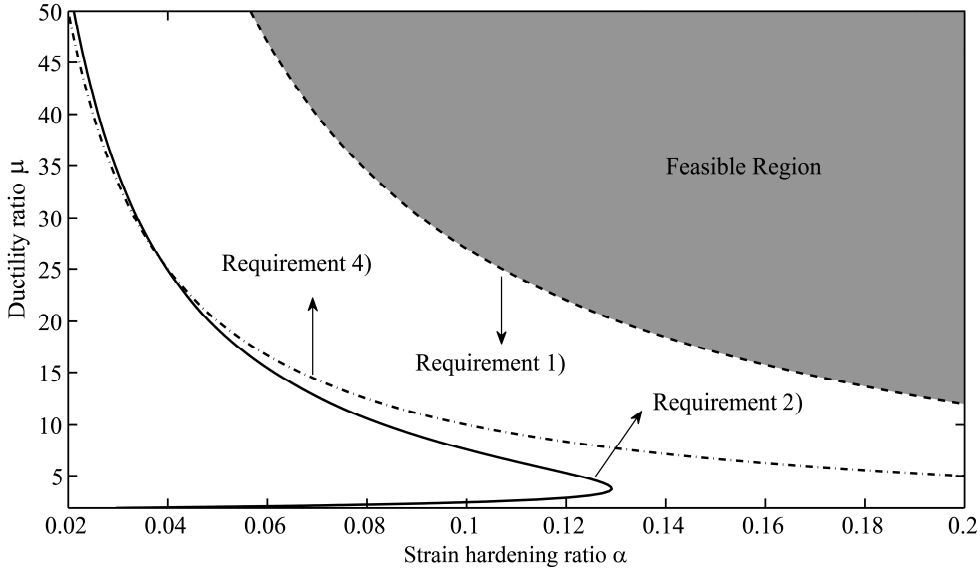

Fig. 182 Feasible region of equivalent linearization of seismic isolation system

6.2. Analysis Procedures

Detailed procedures to perform different analysis methods are presented as below in accordance with the Italian seismic code (D.M., 2008). Application of various analysis methods depends on the complexity of base-isolated buildings. Specific requirements should be satisfied when applying the corresponding analysis method.

6.2.1 Equivalent Static Linear Analysis

In equivalent static linear analysis (SLA), the superstructure of base-isolated buildings is assumed to be a rigid solid translating above the isolation system. Then the effective period for translation is:

$$T_{eff} = 2\pi \sqrt{\frac{M}{K_{eff}}} \tag{96}$$

where M is the mass of superstructure and K_{eff} is the effective stiffness of the isolation system.

The torsional movement about the vertical axis may be neglected in the evaluation of the effective horizontal stiffness and in the simplified linear analysis if, in each of the two principal horizontal directions, the total eccentricity (including the accidental eccentricity) between the stiffness centre of the isolation system and the vertical projection of the centre of mass of the superstructure does not exceed 7.5% of the length of the superstructure transverse to the horizontal direction considered. This is a condition for the application of the simplified linear analysis method.

Besides the requirements in applying equivalent linearization technique, to perform equivalent static linear analysis of base-isolated buildings, the following conditions have to be also met:

1) the effective period T_{eff} satisfies the following condition:

$$3T_{fb} \leq T_{eff} \leq 3 \text{ s} \tag{97}$$

where T_{fb} is the fundamental period of the superstructure assuming a fixed base (could be estimated through a simplified expression).

2) the ratio between the vertical and the horizontal stiffness of the isolation system should satisfy the following expression:

$$\frac{K_v}{K_{eff}} \geq 150 \tag{98}$$

3) the fundamental period in the vertical direction, TV, should be not longer than 0,1 s, where:

$$T_v = 2\pi \sqrt{\frac{M}{K_v}} \tag{99}$$

For civil and industrial buildings, the following conditions are added:

- The superstructure has a height not greater than 20 meters and not more than 5 floors.

- The substructure can be considered infinitely rigid or the natural period is not greater than 0.05 s.

- The largest dimension in plan of the superstructure is less than 50 meters;

- In each of the principal directions of horizontal eccentricity total (excluding the accidental) between the center of rigidity of the isolation system and the vertical projection of the center of mass is not more than 3% of the size of the superstructure transverse to the horizontal direction considered.

As mentioned previously, an iteration procedure should be used to perform equivalent static linear analysis of base-isolated buildings due to the unknown design displacement, which can be described through the following steps:

Step 1: Assuming the initial design displacement d_0 of isolation system;

Step 2: Calculate the equivalent properties (K_{eff} and ξ_{eff}) using the recommended method in code (R&H method) or those proposed in Chapter 4 and 5 (Liu I and Liu II methods);

Step 3: Compute the displacement of isolation systems from the following expression:

$$d_{dc} = \frac{M \cdot S_e\left(T_{eff}, \xi_{eff}\right)}{K_{eff}} \tag{100}$$

where $S_e(T_{eff}, \xi_{eff})$ is the spectral acceleration, taking into account the appropriate value of effective damping ξ_{eff}.

Step 4: Compare d_{dc} with d_0, if the relative error between them is less than 1%, then stop the iteration, otherwise replace d_0 with d_{dc} and go to Step 2.

Step 5: The horizontal forces applied at i^{th} level of the superstructure should be calculated, in each horizontal direction through the following expression:

$$f_i = m_i \cdot S_e\left(T_{eff}, \xi_{eff}\right) \tag{101}$$

6.2.2 Linear Dynamic Analysis

If the behavior of the devices may be considered as equivalent linear but any one of the conditions presented in Chapter 6.2.1 is not met, modal response analysis (RSP) or linear response history analysis (LTHA) may be performed.

If you adopt the modal response spectrum analysis, the vertical component must be taken into account in the cases when the ratio between the vertical stiffness of isolation system K_v and the equivalent horizontal stiffness K_{eff} is lower than 800. The considered elastic spectrum should be reduced for the entire range of periods $T \geq 0.8\ T_{is}$, assuming for the reduction coefficient η, the value corresponding to the equivalent viscous damping ratio ξ_{eff} of the isolation system

Analysis procedures of linear dynamic analysis of base-isolated buildings are presented as below:

Step 1: Assuming the initial design displacement d_0 of isolation system;

Step 2: Calculate the equivalent properties (K_{eff} and ξ_{eff}) using R&H method, Liu I method and Liu II method;

Step 3: Compute the displacement d_{dc} of isolation system from modal response spectrum analysis or linear response history analysis. Note that for modal response spectrum analysis the considered elastic spectrum should be reduced for periods $T \geq 0.8\ T_{is}$ with the equivalent damping ratio ξ_{eff}, while for higher modes with periods $T < 0.8\ T_{is}$ the superstructure damping ratio could be used.

Step 4: Compare d_{dc} with d_0, if the relative error between them is less than 1%, then stop the iteration, otherwise replace d_0 with d_{dc} and go to Step 2.

Step 5: The horizontal forces applied at each level of the superstructure can be directly calculated using linear dynamic analysis.

6.2.3 Nonlinear Dynamic Analysis

If an isolation system cannot be represented by an equivalent linear model, the seismic response should be evaluated by nonlinear time history analysis (NTHA), using an constitutive relationship of the devices which can adequately reproduce

the behavior of the isolation system in the range of deformations and velocities anticipated in the seismic design situation.

Specifically, in this research, bilinear hysteretic behavior of isolation systems is considered as well as the Newmark-β method to solve the nonlinear dynamic analysis.

6.3. Seismic Input Characterization

The structural analyses of base-isolated buildings are in general carried out based on response acceleration spectrum specified in codes, which could be utilized by equivalent static linear analysis and modal response spectrum analysis. However, for linear and nonlinear response history analysis, spectrum-compatible natural records should be considered as seismic inputs. The modeling of the seismic input in both cases is discussed hereafter.

6.3.1 Acceleration Response Spectrum

In DM 2008, two damage limit states (SLO, SLD) and two ultimate limit states (SLV, SLC) are established for the purpose of structural design, as presented in Table 7.

Limit states		Target performance	Return Periods T_R (years)	Probability of exceedance in 50 years
Serviceability	SLO	Immediate Operability	30	81%
limit states	SLD	Damage Control	50	63%
Ultimate	SLV	Life Safety	475	10%
limit states	SLC	Collapse Prevention	975	5%

Table 7
Different limit states considered in DM 2008.

DM 2008 does not use the concept of seismic zones but defines the response spectra in each point of a network covering the entire Italian Territory. According to the location of the building and the return period of seismic hazard, three parameters, a_g, F_o and T_C^* can be provided to generate the elastic acceleration spectrum. Due to space limitation, the detailed shape of 5%-damped horizontal acceleration spectrum and meanings of different parameters can be found in Chapter 3 of DM 2008.

When response spectrum is used, high viscous damping ratio (>0.05) is generally introduced by base isolation system, so the damping reduction factor will be used to get an approximate estimate of high damping elastic response spectra from their 5% counterpart. The expression of damping reduction factor used in DM 2008 was derived by Bommer et al. (Bommer et al., 2000), as shown in Eq. (102), where ξ is applied in decimal form.

$$\eta = \sqrt{\frac{10}{5+100\cdot\xi}} \tag{102}$$

Due to the 2009 L'Aquila earthquake, parameters a_g, F_o and T_C^* are selected based on the location of L'Aquila in Italy, namely, a_g = 0.334, F_o = 2.400 and T_C^* = 0.364. Assuming the investigated base-isolated buildings in this region have the following structural parameters, soil type *C* and topology type *T1*, the 5%-damped elastic acceleration spectra corresponding to different limit states are presented in Fig. 183. In the present study, for the sake of simplicity, only the severest limit state SLC is considered as seismic input.

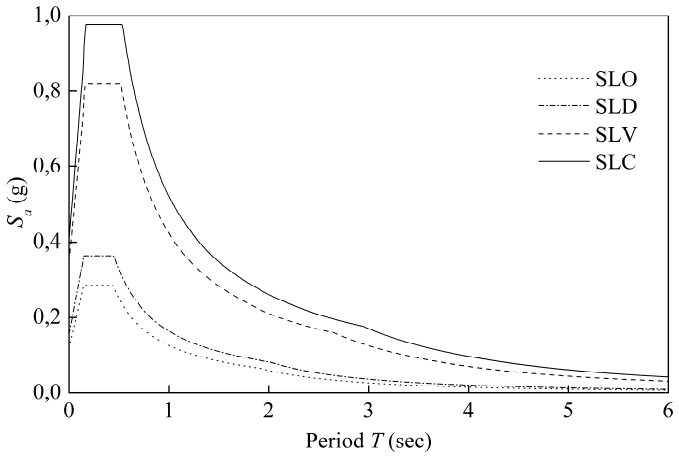

Fig. 183 5%-damped elastic acceleration spectra of different limit states

6.3.2 Natural Acceleration Time-histories

Besides the acceleration response spectra, ultimate limit states in DM 2008 can be also verified through the use of artificial, simulated or natural ground motions. To perform nonlinear time history analysis of base-isolated building, a set of twelve natural ground motions has been compiled from the Pacific Earthquake Engineering

Research Center (PEER, 2010). Note that the ground motions are selected to fit the target response spectrum without consideration of geological conditions and earthquake mechanisms. The digital records of these ground motions and summaries of their characteristics are presented in Fig. 184 and Table 3, respectively.

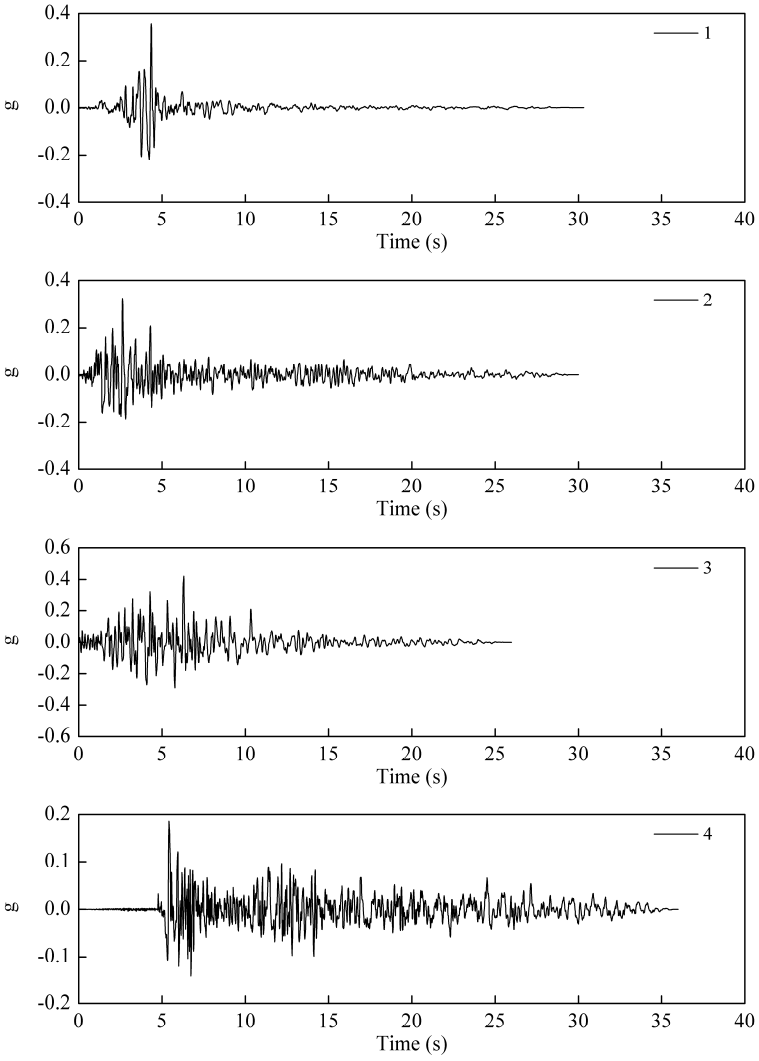

Fig. 184 Digital records of the selected ground motions

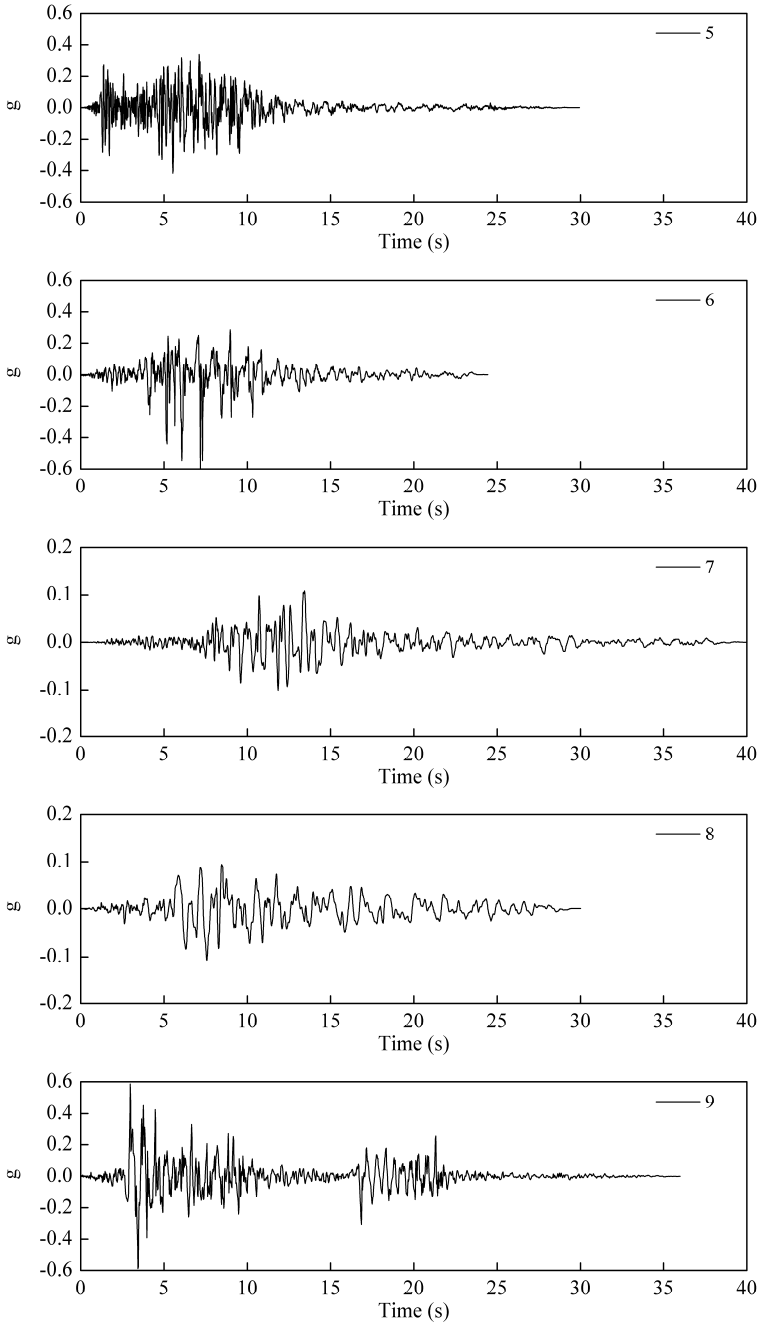

Fig. 184 Digital records of the selected ground motions (continued)

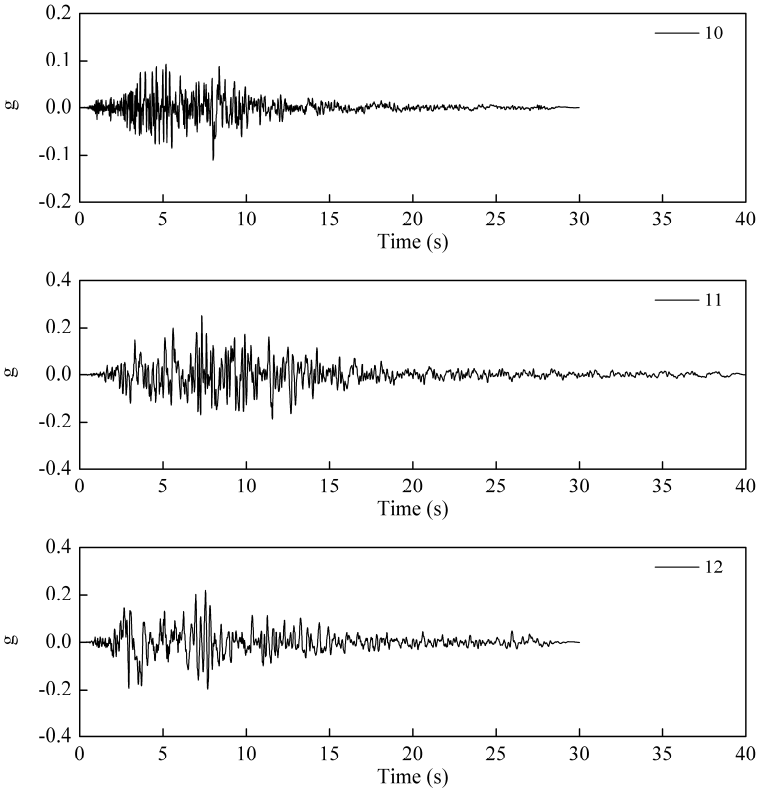

Fig. 184 Digital records of the selected ground motions (continued)

The selected earthquake ground motions should be scaled so that their mean response spectrum is compatible to the target design spectrum corresponding to SLC limit state. The scaling procedure is composed of two phases. At the beginning, the 5%-damped acceleration spectra of these ground motions are computed and shown in Fig. 185.

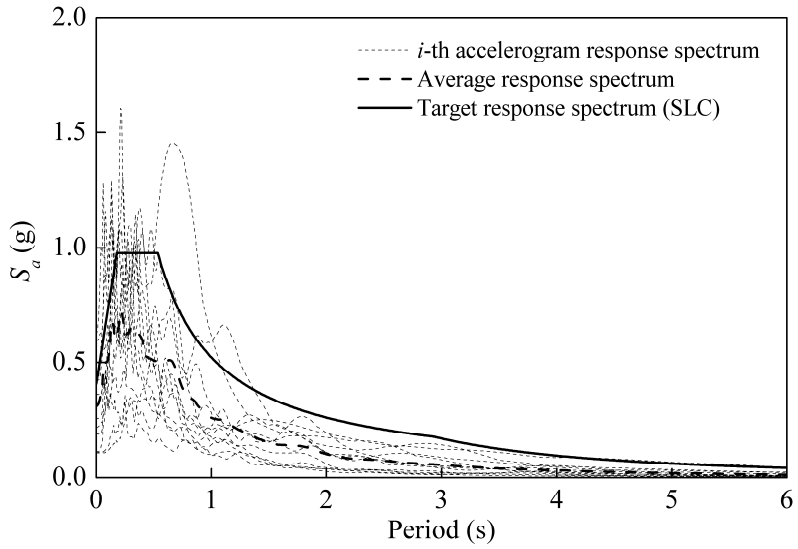

Fig. 185 Original acceleration spectra of the selected ground motions

The first phase is an amplitude scaling method which seeks to minimize a sum (ε) of the weighted squared errors between the geometric mean of the selected ground motions and the target spectral values at various periods. Error ε is defined as:

$$\varepsilon = \sum_{i=1}^{n} w_i \cdot \left(S_1 \cdot y_i - y_{Ti} \right)^2 \tag{103}$$

where w_i is the weighted factor at periods T_i, S_1 the scaling factor for the ground motion of interest, y_i the spectral value for the considered record at period T_i, y_{Ti} the target spectral ordinates at period T_i and n the number of selected target periods.

So, for each selected natural ground motion, the corresponding value of S_1 can be determined by setting the derivative of Eq. (103) with respect to parameter S_1 equal to zero, namely:

$$S_1 = \frac{\sum_{i=1}^{n} w_i y_i y_{Ti}}{\sum_{i=1}^{n} w_i y_i^{\,2}} \tag{104}$$

In this study, 26 target periods (T_i) from the interested period range between 1.5 sec and 4.0 sec with an increment of 0.1 s are considered for the first phase of

scaling procedure. Since the natural period of most base-isolated buildings generally varies between 1.5 s and 3.0 s, all the weighted factors of the target periods are selected to be 1.0. Averaged acceleration spectrum after first scaling phase is presented in Fig. 186.

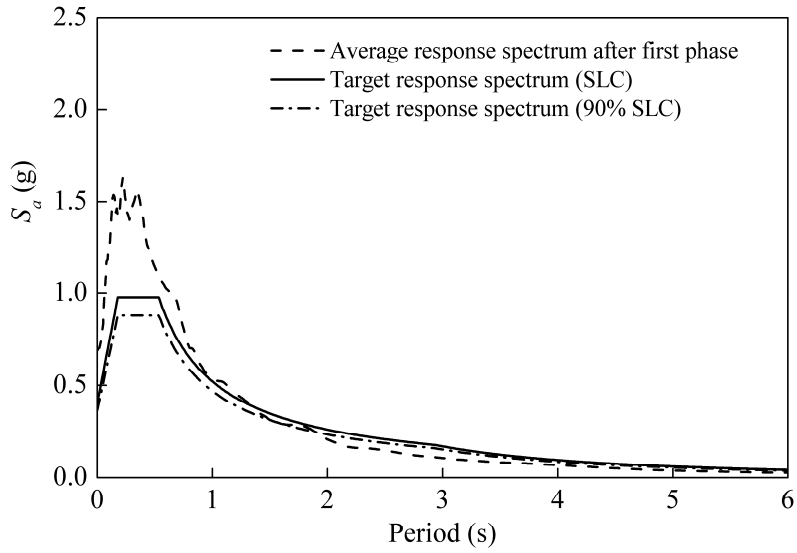

Fig. 186 Average acceleration spectrum after first scaling phase

The second phase, scaling all the ground motions using a unique factor S_2, assures the requirement of DM 2008. Each ground motion is further scaled such that for each period between 0.15 s and $1.2T_{eq}$ with an increment of 0.01 s the average of spectra from all the ground motions does not fall below the corresponding ordinate of the target response spectrum by more than 10%. Period T_{eq} is the equivalent period of base-isolated building under SLC response spectrum.

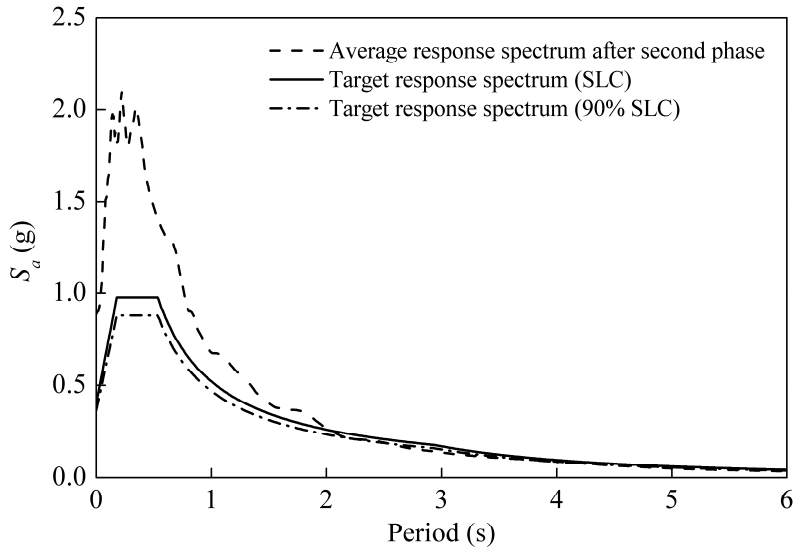

Fig. 187 Average acceleration spectrum after second scaling phase

The final scaling factor *SF* applied to each ground motion is obtained by multiplication of two factors S_1 and S_2 obtained in two scaling phases. Fig. 187 presents the 5%-damped target spectrum and average value of the scaled ground motion records. The final scaling factors are given in Table 8 for each ground motion.

Num	Earthquake	Components	S_1	S_2	*SF*
1	Parkfield	Temblor pre-1969	3.3010	1.2853	4.2428
2	San Fernando	Castaic-Old Ridge Route	4.0048	1.2853	5.1474
3	Managua-Nicaragua-01	Managua- ESSO	1.7466	1.2853	2.2449
4	Imperial Valley-06	Compuertas	5.2072	1.2853	6.6928
5	Mammoth Lakes-01	Convict Creek	1.8900	1.2853	2.4292
6	Victoria- Mexico	Cerro Prieto	0.9713	1.2853	1.2484
7	Coalinga-01	Parkfield-Cholame 2WA	3.2573	1.2853	4.1866
8	Loma Prieta	Foster City-Menhaden Court	2.1673	1.2853	2.7856
9	Cape Mendocino	Petrolia	1.2124	1.2853	1.5583
10	Northridge-01	LA-Wonderland Ave	5.5586	1.2853	7.1445
11	Kobe-Japan	Kakogawa	1.7317	1.2853	2.2258
12	Kocaeli- Turkey	Izmit	1.5340	1.2853	1.9717

Table 8

Scaling factors of the selected earthquake ground motions.

6.4. Investigated Multi-storey Base-isolated Buildings

To examine the results from different analysis methods, i.e., equivalent static linear analysis, response spectrum analysis, linear and nonlinear dynamic analysis, ten multi-storey base-isolated buildings are considered with superstructyures from 3-storey to 12-storey, as shown in Fig. 188. All the superstructyures have the same storey mass m_s (60000 kg) at all the levels and the base mass m_b is assumed to be two times the storey mass, which are same as the MDOF systems described in Chapter 5. Presented in Table 9 is the summary of structrual properties of various superstructures as well as the behavior of base isolation system. The bilinear hysteretic model is specified to base isolation systems. The superstructures are assumed to respond linearly to all earthquake loads. Furthermore, they are assumed to behave rigidly in the axial direction. The reduction in stiffness due to P-Δ effects has not been included in the model. The damping ratio of superstructure is assigned to be 0.05.

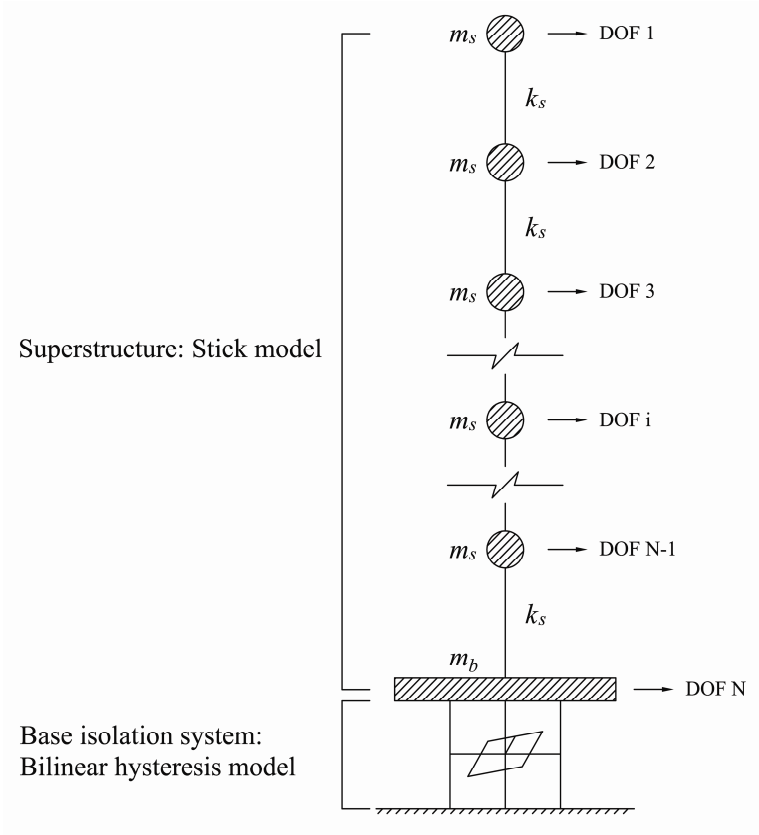

Fig. 188 Layout of the prototype base-isolated buildings examined in this study

MDOF systems	Superstructure		Isolation system	
	Superstructure period (s)	Inter-storey stiffness (N/m)	Normalized yield strength (F_y/W)	Isolated period (s)
3 storey	0.3	132808415	0.02	1.50
4 storey	0.4	122643063	0.04	1.75
5 storey	0.5	116881283	0.06	2.00
6 storey	0.6	113106845	0.08	2.25
7 storey	0.7	110520718	0.10	2.50
8 storey	0.8	108613268	0.12	2.75
9 storey	0.9	107148719	0.14	3.00
10 storey	1.0	105940532	0.16	3.25
11 storey	1.1	105007436	0.18	3.50
12 storey	1.2	104235211	0.20	3.75

Table 9

Structural properties of the investigated base-isolated buildings.

6.5. Results Comparison

As mentionded in DM 2008, the dynamic response of base-isolated buildings should be analyzed in terms of base displacements and storey forces. In the following sections, the results from different equivalent linearization analysis methods are cpmpared with those from nonlinear time history analysis, in which both the equivalent linearization technique recommended in code (R&H method) and those proposed by the authors are used (Liu I and Liu II methods).

6.5.1 Base Displacement

Maximum displacements of the isolation interface for different MDOF systems are presented in Table 10. It can be noted that for all the equivalent linearization analyses (SLA, RSP and LTHA), the maximum displacement of isolation interface computed using Liu methods is larger than that obtained using R&H method. This is because, the equivalent damping ratio from Liu methods is smaller than that from R&H method, which also demonstrates that R&H method overestimates the equivalent damping ratio to some extent.

The relative error between different equivalent linearization analysis methods and NTHA can be observed in Fig. 189. For SLA, it can be seen that R&H method underestimates the maximum displacement and the relative error in general increases with increasing the storey number. However, with Liu I equivalent linearization method, good agreement between SLA and NTHA could be obtained. In addition, the error decreases as the number of storey increases.

For RSP analysis, both R&H and Liu I methods produce nonconservative results, that is the maximum displacement of the isolation systems is significantly underestimated. But, smaller errors can be found for Liu I method than R&H method.

For LTHA, both R&H and Liu II methods yield good estimates of the exact maximum displacement of isolation system. It is found that for storey number less than 6, R&H method is slightly better than Liu II method. However, for storey number greater than 6, estimation accuracy of the results is significantly improved by Liu II method. Using R&H method, relative error between LTHA and NTHA is in general less than 20%, while the relative error will become less than 10% when Liu II method is utilized.

It is expected that LTHA always predicts better maximum displacement of the isolation interface than RSP method because there is no additional requirements in scaling the earthquake ground motions to match the target spectrum and in determining the reduction factor based on damping ratios greater than 5%. But, if the investigated base-isolated building is very complicated, the application of LTHA with equivalent linearization method may require an exorbitant amount of time.

Fortunately, SLA with Liu I method allows the structural designers to assess the response of base-isolated building using a simplified way. In general, Liu I method will always produce better results than R&H method since it is the modified version of R&H method. Again, when compare the structural response between SLA and NTHA, the scaling of the selected ground motions and the choice of the damping reduction factor are of great importance. If both of them are addressed well, SLA with Liu I method could be a very useful tool in the structural design of base-isolated buildings, at least in the preliminary stage of structural design.

Number of storey	SLA		RSP		LTHA		NTHA
	R&H	*Liu I*	*R&H*	*Liu I*	*R&H*	*Liu II*	
3	0.2680	0.2670	0.2638	0.2649	0.3724	0.3753	0.3659
4	0.2133	0.2200	0.2080	0.2149	0.2753	0.2787	0.2513
5	0.1658	0.1777	0.1586	0.1709	0.1994	0.2036	0.1914
6	0.1318	0.1512	0.1223	0.1423	0.1524	0.1600	0.1534
7	0.1085	0.1348	0.1090	0.1227	0.1290	0.1384	0.1396
8	0.0921	0.1235	0.0996	0.1070	0.1134	0.1248	0.1310
9	0.0803	0.1149	0.0864	0.0923	0.1018	0.1133	0.1179
10	0.0713	0.1078	0.0700	0.0776	0.0928	0.1017	0.1019
11	0.0644	0.1015	0.0519	0.0630	0.0851	0.0905	0.1040
12	0.0588	0.0958	0.0310	0.0485	0.0779	0.0798	0.0886

Table 10
Maximum displacements of the isolation interface (m).

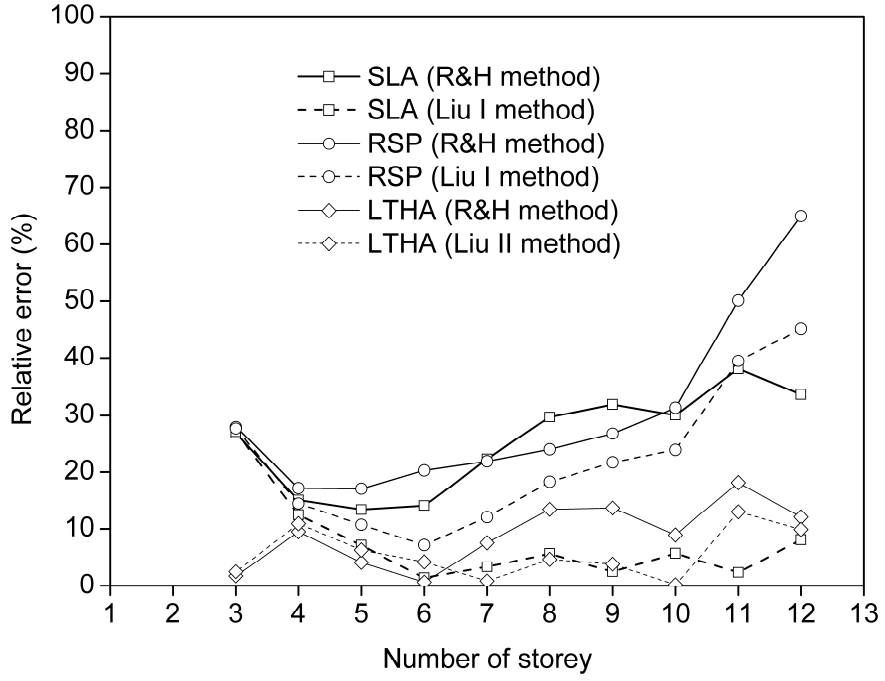

Fig. 189 Relative error of maximum base displacement between different equivalent linearization analyses and nonlinear time history analysis

6.5.2 Storey Shear Force

Besides the maximum displacement of isolation systems, another response indicator of base-isolated buildings is the storey shear force in superstruture. If the maximum displacement of isolation sysytems is predicted accurately, the base shear force can be determined based on the properties (equivalent linear or nonlinear) of isolation system. Here, the study is only focused on the distribution of storey shear force along the height of the superstructure in base-isolated buildings.

As described in Chapter 2.4, various methods are used to determine the lateral force distribution. For the sake of comparison, four methods to determine the lateral force distribution are investigated, including uniform distribution, invert triangular distribution, methods proposed by Protective Systems Committee (PSC) and York and Ryan. In addition, distributions of storey shear force computed by LTHA (with both R&H and Liu II methods) and NTHA are also presented.

Fig.190 shows the normalized storey shear (V_i/V_b) for different base-isolated buildings. It is found that for base-isolated buildings with storey number less than 4 the distribution of storey shear force can be considered to be uniform, namely proportional to the storey mass, which is also recommended in DM 2008. Invert triangular distribution and PSC distribution overestimate the storey shear force when storey number is less than 4. Essentially, the equivalent damping ratio estimated for 3- and 4-storey base-isolated buildings are 0.0023 and 0.0471, respectively, thereby the storey shear could be assumed to proportional to the storey mass.

However, with increasing the storey number of superstructure and varying the properties of the isolation system, the equivalent damping ratio of isolation system increases. Therefore, the acceleration profile can't be considered as uniform along the height of the superstructure. It is seen that York method presents relatively good results for medium storey number when compared with other methods.

PSC method results in the same storey shear force in first floor as that from uniform distribution, while in the superstructure, an inverted triangular distribution is applied. However, this method does not remarkably improve the accuracy in predicting the storey shear distribution along the height of superstructure.

When LTHA is used, the storey shear is found to be accurate at the upper storyes while it is largely overestimated at the lower storeys, especially for base-isolated buildings with relatively high damping ratio.

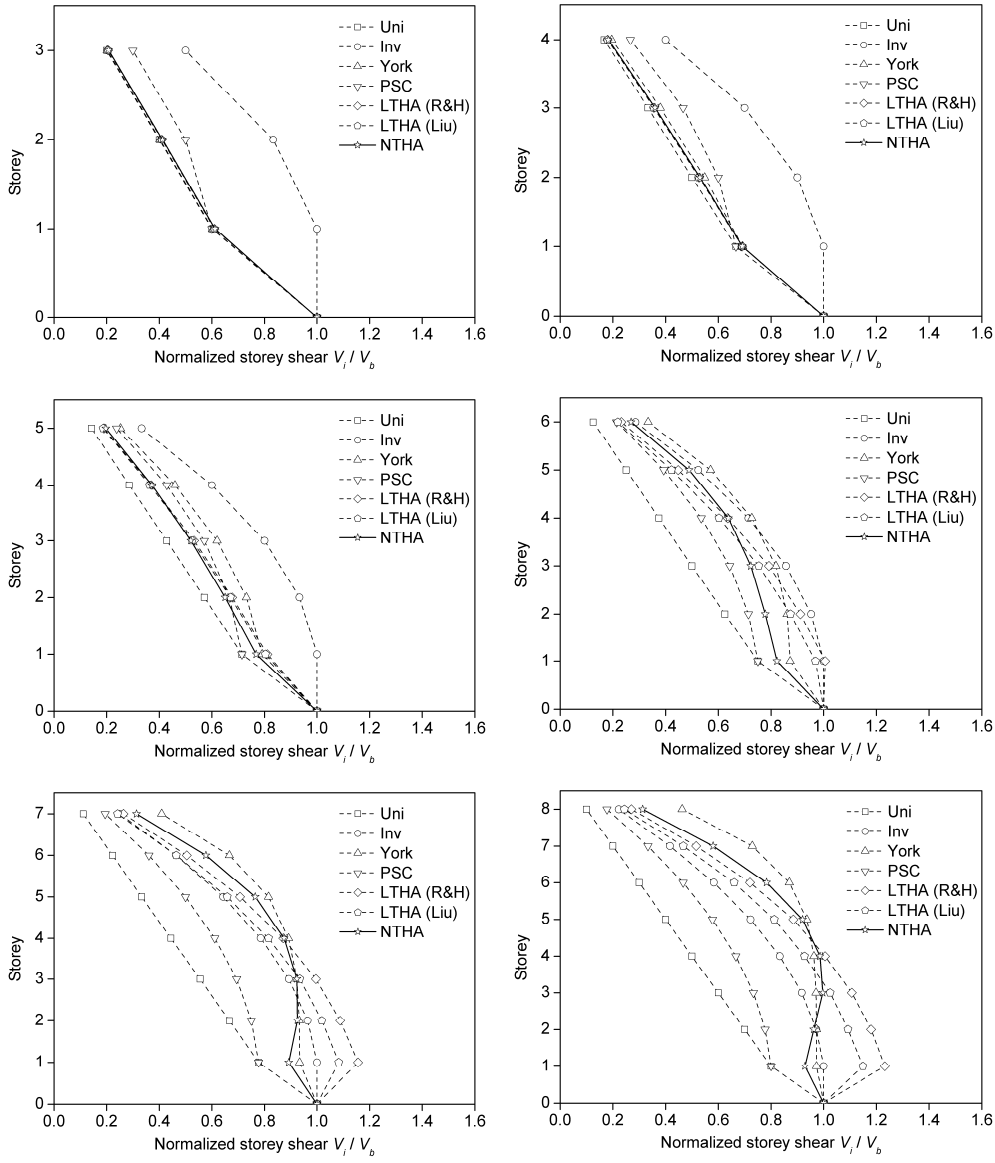

Fig. 190 Normalized storey shear for base-isolated buildings with 3- to 12-storey superstructures

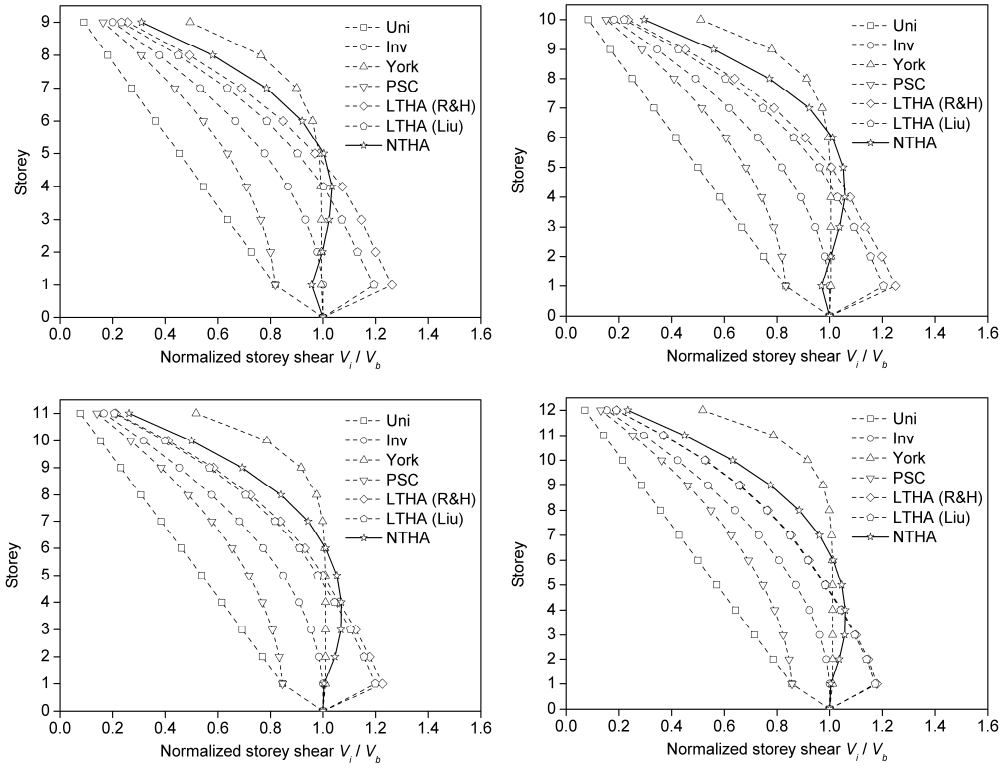

Fig. 190 Normalized storey shear for base-isolated buildings with 3- to 12-storey superstructures (continued)

It is noted that both the uniform and the inverted triangular equivalent-static-force distribution are inadequate to describe the great variety of situations that can be found. In addition, for other methods to estimate the distribution of storey shear, they are only considered to be valid in limited conditions. In fact, the distribution of storey shear along the height of superstructure in base-isolated buildings is significantly related to the distribution of the storey mass and the inter-storey stiffness and more important the equivalent damping of the isolation systems. With increasing the damping ratio of the isolation systems, more seismic force will be translated to superstructure, so the normalized storey shear envelope becomes more bulged, indicating more significant higher-mode contributions.

York method in general presents good estimations of storey shear force distribution for relative low base-isolated buildings (or for MDOF systems with relatively low damping ratio). However, with increasing the damping ratio in base isolation systems, much more high modes effects must be taken into account.

More work need to be done to comprehensively examine the lateral force distribution in multi-storey base-isolated buildings, which is also important for equivalent linearization analysis of base-isolated buildings.

6.6. Summary

In this Chapter, different analysis methods for base-isolated buildings are investigated. In accordance with the specification in DM 2008, four analysis methods, equivalent static linear analysis (SLA), response spectral analysis (RSP), linear time history analysis (LTHA), nonlinear time history analysis (NTHA) are carried out on ten (from 3- to 12-storey) shear-type buildings, equipped with a variety of isolation systems. In addition, both R&H method and Liu methods are considered to estimate the equivalent damping ratio of isolation systems. In Liu methods, Liu I method indicates the method used for SDOF systems derived in Chapter 4, while Liu II method is the method derived for MDOF systems in Chapter 5.

For the prediction of the maximum displacement of isolation interface, it is found that results from LTHA always have a good agreement with those from NTHA. Specifically, LTHA with Liu II method could present better results than that with R&H method in all the considered cases. However, this analysis method will take a great amount of time when the investigated buildings is complicated.

In general, RSP produces larger errors than other analysis methods, in particular for high superstructures. This can be explained that high-mode effects will take place for higher superstructures. Considering the computational time, SLA with Liu I method can be used as an appropriate tool for design of base-isolated buildings.

Regarding the distribution of storey shear force along the superstructure, many different methods are assessed. It is found that for relatively low superstructures uniform distribution is correct, while both uniform distribution and inverted triangular distribution are not sufficient to predict the storey shear force for superstructures with relatively high damping ratio. York method can produce better results for medium damping ratio. However, with increasing the equivalent damping ratio, the difference between the predicted and the exact storey shear force increases. Therefore, much work needs to be done to get insight into the distribution of storey shear force in multi-storey base-isolated buildings.

CONCLUSIONS

The present research investigates the equivalent linearization of base-isolated buildings with bilinear isolation system, in order to maximize the estimation accuracy of the simplified analysis method. From simplicity to complexity, the study is carried out based on the assumption of SDOF and MDOF systems, respectively. To provide a unitary framework, a detailed literature survey about the topic of seismic base isolation system is firstly presented. Then, the prediction accuracy of various equivalent linearization methods was evaluated based on parametric analyses. After that, to improve the estimation accuracy, an improved formula of equivalent damping ratio is proposed for SDOF bilinear systems. With this expression of equivalent damping ratio, more comprehensive study is conducted for MDOF base-isolated buildings. Accordingly, another improved formula for equivalent damping ratio is derived for MDOF systems through correcting the formula used for SODF systems. Finally, several equivalent linearization methods, including R&H method and the proposed methods, are examined in equivalent linear analysis of base-isolated buildings and an effective equivalent linearization method is presented for structural design of base-isolated buildings, at least in the preliminary stage.

Conclusions

On the basis of the findings of the literature reviews, analyses and derivations carried out, and the approaches presented, the conclusions are drawn as following:

- Base isolation systems, as one of the most effective way to mitigate seismic risk, have been widely applied in worldwide. They have become very mature technique and can provide many benefits, not only in the structural performance but also in the cost effectiveness.

- To simplify the design process of base-isolated buildings, many approximate methods are recommended in many specifications. Equivalent linearization analysis method can be considered as an effective tool for the analysis of base-isolated buildings.

- In general, equivalent linearization methods are performed based on the maximum displacement response. In other words, the accuracy of predict-

ing the maximum displacement of isolation systems can be used to examine various equivalent linearization methods.

- The estimation accuracy is strongly related to different assumptions when various equivalent linearization methods are derived or fitted. It can be found that the method that best simulates a given hysteresis type may not be the best one to emulate the response of other hysteresis types.

- Of all the equivalent linearization methods investigated in this research, R&H and B&P methods yield the highest accuracy for high and low ductility ratios, respectively. For other approximate methods, special attention should be paid due to the probable deviations caused by different levels of initial period or inelastic deformation.

- To get more accurate results, period ratio computed based upon secant stiffness could be a desirable alternative and equivalent viscous damping ratio should first increase and then decrease as the ductility ratio increases. However, not only the variation trend but also the quantitative values of equivalent linear properties should be taken into account when deriving a better method.

- Although an equivalent linearization method produces a high accuracy of estimation will also show a low standard deviation, the opposite is not always true. So, when an equivalent linearization method is derived, the estimation accuracy should be considered firstly.

- Recommended in recent structural codes and derived based upon the concept of secant stiffness and equal energy dissipation rule, R&H method underestimates the maximum inelastic displacement on average 20 per cent for systems with displacement ductility ratios less than 10. However, for high ductility ratios, this method provides satisfied accuracy to estimate the actual maximum nonlinear deformation.

- Since B&P method is derived based on ductility ratios up to 6, better accuracy could be always obtained for low ductility ratios than that for high ones. Although the strain hardening ratio in B&P method is assumed to be 0.2, it can be observed that better results can be produced for lower strain hardening ratio.

- The optimal damping ratio for SDOF bilinear systems first increases and then decreases as the ductility ratio increases. With increasing the initial period and strain hardening ratio, the optimal damping ratio decreases.

- To propose an improved equation of equivalent damping ratio, modification of R&H method by introducing a factor may be an appropriate option because of the theoretical background of this method. Furthermore, the boundary conditions and variation trends of equivalent damping ratios can be guaranteed.

- The proposed method for SDOF bilinear systems (Liu I method) accurately predicts the influence of various parameters, such as strain hardening ratio, initial natural period and ductility ratio, on the determination of equivalent damping ratio.

- Based on Liu I method, most of mean approximate to exact displacement ratios range from 0.90 to 1.10, which indicates the relative error between approximate and exact maximum inelastic displacement is less than 10%.

- Validated using the other twelve earthquake ground motions, satisfied accuracy could be also produced by Liu I method. In addition, the computed coefficients of variation are even less than that obtained from the origin seismic loads, indicating high robustness of Liu I method for general SDOF bilinear systems.

- Considering the MDOF base-isolated buildings, incorporation of Mass-proportional damping in the superstructure damping will result in undesirable suppression of the first mode response of base-isolated buildings. As a remedy, Stiffness-proportional damping instead of Rayleigh damping should be applied to the superstructure of base-isolated buildings.

- Estimation accuracy of R&H method for MDOF systems is significantly influenced by the height (or the period) of the superstructure. Larger errors can be obtained for relatively short initial period and for relatively low ductility ratios because of the small ratio of the equivalent period to the superstructure period. In other words, the MDOF systems cannot be simplified to be SDOF systems and high mode effects should be taken into account.

- Similar results can be observed when Liu I method is used. Therefore, both R&H method and Liu I method are not able to predict satisfied estimates of the maximum displacement of isolation interface.

- The optimal damping ratio in general decreases with increasing the initial period of isolation systems. However, it first increases and then decreases as the ductility ratio increases except for isolation systems with relatively short initial periods. Significant change in the optimal damping ratio happens when short initial period is considered. But, for the cases with long initial periods and high ductility ratios, the influence of different superstructures is not so remarkable.

- Plotted against the ratio of equivalent period to superstructure period T_{eq}/T_{fb}, It is found that the optimal damping ratio is underestimated when the ratio T_{eq}/T_{fb} is close to 1. For large T_{eq}/T_{fb}, the optimal damping ratio can be considered to be those computed by Liu I method.

- As a function of T_{eq}/T_{fb}, a factor is introduced to Liu I method to further improve the estimation accuracy of equivalent linearization method for MDOF systems. The newly proposed method (Liu II method) is able to take into account the influence of both isolation systems and superstructures and the prediction accuracy of isolator displacement is significantly improved.

- Regarding the coefficients of variation, results from Liu methods are comparable to those from R&H method not only for SDOF systems but also for MDOF systems. Thus, Liu methods didn't increase the dispersion of results while improving the prediction accuracy.

- In structural codes, the permission of equivalent linearization method is dominated by requirement of equivalent stiffness. Seismic isolation systems with high values of strain hardening ratio and ductility ratios are suitable for the procedure of equivalent linearization. However, in most cases, equivalent linearization of seismic isolation system is not permitted.

- Thus, to apply the code-recommended method (R&H method), several requirements should be met. But, adjusting the bilinear properties of seismic isolation system so as to satisfy the limited condition may become very inconvenient. In addition, the selected isolation bearings may be unavailable on the market.

- For SLA, Liu I method could yield more accurate results than R&H method. More important, Liu I method has no additional requirements in the application of equivalent linearization analysis method.

- For RSP analysis, the maximum displacement of the isolation systems is significantly underestimated by both R&H and Liu I methods. But, smaller errors can be obtained by Liu I method than R&H method.

- LTHA always predicts better maximum displacement of the isolation interface than other analysis methods because the combined use of the iteration procedure and damping reduction factor (η), as is used in the current design practices, may result into the loss of prediction accuracy. But, if the investigated base-isolated building is very complicated, the application of LTHA with equivalent linearization method may require an exorbitant amount of time.

- As a remedy, SLA in combination with Liu I method could be used for analysis and design of base-isolated buildings, at least in the preliminary stage. In addition, Liu I method could present better results than R&H method in a wider parameter space. Therefore, the requirements specified in codes could be omitted.

- Distribution of lateral shear force along the height of superstructure is strongly related to the properties of both isolation system and the superstructure. Both uniform distribution and inverted triangular distribution are not sufficient to predict the storey shear force for superstructures with relatively high damping ratio.

- PSC method, resulting in the storey shear forces between those from uniform distribution and inverted triangular distribution, does not remarkably improve the accuracy in predicting the storey shear distribution along the height of superstructure.

- It is seen that York method presents relatively good results for medium storey number when compared with other methods. But for superstructures with large storey number and high damping ratio, the storey shear forces are underestimated in low storeys and overestimated in high storeys.

- Due to the good accuracy for bilinear systems with both low and high ductility ratios, Liu I method can be used not only for base-isolated buildings but also for other buildings with small ductility ratio when applying direct displacement-based design (DDBD).

Recommendations for Future Investigations

Although the present study investigates various equivalent linearization methods and proposes improved equivalent linearization methods for SDOF and MDOF bilinear systems, respectively, to properly perform equivalent linear analysis of base-isolated buildings there are still many factors and uncertainties need to be addressed.

- The hysteretic behavior of isolation systems is assumed to be bilinear. Other hysteretic models should be also addressed using the similar process in the future research.

- Equivalent linear analysis of 3-Dimension base-isolated buildings needs to be investigated as well as the potential torsion effect.

- The vertical action of ground motions should also be examined, which could cause the over-turning of base-isolated buildings. Specifically, for friction pendulum bearings, normal force during the earthquake has significant effect on the friction coefficient, thereby influences the global performance of isolation system.

- This study assumes the inherent viscous damping of isolation systems is zero (i.e., $\xi_0 = 0$). But, the effect of inherent viscous damping on the proposed equivalent linearization methods should be examined.

- As mentioned by many researchers, determination of equivalent damping ratios is significantly related to the characteristics of inputted earthquake ground motions, for instance, the near-fault ground motion effects. However, this is not considered in the present study and could be studied in the future work.

- It is found that none of the existing methods is able to accurately estimate the lateral force distribution along the height of superstructure in base-

isolated buildings. Much work needs to be done to propose a more precise model for the distribution of storey shear force.

- To compare the results from response spectral analysis and time history analysis of base-isolated buildings, earthquake ground motions should be scaled to match the target response spectrum. How to apply the scaling procedure so that both results are comparable could be interesting.

- To perform equivalent static linear analysis of base-isolated buildings, damping reduction factor is often involved. How to properly determine the damping reduction factor is very important to the accuracy of equivalent linear analysis and could be another interesting research topic.

BIBLIOGRAPHY

AASHTO, (2002), Guide Specifications for Seismic Isolation Design. American Association of State Highway and Transportation Officials, 444 North Capitol Street, N.W. Suite 249, Washington, DC.

AIJ, (2001), Recommendation for Design of Base Isolated Buildings, Architectural Institute of Japan (AIJ), 74-93.

Alhana C. and Altun M., (2009), Performance of Non-Linear Base Isolation Systems Designed According to Uniform Building Code. Proceedings of the 5th International Advanced Technologies Symposium (IATS'09), May, Karabuk, Turkey.

Almazán J.L., De La Llera J.C., Inaudi J.A., (1998), Modelling aspects of structures isolated with the frictional pendulum system, Earthquake engineering & structural dynamics, 27, 8, 845-867.

Almazán J.L. and De la Llera J.C., (2002), Analytical model of structures with frictional pendulum isolators, Earthquake engineering & structural dynamics, 31, 2, 305-332.

Al-Shatnawi A., (2001), Developments for Complex Inelastic Large-scale Simulations and Parameter Estimation, with emphasis on Large Strain, Softening and Localization Phenomena, Doctoral Dissertation, University of Akron, Department of Civil Engineering.

American Society of Civil Engineers (ASCE), (2005), ASCE SEI7-05: Minimum design loads for buildings and other structures, ASCE publications.

Amin A., Alam M.S., Okui Y., (2002), An improved hyperelasticity relation in modeling viscoelasticity response of natural and high damping rubbers in compression: experiments, parameter identification and numerical verification, Mechanics of materials, 34,2, 75-95.

Amin A., Lion A., Sekita S., Okui Y., (2006), Nonlinear dependence of viscosity in modeling the rate-dependent response of natural and high damping rubbers in compression and shear: Experimental identification and numerical verification, International Journal of Plasticity, 22, 9, 1610-1657.

Andriono T. and Carr A.J., (1991), A simplified earthquake resistant design method for base-isolated multistory structures. Bulletin of the New Zealand National Society for Earthquake Engineering, 24, 3, 238–250.

Andriono T. and Carr A.J., (1991), Reduction and distribution of lateral seismic inertia forces on base-isolated multistory structures, Bulletin of the New Zealand National Society for Earthquake Engineering, 24, 3, 225–237.

Bedrinana L.A., (2011), Seismic risk and cost-effectiveness of base isolated buildings in Peru, Bulletin of the International Institute of Seismology and Earthquake Engineering, 45, 97-102.

Bhuiyan A.R. Okui Y., Mitamura H., Imai T., (2009), A rheology model of high damping rubber bearings for seismic analysis: Identification of nonlinear viscosity, International Journal of Solids and Structures, 46, 7, 1778-1792.

Bhuiyan A.R., Okui Y., Mitamura H., Imai T., (2009), A rheology model of high damping rubber bearings for seismic analysis: identification of nonlinear viscosity, International Journal of Solids and Structures, 46, 7, 1778-1792.

Blandon C.A. and Priestley M.J.N., (2005), Equivalent viscous damping equations for direct displacement based design, Journal of earthquake Engineering, 9, 2, 257-278.

Bommer J.J., Elnashai A.S., Weir A.G., (2000), Compatible acceleration and displacement spectra for seismic design codes, Proceedings of the 12th World Conference on Earthquake Engineering, Auckland, New Zealand.

Box G.E. and Draper N.R., (1987), Empirical model-building and response surfaces, John Wiley & Sons.

Branco M. and Guerreiro L.M., (2011), Seismic rehabilitation of historical masonry buildings, Engineering Structures, 33, 5, 1626-1634.

Briseghella B., Zordan T., Liu T., Mazzarolo E., (2013), Friction Pendulum System as a Retrofit Technique for Existing Reinforced Concrete Building, Structural Engineering International, 23, 2, 219-224.

Briseghella B., Zordan T., Romano A., Zambianchi L., Simone G., Liu T., (2012), Lift-up and Base Isolation as a Retrofit Technique for RC Existing Building, Proceedings of 15th World Conference on Earthquake Engineering, Lisbon, Portugal.

BSSC, (2003), NEHRP recommended provisions for seismic regulations for new buildings and other structures. Washington, DC: FEMA 450, developed by BSSC for FEMA.

Buckle I.B. and Mayes R.M., (1990), Seismic isolation: History, application, and performance-A world view, Earthquake spectra, 6, 2, 161-201.

Cardone D., Dolce M., Gesualdi G., (2009), Lateral force distributions for the linear static analysis of base-isolated buildings, Bulletin of Earthquake Engineering, 7, 3, 801-834.

Caughey T.K., (1960), Classical normal modes in damped linear systems, Journal of Applied Mechanics, 27, 269-271.

CEN (Comité Européen de Normalisation), (2004), Eurocode8: design provisions for earthquake resistance of structures: part 1: general rules, seismic actions and rules for buildings, EN 1998–1:2004.

Charney F.A., (2008), Unintended consequences of modeling damping in structures, Journal of Structural Engineering, 134, 4, 581-592.

Chinese Standard, G.B., (2008), 50011-2010, Code for Seismic Design of Buildings, Chinese Building Press, Beijing, China.

Chopra A.K., (2007), Dynamics of Structures: Theory and applications to earthquake engineering, 3rd Ed., Prentice-Hall, Englewood Cliffs, N.J. USA.

Clough R. and Penzien J., (2003), Dynamics of structures, Computer and Structures, Inc., Berkeley, California, USA.

Code I.B., (2008), D.M. 14.01. 2008: Norme Tecniche per le Costruzioni, Italian Ministry of Infrastructures and Transportation: Rome, Italy.

Constantinou M., Mokha A., Reinhorn A., (1990), Teflon bearings in base isolation II: Modeling, Journal of Structural Engineering, 116, 2, 455-474.

Constantinou M.C., Winters C.W., Theodossiou D., (1993), Evaluation of SEAOC/UBC analysis procedures. Part 2: flexible superstructure, Proceedings of ATC-17-1 seminar on seismic isolation, passive energy dissipation and active control, San Francisco, CA, USA.

Dall'Asta A. and Ragni L., (2006), Experimental tests and analytical model of high damping rubber dissipating devices, Engineering structures, 28, 13, 1874-1884.

Di Sarno L., Chioccarelli E., Cosenza E., (2011), Seismic response analysis of an irregular base isolated building, Bulletin of Earthquake Engineering, 9, 5, 1673-1702.

Dicleli M. and Buddaram S., (2007), Comprehensive evaluation of equivalent linear analysis method for seismic-isolated structures represented by sdof systems, Engineering Structures, 29, 8, 1653-1663.

Erduran E., (2012), Evaluation of Rayleigh damping and its influence on engineering demand parameter estimates, Earthquake Engineering & Structural Dynamics, 41, 14, 1905-1919.

Eröz M. and DesRoches R., (2008), Bridge seismic response as a function of the Friction Pendulum System (FPS) modeling assumptions, Engineering Structures, 30, 11, 3204-3212.

Federal Emergency Management Agency (FEMA), (1997), NEHRP guidelines for the seismic rehabilitation of buildings. Report FEMA 273. Washington (DC): FEMA.

Federal Emergency Management Agency (FEMA), (2005), Improvement of inelastic seismic analysis procedures, Report FEMA-440, Washington, DC, USA.

Franchin P., Monti G., Pinto P.E., (2001), On the accuracy of simplified methods for the analysis of isolated bridges, Earthquake Engineering & Structural Dynamics, 30, 3, 363-82.

Gulkan P. and Sozen M.A., (1974), Inelastic responses of reinforced concrete structure to earthquake motions, ACI Journal Proceedings, 71, 12, 604-610.

Guyader A.C. and Iwan W.D., (2004), An improved capacity spectrum method employing statistically optimized linearization parameters. Proceedings of the 13th World Conference on Earthquake Engineering, Vancouver, Canada.

Guyader A.C. and Iwan W.D., (2006), Determining Equivalent Linear Parameters for Use in a Capacity Spectrum Method of Analysis, Journal of Structural Engineering, 132, 1, 59-67.

Hall J.F., (2006), Problems encountered from the use (or misuse) of Rayleigh damping, Earthquake Engineering & Structural Dynamics, 35, 5, 525-545.

Hwang J.S. and Chiou J.M., (1996), An equivalent linear model of lead-rubber seismic isolation bearings, Engineering Structures, 18, 7, 528-536.

Hwang J.S. and Ku S.W., (1997), Analytical modeling of high damping rubber bearings, Journal of Structural Engineering 123, 8, 1029-1036.

Hwang J.S. and Sheng L.H., (1993), Effective stiffness and equivalent damping of base isolated bridges, Journal of Structural Engineering, 119, 10, 3094-3101.

Hwang J.S. and Wang J.C., (1998), Seismic response prediction of HDR bearings using fractional derivatives Maxwell model, Engineering Structures, 20, 9, 849-856.

Hwang J.S., (1996), Evaluation of Equivalent Linear Analysis Methods of Bridge Isolation, Journal of Structural Engineering, 122, 8, 972-976.

Hwang J.S., Wu J.D., Pan C.T., Yang G., (2002), A mathematical hysteretic model for elastomeric isolation bearings, Earthquake Engineering & Structural Dynamics 31, 4, 771-789.

Iizuka M., (2000), A macroscopic model for predicting large-deformation behaviors of laminated rubber bearings, Engineering structures, 22, 4, 323-334.

International Code Council (ICC), (2000), IBC: chap 16: seismically isolated structures, USA.

International Conference of Building Officials (ICBO), (1991), UBC: Earthquake regulations for seismic isolated structures. In: Uniform building code, USA.

International Conference of Building Officials (ICBO), (1997), UBC: Earthquake regulations for seismic isolated structures. In: Uniform building code, USA.

Islam A.B.M., Hussain R.R., Jameel M., Jumaat M.Z., (2012), Non-linear time domain analysis of base isolated multi-storey building under site specific bi-directional seismic loading, Automation in construction, 22, 554-566.

Islam A.S., Ahmad S.I., Jameel M., Zamin M.J., (2010), Seismic base isolation for buildings in regions of low to moderate seismicity: practical alternative design, Practice Periodical on Structural Design and Construction,17, 1, 13-20.

Iwan W.D. and Gates N.C., (1979), Estimating earthquake response of simple hysteretic structures, Journal of the Engineering Mechanics Division, 105, 3, 391-405.

Iwan W.D. and Gates N.C., (1979), The effective period and damping of a class of hysteretic structures, Earthquake Engineering & Structural Dynamics, 7, 3, 199-211.

Iwan W.D., (1980), Estimating inelastic response spectra from elastic spectra, Earthquake Engineering & Structural Dynamics, 8, 4, 375-388.

acobsen L.S., (1930), Steady forced vibrations as influenced by damping, ASME Transactions, 52, 15,169-181.

Jangid R.S. and Datta T.K., (1995), Seismic behaviour of base-isolated buildings: a state-of-the-art review, Proceedings of the ICE-Structures and Buildings, 110, 2, 186-203.

Jara M. and Casas J.R., (2006), A direct displacement-based method for the seismic design of design of bridges on bilinear isolation devices, Engineering Structures, 28, 6, 869-879.

Jara M., Jara J.M., Olmos B.A., Casas J.R., (2012), Improved procedure for equivalent linearization of bridges supported on hysteretic isolators, Engineering Structures, 35, 99-106.

Kaelo P. and Ali M.M., (2007), Integrated crossover rules in real coded genetic algorithms, European Journal of Operational Research, 176, 1, 60-76.

Kalpakidis I.V. and Constantinou M.C., (2009), Effects of heating on the behavior of lead-rubber bearings. I: Theory. Journal of structural engineering, 135, 12, 1440-1449.

Kalpakidis I.V. and Constantinou M.C., (2009), Effects of heating on the behavior of lead-rubber bearings. II: Verification of theory. Journal of structural engineering, 135, 12, 1450-1461.

Kalpakidis I.V., Constantinou M.C., Whittaker A.S., (2010), Modeling strength degradation in lead-rubber bearings under earthquake shaking, Earthquake Engineering & Structural Dynamics, 39, 13, 1533-1549.

Kelly J. M., Skinner R. I., Heine A. J. (1972), Mechanisms of energy absorption in special devices for use in earthquake resistant structures, Bulletin of the New Zealand National Society for Earthquake Engineering, 5, 3, 63-88.

Kelly J.M. and Tsztoo D.F., (1977), Energy absorbing devices in structures under earthquake loading, Proceedings of the 6th World Conference on the Earthquake Engineering, New Delhi, India, 1369-1374.

Kelly J.M., (1986), Aseismic base isolation: Review and bibliography, Soil Dynamics and Earthquake Engineering, 5, 4, 202-216.

Kelly T.E., (2001), Base isolation of structures: design guidelines, Holmes Consulting Group Ltd.

Khoshnoudian F. and Mehrparvar B., (2008), Evaluation of IBC equivalent static procedure for base shear distribution of seismic isolated structures, Journal of Earthquake Engineering, 12, 5, 681-703.

Kikuchi M., Nakamura T., Aiken I.D., (2010), Three-dimensional analysis for square seismic isolation bearings under large shear deformations and high axial loads. Earthq, Earthquake Engineering & Structural Dynamics, 39, 13, 1513-1531.

Kilar V., Petrovčič S., Koren D., Šilih S., (2013), Cost viability of a base isolation system for the seismic protection of a steel high-rack structure, International Journal of Steel Structures, 13, 2, 253-263.

Kobayashi M. and Matsuda S., (2012), A Study on Vertical Distribution of Shear Force Coefficient for Seismic Design of Seismically Isolated Buildings, Proceedings of the 15th World Conference on the Earthquake Engineering, September, Lisbon, Portugal.

Koh C.G. and Kelly J.M., (1990), Application of fractional derivatives to seismic analysis of base isolated models, Earthquake Engineering & Structural Dynamics, 19, 2, 229-241.

Komur M.A., Karabork T., Deneme I.O., (2011), Nonlinear Dynamic Analysis of Isolated and Fixed-Base Reinforced Concrete Structures, Gazi University Journal of Science, 24, 3, 463-475.

Kowalsky M.J., (1995), Displacement based design: a methodology for seismic design applied to RC bridge columns, Master's thesis, San Diego, CA: University of California.

Kunde M.C. and Jangid R.S., (2003), Seismic behavior of isolated bridges: A-state-of-the-art review, Electronic Journal of Structural Engineering, 3, 2, 140-169.

Kwan W.P. and Billington S.L., (2003), Influence of hysteretic behavior on equivalent period and damping of structural systems, Journal of Structural Engineering,129, 5, 576-585.

Lee C.S., Goda K., Hong H.P., Cost-Effectiveness of Tuned Mass Damper and Base Isolation, Proceedings of the 14th World Conference on Earthquake Engineering. October, Beijing, China

Lee D.G., Hong J.M., Kim J., (2001), Vertical distribution of equivalent static loads for base isolated building structures, Engineering structures, 23, 10, 1293-1306.

Léger P. and Dussault S., (1992), Seismic-energy dissipation in MDOF structures, Journal of Structural Engineering, 118, 5, 1251-1269.

Lin Y.Y. and Miranda E., (2009), Evaluation of equivalent linear methods for estimating target displacements of existing structures, Engineering structures, 31, 12, 3080-3089.

Liu T., Zordan T., Briseghella B., Zhang Q., (2014a), Evaluation of equivalent linearization analysis methods for seismically isolated buildings characterized by SDOF systems, Engineering Structures, 59, 619-634.

Liu T., Zordan T., Briseghella B., Zhang Q., (2014b), An improved equivalent linear model of seismic isolation system with bilinear behavior, Engineering Structures, 61, 113-126.

Liu T., Zordan T., Briseghella B., Zhang Q., (2014c), Simplified Linear Static Analysis for Base-isolated Building with FPS Systems, Structural Engineering International (in press).

Liu T., Zordan T., Zhang Q., Briseghella B., (2014d), Equivalent Viscous Damping of Bilinear Hysteretic Oscillators, Journal of Structural Engineering (in press).

JPWRI, (1992), Manual for Menshin Design of Highway Bridges, Japanese Public Works Research Institute, Tsukuba, Japan.

MATLAB, (2009), V.7.8. 0.347 (R2009a), MathWorks Inc., Natick, MA.

Matsagar V. A. and Jangid R.S., (2003), Seismic response of base-isolated structures during impact with adjacent structures, Engineering Structures, 25, 10, 1311-1323.

Matsagar V.A. and Jangid R.S., (2004), Influence of isolator characteristics on the response of base-isolated structures, Engineering Structures, 26, 12, 1735-1749.

Matsagar V.A. and Jangid R.S., (2008), Base isolation for seismic retrofitting of structures, Practice Periodical on Structural Design and Construction,13, 4, 175-185.

Mavronicola E. and Komodromos P., (2011), Assessing the suitability of equivalent linear elastic analysis of seismically isolated multi-storey buildings. Computers & Structures, 89, 21, 1920-1931.

Mazzoni S., McKenna F., Fenves G.L., (2007), OpenSees Command Language Manual, Pacific Earthquake Engineering Research Center, University of California at Berkeley, CA, USA.

Michalewicz Z., Dasgupta D., Le Riche R.G., Schoenauer M., (1996), Evolutionary algorithms for constrained engineering problems, Computers & Industrial Engineering, 30, 4, 851-70.

Miranda E. and Ruiz-García J., (2002), Evaluation of approximate methods to estimate maximum inelastic displacement demands, Earthquake Engineering & Structural Dynamics, 31, 3, 539-560.

Mitu A.M., Sireteanu T., Baldovin D., (2010), On the Efficiency of a Base Isolation System, ANALELE UNIVERSITĂȚII. “EFTIMIE MURGU” REŞIȚA. ANUL XVII, NR. 1.

Miyamoto, (2008), Sichuan China M8 earthquake e Lessons learned, Earthquake Field Investigation Report, Global Risk Miyamoto and Miyamoto International.

Miyamoto, (2009), L’Aquila Italy M6.3 Earthquake Field Investigation Report, Global Risk Miyamoto and Miyamoto International.

Miyamoto, (2011a), Christchurch, New Zealand Earthquake Field Investigation Report, Global Risk Miyamoto and Miyamoto International.

Miyamoto, (2011b), Tohoku earthquake and Tsunami Field Investigation Report, Global Risk Miyamoto and Miyamoto International.

Naeim F. and Kelly J.M., (1999), Design of Seismic Isolated Structures: From Theory to Practice, John Wiley and Sons: Hoboken, NJ, USA.

Nagarajaiah S., Reinhorn A.M., Constantinou M.C., (1991), Nonlinear dynamic analysis of 3-D-base-isolated structures, Journal of Structural Engineering, 117, 7, 2035-2054.

NEHRP, (1997), Federal emergency management agency (FEMA-273): guidelines for the seismic rehabilitation of buildings, USA.

Newmark N.M., (1959), A Method of Computation for Structural Dynamics, Journal of the Engineering Mechanics Division, 85, 3, 67-94.

Ou J.P., Wu B., Long X., (1998), Aseismic Design Methods of Passive Energy Dissipation Systems, Earthquake Engineering and Engineering Vibration,18, 2, 98-107 (In Chinese).

Ozdemir G. and Dicleli M., (2012), Effect of lead core heating on the seismic performance of bridges isolated with LRB in near-fault zones, Earthquake Engineering & Structural Dynamics, 41, 14, 1989-2007.

Pacific Earthquake Engineering Research Center, (2010), PEER: Ground Motion Database, 2010 Beta Version.
http://peer.berkeley.edu/peer_ground_motion_database.

Pan P., Ye L., Shi W., Cao H., (2012), Engineering practice of seismic isolation and energy dissipation structures in China, Science China Technological Sciences, 55, 11, 3036-3046.

Pan P., Zamfirescu D., Nakashima M., Nakayasu N., Kashiwa H., (2005), Base-isolation design practice in Japan: introduction to the post-Kobe approach. Journal of Earthquake engineering, 9, 1, 147-171.

Pant D.R., Wijeyewickrema A.C., ElGawady M.A., (2013), Appropriate viscous damping for nonlinear time-history analysis of base-isolated reinforced concrete buildings, Earthquake Engineering & Structural Dynamics, 42, 15, 2321-2339.

Robinson W.H., (1976), A lead-rubber shear damper, Bulletin of the New Zealand National Society for Earthquake Engineering, 4, 251-259.

Robinson W.H., (1982), Lead-rubber hysteretic bearings suitable for protecting structures during earthquakes, Earthquake Engineering & Structural Dynamics, 10, 4, 593-604.

Robinson W.H., (1995), Recent research and applications of seismic isolation in New Zealand, Bulletin of the New Zealand National Society for Earthquake Engineering, 28, 253-264.

Rosenblueth E. and Herrera I., (1964), On a kind of hysteretic damping, Journal of Engineering Mechanics Division ASCE, 90, 4, 37-48.

Ryan K.L. and Polanco J., (2008), Problems with Rayleigh damping in base-isolated buildings, Journal of Structural Engineering, 134, 11, 1780-1784.

Ryan K.L. and York K., (2007), Vertical distribution of seismic forces for simplified design of base-isolated buildings, In ASCE Structures Congress, May, Long Beach, CA, USA.

Ryan K.L., Kelly J.M., Chopra A.K., (2005), Nonlinear model for lead-rubber bearings including axial-load effects, Journal of engineering mechanics, 131, 12, 1270-1278.

Sanchez J., Masroor A., Mosqueda G., Ryan K., (2013), Static and dynamic stability of elastomeric bearings for seismic protection of structures, Journal of structural engineering,139, SPECIAL ISSUE: NEES 1: Advances in Earthquake Engineering, 1149-1159.

SAS, (1999), SAS/STAT user's guide: Introduction to Regression Procedures, version 8[M], SAS Institute Inc., Cary, NC, USA.

Sayani P.J. and Ryan K.L., (2009), Comparative evaluation of base-isolated and fixed-base buildings using a comprehensive response index, Journal of Structural Engineering, 135, 6, 698-707.

Shatnawi A.S., Najmi A.S., Mu'tasim S., Amareen I.M., (2008), Non-Linear Seismic Response of Base-Isolated Frame Structures Using Rubber Bearings, Jordan Journal of Civil Engineering, 2, 2, 152-171.

Skinner R.I., Kelly J.M., Heine A.J., (1975), Hysteretic Dampers for earthquake resistant structures, Earthquake Engineering & Structural Dynamics, 3, 3, 287-296.

Skinner R.I., Robinson W.H., McVerry G.H., (1993), An introduction to seismic isolation, John Wiley & Sons Ltd, Chichester, West Sussex, UK.

Soong T.T. and Constantinou M.C., (1994), Passive and Active Structural Vibration Control in Civil Engineering; Springer-Verlag: New York, NY, USA.

Structural Engineers Association of Northern California (SEAONC), (1986), Tentative Seismic Isolation Design Requirements, San Francisco, California.

Symans M.D., Cofer W.F., Fridley K.J., (2003), Base isolation and supplemental damping systems for seismic protection of wood structures: Literature review, Earthquake Spectra, 18, 3, 549-572.

Takayama M. and Morita K., (2002), A Study on the Regulations for Seismic Design of Base-Isolated Buildings, Summaries of technical paper of annual meeting architecture institute of Japan, B-2, 473-474.

Takeda T., Sozen M.A., Nielsen N.N., (1970), Reinforced concrete response to simulated earthquakes, Journal of the Structural Division, 96, 12, 2557-2573.

Taylor A.W., Lin A.N., Martin J.W., (1992), Performance of elastomers in isolation bearings: A literature review, Earthquake spectra, 8, 2, 279-303.

Tena-Colunga A. and Zambrana-Rojas C., (2006), Dynamic torsional amplifications of base-isolated structures with an eccentric isolation system, Engineering structures, 28, 1, 72-83.

Thakare P.P. and Jaiswal O.R., (2011), Comparative Study of Fixed Base and Base Isolated Building using Seismic Analysis, International Journal of Earth Sciences and Engineering, 4, 6, 520-525.
Touaillon J., (1870), U.S. Patent No. 99,973. Washington, DC: U.S. Patent and Trademark Office.

Tsai C.S., Chen B.J., Chiang T.C., (2003), Experimental and computational verification of reasonable design formulae for base-isolated structures, Earthquake Engineering & Structural Dynamics, 32, 9, 1389-1406.

Tsai C.S., Chiang T.C., Chen B.J., Lin S.B., (2003), An advanced analytical model for high damping rubber bearings, Earthquake engineering & structural dynamics, 32, 9, 1373-1387.

Tulei E., Cretu D., Ghindea C., Cruciat R., (2010), Efficiency of Passive Control Devices in Rehabilitation of a Building in the Seismic Conditions of Romania, Proceedings of the 14th European Conference on Earthquake Engineering, 30 August - 03 September, Ohrid, Macedonia.

Wen Y.K., (1976), Method of random vibration of hysteretic systems, Journal of the Engineering Mechanics Division, 102, 2, 249-263.

Westermo B. and Udwadia F., (1983), Periodic response of a sliding oscillator system to harmonic excitation, Earthquake engineering & structural dynamics, 11, 1, 135-146.

Wiles J.I., (2008), An overview of the technology and design of base isolated buildings in high seismic regions in the United States, K-State Electronic Report.

Wilson E.L., (2000), Three Dimensional Static and Dynamic analysis of Structures (3rd Edition), Computers and Structures, Inc. Berkeley, California, USA.

Winters C.W. and Constantinou M.C., (1993), Evaluation of static and response spectrum analysis procedures of SEAOC/UBC for seismic isolated structures, Technical Report NCEER-93-0004, National Center for Earthquake Engineering Research, Buffalo, NY, USA.

Wu H., (2010), Vibration control of a building model with base isolation, Proceedings of the 20th International Congress on Acoustics, 23-27 August, Sydney, Australia.

Yamamoto S., Kikuchi M., Ueda M., Aiken I.D., (2009), A mechanical model for elastomeric seismic isolation bearings include the influence of axial load. Earthq, Earthquake Engineering & Structural Dynamics, 38, 2, 157-180.

York K. and Ryan K.L., (2008), Distribution of lateral forces in base-isolated buildings considering isolation system nonlinearity, Journal of Earthquake Engineering, 12, 7, 1185-1204.

Zayas V., Low S., Mahin S., (1987), The FPS Earthquake Resisting System; Report No. UCB/EERC-87/01; University of California: Berkeley, CA, USA.

Zayas V.A., Low S.S., Mahin S.A., (1990), A simple pendulum technique for achieving seismic isolation, Earthquake spectra, 6, 2, 317-333.

Zekioglu A., Darama H., Erkus B., (2009), Performance-based seismic design of a large seismically isolated structure: Istanbul Sabiha Gökçen International Airport Terminal Building, In SEAOC 2009 Convention Proceedings, 409-427.

Zordan T., Liu T., Briseghella B., Zhang Q., (2014), An improved linear model for base isolated structures with lead rubber bearings, Engineering Structures (in press).